Deformation of the lithosphere during the formation of continental rifted margins

Thesis submitted in accordance with the requirements of the University of Liverpool for the degree of Doctor in Philosophy

By Ludovic Jeanniot

October 2014

Abstract

Deformation of the lithosphere during the formation of continental rifted margins

Ludovic Jeanniot

This thesis investigates lithosphere and asthenosphere deformation during intracontinental rifting leading to breakup and seafloor spreading initiation. Continental rifted margins results from the separation of a continental crust after lithosphere stretching and thinning, but their observations are poorly related to lithosphere and asthenosphere deformation. The strategy of my thesis is to use a kinematic modelling approach to examine the formation of magma-poor rifted margins. Decompressional melting is also predicted. The kinematic model consisting of pure-shear for the 15km upper brittle seismogenic lithosphere above buoyancy driven upwelling divergent flow (UDF) is used to advect temperature and material. A series of numerical experiments using this hybrid deformation model explores the conditions under which mantle exhumation is possible within the Ocean-Continent Transition (OCT) of magma-poor rifted margins. Mantle exhumation is possible and can persist over a long period of time by using a combination of shallow decoupling depth between pure-shear and UDF, narrow pure-shear region, slow spreading rate, no buoyancy and low asthenosphere temperature. However, the application of this hybrid deformation model to specific rifted margins cannot explain their thermal and subsidence evolution and complex architecture if the mode of lithosphere deformation does not evolve. A kinematic finite element model is therefore used to generate a sequence of lithosphere deformation events. The lithosphere deformation mode is similar to the previous hybrid mode but consists of (1) pure-shear induced passive upwelling and (2) buoyancy induced upwelling which is used to speed up lithosphere thinning. Each lithosphere deformation event has specific event timing, pure-shear width, half-spreading rate, buoyancy upwelling rate and lateral deformation migration. This kinematic model is applied to the present-day Iberia-Newfoundland and the fossil analogue Alpine Tethys rifted margins. Pure-shear widths and lateral deformation migration are constrained by the crustal architecture of the observed rifted margin. Lateral migration of deformation produce an asymmetry of their conjugate. Conversely, the event timing, half-spreading and buoyancy rates are constrained by the subsidence and melting generation histories and observed mantle exhumation. The pure-shear width evolves from wide to narrow and the half-spreading rate increases during rifting leading to continental breakup. Buoyancy upwelling plays an important role at the beginning of rifting. Melt retention is required to permit mantle exhumation.

'In all representations of this kind we have, however, to guard against the assumptions of a general arrangement of any kind; indeed, considering the almost incomprehensible variety of the occurrences, a systematic search for regularity is not without danger, because the inquiring mind is so easily led astray from the path of sound synthesis'

(Suess, 1891)

Acknowledgments

Firstly I would like to thank Nick Kusznir for his admirable supervision, enthusiasm and intelligence. Thanks also for giving me the opportunity to do this PhD and for his impressive patience during my last few months of writing.

I thank everyone who has been involved in the MM3 project (BP, ConocoPhillips, HESS, BR Petrobras, Statoil, Shell, TOTAL, BG Group, BHP-Billiton), for finances and support. I am thankful to Geoffroy Mohn, Gianreto Manatschal, Marco Beltrando, Julie Tugend, Jakob Skogseid and Craig Schneider for the numerous discussions that took place during field excursions all over the Alps, in Strasbourg or in the Pyrenees.

Jolante Van Wijk is appreciatively acknowledged for letting me come at the University of Houston and for teaching me dynamic modelling. Also thanks to Erica Greenhalgh for showing me around Houston.

I wish to dedicate especially my gratitude to my VIVA examiners Elisabeth Mariani and Gwenn Péron-Pinvidic for the 4 hours discussion! I appreciate the time you spent to read my thesis and all the constructive comments you gave me.

Thanks to all my colleagues in Liverpool especially to the best office mate I have ever had, Leanne Cowie, to her patience with my English and her kindness in helping me with any issues (administratively or personal) I have been encountered. Thanks to John, Simon and Oliver for their cheerfulness this last year. I would also especially like to thank Steve H., Tom, Kirstie, Kelly, Amaya, Steve C., Felix, Henri, Charlotte and everybody else in the department. Basically, thanks to Liverpool for being one the best cities I have ever lived in.

Thank you to Jo for having cheered me up this year, and the Liverpool Merseyswingers for these stimulating Wednesdays indispensable for unwinding.

Final thanks to my parents, my brother and his new family. I am still not sure they really understand what I am doing, but at least they realized after a year or two of my PhD that I am not an archaeologist!

Contents

Chapter 1

Introduction

1.1 Aims

The formation of a new ocean during plate tectonics requires stretching, thinning and breakup of a continental lithospheric plate into two or more fragments. Stretching and thinning of continental crust and lithosphere during continental rifting leads to mantle upwelling, which at some point generates melt by mantle decompression creating a new oceanic crust. The aim of my PhD is to examine lithosphere deformation during continental rifting leading to breakup and seafloor spreading initiation.

1.1.1 The formation of continental rifted margins

In the interest of the scientific community, I give several definitions to understand what the concepts are and the definitions of the important words that are used in this thesis.

Continental rifting

Rifts are defined by Sengör and Burke (1978) as '*elongated depressions beneath which the entire thickness of the lithosphere has ruptured under extension. Continental rifting occurs in diverse tectonic environments resulting from the continuous evolution of the plate mosaic of the Earth and also from the interaction between mantle processes and the overlying lithosphere*'. Two sorts of rift are identified: passive and active rifts (Turcotte and Emerman, 1983). Active rifts are associated with mantle convection (Morgan, 1972) and passive rifts relate to the tensional failure of the lithosphere to pre-existing tensional stresses (Turcotte and Oxburgh, 1973). Some continental rifts evolve into oceans; others are aborted after few kilometres of extension (Turcotte and Emerman, 1983).

Breakup of the continental crust and lithospheric mantle

In this thesis, continental rifting leading to an ocean is examined. During continental rifting, stretching and thinning of the continental lithosphere lead to the rupture and separation of the continental crust (i.e. crustal breakup) and the lithospheric mantle (i.e. lithosphere mantle breakup) (Franke, 2013). Crustal breakup allows the complete separation of the continental crust into two crustal plates allowing, if no melt is generated at that time, to exhume mantle on the seafloor. Breakup of the mantle lithosphere occurs when the original asthenospheric mantle is either exhumed on the seafloor or is underplated beneath the continental crust. The relative timing of crustal and lithospheric mantle breakup may be important to describe the type of continental rifted margins.

Continental rifted margins

The breakup and separation during continental rifting of a continental lithospheric plate into two or more fragments result in the formation of conjugate rifted margins. Continental rifted margins are the transition between a continental crust of approximately 30-40km thickness and much thinner oceanic crust ~6-7km thick. Seismic analysis imaging continental rifted margins show a broad range of margin architectures. Some rifted margins

show a sharp Ocean-Continent Transition (OCT) (e.g. Black Sea; Florineth and Froitzheim, 1994), others show a smoother transition with a hyper-extended continental crustal domain which sometimes exhibits large domains of exhumed mantle between unequivocal continental and oceanic crust (Boillot et al., 1987; Manatschal et al., 2001; Van Avendonk et al., 2006; Péron-Pinvidic and Manatschal, 2009). This broad range of architecture is related to the presence or absence of significant amount of volcanic supply and distinguishes magma-poor from volcanic rifted margins as illustrated in Figure 1.1. Volcanic margins are the most worldwide margins while the magma-poor type represents a minority. My thesis focuses on magma-poor rifted margins because these margins have large amounts of observations, including mantle rocks exposed on the seafloor, seismic reflection and refraction and well datasets.

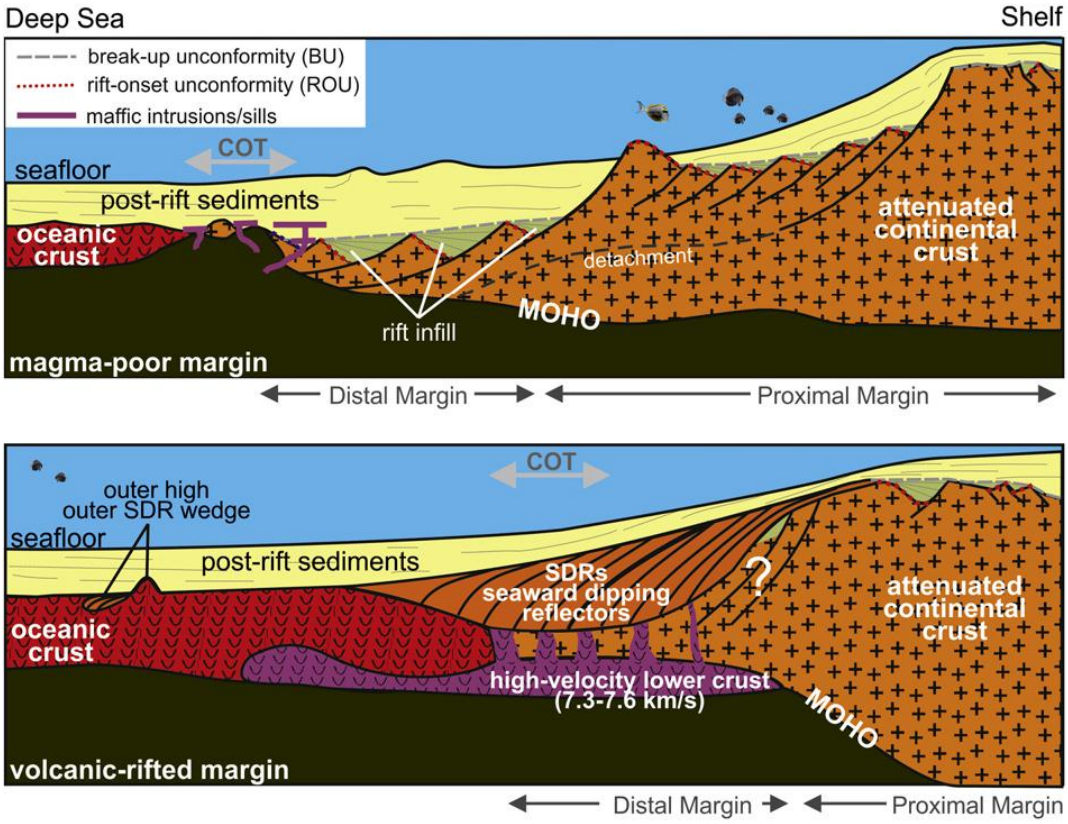

Figure 1.1: Magma-poor vs. magma-rich rifted margin architecture (Franke, 2013).

The architecture-type of magma-poor rifted margins

A simplified architecture of a magma-poor rifted margins is proposed in Figure 1.2 (Tugend et al., 2014). The figure shows the different terminologies from recent studies relying either on geological field observations and geophysical approaches. From the proximal to the most distal domains, rifted margins comprise (1) a stretched and slightly thinned continental crust of ~30km, (2) a necking zone where the continental crust thins to approximately 10km, (3) a hyper-thinned continental crust domain, (4) a zone of exhumed continental mantle (ZECM) with continental slivers and embryonic oceanic crust, and (5) an oceanic crust. OCT's are defined within the points 3, 4 until 5.

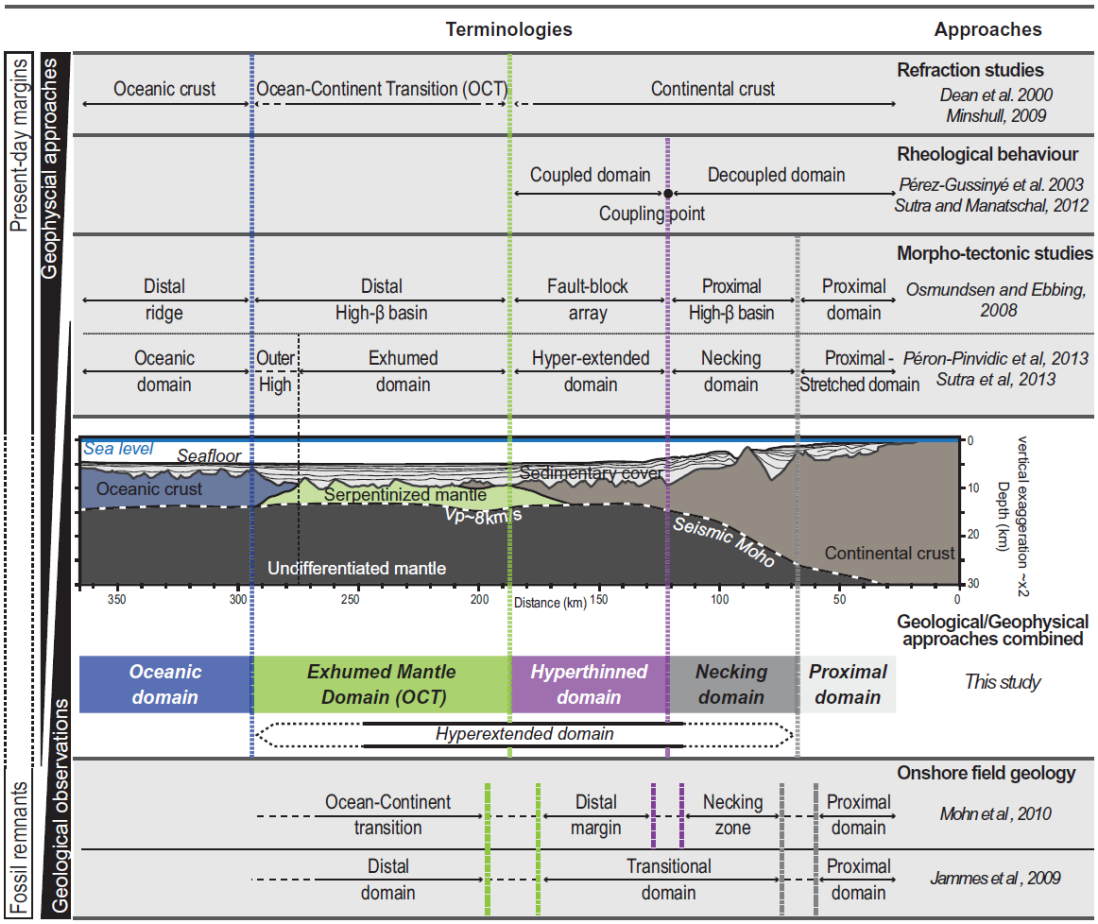

Figure 1.2: The architecture type of magma-poor rifted margins derived from geological and geophysical observations.

The evolution-type of magma-poor rifted margins

The study, description and recognition of magma-poor rifted margins permitted to reconstitute the formation of magma-poor rifted margins. Whitmarsh et al. (2001) and many other authors (Manatschal and Bernoulli, 1999; Cannat et al., 2009; Péron-Pinvidic and Manatschal, 2009) believe that intracontinental rifting leading to breakup and seafloor spreading follows a polyphase evolution. The following gives the definitions used in this thesis for the 4 stages leading to the formation of magma-poor rifted margins (Figure 1.3):

Distributed stretching and thinning: Distributed stretching and thinning, defined as 'stretching' by Péron-Pinvidic and Manatschal (2009), is a deformation phase that occurs over a broad region (>100km, Brun & Choukroune, 1983) and is characterised by high-angle extensional normal faulting in the upper 10-15km brittle seismogenic lithosphere (i.e. upper crust), associated with half-graben subsidence developing independent sedimentary basins (Jackson, 1987). The continental crust and lithosphere are slightly stretched and thinned.

Localised stretching and thinning: This phase, defined as the 'thinning' mode by Péron-Pinvidic and Manatschal (2009), results in localised deformation within a narrow region (<100km). The continental crust and lithosphere are extremely thinned until the creation of a conjugate system of detachment faults that accommodates crustal and mantle exhumation (e.g. Alpine Tethys, Iberia-Newfoundland, Reston et al., 1996; Manatschal, 2004; Reston and McDermott, 2011). The latest stage of thinning may lead to the formation of hyper-thinned crustal domain (e.g. West-African Margin, Contrucci et al., 2004), mantle exhumation and embryonic oceanic crust.

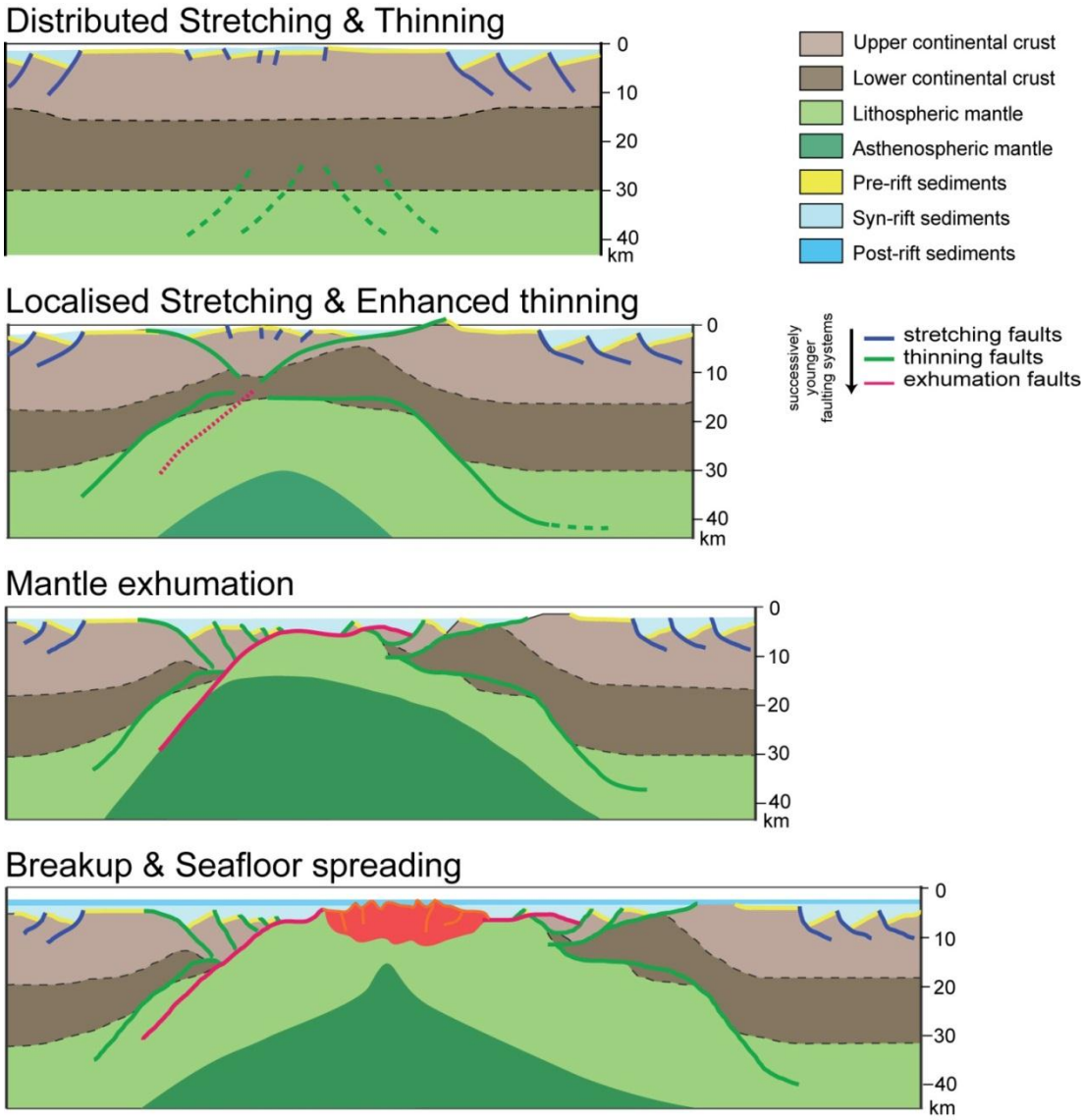

Figure 1.3: The development of continental lithosphere stretching and thinning leading to breakup and seafloor spreading initiation for magma-poor rifted margins (modified from Péron-Pinvidic and Manatschal, 2009). A sequence of four stages have been identified form observations of rifted margins seismic data and geological field studies of exhumed rifted margins: stretching and thinning; stretching with enhanced thinning; mantle exhumation and seafloor spreading. The different types of faulting (stretching, thinning and exhumation faults) during these stages are also shown.

Mantle exhumation: Extreme thinning of the continental crust and lithosphere leads to the breakup of the crust which allows mantle exhumation to occurs, only if no consequential melting is generated and extracted prior crustal breakup to form an oceanic crust (e.g. Iberia and Newfoundland margins, Boillot et al., 1987; Reid, 1994; Jagoutz et al., 2007; Bronner et al., 2011). The type of exhumed mantle is dependent to the relative timing of crustal and lithosphere mantle breakup (Franke, 2013); sub-continental mantle is exhumed if the lithosphere mantle breakup occurs after crustal breakup. Otherwise prior to crustal breakup, asthenospheric mantle is exhumed.

Seafloor spreading initiation: Seafloor spreading occurs when thermal and/or mechanical processes are localised in a narrow region of ~20km (i.e. ridge axis). The seafloor that spreads may be composed of exhumed mantle, oceanic crust or a mix of mantle and continental crust. In this thesis, we consider seafloor spreading initiation as the latest deformation event that lead to an equilibrated formation of oceanic crust or exhumed mantle.

Continental breakup

Continental breakup is a broad concept defining late stages of continental rifting during breakups of the continental crust and lithospheric mantle, and seafloor spreading. In this meaning, continental breakup cannot be defined as a point in time. However, Cannat et al. (2009) suggested that the installation of a ridge-type thermal regime (active heat balance, i.e. Figure 1.4), was the most practical definition for continental breakup. Understanding the thermal evolution of the lithosphere during continental breakup is important to predict magmatism at continental rifted margins. Cannat et al. (2009) proposed an evolution of lithosphere thermal structure from intracontinental rifting to breakup and seafloor spreading initiation for the formation of magma-poor rifted margins (Figure 1.4). At the beginning of rifting, the base of the lithosphere remains deep and close to its original

depth, then it shallows rapidly leading to decompressional melting, and finally it stabilizes at shallow depth. This thesis aims to quantify this thermal evolution by examining the relative timing of melt initiation and crustal rupture during rifting.

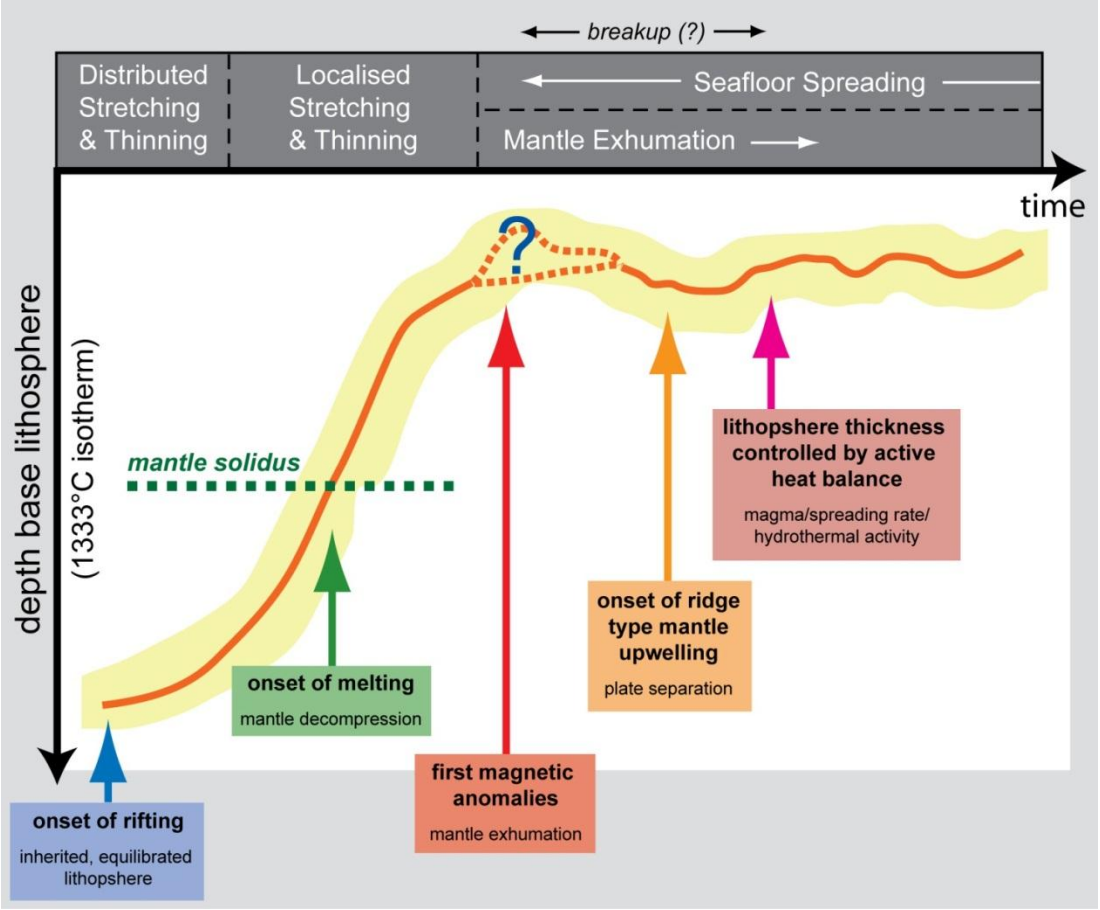

Figure 1.4: Interpreted evolution of the thinning of the base of the lithosphere defined with the isotherm 1333°C during the polyphase evolution of rifting and its relationship to the onset of rifting, melting, magnetic anomaly generation and seafloor spreading (modified from Cannat et al. (2009)).

1.1.2 Modes of lithosphere deformation

The processes of lithosphere deformation during continental rifting remain obscure because there is no direct observational evidence of the mantle behaviour during continental breakup. Nevertheless, geoscientists have found indirect access by examining existing and fossil continental rifted margins. Although the magmatism history, distinguishing volcanic from magma-poor rifted margins, may be controlled by a combination of factors including the thermal structure (Spiegelman, 1993; Reston and Morgan, 2004), spreading rate and rifting duration (Winterbourne et al., 2009), active upwelling (Holbrook et al., 2001) or small-scale convection (Pinheiro et al., 1996), how the lithosphere deforms during continental breakup remains an important question.

Two types of lithosphere deformation are defined as passive and active mode of deformation:

Pure-shear and simple shear: Pure-shear and simple shear extension of the lithosphere produce two different rift morphologies (Figure 1.5). McKenzie (1978) used a pure-shear deformation mode to describe symmetric lithosphere deformation during intracontinental rifting. The lithosphere is stretched with a constant spreading rate which imposes uniform and homogenous passive upwelling beneath a specific region that can be broad or narrow, and accommodated by conjugated symmetrical normal faults. The asymmetric analogue is a simple shear mode (Wernicke et al., 1981), where a detachment fault divides the lithosphere into two plates (lower and upper, or hanging wall and footwall). In this thesis, pure-shear is commonly used to describe passive extension. In chapter 3 and 4, I explore the lateral migration of the deformation axis, which results in the asymmetry of the rift morphology, thus similar to simple-shear.

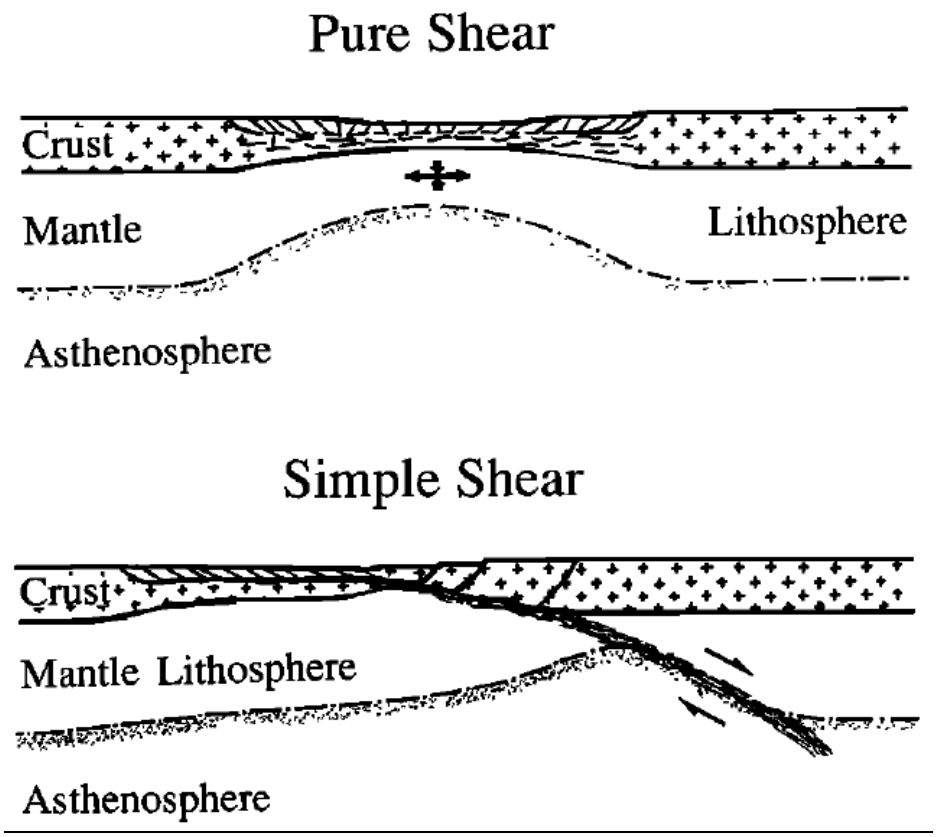

Figure 1.5: Pure-shear and simple shear deformation (Buck et al., 1988).

Upwelling-divergent flow: Upwelling-divergent flow has been used to describe lithosphere and asthenosphere deformation at ocean ridges (Figure 1.6 Morgan, 1987). The difference with pure and simple shear is the active definition of the mode, driven by a constant extension and axial upwelling rates. The ratio between the extensional and axial rates characterizes the degree of active upwelling or buoyancy (Batchelor, 2000; Braun et al., 2000). In this context, the deformation is focused to a narrow axial region (i.e. mid-ocean ridge). This active mode is consistent with continental breakup defined as the active heat balance by Cannat et al. (2009).

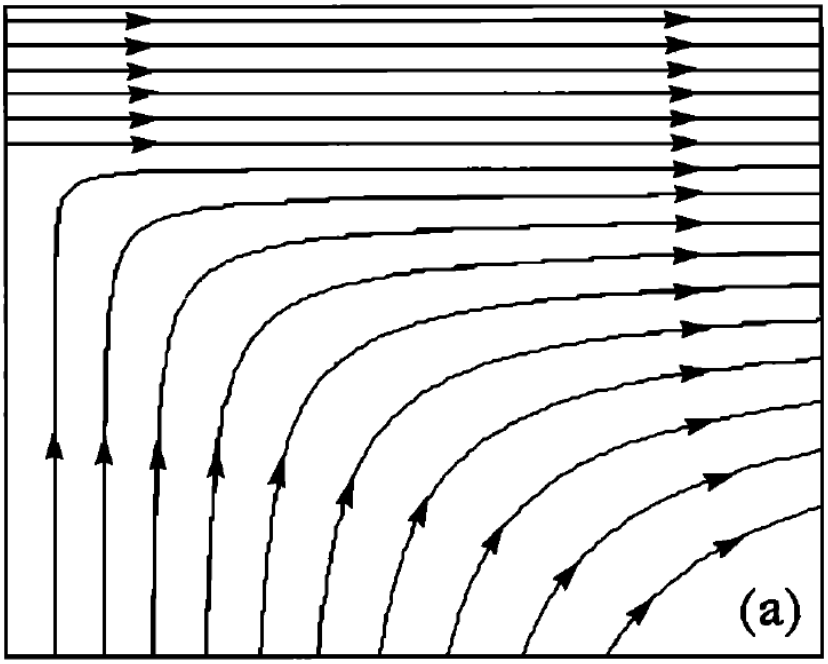

Figure 1.6: Upwelling-divergent flow deformation mode (Morgan, 1987).

Fletcher et al. (2009) examined pure-shear and upwelling-divergent flow lithosphere deformation mode end-members applied to continental breakup and their consequences for decompressional melting and crustal breakup. They explored the relative timing of melt initiation and crustal breakup in order to predict the conditions under which mantle exhumation may occur. They proposed that the presence or absence of exhumed mantle was not only controlled by asthenosphere temperature, mantle depletion or the rate of lithosphere stretching and thinning, but also that the mode of lithosphere deformation was critically important. The resulting lithosphere and asthenosphere deformation of pure-shear and upwelling divergent flow deformation modes is shown in Figure 1.7. Fletcher et al. (2009) argued that deformation by pure-shear was unlikely to predict mantle exhumation, whereas deformation by upwelling-divergent flow was more likely to predict a magma-poor rifted margin with exhumed mantle within the OCT.

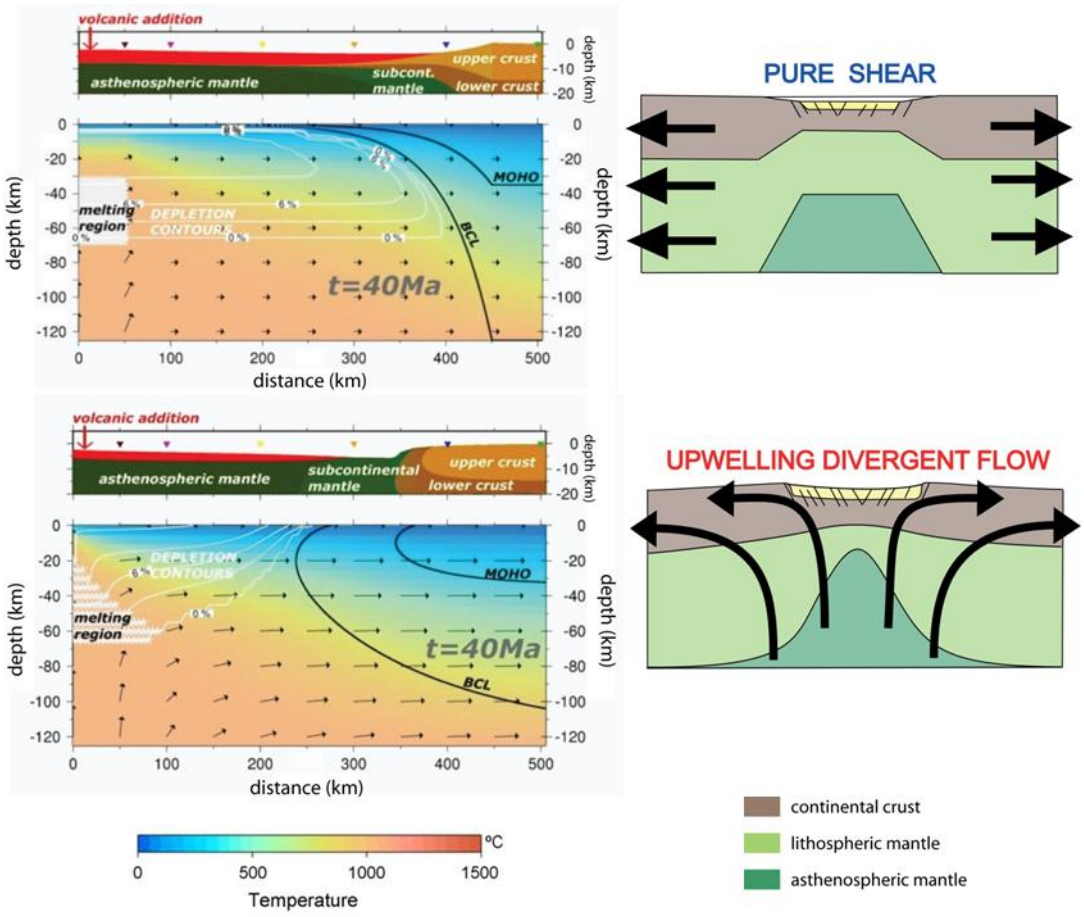

Figure 1.7: Temperature and material advection and sketches of two end-members deformation modes according to Fletcher et al. (2009): pure-shear and upwelling-divergent flow.

However, observations at slow-spreading ocean ridges and magma-poor rifted margins suggest a more complex evolution of continental rifting leading to breakup that cannot be explained by simple end-members lithosphere deformation modes. Cannat (1996) shows that the deformation at slow-spreading ocean ridges is dominantly controlled by extensional faulting for the seismogenic 10-15km upper lithosphere, with upwelling-divergent flow for the remaining ductile lithosphere and asthenosphere. This mechanical and thermal behaviour of the lithosphere and asthenosphere may also be applicable to intracontinental rifting (Cannat et al., 2009), where normal faulting within the 10-15km

upper crust (Jackson, 1987) represent the first accommodation of the extension (Figure 1.8). However, the main difference between intracontinental rifting and slow-spreading ocean ridges is the width within which the lithosphere deformation is focused.

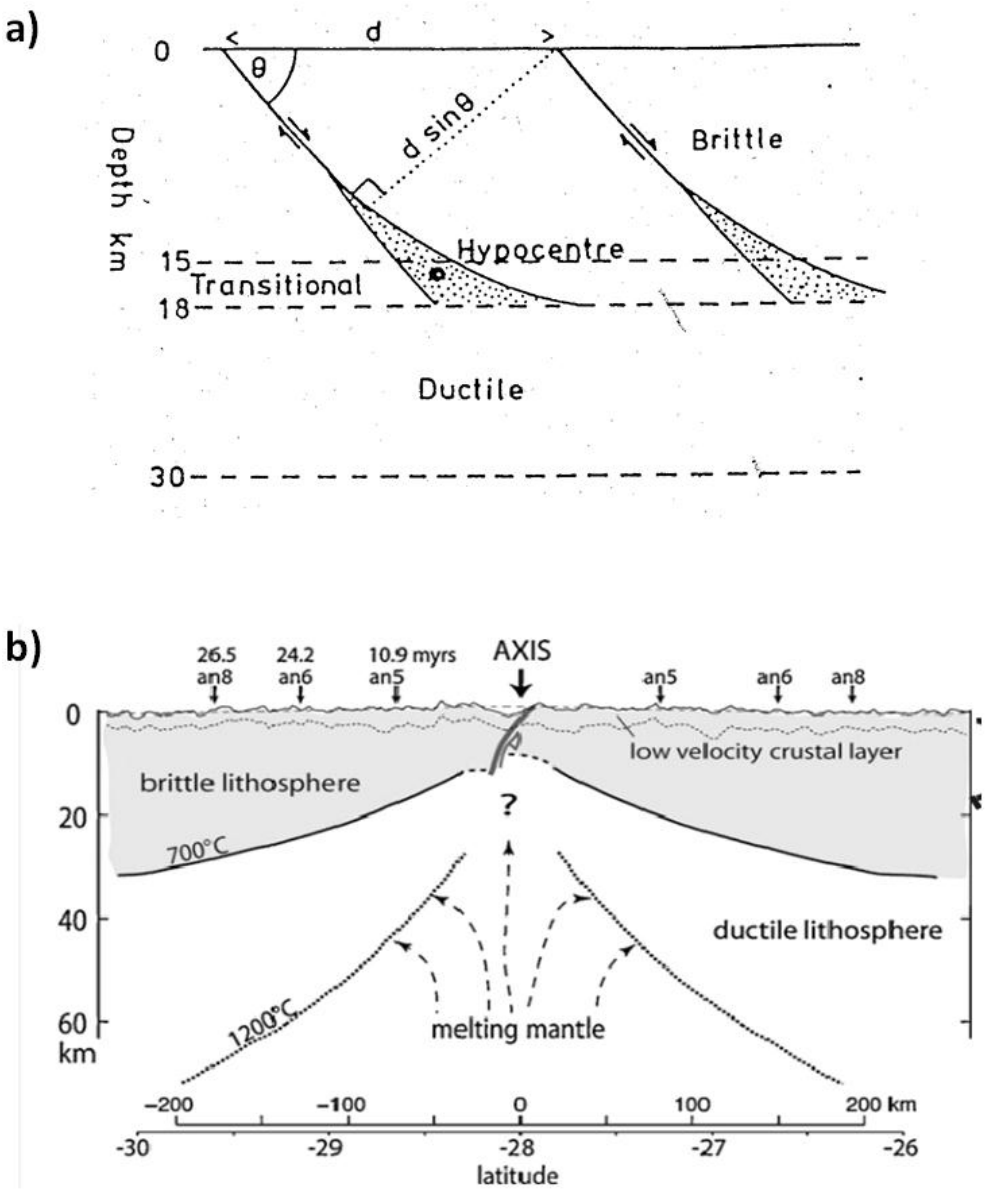

Figure 1.8: Extensional faulting in the topmost upper 10-15km seismogenic lithosphere **a)** during intracontinental rifting (Jackson, 1987) and **b)** at slow-spreading ocean ridges (Cannat et al., 2009).

These observations at magma-poor rifted margins and slow-spreading ocean ridges described above do not only introduce new concepts of how the lithosphere deforms during continental rifting leading to breakup, but they also require new models of lithosphere deformation.

1.2 Strategy and plan

The strategy used in my PhD is to relate conceptual models, numerical modelling and observations at magma-poor rifted margins in order to investigate lithosphere deformation modes responsible for the crustal thinning and rupture, melting and resulting subsidence histories that lead to complex rifted margins architecture. Determining lithosphere deformation modes during continental breakup is important for our understanding of plate tectonics. In addition, understanding lithosphere deformation, crustal and OCT structure, Continent-Ocean Boundary location, melt generation, and heat flow and subsidence histories is also important to the hydrocarbon industry.

1.2.1 Modelling approach

Numerous numerical model experiments have been carried out to investigate continental breakup and rifted margins formation. In this section I give the definition of the dynamic and kinematic modelling approaches.

Dynamic modelling

The mode of deformation in dynamic modelling is defined by constitutive equations where the rheology is fully thermo-mechanically coupled (Fernàndez & Ranalli, 1997). This permits the model to be self-consistent with actual rock-rheology fundamental processes. The deformation is initiated using initial anomalies implanted within the lithosphere. Harry and Grandell (2007) used initial anomalies in the continental crustal thickness and initial weakness of the rheology of the continental crust to reproduce a similar architecture to Galicia Bank and Flemish Cap. Lavier and Manatschal (2006) constrained their initial

conditions from derived geological and geophysical observations on the Iberia-Newfoundland and the Alpine Tethys rifted margins. These dynamic models show a complex evolution determined by the initial rheological properties of continental crust and mantle, but they may result in unexpected predictions, which make them difficult to apply to specific rifted margins architecture and calibrated against real data observations.

Kinematic modelling

Deformation modes in kinematic models are prescribed by flow velocity fields. Kinematics models omit rheological properties and the physics of its evolution, but their simplicity of use allows quantitative calibration. Therefore we privilege the kinematic approach, rather than dynamic, not only because I aim to apply a model of lithosphere deformation to the Iberia-Newfoundland rifted margins but because we want to constrain the model, through a series of numerical experiments, using strong geological and geophysical observations. Kinematic models have been already applied to specific case histories in order to predict subsidence, heat flow or the architecture of the sedimentary basins and rifted margins (e.g. Beaumont et al., 1982, Kusznir & Karner, 2007); however, there is no existing study that can determine the full deformation history in lithospheric extension context, constrained and quantitatively calibrated using real observations and interpretations.

During my PhD I developed a kinematic model of lithosphere deformation during continental rifting leading to breakup and seafloor spreading. This model is called FEmargin (Finite-Element margin) and uses prescribe flow velocity field to advect lithosphere and asthenosphere material and temperature.

1.2.2 Thesis plan

The contents of each chapter are summarized as follows. Chapters 2, 3 and 4 are presented in a paper format suitable for publication in scientific journals. As a consequence, there is some duplication of information between these chapters.

Chapter 2: In this chapter I examine a hybrid model of lithosphere deformation during continental breakup, consisting of pure-shear above upwelling divergent flow (Figure 1.9), to explore magma-poor rift margin architecture and particularly the conditions under which mantle may exhume. This chapter relies on the continuity of the work of Fletcher et al., 2009, where numerical experiments are carried out to give insight of the optimum conditions for mantle exhumation to occur.

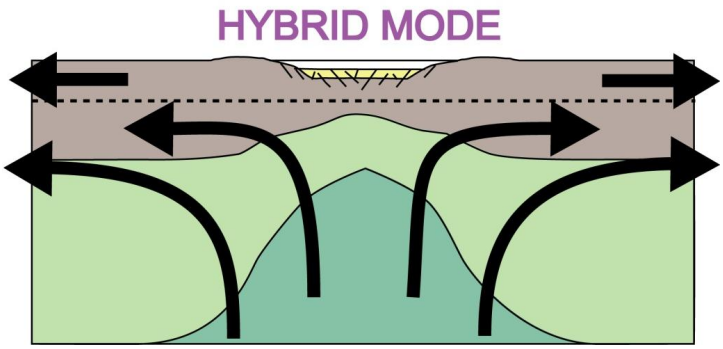

Figure 1.9: By analogy to the deformation processes occurring during intracontinental rifting and at slow spreading ocean ridges (Figure 1.8), a more realistic lithosphere deformation mode for magma-poor continental breakup is pure-shear for the colder brittle upper 10-15 km above upwelling-divergent flow for the remaining lithosphere and asthenosphere.

Chapter 3: The application of the hybrid model described in chapter 2 to natural laboratories at rifted continental margins is not possible with a non-evolving lithosphere deformation mode because of the polyphase evolution of rifting leading to continental breakup. In this chapter I develop a more complex and powerful geodynamic model (FEmargin). The model uses a series of evolving lithosphere deformation mode events kinematically driven. In order to validate the sequence of lithosphere deformation evens, and also give insight of the main stages of rifting, I apply the model to two conjugate margin profiles across the Iberia-Newfoundland (Figure 1.10). The model is

quantitatively calibrated against the rifted margin architecture using the observed continental crust thickness and present-day water-loaded subsidence, and against the evolution of rifting using observed melting and subsidence histories.

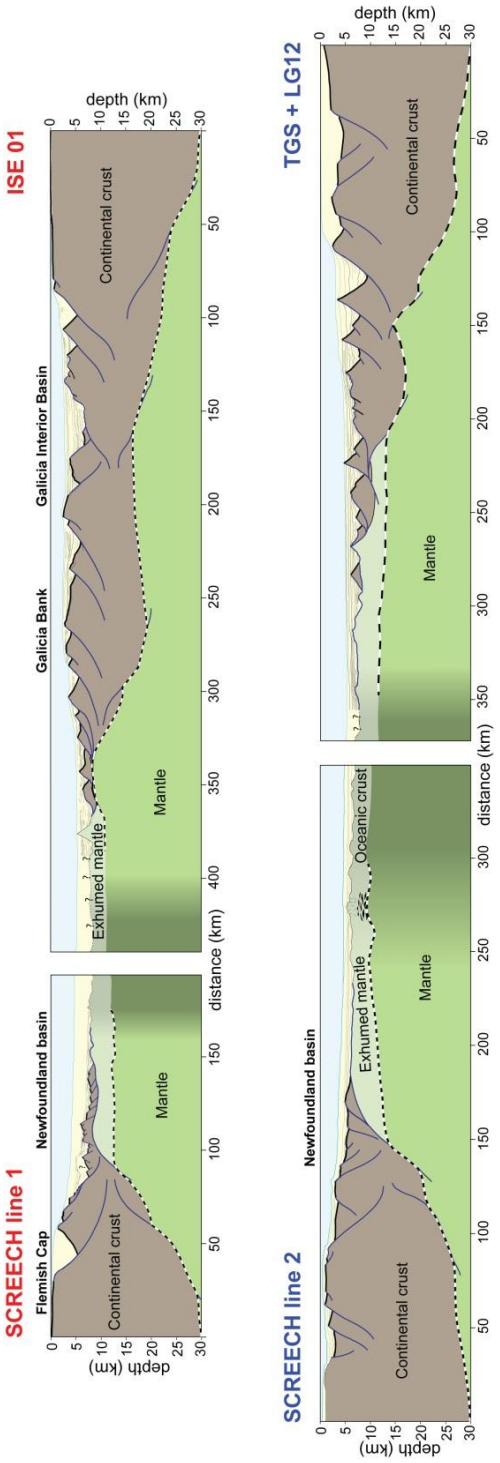

Figure 1.10: Cross-section interpretation of the northern and southern Iberia-Newfoundland conjugate rifted continental margins (modified from Sutra et al., 2013).

Chapter 4: In this chapter the new kinematic model is used to examine the isostatic and thermal evolution during the formation of continental rifted margins and to give insight into the lithosphere and asthenosphere deformation. For this purpose, I apply the model to the Alpine Tethys margins with particular focus on the Briançonnais domain. The Briançonnais is a continental ribbon between two hyper-extended basins (Figure 1.11), which underwent a complex vertical motion consisting of initial uplift followed by rapid subsidence. Modelling is also used to predict P-T-t histories and geothermal gradient evolution for comparison with observations.

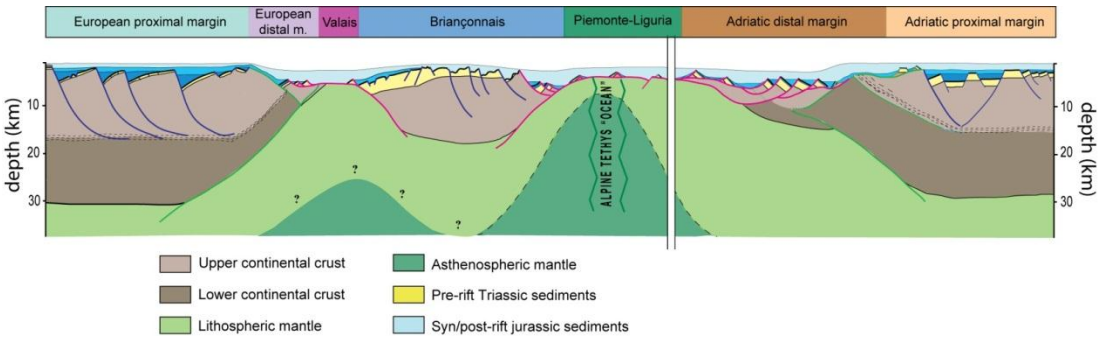

Figure 1.11: Cross-section during the late Jurassic (145Ma) of the Alpine Tethys crustal rifted margins architecture (modified from Mohn et al. (2010)).

Chapter 5: This chapter summarises the previous studies and includes a general discussion about lithosphere deformation, continental rifted margin architecture, thermal evolution and melting history during continental rifting leading to breakup and seafloor spreading initiation. It also suggests further work.

REFERENCES

Batchelor, G. K. (2000). *An Introduction to Fluid Dynamics*. Cambridge University Press.

Beaumont, C., Keen, C. E., & Boutilier, R. (1982). On the evolution of rifted continental margins: comparison of models and observations for the Nova Scotian margin (Canada). *Geophysical Journal*, *70*, 667–715.

Cannat, M., 1996, How thick is the magmatic crust at slow spreading oceanic ridges?: Journal of Geophysical Research: Solid Earth, v. 101, p. 2847-2857.

Boillot, G., Winterer, E. L., & Meyer, A. W. (1987). Leg 103. In *Proc. Ocean Drill. Program, Initial Reports* (Vol. 103, p. 663).

Braun, M. G., Hirth, G., & Parmentier, E. M. (2000). The effects of deep damp melting on mantle flow and melt generation beneath mid-ocean ridges. *Earth and Planetary Science Letters*, *176*(3–4), 339–356.

Bronner, A., Sauter, D., Manatschal, G., Péron-Pinvidic, G., & Munschy, M. (2011). Magmatic breakup as an explanation for magnetic anomalies at magma-poor rifted margins. *Nature Geoscience*, *4*(8), 549–553.

Brun, J., Choukroune, P., Armoricain, C., & Structurale, E. (1983). Normal faulting, block tilting, and décollement in a stretched crust, *2*(4), 345–356.Cannat, M., G. Manatschal, D. Sauter, and G. Peron-Pinvidic, 2009, Assessing the conditions of continental breakup at magma-poor rifted margins: What can we learn from slow spreading mid-ocean ridges?: Comptes Rendus Geoscience, v. 341, p. 406-427.

Buck, W. R., Martinez, F., Steckler, M. S., Cochran J. R. (1988).Thermal consequences of lithospheric extesnion: Pure and simple Lithosphere. *Tectonics*, *7*(2), 213–234.

Contrucci, I., Klingelhöfer, F., Perrot, J., Bartolome, R., Gutscher, M., Sahabi, M., … Rehault, J. (2004). The crustal structure of the NW Moroccan continental margin from wide-angle and reflection seismic data. *Geophysical Journal International*, *159*(1), 117–128.

Fernàndez, M., & Ranalli, G. (1997). The role of rheology in extensional basin formation modelling. *Tectonophysics*, *282*, 129–145.

Fletcher, R., N. Kusznir, and M. Cheadle, 2009, Melt initiation and mantle exhumation at the Iberian rifted margin: Comparison of pure–shear and upwelling-divergent flow models of continental breakup: Comptes Rendus Geoscience, v. 341, p. 394-405.

Florineth, D., and N. Froitzheim, 1994, TRANSITION FROM CONTINENTAL TO OCEANIC BASEMENT IN THE TASNA NAPPE (ENGADINE WINDOW, GRAUBUNDEN, SWITZERLAND)-EVIDENCE FOR EARLY CRETACEOUS OPENING OF THE VALAIS OCEAN: Schweizerische Mineralogische und Petrographische Mitteilungen, v. 74, p. 437-448.

Franke, D. (2013). Rifting, lithosphere breakup and volcanism: Comparison of magma-poor and volcanic rifted margins. *Marine and Petroleum Geology*, *43*, 63–87.Harry, D. L., and S. Grandell, 2007, A dynamic model of rifting between Galicia Bank and Flemish Cap during the opening of the North Atlantic Ocean: Geological Society, London, Special Publications, v. 282, p. 157-172.

Holbrook, W. S., H. C. Larsen, J. Korenaga, T. Dahl-Jensen, I. D. Reid, P. B. Kelemen, J. R. Hopper, G. M. Kent, D. Lizarralde, S. Bernstein, and R. S. Detrick, 2001, Mantle thermal structure and active upwelling during continental breakup in the North Atlantic: Earth and Planetary Science Letters, v. 190, p. 251-266.

Jackson, J. a. (1987). Active normal faulting and crustal extension. *Geological Society, London, Special Publications*, *28*(28), 3–17.

Jagoutz, O., Müntener, O., Manatschal, G., Rubatto, D., Péron-Pinvidic, G., Turrin, B. D., & Villa, I. M. (2007). The rift-to-drift transition in the North Atlantic: A stuttering start of the MORB machine? *Geology*, *35*(12), 1087–1090.

Kusznir, N. J., & Karner, G. D. (2007). Continental lithospheric thinning and breakup in response to upwelling divergent mantle flow: application to the Woodlark, Newfoundland and Iberia margins. *Geological Society, London, Special Publications*, *282*(1), 389–419.

Lavier, L. L., and G. Manatschal, 2006, A mechanism to thin the continental lithosphere at magma-poor margins: Nature, v. 440, p. 324-328.

Manatschal, G., and D. Bernoulli, 1999, Architecture and tectonic evolution of nonvolcanic margins: Present-day Galicia and ancient Adria: Tectonics, v. 18, p. 1099-1119.

Manatschal, G., N. Froitzheim, M. Rubenach, and B. D. Turrin, 2001, The role of detachment faulting in the formation of an ocean-continent transition: Insights from the Iberia Abyssal Plain: Geological Society, London, Special Publications, v. 187, p. 405-428.

Manatschal, G. (2004). New models for evolution of magma-poor rifted margins based on a review of data and concepts from West Iberia and the Alps. *International Journal of Earth Sciences*, *93*(3), 432–466.

McKenzie, D., 1978, Some remarks on the development of sedimentary basins: Earth and Planetary Science Letters, v. 40, p. 25-32.

Mohn, G., G. Manatschal, M. Beltrando, E. Masini, and N. Kusznir, 2012, Necking of continental crust in magma-poor rifted margins: Evidence from the fossil Alpine Tethys margins: Tectonics, v. 31.

Morgan, J. P., 1987, Melt migration beneath mid-ocean spreading centers: Geophysical Research Letters, v. 14, p. 1238-1241.

Péron-Pinvidic, G., and G. Manatschal, 2009, The final rifting evolution at deep magma-poor passive margins from Iberia-Newfoundland: a new point of view: International Journal of Earth Sciences, v. 98, p. 1581-1597.

Pinheiro, L. M., R. C. L. Wilson, R. Pena dos Reis, R. B. Whitmarsh, and A. Ribeiro, 1996, The western Iberia margin: a geophysical and geological overview: PROCEEDINGS-OCEAN DRILLING PROGRAM SCIENTIFIC RESULTS, p. 3-26.

Reid, I. D. (1994). Crustal structure of a nonvolcanic rifted margin east of Newfoundland. *Journal of Geophysical Research: Solid Earth (1978–2012)*, *99*(B8), 15161–15180.

Reston, T. J., Krawczyk, C. M., & Klaeschen, D. (1996). The S reflector west of Galicia (Spain): Evidence from prestack depth migration for detachment faulting during continental breakup. *Journal of Geophysical Research: Solid Earth (1978–2012)*, *101*(B4), 8075–8091Reston, T. J., and J. P. Morgan, 2004, Continental geotherm and the evolution of rifted margins: Geology, v. 32, p. 133-136.

Reston, T. J., & McDermott, K. G. (2011). Successive detachment faults and mantle unroofing at magma-poor rifted margins. *Geology*, *39*(11), 1071–1074.

Sengör, A. M., & Burke, K. (1978). Relative timing of rifting and volcanism on Earth and its tectonic implications. *Geophysical Research Letters*, *5*(6), 419–421.

Spiegelman, M., 1993, Physics of melt extraction: Theory, implications and applications: Philosophical Transactions of the Royal Society of London. Series A: Physical and Engineering Sciences, v. 342, p. 23-41.

Tugend, J., Manatschal, G., & Kusznir, N. J. (2014). Characterizing , identifying and mapping structural domains at rifted continental margins : insights from the Bay of Biscay margins and its Pyrenean fossil analogue, *16*, 8416.

Turcotte, D. L., & Oxburgh, E. R. (1973). Mid-plate Tectonics. *Nature*, *244*, 337–339.

Turcotte, D.L., & Emerman, H. (1983). Mechanisms of active and passive rifting. 39-50. *Science*, *94*, 39–50.

Turcotte, D. L., & Schubert, G. (2002). *Geodynamics*. University Press.

Van Avendonk, H. J. A., W. S. Holbrook, G. T. Nunes, D. J. Shillington, B. E. Tucholke, K. E. Louden, H. C. Larsen, and J. R. Hopper, 2006, Seismic velocity structure of the rifted margin of the eastern Grand Banks of Newfoundland, Canada: Journal of Geophysical Research: Solid Earth (1978–2012), v. 111.

Wernicke, B., 1981, Low-angle normal faults in the Basin and Range province: Nappe tectonics in an extending orogen: Nature, v. 291, p. 645-648.

Whitmarsh, R. B., G. Manatschal, and T. A. Minshull, 2001, Evolution of magma-poor continental margins from rifting to seafloor spreading: Nature, v. 413, p. 150-154.

Winterbourne, J., A. Crosby, and N. White, 2009, Depth, age and dynamic topography of oceanic lithosphere beneath heavily sedimented Atlantic margins: Earth and Planetary Science Letters, v. 287, p. 137-151.

Chapter 2

How does the lithosphere deformation mode during continental breakup affect mantle exhumation?

Preface

This chapter is a paper format and is aim to be submitted in Comptes rendu Geoscience

How does the lithosphere deformation mode during continental breakup affect mantle exhumation?

Ludovic Jeanniot[1], Nick Kusznir[1] and Gianreto Manatschal[2]

[1]Department of Earth, Ocean and Ecological Sciences, University of Liverpool, Liverpool, L69 3GP, UK

[2]IPGS-EOST, UDS-CNRS, Strasbourg, France

ABSTRACT

We carry out a series of numerical experiments to investigate under which conditions mantle exhumation can occur at magma-poor rifted margins. A hybrid lithosphere deformation model with pure-shear in the upper brittle seismogenic lithosphere above upwelling-divergent flow is used to advect lithosphere and asthenosphere material and temperature, and to predict continental crustal separation and decompression melting. The relative timing of melt initiation and continental crustal separation determine the occurrence or absence of exhumed mantle on the seafloor. We show that mantle exhumation is only possible under certain conditions consisting of a narrow pure-shear deformation region, passive upwelling, a shallow decoupling depth between pure-shear and upwelling divergent flow deformation or cold asthenosphere temperature. Mantle exhumation may only occur for a long period of time by using a combination of these conditions. Melt retention within the mantle plays an important role for delaying melt extraction and therefore allowing mantle exhumation. The predicted subsidence history and crustal architecture at rifted margins is examined.

2.1 Introduction

Magma-poor rifted margins show a region of serpentinized exhumed mantle within the Ocean-Continent Transition (OCT). Mantle exhumation requires that the stretched and thinned continental crust separates prior to the onset of significant decompression melting. While the relative timing of melt initiation and continental crustal separation, and therefore mantle exhumation, are controlled by the asthenosphere potential temperature, mantle depletion and the rate of lithosphere stretching and thinning, Fletcher et al. (2009) have shown that the deformation modes of lithosphere and asthenosphere are also important. They examined two end-members of lithosphere deformation modes; pure-shear and upwelling divergent flow (Figure 2.1).

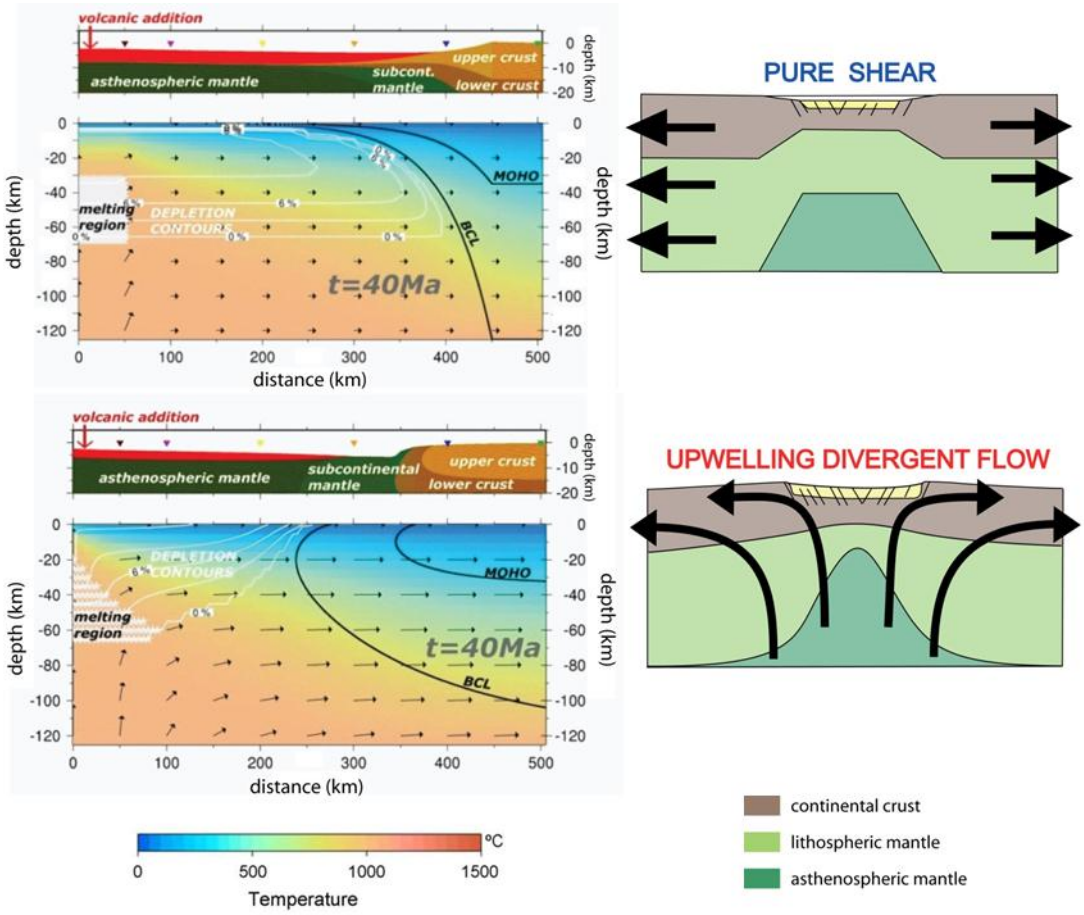

Figure 2.1: Temperature and material advection and sketches of pure-shear and upwelling-divergent flow end-members deformation modes according to Fletcher et al., 2009.

They showed that for the Iberia-Newfoundland conjugate rifted margins, modelling of continental lithosphere stretching and thinning by pure-shear resulted in decompression melting before continental crustal rupture, unless there was initially a cold or geochemically depleted mantle, while stretching and thinning by upwelling-divergent flow (UDF) resulted in crustal separation prior to melt initiation. It has been suggested that the upwelling-divergent "corner flow" deformation mode, introduced by Morgan (1982), may be required to explain the formation of exhumed mantle and therefore may be important in the formation of non-volcanic rifted margins (Davis and Kusznir, 2004).

However observations at magma-poor rifted margins including Iberia-Newfoundland show a particular OCT architecture (Péron-Pinvidic and Manatschal, 2009) suggesting a complex continental rifting evolution that cannot be explained by simplistic end-member pure-shear or corner-flow deformation modes of lithosphere stretching and thinning. Mohn et al. (2012) showed that the architecture of a magma-poor rifted margin is subdivided into a proximal domain of approximately 30km continental crustal thickness, a necking zone where the continental crust thins considerably, a distal domain that includes thinned continental crust, a zone of exhumed continental mantle (ZECM) within the OCT and an oceanic domain. Mantle exhumation can be found accompanied with continental ribbons, dykes and embryonic oceanic crust (Péron‐Pinvidic et al., 2007).

A more realistic hybrid model of lithosphere deformation for magma-poor rifted margins can be explored by analogy with observations of lithosphere deformation processes occurring at slow spreading ocean ridges. Cannat et al. (2009) showed that the uppermost 10-15km are made of strong brittle lithosphere and that extension within this layer is accommodated by normal faulting and magmatic intrusions. During intracontinental rifting, McKenzie (1987) uses pure-shear to deform the lithosphere which is also accommodated by extensional normal faulting in the topmost upper 10-15km lithosphere (Jackson, 1987) Therefore, we suggest that deformation in this upper brittle layer of the lithosphere may be

represented by pure-shear at slow-spreading ocean ridges. Below the pure-shear layer, the deformation within the lithosphere and asthenosphere occurs by UDF. The two lithosphere deformation modes, pure-shear above UDF, are separated by a decoupling horizon.

The objective of this paper is to explore this hybrid model of lithosphere deformation and the relative contribution of pure-shear and upwelling-divergent "corner flow" deformation mode in order to investigate under which conditions mantle exhumation may occur. A series of numerical experiments exploring the model sensitivity to the deformation modes and initial conditions is carried out to explore the relative timing of continental crustal separation, melting and subsidence histories and the final architecture of rifted margins.

2.2 Model formulation

We represent lithosphere and asthenosphere deformation by a 2-D flow field, which is used to advect both material and temperature. Pure-shear has been used to describe lithosphere deformation during intracontinental rifting (McKenzie, 1978). Upwelling-divergent flow (UDF) has been used to describe lithosphere and asthenosphere deformation at ocean ridges (Morgan, 1987). Pure-shear and UDF have both been examined by Fletcher et al. (2009) as end-members models describing breakup processes.

2.2.1 Lithosphere deformation

The hybrid lithosphere deformation model consists of a combination of both pure-shear and upwelling-divergent flow components as illustrated in Figure 2.2.

Pure-shear deformation mode

Pure-shear deformation is applied to the topmost 15km of the upper continental and oceanic lithosphere. It corresponds to the cooler brittle seismogenic layer (Cannat, 1996), which deforms primarily by extensional faulting. We consider that the lithosphere is stretched with a constant half extension rate V_x^0 and that the pure-shear deformation occurs within a fixed width W axial zone in the lithosphere and asthenosphere (Figure 2.3a).

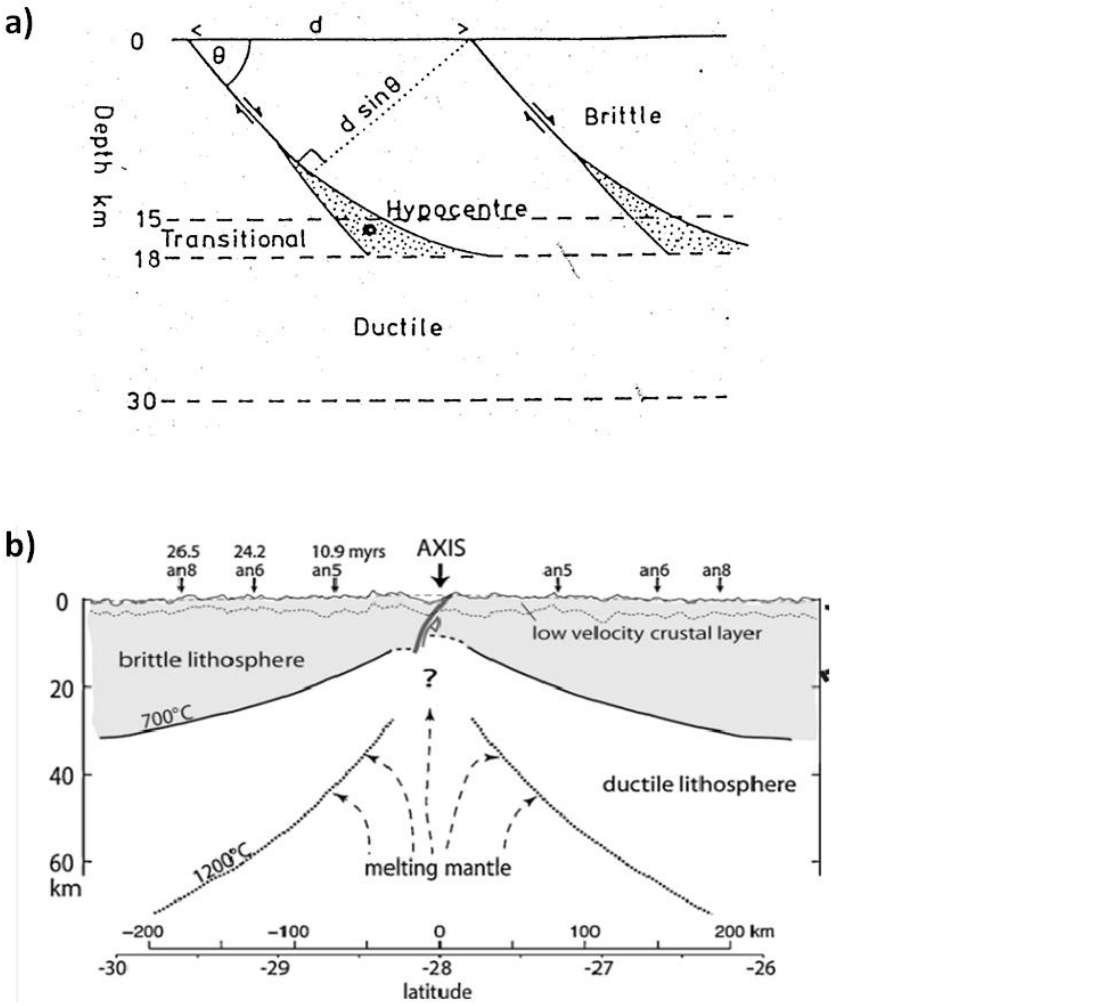

Figure 2.2: By analogy to the deformation processes occurring **a)** during intracontinental rifting (Jackson, 1987) and **b)** at slow spreading ocean ridges (Cannat et al 2009), a more realistic lithosphere deformation mode for magma-poor continental breakup is **c)** pure-shear for the colder brittle upper 12-15 km above UDF for the remaining lithosphere and asthenosphere.

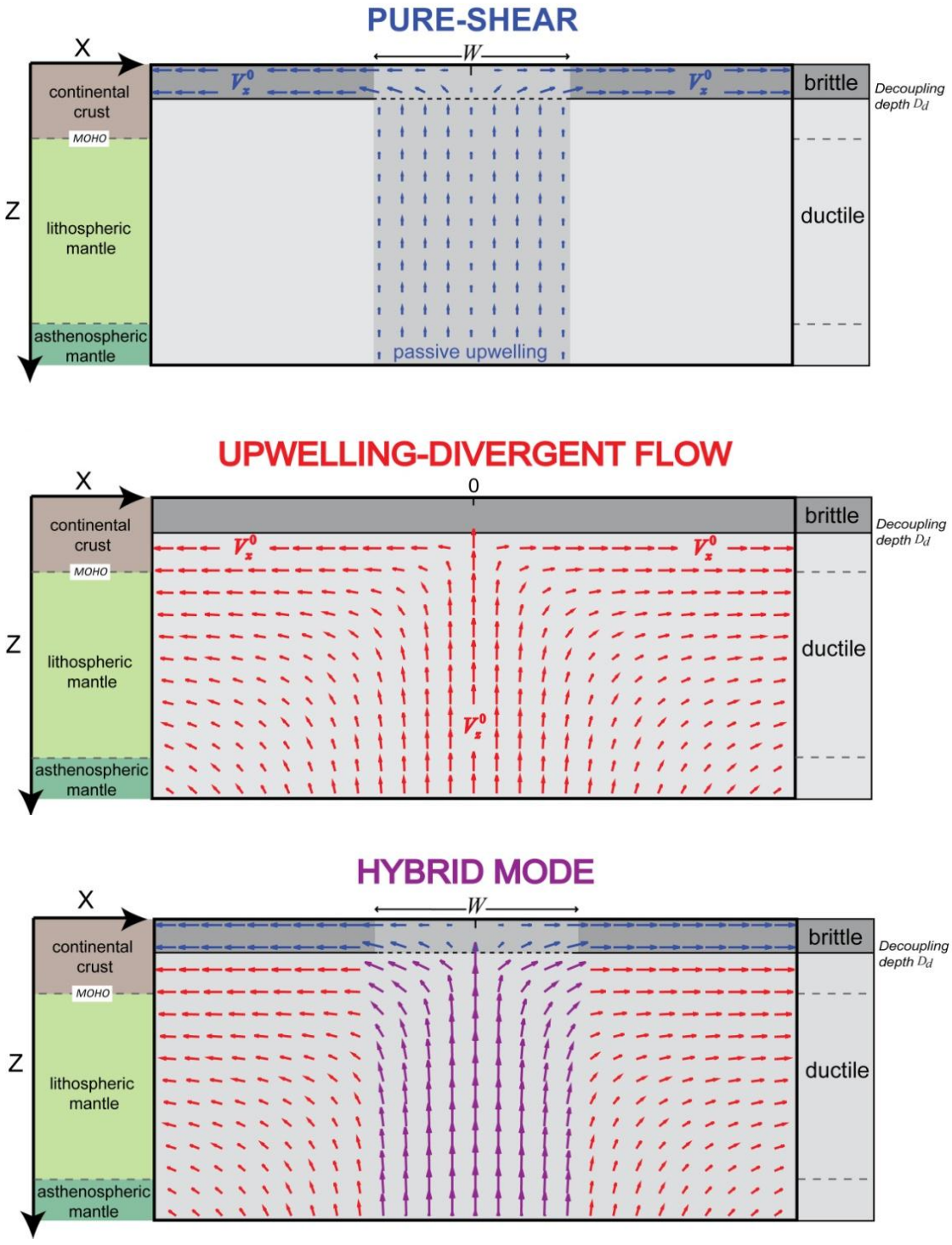

Figure 2.3: 2-D flow vector of the hybrid deformation mode with **a)** pure-shear deformation mode applied for the colder brittle upper 12-15 km lithosphere enhancing a passive upwelling beneath the pure-shear region and **b)** upwelling-divergent flow deformation mode. **c)** The hybrid deformation mode flow vector field corresponds to the combination of both pure-shear and UDF.

In order to satisfy volume conservation, beneath this topmost lithosphere layer and within the pure-shear region W, passive upwelling is assumed to occur at a constant rate:

$$V_z^0 = V_x^0 \frac{D_d}{W_{1/2}} \quad (1)$$

where D_d is the decoupling depth separating pure-shear and upwelling divergent flow deformation modes and $W_{1/2}$ is the half pure-shear width.

Upwelling-divergent 'corner flow' deformation mode

Upwelling-divergent flow is assumed to be the main deformation mode occurring for the remaining (deeper) lithosphere and asthenosphere (Figure 2.3b). The difference with pure-shear is the active definition of the mode, driven by a constant extension and axial upwelling rates. The UDF is characterized by a corner flow solution as described by Batchelor (2000). The flow-field is defined with a constant half-spreading rate V_x^0 at the decoupling depth boundary and a constant axial upwelling rate V_z^0. For passive upwelling in response to plate divergence the ratio V_z^0/V_x^0 = 2/π (Morgan, 1987). Braun et al. (2000) show that thermal and melt buoyancy increases vertical flows at slow spreading ocean ridges. In this context, the deformation is focused to a narrow axial region (i.e. mid-ocean ridge). This active mode is consistent with continental breakup defined as the active heat balance by Cannat et al. (2009).

Both pure-shear and UDF deformation fields are summed giving the velocity field shown in Figure 2.3c.

2.2.2 Material advection

A Lagrangian (x, z) space coordinate frame system is used to track advected lithosphere and asthenosphere material. The numerical material advection model uses a grid-node resolution of 5km horizontally and 2.5km vertically, and a time-step of 50000yrs. The tracker particles nodes move in space with time following vectors generated by the hybrid

flow-field. Regridding is required when the horizontal distance between two tracker particles nodes is greater than 10km; a new node is created between them. Regridding also takes into account the modified volume representing by tracker particles. Tracker particles allow us to characterize and follow the evolution of boundaries such as the Moho and the base of the continental lithosphere which are initially assumed to be horizontal. Tracker particles are assigned density parameters which allow the differentiation of the continental crust ($\rho_c = 2850$kg.m^{-3}) from lithospheric and asthenospheric mantle ($\rho_m = 3330$kg.m^{-3}). Thermal conductivities for the continental crust is $k_c = 2.6$W.m^{-1}.K^{-1} and $k_m = 3.14$W.m^{-1}.K^{-1} for the mantle (Chapman, 1986; McKenzie et al., 2005; Parsons and Sclater, 1977).

2.2.3 Temperature advection

The temperature field modelling uses an Eulerian (x, z) coordinate reference frame system. The finite difference thermal model also runs at grid-node resolution of 5km horizontally and 2.5km vertically, and a time-step of 50000yrs. Temperature behaviour during advection is described by the solution of the diffusion-advection equation:

$$\frac{\partial T}{\partial t} = \frac{1}{\rho C_p}\nabla(\mathrm{k}\nabla\mathrm{T}) - \boldsymbol{V}(\nabla T + h) + \frac{A_0}{\rho C_p} e^{-\frac{z}{a_r}} \qquad (2)$$

where T is temperature, C_p is the specific heat, k and ρ are respectively the thermal conductivity and density either for continental crust and mantle, and h is the adiabatic gradient as described by McKenzie and Bickle (1988).

Pure-shear and upwelling-divergent deformation modes are represented by a velocity field $\boldsymbol{V}$, used to advect temperature. The exponential radiogenic heat source productivity used is described by Turcotte and Schubert (2002); A_0 is the surface radiogenic heat productivity and a_r is its depth decay length.

2.2.4 Initial lithosphere thermal structure and topography

The initial continental lithosphere geotherm is assumed to be in thermal equilibrium. The initial lithosphere thickness is 135km and the temperature of the lithosphere-asthenosphere boundary set at 1333°C. A value of the radiogenic heat production $A_0 = 2.2e^{-6}$ W.m^{-2} for the upper continental crust is used to produce an initial continental geothermal gradient of approximately 30°C.km^{-1} if the initial continental crust is 35km thick. The depth decay length a_r is assumed to be the half of the continental crust thickness which predicts a radiogenic heat flow of 38.5mW.m^{-2}.

The initial oceanic lithosphere thermal structure, 125km thick, is defined using a linear geothermal gradient as shown in Figure 2.4a (McKenzie, 1978; Sclater et al., 1980). The radiogenic heat production of basalts and gabbros of the oceanic crust may be ignored. The isostatic model reference is the equilibrium McKenzie (1978) oceanic lithosphere so that the temperature difference between the initial continental geotherm and the linear oceanic geotherm predicts an initial elevation.

2.2.5 Decompressional melting parameterization

Temperature advection results in decompressional melting of ascending asthenospheric mantle. When the continental lithosphere geotherm crosses the solidus of dry peridotite, melt is generated (Figure 2.4b). We use the methodology and the parameterization of Katz et al. (2003) to predict decompression melting. The temperature field is interpolated within the material grid in order to track melt fraction at each time step. The rate of melt production at each time step depends on the incremental increase in melt fraction. The volume of melt extracted is evenly distributed at the surface within the pure-shear region W, from which melt thickness is then calculated. The new oceanic crust so generated deforms by pure-shear, within the material deformation field; it is stretched and thinned within the pure shear region but spreads normally outside. The reference magmatic addition density is $\rho_v = 2850$ kg.m^{-3}.

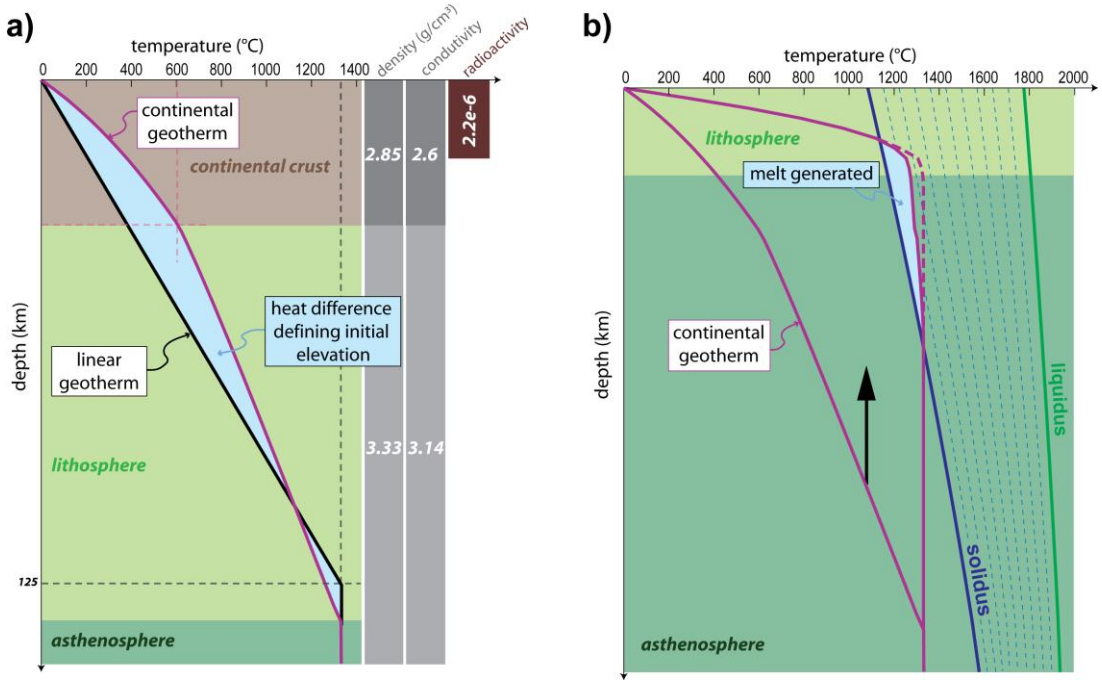

Figure 2.4: **a)** Initial conditions, oceanic linear geotherm and continental geotherm. **b)** Melt generation is predicted by decompressional melting using the parameterization and methodology of Katz et al., 2003. The dash line shows the predicted geotherm without correction of latent heat of fusion.

The efficiency with which melt is extracted after its generation and brought to the surface is an open question. In order to explain magma-poor rifted margins with exhumed mantle within the OCT, Müntener et al. (2010) suggested that the melt may be stored in the mantle rather than being efficiently extracted to form an oceanic crust. Because of the occurrence of melt infiltration and embryonic oceanic crust within the zone of exhumed mantle, the efficiency of melt extraction may evolve in time. Two approaches to addressing melt retention may be examined. One is that the melt is only extracted after it reaches a threshold amount of melt fraction. On the other hand, the efficiency of melt extraction may be used to describes the process by which a percentage of melt always stays in the mantle (Cannat et al., 2004; Lizarralde et al., 2004).

2.2.6 Crustal breakup

Mantle exhumation occurs when detachment faults cut into the lithospheric mantle and pull it out to the seafloor. In this paper, we define crustal breakup as the point in time when the continental crust is no longer continuous and we start to expose mantle on the seabed. Separation of the continental crust follows crustal breakup. However, because our model represents upper lithosphere deformation by pure-shear and does not include faults, we define crustal breakup using either a critical continental crustal thickness or a critical crustal thinning factor. In previous published papers (Minshull et al., 2001; Pérez-Gussinyé et al., 2006), the critical thinning factor used varied from $\gamma_{crit} = 0.67$ to 0.98 ($\beta = 3$ and 50). In this paper, we consider that rupture and separation of the continental crust occurs at a critical continental crust thickness, Ct_{crit} =3.5km, corresponding to a crustal thinning factor, $\gamma_{crit} = 0.9$ ($\beta = 10$), if the initial continental crust is 35km thick. Consequently, we assume that mantle exhumation has occurred if the continental crust is thinner than 3.5km.

2.3 Reference model of rifting, continental breakup and seafloor spreading initiation

We explore thermal and material advection during continental rifting leading to breakup and the resulting subsidence and melt generation using the hybrid lithosphere deformation model. For sensitivity tests of model parameters in the section 3.2.4, we define a reference model. The reference model has a pure-shear width set at 100km, half-spreading rate of $V_x^0 = 15$ mm.yr^{-1} and a corner flow V_z^0/V_x^0 of 1. The decoupling depth between pure-shear and upwelling-divergent flow is fixed at 15km. Asthenosphere temperature is set at 1333°C, initial continental crust thickness at 35km and the lithosphere thickness at 135km. The initial topography is 390m. The model is run for 20 Myr. Model parameters and values are summarized in Table 2.1.

Table 2.1: Table of constants and physical parameters

Variable	Meaning	value	units
Ak	Lithosphere thickness for a linear oceanic geotherm	125	km
At	Initial lithosphere thickness	135*	km
A_0	Heat production	$2.2e^{-6}$	$W.m^{-2}$
a_r	Radiogenic layer thickness	$Ct/2$	km
C_p	specific heat	1180	$J.kg^{-1}.K^{-1}$
Ct	Initial crustal thickness	35*	km
Ct_{crit}	Critical crustal thickness	3.5*	km
D_d	Decoupling depth	15*	km
g	Gravitational acceleration	9.81	$m^2.s^{-1}$
h	Adiabatic gradient	-	$°C.km^{-1}$
k_c	Reference crustal thermal conductivity	2.6	$W.m^{-1}.K^{-1}$
k_m	Reference mantle thermal conductivity	3.14	$W.m^{-1}.K^{-1}$
k	Thermal conductivity at (X,Z)	-	$W.m^{-1}.K^{-1}$
LF	Latent fusion	400	$kJ.kg^{-1}$
M_{cpx}	Weight fraction of clinopyroxene being melted	0.16	%
$T°$	Base lithosphere temperature	1333*	°C
T	Temperature at (X,Z)	-	°C
t	time	-	Myr
V_x^0	half-spreading rate - characteristic horizontal velocity for pure-shear and upwelling-divergent flow	15*	$mm.yr^{-1}$
V_z^0	upwelling rate - characteristic vertical velocity for upwelling-divergent flow	15*	$mm.yr^{-1}$
$\boldsymbol{V}$	Local velocity vector at (X,Z)	-	$mm.yr^{-1}$
W	Pure-shear width	100*	km
X	Horizontal coordinate	-	km
Z	Vertical coordinate	-	km
α	Thermal expansion coefficient	$3.28e^{-5}$	$°C^{-1}$
β	Stretching factor	-	-
β_{crit}	Critical stretching factor	10*	-
γ	Thinning factor	-	-
γ_{crit}	Critical thinning factor	0.9*	-
ρ_c	Reference crustal density	2850	$kg.m^{-3}$
ρ_m	Reference mantle density	3330	$kg.m^{-3}$
ρ_v	Reference volcanic addition density	2850	$kg.m^{-3}$
ρ_w	Density of water	1040	$kg.m^{-3}$
ρ	Density at (X,Z)	-	$kg.m^{-3}$

* Stated for the reference model

2. How does the lithosphere deformation mode during continental breakup affect mantle exhumation?

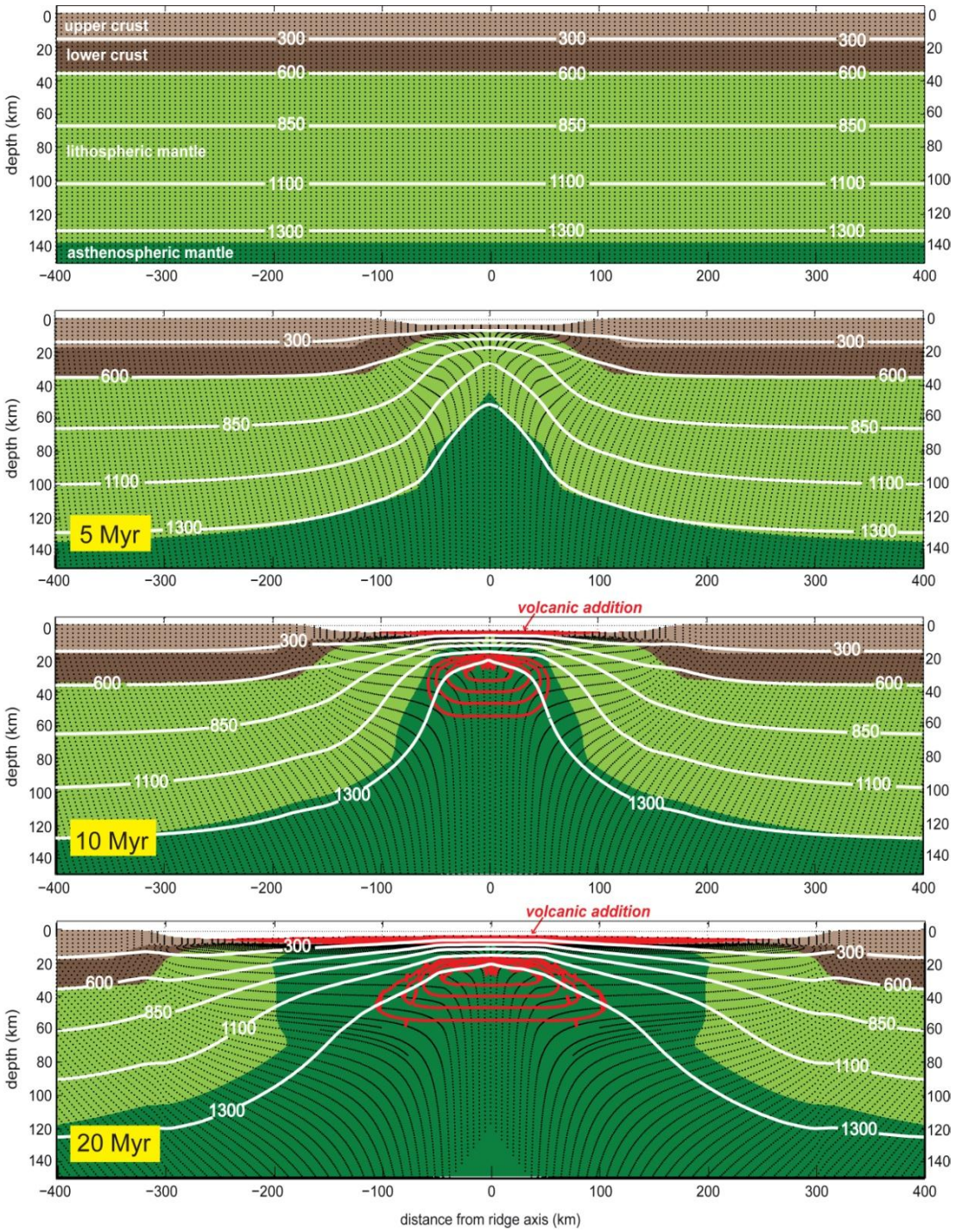

Figure 2.5: Temperature and material advection evolution from t=0 to t=20 Myr. Isotherms (°C) are shown as white lines and melt fractions as red lines. Each red line increases the melt fraction of 0.03%. Black nodes represent tracker particles.

2.3.1 Model behaviour

The behaviour of the reference model to material and temperature advection is shown in Figure 2.5 at 5, 10 and 20Myr. At 5Myr, after 75km of extension, the continental crust and lithosphere has stretched and thinned respectively by a beta factor of approximately 7 and 2.25. Decompression melting is initiated at 60km depth at 5.5Myr and crustal breakup occurs at 6Myr. The maximum melt fraction at 10Myr is 0.15 and has created a volcanic addition 3.8km thick.

2.3.2 Relative timing of melt initiation and crustal breakup

We examine the relative timing of crustal breakup and melt initiation in order to explore under which conditions mantle may exhume. Figure 2.6 shows the reference model evolution of the volcanic addition and the thinning factor of the continental crust and lithosphere as a function of time. Crustal breakup is predicted at 6Myr, and decompressional melt is initiated at 5.5Myr. Therefore, the reference model does not predict mantle exhumation. This prediction is valid only if the melt generated is instantaneously and efficiently extracted. The evolution of the volcanic addition shows that a steady state is not reached at 20Myr; it has a thickness of 5.2km and is still increasing with time.

We examine the reference model sensitivity to melt retention distinguishing two processes: a threshold melt fraction and a fractional efficiency of melt extraction.

(1) ***Threshold melt fraction:*** It is possible that melt is retained within the mantle until it reaches a threshold melt fraction, after which it is extracted to the surface to form an oceanic crust. If the threshold melt fraction is 0%, melt extraction is instantaneous. An example of 8% retention delays melt extraction of about 2Myr, giving a window of 0.7Myr to exhume mantle (Figure 7a).

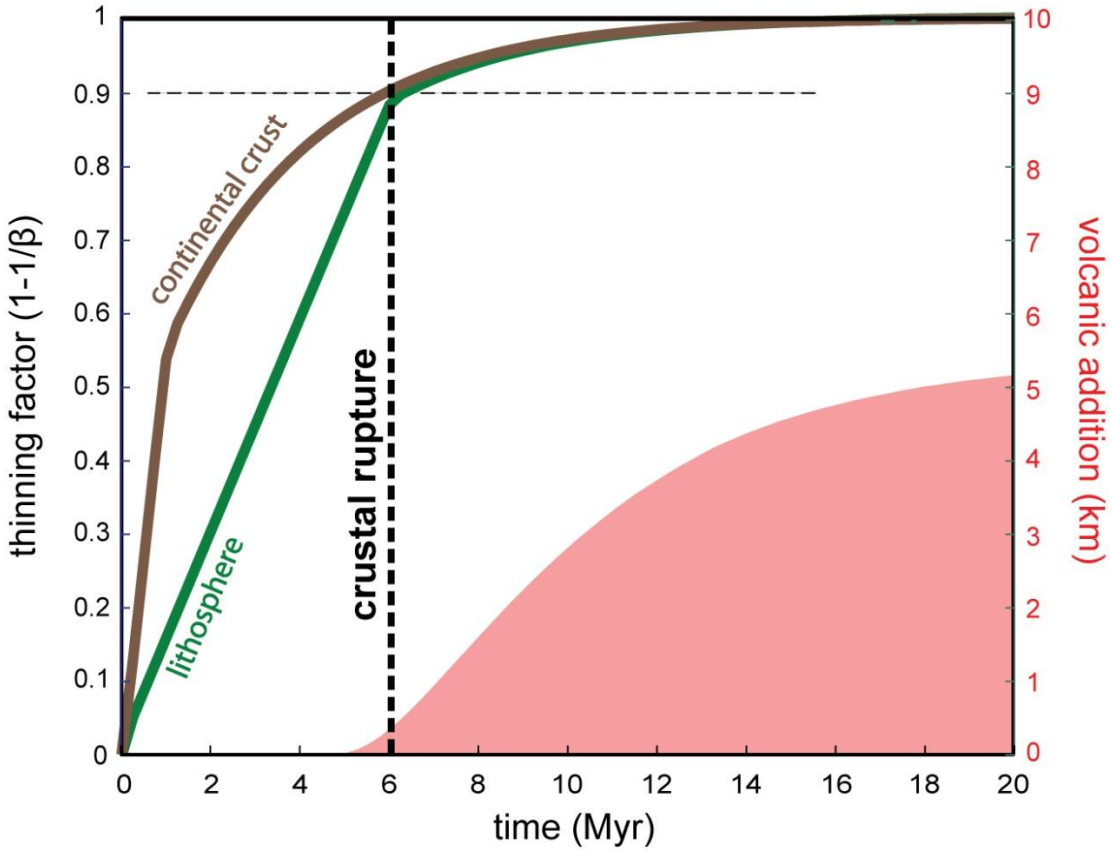

Figure 2.6: Relative timing of crustal breakup and melt generation. The evolution of extracted melt thickness (y-right axis) and continental lithosphere and crustal thinning (y-left axis) is shown as a function of time.

(2***) Efficiency:*** It is possible that only a certain fraction of melt is extracted to the surface (Figure 2.7b). This process decreases the volume of extracted melt, i.e. volcanic addition, but it does not delay the timing of melt extraction.

The sensitivity to these two processes of melt retention together is shown with the grey area in Figure 2.7.

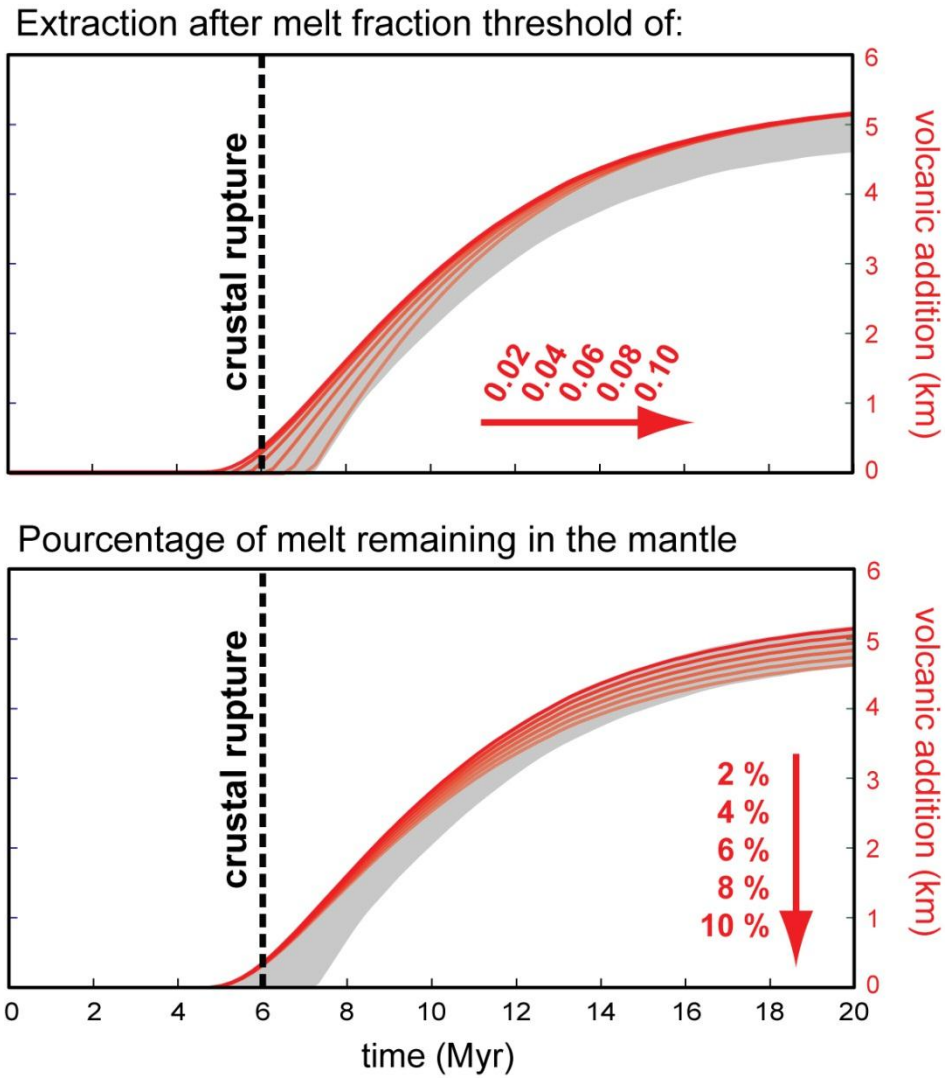

Figure 2.7: Numerical experiments testing the sensitivity to ***a)*** the instantaneousness and **b)** the efficiency of melt extraction. Grey area combines both retention predictions.

2.3.3 Subsidence history

The lithosphere density distribution due to crustal thinning, change in geothermal gradient and volcanic addition may be used to calculate subsidence or uplift, assuming local isostasy. Subsidence below sea-level is assumed to be water-loaded. Initial elevation and topography above sea-level is assumed to be air-loaded. Thermal loads are calculated from the lateral temperature variation between the evolving thermal structure and the initial linear oceanic

thermal structure described in the previous section. Subsidence history along the rift axis at 5, 10 and 20Myr is shown in Figure 2.8 for the reference model. Volcanic addition is included as an increase in crustal thickness. At 20Myr, model predictions show a bathymetry of about 2700m at the ocean ridge, and approximately 4500m in the abyssal plain. These results are consistent with the depth of the oceans on Earth relative to their age (Sclater et al., 1980).

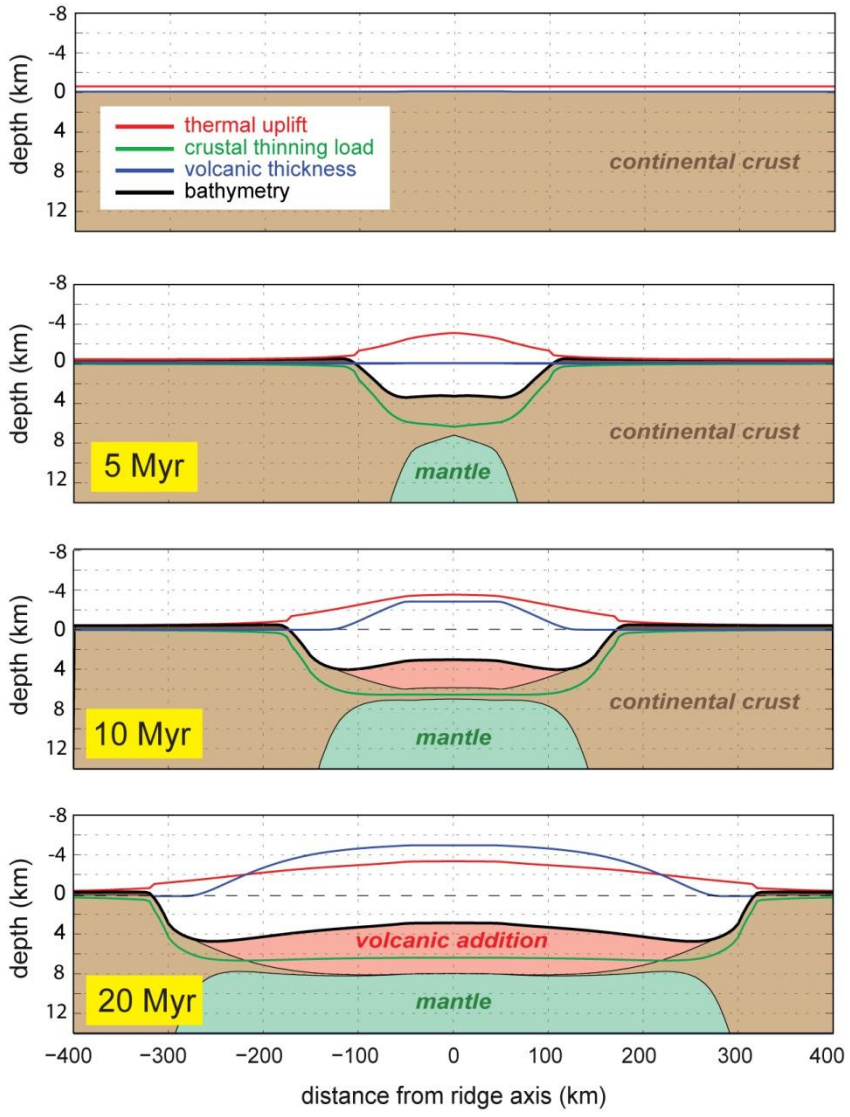

Figure 2.8: Subsidence history snapshots at 5, 10 and 20 Myr, showing the evolution of thermal uplift, crustal thinning load, volcanic thickness and predicted bathymetry.

2.3.4 Rifted margin crustal architecture

The conjugate rifted margins of the reference model are symmetric as shown in Figure 2.8. The rifted margin width, where the continental crust thins from 35km to zero thickness, is approximately 50km wide. In the necking zone, the continental crustal thickness drops from 35 to 10km thick within a region 25km wide. This necking zone is followed by a domain 25km wide of thinned continental crust less than 10km thick. The reference model predicts no mantle exhumation as mentioned earlier.

2.4 Model sensitivity to lithosphere deformation

In this section, we use a series of numerical experiments to explore the relative timing of melt generation and crustal breakup for the hybrid lithosphere deformation mode with balanced pure-shear and UDF (D_d). We test the hybrid model sensitivity to the pure-shear width W, half spreading deformation rate V_x^0 and the corner flow V_z^0/V_x^0 ratio. We change one parameter at a time, with respect of the reference model.

2.4.1 Decoupling depth D_d

The decoupling depth between pure-shear and UDF controls the relative contribution of these two deformation modes in the hybrid model. The thickness of the pure-shear layer has an important influence on the vertical flow velocity; the deeper the decoupling depth, the faster is the passive upwelling rate. The relative timing of melt initiation and crustal breakup for decoupling depths of 7.5, 15 and 22.5km is examined in Figure 2.9a. Two effects are observed; (1) a shallow decoupling depth delays the timing of decompressional melting and (2) the timing of crustal breakup is quickened. With a shallow decoupling depth of 7.5km, a window of about 2Myr between crustal breakup and the onset of melting permits mantle exhumation while for a deeper pure-shear deformation layer of 22.5km, crustal breakup about 2.5Myr after melt initiation. These predictions are consistent with the results obtained by Fletcher et al. (2009) for pure-shear or UDF end-members.

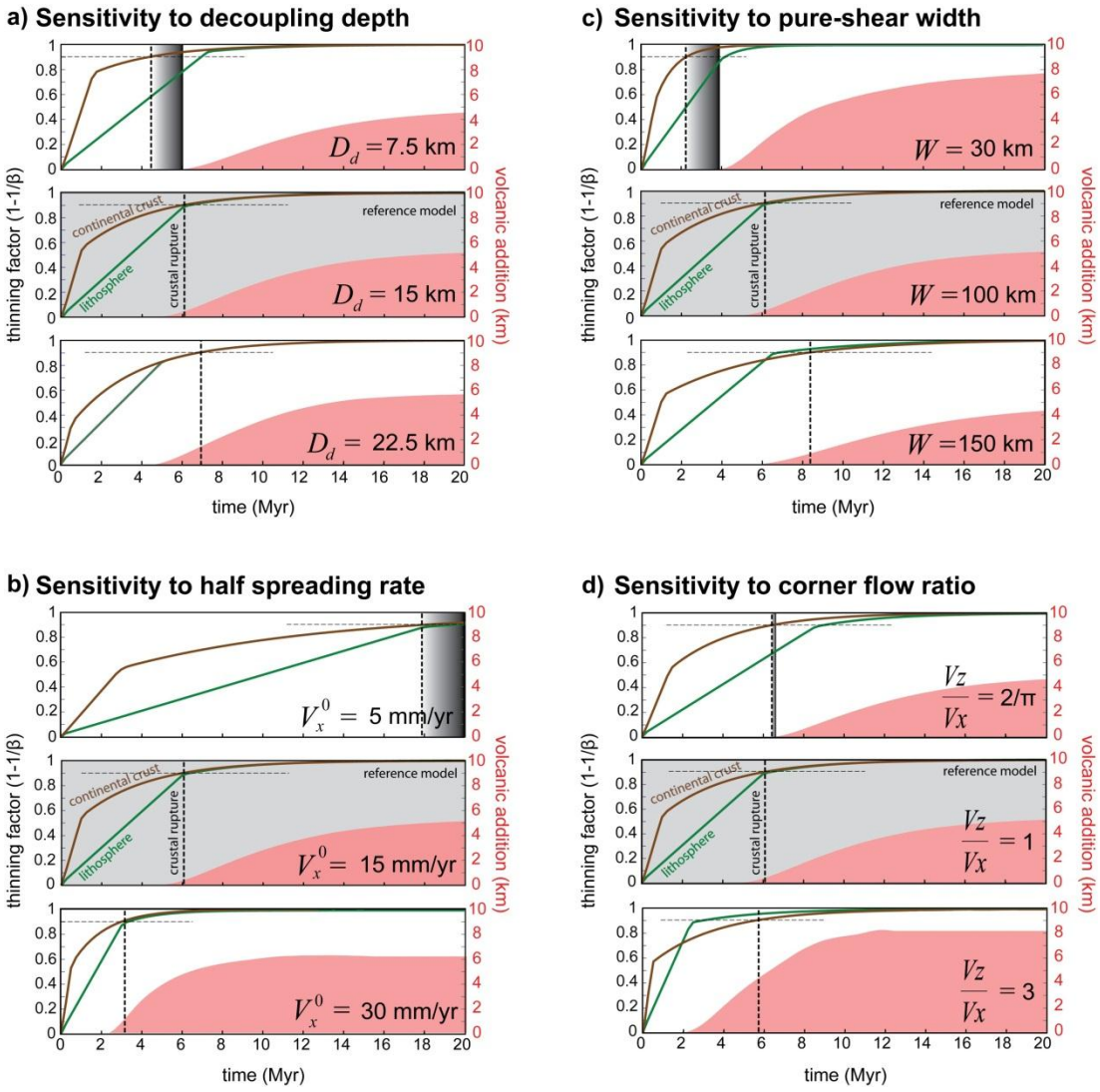

Figure 2.9: Sensitivity tests to the deformation parameterization. The evolution of volcanic addition (y-right axis) and continental lithosphere and crustal thinning (y-left axis) is shown as a function of time. Black dash line show when mantle should have exhumed after melt generation, and the grey area represents the timing of mantle exhumation.

2.4.2 Pure-shear width W

The pure-shear deformation mode only deforms the continental crust. The passive upwelling generated within the pure-shear region is inversely proportional to the width of that region (**Eq. 1**). Consequently, changes of pure-shear width have similar implication for the timing of crustal breakup and for decompressional melt initiation; both occur sooner

with a narrow pure-shear region, and later with a wider region. However, Figure 2.9b shows that continental crustal thinning progresses more rapidly than lithosphere thinning; a narrow pure-shear deformation region W =30km advances crustal breakup by 4Myr with respect to the reference model, while it quickens melt initiation by only 2Myr. This predicts a 2Myr window of mantle exhumation. A narrower pure-shear region generates a larger amount of decompressional melt which is distributed only within this narrow region. Thus, it creates a thick volcanic addition.

2.4.3 Half spreading rate V_x^0

Figure 2.9c shows model predictions of melt thicknesses and continental crustal thinning factor during rifting evolution using a constant half-spreading rate of V_x^0 =5, 15 and 30mm.yr^{-1}. A slow extension rate delays both the timing of decompressional melting and crustal breakup; a half spreading rate of $V_x^0 = 5$mm.yr^{-1} allows continental crustal rupture after 18Ma of rifting while no melt is generated. A faster half-spreading rate of $V_x^0 =$ 30mm.yr^{-1} initiates decompressional melting about 1Myr before crustal breakup. While the reference model does not get to an equilibrium volcanic addition before 20Myr, a higher deformation rate reaches that steady state at 12Myr giving a volcanic addition 6.2km thick.

2.4.4 Corner flow V_z^0/V_x^0 ratio

The velocity V_z^0/V_x^0 ratio affects the upwelling-divergent flow part-field of the hybrid deformation model. A velocity ratio of $2/\pi$ corresponds to passive upwelling only (Morgan, 1987) and no buoyancy contribution. Buoyancy increases that ratio and upwelling rate (Braun et al., 2000). Increasing the ratio V_z^0/V_x^0 is expected to have a significant impact on the timing of decompressional melting initiation and lesser implication on crustal breakup. This is shown in Figure 2.9d. The effect of buoyancy to the timing of crustal breakup is negligible as expected; faster upwelling rate slightly brings forward the time of crustal breakup of few 100,000yrs. The main impact of increased buoyancy is for melt generation. At a constant half-spreading rate $V_x^0 = 15$mm.yr^{-1}, a ratio $V_z^0/V_x^0 = 3$ initiates melting at

2Myr and produces a larger amount of melt with a steady state oceanic crust thickness of 7.9km reached after 12Myr. Mantle exhumation is not predicted using active buoyancy driven upwelling. Conversely, passive upwelling generates melt at 6Myr and permits a short duration (~200,000yrs) for mantle to be exhumed.

2.5 Model sensitivity to initial conditions

The relative timing of melt initiation and crustal breakup using a hybrid deformation model may be dependent on initial conditions such as the asthenosphere temperature and the initial thickness of continental crust and lithosphere. This dependency is examined in this section. These parameters do not change the kinematics of the hybrid deformation model. Consequently, the effects of initial conditions are not expected to significantly change the timing of crustal breakup. However, melt generation is dependent on the initial continental thermal structure and the asthenosphere temperature. We change one parameter at a time and compare the sensitivity test results against the reference model.

2.5.1 Asthenosphere temperature

We use an average asthenosphere temperature of 1333°C in the reference model (Parsons and Sclater, 1977; Sclater et al., 1980). Nevertheless, petrology and thermal models do not always agree on a universal and constant value of the lithosphere basal temperature, (e.g. Stein and Stein (1992) estimates the asthenosphere temperature around 1450°C). We examine the effects that a change of the asthenosphere temperature would have on the timing of melt initiation in Figure 2.10a. A reduced asthenosphere temperature $At = 1233$°C slightly delays of 2Myr the timing of decompressional melting initiation and greatly decreases the amount of melt produced; the steady-state volcanic addition is 1km. Conversely, a high asthenosphere temperature of $At = 1433$°C causes melt initiation 3Ma prior to crustal breakup. Mantle exhumation is therefore favoured by a low asthenosphere temperature.

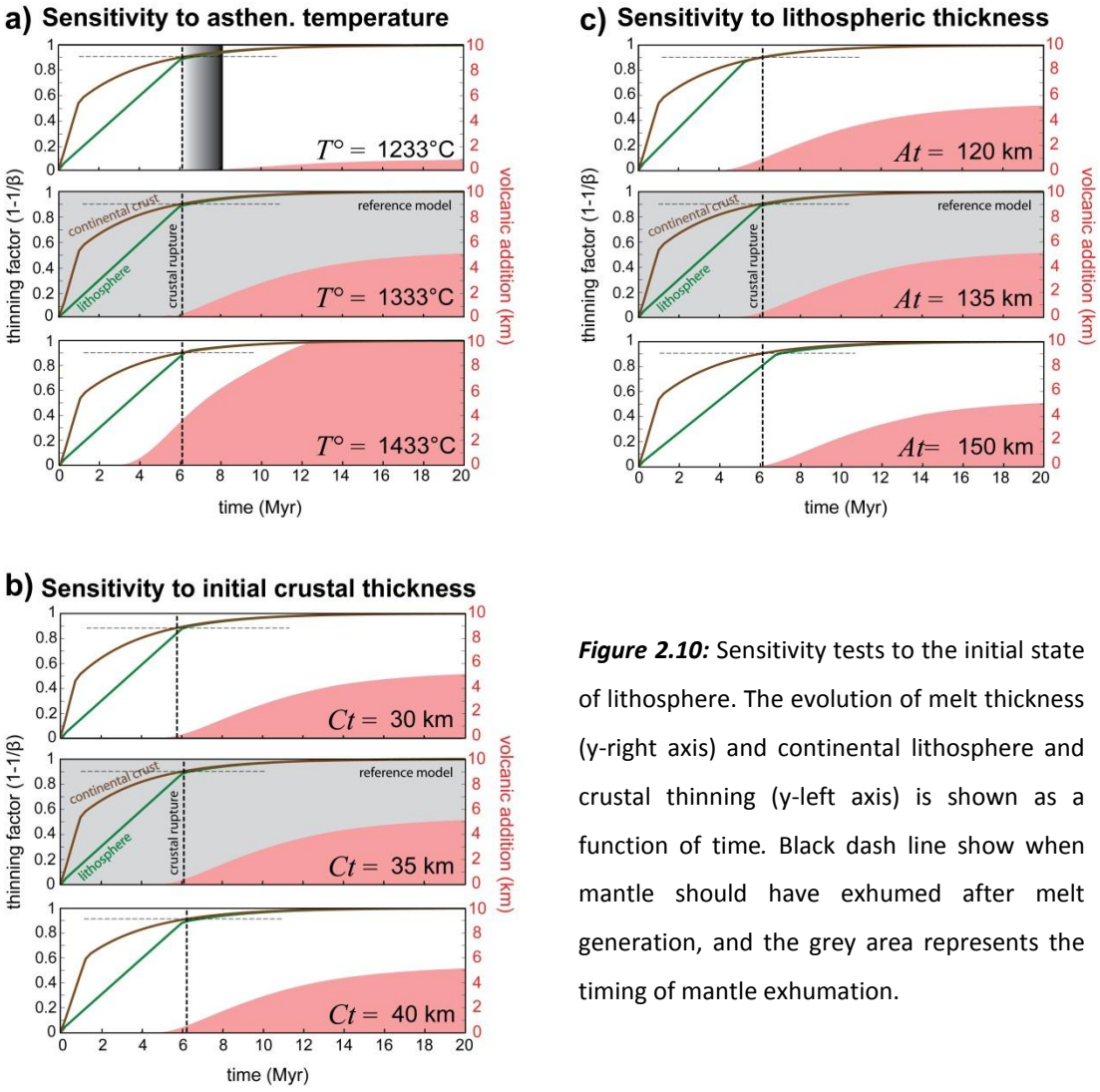

Figure 2.10: Sensitivity tests to the initial state of lithosphere. The evolution of melt thickness (y-right axis) and continental lithosphere and crustal thinning (y-left axis) is shown as a function of time. Black dash line show when mantle should have exhumed after melt generation, and the grey area represents the timing of mantle exhumation.

2.5.2 Initial lithosphere thickness

The continental lithosphere-asthenosphere boundary depth cannot be considered as globally constant and recent studies shows disparities and controversial results (Hamza and Vieira, 2012). We use in the reference model an average continental lithosphere thickness of 135km. We explore in Figure 2.10b the relative timing of melt initiation and crustal breakup sensitivity to an initial continental lithosphere thickness of 120 and 150km. A thin initial continental lithosphere thickness of 120km permits decompressional melt approximately 1Myr before continental crustal rupture, while a thicker initial continental

lithosphere 150km thick initiates melt at about the same time as crustal breakup. Consequently, the thickness of the initial lithosphere does not primarily affect the timing of melt generation.

2.5.3 Initial crustal thickness

Christensen and Mooney (1995) summarized continental crust thicknesses over the world and suggested an average crustal thickness of about 40km, with a range from 16 to 72km. However, this range spans orogenic crust and continental crust at rifted margins. We examine in Figure 2.10c initial continental crust of thicknesses ranging from 30 to 40km thick. An initially thick continental crust slightly delays crustal breakup and also creates a higher geotherm which gives slightly earlier melting. The difference of timing of the crustal breakup or melt initiation either using an initial continental crust thickness 30km or 40km is less than 100,000yrs. Therefore the initial continental crust thickness does not significantly change the relative timing of crustal breakup and melt initiation.

2.6 Discussion

The upwelling-divergent flow and pure-shear deformation modes are two end-members that individually describe ocean ridge processes and intracontinental rifting respectively. We suggest that the process of lithosphere continental breakup can be best described by using a combination of both deformation modes. The model of Cannat (1996) proposed for slow-spreading ocean ridges suggests that deformation occurs by extensional faulting and magmatic intrusions in the topmost 10-15km brittle seismogenic layer. We approximate this deformation pattern by using pure-shear above a ductile lithosphere-asthenosphere which would be deformed by UDF. We propose that similar deformation modes may be applicable to intracontinental rifting processes leading to breakup and the formation of magma-poor rifted margin. The main focus of this study was to explore this hybrid deformation model to specifically examine under which conditions mantle exhumation is

possible. We explored the sensitivity of the hybrid model behaviour to lithosphere deformation parameterization and initial conditions.

2.6.1 Summary

Numerical experiments suggest that the hybrid continental lithosphere deformation mode can initiate mantle exhumation before the onset of decompression melting only under certain conditions. Mantle exhumation is predicted either if the decoupling depth is shallow, the pure-shear deformation region is narrow, the half-spreading rate is slow, the velocity ratio V_z^0/V_x^0 corresponds to passive upwelling or the asthenosphere temperature is low. Conversely, mantle exhumation is not predicted if high values of these parameters are used.

Sensitivity to decoupling depth

The decoupling depth has been defined as the horizon separating the extending brittle layer represented by pure-shear above deeper UDF. Model sensitivity tests show that only models using shallow decoupling depths can predict mantle exhumation. Although this parameter has a significant impact on the relative timing of melt initiation and crustal breakup, the thickness of the pure-shear layer may be constrained by observations. At the beginning of continental rifting, proximal domains of rifted margins show extensional faults flattened into the more ductile middle crust also at 10-12km depth (Manatschal, 2004). Then the thinning of the continental crust leads later to create exhumation and detachments faults that cut into the mantle and pull it out at the seafloor; these exhumation faults are also initiated between 10 to 12km (Manatschal et al., 2001). Finally at slow spreading ocean ridges, detachment faulting occurs for the topmost 10km of the brittle lithosphere (deMartin et al., 2007). Therefore, the decoupling depth may remain globally the same during all the process of continental rifting leading to breakup. Our model prediction for a decoupling depth of 10-12km gives a similar timing for both melt initiation and crustal breakup, although slightly in favour of mantle exhumation. Consequently, we

suggest that mantle exhumation would be likely dependent on the other parameters rather than the decoupling depth.

Sensitivity to pure-shear width

Modelling shows that a wide pure-shear width is unlikely to exhume mantle prior to significant melt generation. Conversely, a narrow pure-shear region is suggested to accelerate the thinning of the continental crust faster than the lithosphere so that it separates before the onset of decompression melting. Observation at magma-poor rifted margins such as Iberia-Newfoundland (Figure 2.10), which has experienced mantle exhumation, shows that the deformation during the early stage of rifting was distributed over a wide region and not localized (Péron‐Pinvidic et al., 2007). Extensional faulting occurring at slow spreading ocean ridges occurs however within a narrow area of about 20-25km width (Cannat et al., 1997; Cannat et al., 2009). Therefore pure-shear widths must evolve from broad to narrow during continental rifting leading to breakup. Our numerical experiments cannot explain the occurrence or absence of mantle exhumation only using the deformation width.

Half-spreading and upwelling rate

Numerical experiments suggest that the half-spreading rate has the most significant impact on both timing of melt initiation and crustal breakup. Slow extension rates will enable mantle exhumation if the upwelling rate remains passive. The observed magmatic evolution at magma-poor rifted margins could help to better constrain the models. The oceanic crustal thickness evolution prediction for models using slow spreading rates shows that the accretion of melt takes a long time to reach a steady-state, unless buoyancy is included. The recognition of magma in seismic sections of magma-poor rifted margin show however an excess production of volcanic material prior to continental breakup (i.e. J-anomaly, Bronner et al. (2011)) which suggest that the oceanic crust reaches a thick thickness in a short period of time. Therefore, either the half-spreading rate accelerates from continental rifting

to breakup, or the upwelling rate is active. However, we show that the contribution of buoyancy induced upwelling tends to prevent mantle exhumation. Consequently, half-spreading rate and buoyancy upwelling rate may evolve from slow to fast suggesting again an evolution of the lithosphere deformation.

Asthenosphere temperature

The model predicts that asthenosphere temperature has an important implication on the timing of melt initiation. A hot asthenospheric temperature generates melt sooner than if it was cold. However, the value of asthenosphere temperature remains subject of debate. Reston and Morgan (2004) suggest that the subcontinental lithospheric mantle may have a potential temperature cooler than 1300°C, and that to explain the occurrence of 6-7km volcanic addition, the potential temperature of an oceanic lithosphere is hotter. Thus, an increase of the asthenospheric temperature may occur during continental rifting leading to breakup.

2.6.2 Timing of crustal breakup

Regardless of the lithosphere deformation and initial conditions parameterization, uncertainties remain concerning the validity of defining a critical continental crustal thickness or thinning factor to predict mantle exhumation because faulting is not modelled. The thickness of the most distal continental crust of the two pair Iberia-of Newfoundland conjugate rifted margins (Sutra et al., 2013) suggests that the northern section experienced a greater thinning of the continental crust (~2km) before it broke up whereas the southern section seems to separate earlier at a greater crustal thickness (~4-5km). This observation is not well constrained but is likely to be related to the deformation rate and rheology.

2.6.3 Duration of mantle exhumation

Péron-Pinvidic and Manatschal (2009) suggested that mantle exhumation took place along the Iberia-Newfoundland conjugate rifted margins for a duration between 5 and 15Myr,

and can develop a zone of exhumed serpentinized mantle 30-150km wide (Sibuet et al., 2007; Whitmarsh et al., 2001). Our model predictions are not consistent with these observations. Model predicted durations of mantle exhumation are typically 2Myr duration. One of the causes of the predicted short mantle exhumation durations may be due to the analytical solution of the pure-shear deformation mode which focuses the passive upwelling beneath the pure-shear deformation region. The focussed passive upwelling is combined with the UDF rate which inevitably accelerates melting. Although the passive upwelling rate beneath the pure-shear deformation is limited by the thickness of the brittle layer as seen in **eq.1**, this rate may remain significant even at shallow decoupling depth.

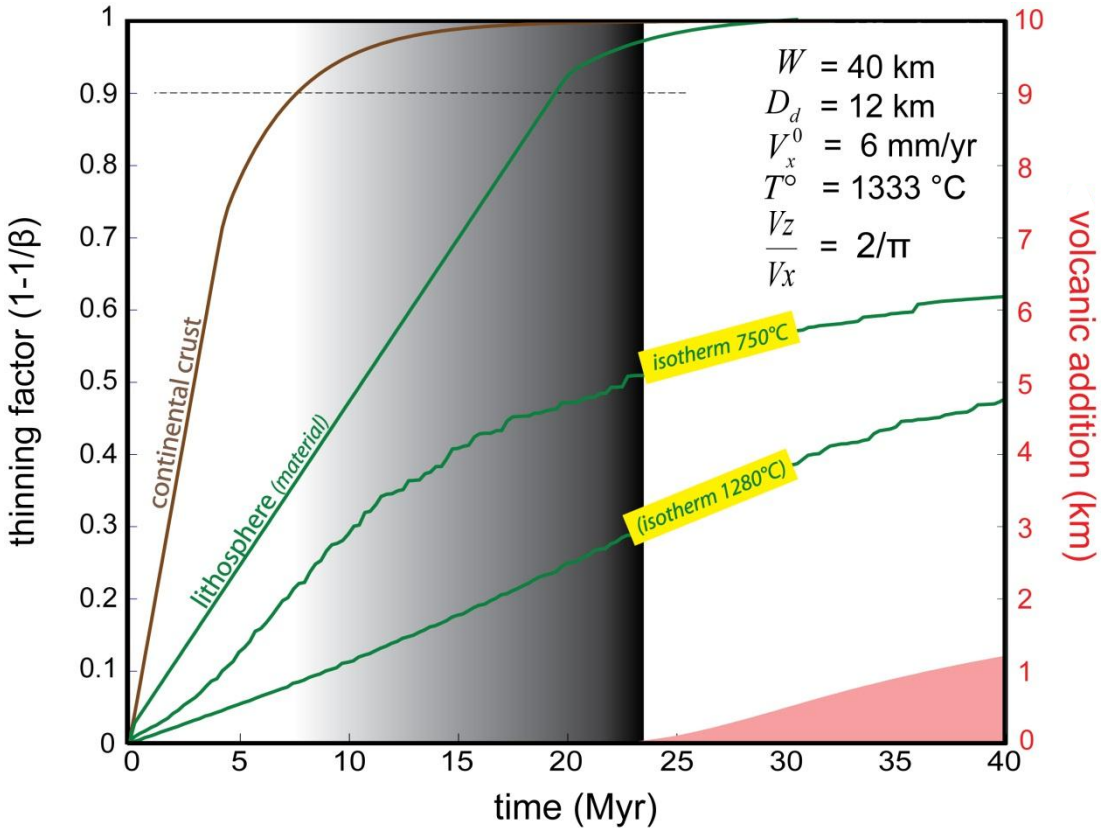

Figure 2.11: 'Optimum' lithosphere deformation model evolution leading to continental breakup enhancing mantle exhumation.

In order to get a longer duration of mantle exhumation, we suggest using a combination of lithosphere deformation parameter values as shown in Figure 2.11. That optimum example model uses a decoupling depth D_d = 12km, a narrow pure-shear width W =50km, a half-spreading rate V_x^0 = 6mm.yr^{-1} and no buoyancy induced upwelling. Initial continental crust and lithosphere thicknesses are respectively 35 and 135km thick. A combination of these parameter values predicts that continental crustal ruptures at 8Myr and melt initiates at 23Myr which gives 15Myr duration for mantle exhumation. Additionally, we show in Figure 1.11 the evolution of the 750°C and 1280°C isotherms.

2.6.5 Continental breakup

Continental breakup is often defined representing the late stages of continental rifting during breakups of the continental crust and lithospheric mantle, and seafloor spreading. In this meaning, continental breakup cannot be defined as a point in time. However, Cannat et al. (2009) suggested that the installation of a ridge-type thermal regime (or active heat balance), was the most practical definition for continental breakup. The same authors proposed an evolution of lithosphere thermal structure from intracontinental rifting to breakup and seafloor spreading initiation for the formation of magma-poor rifted margins (Figure 2.12). At the beginning of rifting, the base of the lithosphere remains deep and close to its original depth, then it shallows rapidly leading to decompressional melting, and finally it stabilizes at shallow depth.

In Figure 2.12, we ask if it is possible to delimit continental breakup using the definition of Cannat et al. (2009). The optimum lithosphere deformation model allowing mantle exhumation to occur over a long period of time is compared to the thermal evolution type of magma-poor rifted margins. Although in both cases mantle exhumation is possible, the prediction thermal evolution from this study cannot be compared to the thermal evolution suggested by Cannat et al. (2009) because our model predictions do not lead to an active heat balance. In our optimum model prediction, the lithosphere-asthenosphere isotherm

boundary (1280°C) still shallows with time but starts its equilibration at about 38Myr. As a consequence, continental breakup cannot be defined with our numerical experiments because another process is missing in this study.

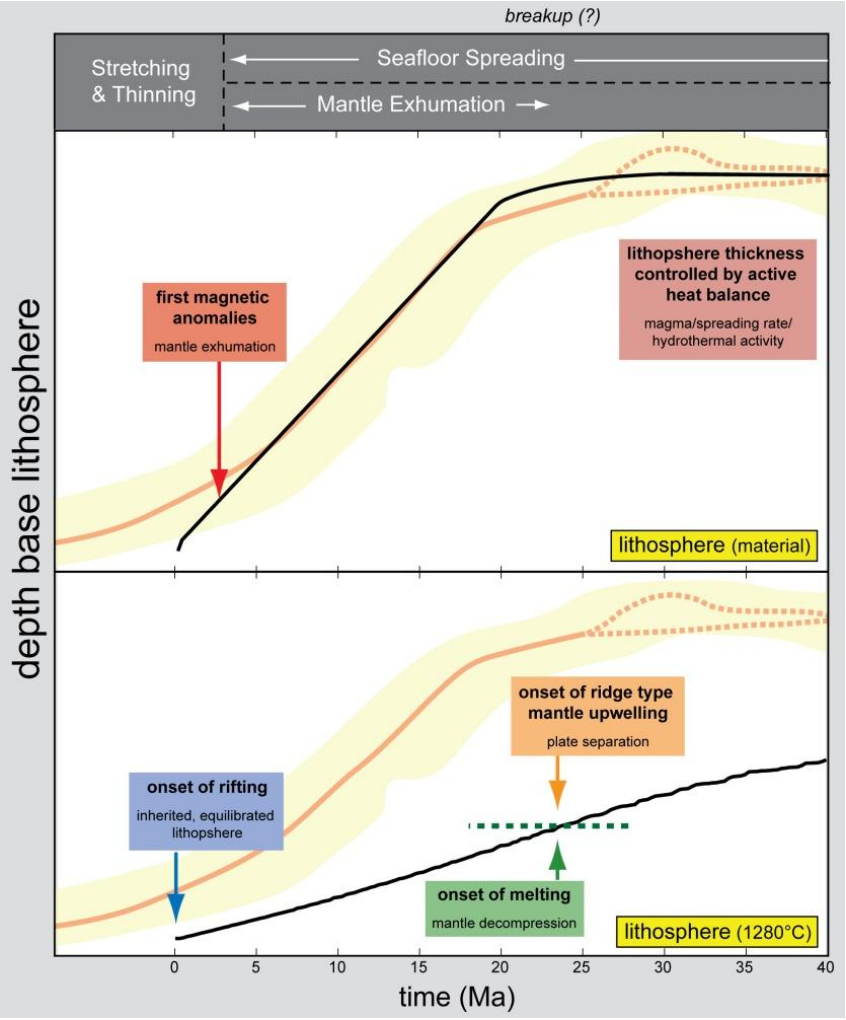

Figure 2.12: Lithosphere thermal structure evolution predicted from our preferred model. Both lithosphere thermal structure evolution predictions are compared with the Cannat et al. (2009) thermal evolution (orange and yellow trends).

2.6.6 Melt retention

The process of melt retention is shown to occur during the formation of magma-poor rifted margins (e.g. Iberia-Newfoundland - Müntener & Manatschal, 2006; Alpine Tethys - Müntener et al., 2010). However, uncertainties remain concerning the amount of melt being extracted during continental rifting processes. Since mantle exhumation can be accompanied by dyking and embryonic oceanic crust (Sutra et al., 2013), it may be too simplistic to define mantle exhumation only as the relative timing of crustal breakup and melt initiation. Much work needs to be carried out to better recognize magma in seismic sections, its emplacement mechanisms and the relative rate of extraction and intrusion. Our numerical experiments show that melt extraction after a threshold melt fraction has a significant impact that can delay melt extraction and therefore enable mantle exhumation. However, observations at magma-poor rifted margins show dyking and embryonic oceanic crust within their OCT suggesting a more complex relationship between the threshold and the efficiency of melt extraction. Cannat et al. (2004) suggested that the melt may be spread more widely within the mantle if the pure-shear deformation width is wide, because the melt is retained if the flow lines are more horizontal (Faul, 2001).

2.6.6 Evolving lithosphere deformation modes

This study identifies an important limitation of kinematic modelling. The use of pure-shear or upwelling-divergent flow end-member deformation modes as described by Fletcher et al. (2009), or a hybrid lithosphere deformation mode consisting of pure-shear above UDF cannot explain alone the complex crustal architecture and thermal evolution observed at magma-poor rifted margin. The decoupling depth controlling the relative contribution of these two deformation modes in the hybrid model may not evolve during rifting and is not the solution to this investigation. Conversely, the other model parameters whose sensitivity we have tested, pure-shear width, half-spreading rate, buoyancy and asthenospheric temperature, are subject to a variation with time. Consequently, the crustal architecture of

continental rifted margin may be better explained using evolving lithosphere deformation modes.

2.7 Conclusion

A hybrid model of lithosphere deformation, consisting of pure-shear for the topmost 10-15km of the lithosphere above an upwelling divergent flow, better describe the continental lithosphere evolution from continental rifting leading to breakup and seafloor spreading initiation during the formation of magma-poor rifted margins. The decoupling depth between pure-shear and UDF is relatively well constrained at 10-15km depth. However, the variations of the half-spreading rate, upwelling rate and pure-shear width can be used to predict mantle exhumation at magma-poor rifted margins.

Mantle exhumation is possible if using a combination of slow half-spreading rate, wide pure-shear width, low asthenosphere temperature or passive upwelling. However, a combination of these parameters cannot produce enough melt and does not allow a ridge-type thermal regime in the good amount of time. Therefore, we suggest that melt retention play an important role to delay melt extraction while the extension rate may be faster, the pure-shear width narrower, the asthenosphere temperature hotter and the upwelling rate more active. In addition, an evolution of these parameters is not excluded and would better explain the occurrence of exhumed mantle at magma-poor rifted margins.

ACKNOWLEDGMENT

We thank Jakob Skogseid (Statoil) for his comments on the numerical experiments. We also acknowledge the MM3 (Margin Modelling Phase 3) partners (BP, ConocoPhillips, HESS, BR Petrobras, Statoil, Shell, TOTAL, BG Group, BHP-Billiton).

REFERENCES

Batchelor, G. K., 2000, An Introduction to Fluid Dynamics, Cambridge University Press.

Braun, M. G., G. Hirth, and E. M. Parmentier, 2000, The effects of deep damp melting on mantle flow and melt generation beneath mid-ocean ridges: Earth and Planetary Science Letters, v. 176, p. 339-356.

Bronner, A., D. Sauter, G. Manatschal, G. Péron-Pinvidic, and M. Munschy, 2011, Magmatic breakup as an explanation for magnetic anomalies at magma-poor rifted margins: Nature Geoscience, v. 4, p. 549-553.

Cannat, M., 1996, How thick is the magmatic crust at slow spreading oceanic ridges?: Journal of Geophysical Research: Solid Earth, v. 101, p. 2847-2857.

Cannat, M., J. Cann, and J. Maclennan, 2004, Some hard rock constraints on the supply of heat to mid-ocean ridges: Geophysical Monograph Series, v. 148, p. 111-149.

Cannat, M., Y. Lagabrielle, H. Bougault, J. Casey, N. de Coutures, L. Dmitriev, and Y. Fouquet, 1997, Ultramafic and gabbroic exposures at the Mid-Atlantic Ridge: Geological mapping in the 15 N region: Tectonophysics, v. 279, p. 193-213.

Cannat, M., G. Manatschal, D. Sauter, and G. Peron-Pinvidic, 2009, Assessing the conditions of continental breakup at magma-poor rifted margins: What can we learn from slow spreading mid-ocean ridges?: Comptes Rendus Geoscience, v. 341, p. 406-427.

Chapman, D. S., 1986, Thermal gradients in the continental crust: Geological Society, London, Special Publications, v. 24, p. 63-70.

Christensen, N. I., and W. D. Mooney, 1995, Seismic velocity structure and composition of the continental crust: A global view: Journal of Geophysical Research: Solid Earth, v. 100, p. 9761-9788.

Davis, M., and N. J. Kusznir, 2004, Depth-dependent lithospheric stretching at rifted continental margins: Proceedings of NSF Rifted Margins Theoretical Institute, p. 92-136.

deMartin, B. J., R. A. Sohn, J. P. Canales, and S. E. Humphris, 2007, Kinematics and geometry of active detachment faulting beneath the Trans-Atlantic Geotraverse (TAG) hydrothermal field on the Mid-Atlantic Ridge: Geology, v. 35, p. 711-714.

Faul, U. H., 2001, Melt retention and segregation beneath mid-ocean ridges: Nature, v. 410, p. 920-923.

Fletcher, R., N. Kusznir, and M. Cheadle, 2009, Melt initiation and mantle exhumation at the Iberian rifted margin: Comparison of pure–shear and upwelling-divergent flow models of continental breakup: Comptes Rendus Geoscience, v. 341, p. 394-405.

Hamza, V. M., and F. P. Vieira, 2012, Global distribution of the lithosphere-asthenosphere boundary: a new look: Solid Earth Discussions, v. 4, p. 279-313.

Katz, R. F., M. Spiegelman, and C. H. Langmuir, 2003, A new parameterization of hydrous mantle melting: Geochemistry Geophysics Geosystems, v. 4.

Lizarralde, D., J. B. Gaherty, J. A. Collins, G. Hirth, and S. D. Kim, 2004, Spreading-rate dependence of melt extraction at mid-ocean ridges from mantle seismic refraction data: Nature, v. 432, p. 744-747.

Manatschal, G., 2004, New models for evolution of magma-poor rifted margins based on a review of data and concepts from West Iberia and the Alps: International Journal of Earth Sciences, v. 93, p. 432-466.

Manatschal, G., N. Froitzheim, M. Rubenach, and B. D. Turrin, 2001, The role of detachment faulting in the formation of an ocean-continent transition: Insights from the Iberia Abyssal Plain: Geological Society, London, Special Publications, v. 187, p. 405-428.

McKenzie, D., 1978, Some remarks on the development of sedimentary basins: Earth and Planetary Science Letters, v. 40, p. 25-32.

McKenzie, D., and M. J. Bickle, 1988, The Volume and Composition of Melt Generated by Extension of the Lithosphere: Journal of Petrology, v. 29, p. 625-679.

McKenzie, D., J. Jackson, and K. Priestley, 2005, Thermal structure of oceanic and continental lithosphere: Earth and Planetary Science Letters, v. 233, p. 337-349.

Minshull, T. A., S. M. Dean, R. S. White, and R. B. Whitmarsh, 2001, Anomalous melt production after continental break-up in the southern Iberia Abyssal Plain: Geological Society, London, Special Publications, v. 187, p. 537-550.

Mohn, G., G. Manatschal, M. Beltrando, E. Masini, and N. Kusznir, 2012, Necking of continental crust in magma‐poor rifted margins: Evidence from the fossil Alpine Tethys margins: Tectonics, v. 31.

Morgan, J. P., 1987, Melt migration beneath mid-ocean spreading centers: Geophysical Research Letters, v. 14, p. 1238-1241.

Müntener, O., & Manatschal, G. (2006). High degrees of melt extraction recorded by spinel harzburgite of the Newfoundland margin: The role of inheritance and consequences for the evolution of the southern North Atlantic. *Earth and Planetary Science Letters*, *252*(3–4), 437–452.

Müntener, O., G. Manatschal, L. Desmurs, and T. Pettke, 2010, Plagioclase peridotites in ocean–continent transitions: refertilized mantle domains generated by melt stagnation in the shallow mantle lithosphere: Journal of Petrology, v. 51, p. 255-294.

Parsons, B., and J. G. Sclater, 1977, An analysis of the variation of ocean floor bathymetry and heat flow with age: Journal of Geophysical Research, v. 82, p. 803-827.

Pérez-Gussinyé, M., J. P. Morgan, T. J. Reston, and C. R. Ranero, 2006, The rift to drift transition at non-volcanic margins: Insights from numerical modelling: Earth and Planetary Science Letters, v. 244, p. 458-473.

Péron-Pinvidic, G., and G. Manatschal, 2009, The final rifting evolution at deep magma-poor passive margins from Iberia-Newfoundland: a new point of view: International Journal of Earth Sciences, v. 98, p. 1581-1597.

Péron‐Pinvidic, G., G. Manatschal, T. A. Minshull, and D. S. Sawyer, 2007, Tectonosedimentary evolution of the deep Iberia‐Newfoundland margins: Evidence for a complex breakup history: Tectonics, v. 26.

Reston, T. J., and J. P. Morgan, 2004, Continental geotherm and the evolution of rifted margins: Geology, v. 32, p. 133-136.

Sclater, J., C. Jaupart, and D. Galson, 1980, The heat flow through oceanic and continental crust and the heat loss of the Earth: Reviews of Geophysics, v. 18, p. 269-311.

Sibuet, J. C., S. P. Srivastava, M. Enachescu, and G. D. Karner, 2007, Early Cretaceous motion of Flemish Cap with respect to North America: implications on the formation of Orphan Basin and SE Flemish Cap–Galicia Bank conjugate margins: Geological Society, London, Special Publications, v. 282, p. 63-76.

Stein, C. A., and S. Stein, 1992, A model for the global variation in oceanic depth and heat flow with lithospheric age: Nature, v. 359, p. 123-129.

Sutra, E., G. Manatschal, G. Mohn, and P. Unternehr, 2013, Quantification and restoration of extensional deformation along the Western Iberia and Newfoundland rifted margins: Geochemistry, Geophysics, Geosystems, v. 14, p. 2575-2597.

Turcotte, D. L., and G. Schubert, 2002, Geodynamics, University Press.

Whitmarsh, R. B., G. Manatschal, and T. A. Minshull, 2001, Evolution of magma-poor continental margins from rifting to seafloor spreading: Nature, v. 413, p. 150-154.

Chapter 3

Constraining lithosphere deformation modes during continental breakup for the Iberia-Newfoundland conjugate rifted margins

Preface

This chapter is a paper format and has been submitted to Tectonophysics

Constraining lithosphere deformation modes during continental breakup for the Iberia-Newfoundland conjugate rifted margins

Ludovic Jeanniot[1], Nick Kusznir[1], Geoffroy Mohn[2], Gianreto Manatschal[3] and Leanne Cowie[1]

[1]Department of Earth, Ocean and Ecological Sciences, University of Liverpool, Liverpool, L69 3GP, UK

[2]Department of Geosciences and Environmental Sciences, Université de Cergy-Pontoise, Cergy-Pontoise, France

[3]IPGS-EOST, UDS-CNRS, Strasbourg, France

ABSTRACT

A kinematic model of lithosphere and asthenosphere deformation has been used to investigate lithosphere deformation modes during continental breakup. The model has been applied to two conjugate profiles across the Iberia-Newfoundland rifted margins and quantitatively calibrated using observed present-day water loaded subsidence and crustal thickness, together with observed mantle exhumation, subsidence and melting generation histories. The kinematic model uses an evolving-prescribed flow-field to deform the lithosphere and asthenosphere from which continental crustal thinning and breakup, lithosphere thermal evolution, melt initiation and subsidence are predicted. We explore the sensitivity of model predictions to accelerating extension rate, deformation migration and buoyancy induced upwelling. The best fit calibrated models of lithosphere deformation evolution for the Iberia-Newfoundland conjugate margins require: (1) an initial broad

region of lithosphere deformation with passive upwelling, (2) lateral migration of deformation, (3) an increase in extension rate with time, (4) focussing of the deformation and (5) buoyancy induced upwelling. The model prediction of exhumed mantle at the Iberia-Newfoundland margins, as observed, requires a critical threshold of melting to be exceeded before melt extraction. The preferred calibrated models predict faster extension rates and earlier continental crustal rupture and mantle exhumation for the Iberia Abyssal Plain - Flemish Pass conjugate margin profile than for the Galicia Bank – Flemish Cap profile to the north. The predicted N-S differences in the deformation evolution give insights into the 3D evolution of Iberia-Newfoundland margin breakup.

3.1 Introduction

How the lithosphere and asthenosphere deform during continental rifting leading to breakup is poorly understood. Observations at present-day and fossil analogue magma-poor rifted margins shows hyper-thinned continental crust and lithosphere (e.g. West-African Margin, Contrucci et al., 2004), detachments faults (e.g. Alpine Tethys, Iberia-Newfoundland, Reston et al., 1996; Manatschal, 2004; Reston and McDermott, 2011), exhumed mantle and scattered embryonic oceanic crust (e.g. Iberia and Newfoundland margins, Reid, 1994; Jagoutz et al., 2007; Bronner et al., 2011), which cannot be explained by simplistic lithosphere deformation modes. Fletcher et al. (2009) explored two deformation mode end-members, pure-shear and upwelling divergent flow, in order to examine the continental breakup process. They showed that these deformation modes play an important role on the resulting architecture of rifted margins and the relative timing of melt generation and crustal breakup. Nevertheless these two lithosphere deformation mode end-members taken individually cannot predict the observed rifted margin architecture.

This study aims to give insights into the main lithosphere deformation processes during continental breakup and to determine the lithosphere deformation history of the Iberia-

Newfoundland rifted margins that led to their present-day configuration. Dynamic numerical models have previously been applied to the formation of the Iberia-Newfoundland conjugate rift system (e.g. Huismans and Beaumont, 2011). The mode of deformation in this modelling approach is defined by constitutive equations where the rheology is fully thermo-mechanically coupled, permitting the model to be self-consistent with actual rock-rheology fundamental processes (Fernàndez & Ranalli, 1997). As a consequence, initial anomalies must be implanted within the lithosphere in order to initiate the deformation. For example, Harry and Grandell (2007) used initial anomalies in the continental crustal thickness and initial weakness of the rheology of the continental crust to reproduce a similar architecture to Galicia Bank and Flemish Cap. Lavier and Manatschal (2006) constrained their initial conditions from derived geological and geophysical observations on the Iberia-Newfoundland and the Alpine Tethys rifted margins and they proposed a polyphase continental rifting evolution of the Iberia-Newfoundland margins. These dynamic models show a complex evolution determined by the initial rheological properties of continental crust and mantle, but they may result in unexpected predictions, which make them difficult to apply to specific rifted margins architecture and calibrated against real data observations.

We privilege the kinematic approach, rather than dynamic, not only because we aim to apply a model of lithosphere deformation to the Iberia-Newfoundland rifted margins but because we want to constrain the model, through a series of numerical experiments, using strong geological and geophysical observations. Deformation modes in kinematic models are prescribed by flow velocity fields. Kinematics models omit rheological properties and the physics of its evolution, but their simplicity of use allows quantitative calibration. Kinematic models have been already applied to specific case histories in order to predict subsidence, heat flow or the architecture of the sedimentary basins and rifted margins (e.g. Beaumont et al., 1982, Kusznir & Karner, 2007); however, there is no existing study that can

determine the full deformation history in lithospheric extension context, constrained and quantitatively calibrated using real data observations.

Two main lithosphere deformation modes are defined in the kinematic model: (1) pure-shear inducing passive upwelling and (2) buoyancy induced upwelling. The pure-shear deformation mode is the dominant mode and is controlled by its deformation width and half spreading rate. The contribution of buoyancy gives additional upwelling and speeds up lithosphere thinning. Because a single lithosphere deformation mode cannot explain complex rifted margins architecture, we prescribe a sequence of lithosphere deformation event represented by a succession of flow-field. The kinematic model uses a fluid-flow model to represent a sequence of lithosphere deformation modes to advect temperature and material during continental rifting leading to breakup and seafloor spreading initiation. As a consequence, we control the evolution of continental rifting until breakup and seafloor spreading, which enable the quantitative calibration. The model incorporates lateral jumps or migration of the modes of lithosphere deformation. The lithosphere deformation and its consequences on crustal breakup and melt initiation using each deformation component is examined and illustrated.

The conjugate Iberia-Newfoundland rifted margins are an ideal natural laboratory because these are magma-poor rifted margins and they are among the best studied rifted margin systems of the world. The Iberia-Newfoundland sections, located in the North Atlantic, started to rift during Middle-Late Jurassic before the localisation of the deformation during the early Cretaceous (145-130Ma) leading to continental breakup at the Albian-Aptian boundary (~112Ma) (Tucholke and Sibuet, 2007; Tucholke et al., 2007; Bronner et al., 2011; Sutra et al., 2013). Two pairs of conjugate margins are studied and modelled in this work; one across the Galicia Bank-Flemish Cap and the other one across the southern Iberia Abyssal Plain-Flemish Pass (Figure 3.1 and Figure 3.2).

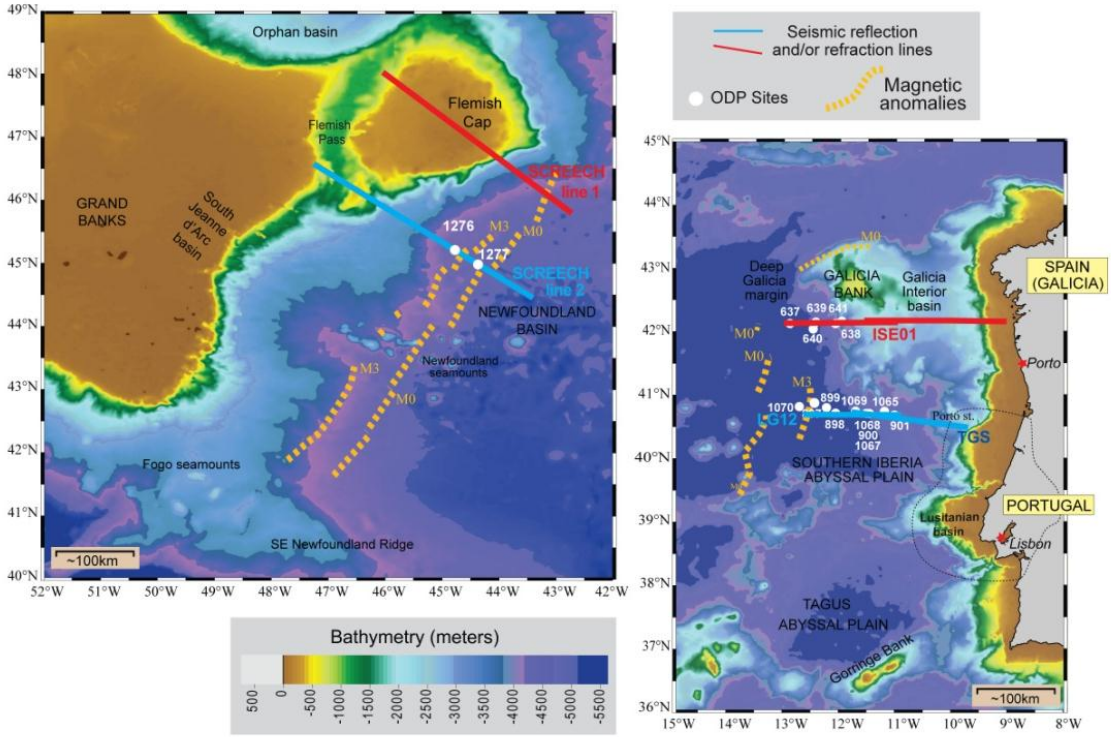

Figure 3.1: Bathymetry of the Iberia-Newfoundland rifted margins in the Atlantic North, with the position of the 2 conjugated margin profiles corresponding to SCREECH 1-ISE01 for the northern section and SCREECH 2-TGS/LG12 for the southern section. The ODP drill holes discussed in this paper and the magnetic anomalies M0 and M3 are marked on the map.

Our modelling of the Iberia-Newfoundland conjugate rifted margins uses 2 forms of calibration:

(1) ***The final rifted margin crustal architecture:*** The model predictions of the conjugate rifted margin crustal architecture must fit the observed present-day water-loaded subsidence and crustal thickness, obtained from flexural backstripping and gravity inversion respectively.

(2) ***The evolution of rifting:*** The timing of mantle exhumation, melt initiation and the subsidence history, deduced from existing datasets, are used to constrain the lithosphere deformation modes during rifting.

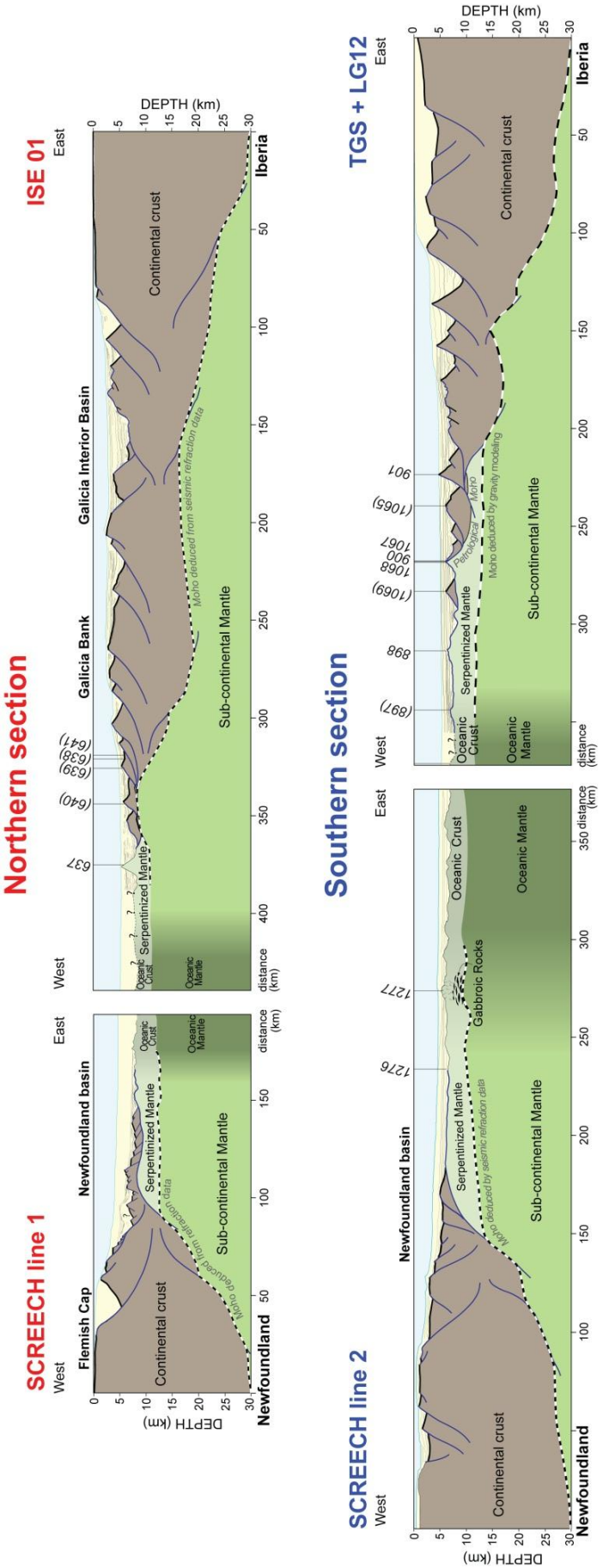

Figure 3.2: Interpreted northern and southern cross-sections for the Iberia-Newfoundland conjugate margins crustal profiles (modified from Sutra et al., 2013), given my gravity inversion and seismic profiles (see section 3.3.4 for references).

We will examine and discuss the development of rifting for both conjugate margin pairs of Iberia-Newfoundland and explore whether they are synchronous or diachronous. The study also investigates how mantle exhumation may persist in time without decompressional melting forming an oceanic crust.

3.2 Model formulation

This section presents the formulation of the kinematic model that has been developed to deform lithosphere and asthenosphere during rifting processes leading to continental breakup and seafloor spreading. Kinematic modelling using a single deformation flow-field cannot be used to describe the complex evolution of deformation processes and the resulting architecture observed at magma-poor rifted margins. While Fletcher et al. (2009) explored two lithosphere deformation mode end-members, pure-shear and upwelling divergent flow leading to continental breakup, we use a sequence of deformation modes so that lithosphere and asthenosphere deformation can evolve kinematically.

3.2.1 How does the lithosphere deform?

The evolution of rifted margins derived from observations and interpretations at magma-poor rifted margin (Péron-Pinvidic and manatschal, 2009) or based on numerical modelling (Lavier and Manatschal, 2006; Huisman and Beaumont, 2011) favour the idea of an evolving lithospheric deformation process from intracontinental rifting leading to mantle exhumation, lithosphere breakup and seafloor spreading initiation. Similar extensional faulting occurs in the cool brittle 15-20km upper lithosphere with ductile distributed deformation in the lithosphere below, either during continental rifting (Jackson, 1987) or at slow-spreading ocean ridges (Cannat et al., 2009). However, the width within which extension faults occurs are different for both previous tectonic contexts; the deformation may be distributed over a wide region at the beginning of rifting (Brun and Choukroune, 1983) and is focus within a narrow region of about 10-20 km at slow and ultraslow spreading ocean ridges (Wilson, 1989; Cannat et al., 2009). As a consequence, we

approximate the deformation of the lithosphere using similar mode of deformation from continental rifting to breakup, where the width of the deformation evolves.

3.2.2 Generation of flow-fields

The flow-fields that are used to advect temperature and material are generated by a finite-element viscous flow model which uses a 6 noded triangular element grid. We calculate two distinct component types of flow-field; (1) a pure-shear mode inducing passive upwelling below and (2) an additional active upwelling due to buoyancy. The finite-element viscous flow solution generates flow-fields using a Newtonian layered viscosity structure which is shown in Figure 3a. The difference of viscosity set for each layer generates a flow; thus only the viscosity ratio between the layers is important. A low viscosity of 10^{20} Pa.s is set for the upper 20km lithosphere within a pure-shear deforming region of width W. This pure-shear region approaches the brittle upper lithosphere deforming by normal faulting. The width W can be varied from broad to narrow. Outside the pure-shear region, the brittle upper lithosphere is set to 20km thick with a high viscosity of 10^{23} Pa.s. Beneath the brittle layer and the pure-shear deformation region, between 20 and 100km depth, the viscosity is set at 10^{21} Pa.s. The viscosity is set at 10^{20} Pa.s between 100 and 660km, and at 10^{22} Pa.s for the remaining mantle.

Pure-shear + passive upwelling

Pure-shear is often used to describe the deformation mode occurring during intracontinental rifting (McKenzie, 1978). In our model pure-shear and passive upwelling flow field are kinematically driven by the half-spreading rate V_x^0 applied to the topmost seismogenic brittle layer (Figure 3.3a). Outside the pure-shear deformation region the following boundary conditions are applied:

$$V_x(z = 0) = \pm V_x^0$$

$$V_z(z = 0) = 0$$

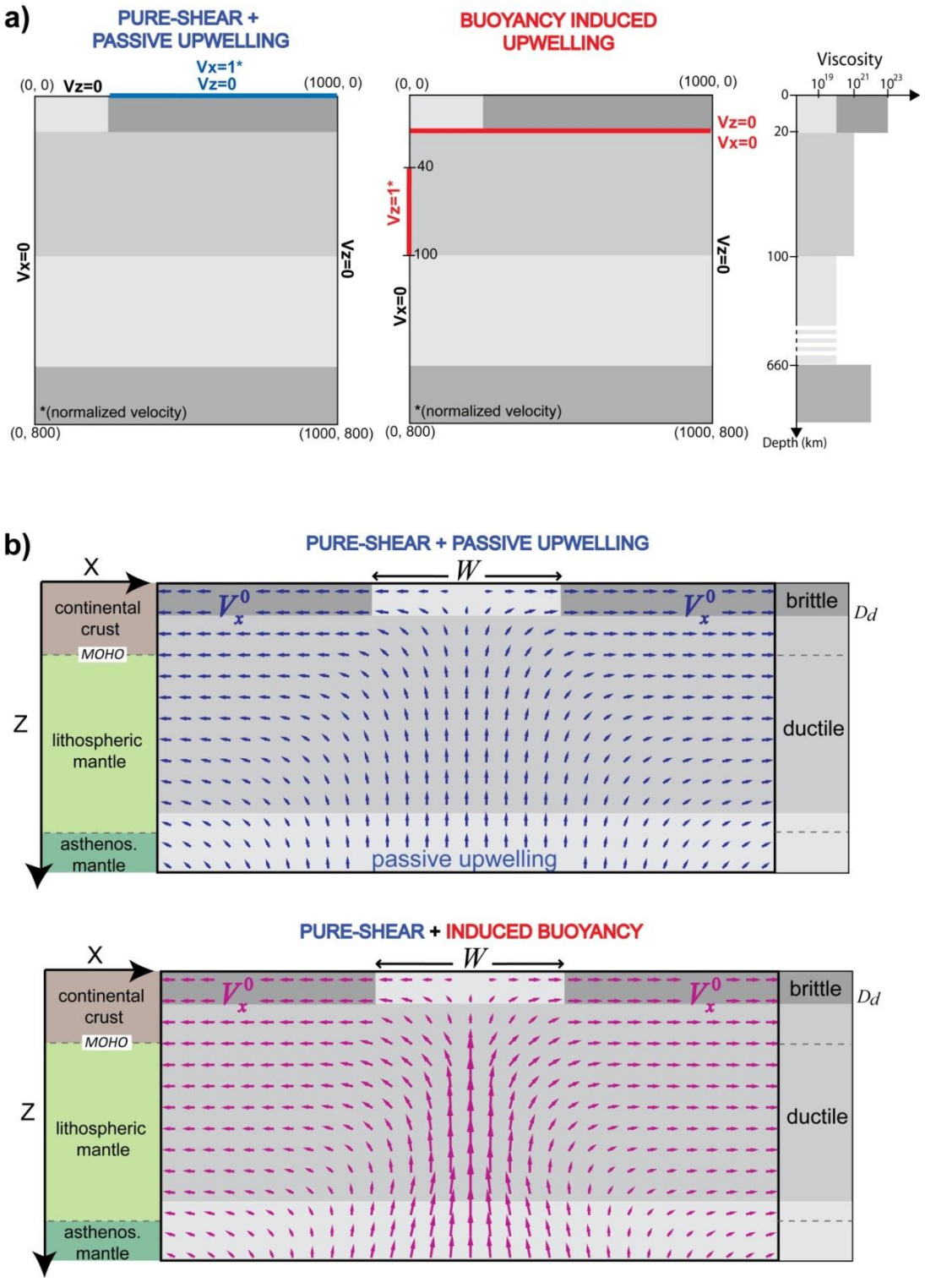

Figure 3.3: Boundary conditions of the 2D finite-element viscous flow model using a Newtonian layered viscosity structure and their resulting flow vectors for **a)** pure-shear + passive upwelling and **b)** buoyancy induced upwelling. W is the pure-shear deformation width. D_d is the decoupling depth between the upper brittle seismogenic layer and the ductile lithosphere and asthenosphere below.

while under the axial region

$$V_x(x = 0) = 0$$

and at the edge of the grid

$$V_z(x = edge) = 0$$

The resulting flow vectors generated by the finite-element viscous flow model are shown in Figure 3.3b. The imposed divergence of the strong viscosity upper layer generates localized pure-shear deformation within the localised low viscosity layer and passive upwelling beneath that region. In contrast to the pure-shear lithosphere deformation end-member of Fletcher et al. (2009), where passive upwelling prescribed within a fixed deformation width resulted in increasing upwelling velocities, the passive upwelling resulted from our model is more distributed in depth so that the deeper upwelling velocities are less (Figure 3.3b).

Buoyancy induced upwelling

The importance of buoyancy induced upwelling during seafloor spreading has been suggested many times by (Forsyth et al., 1998; Spiegelman and Reynolds, 1999; Braun et al., 2000; Nielsen and Hopper, 2004). Buoyancy induced upwelling is likely to be important during continental lithosphere breakup because it gives an upwelling rate greater than that due to passive upwelling alone. We consider that buoyancy upwelling is an amplifier of lithosphere deformation adding to that from pure-shear and passive upwelling. In our kinematic model buoyancy upwelling is driven by an axial upwelling rate V_z^0 (Figure 3.3a). Between 40 and 100km depth, the buoyancy induced upwelling is set to:

$$V_z(x = 0) = V_z^0$$

The buoyancy induced upwelling is assumed not to penetrate the cold seismogenic lithosphere. As a consequence in our kinematic model, buoyancy induced upwelling is not permitted above a buoyancy penetration depth of D_b. D_b is set at 20km in most models. The flow boundary conditions are set as follows:

$$V_x(z = D_b) = 0$$

$$V_z(z = D_b) = 0$$

At the axis:

$$V_x(x = 0) = 0$$

At the model edge:

$$V_z(x = edge) = 0$$

The flow-field generated by buoyancy induced upwelling is added to the pure-shear and passive upwelling flow vectors and is illustrated in Figure 3.3b. The buoyancy contribution creates an axial upwelling that generates small-scale convection beneath that layer. The upper depth of buoyancy induced upwelling, D_b, may be varied from deep to shallow.

For this study we make the approximation that these deformation flow-fields are not controlled by the viscosity structure. The viscosity structure is likely to evolve through rifting which defines the boundary between kinematic and dynamic approaches (Lavier and Manatschal, 2006; Schmeling, 2010; Huismans and Beaumont, 2011). For example, the presence of hydrated lithospheric mantle, dehydration of mantle or the onset of melting would change the rheology and so the flow velocity field (Hirth and Kohlstedt, 1996; Braun et al., 2000). In order to approximate the evolution of the lithosphere deformation mode, we kinematically prescribe a succession of deformation events. Each event has a start and an end. Either purely successive or simultaneous rift events are allowed. The parameterization of each event includes half-spreading and buoyancy upwelling rates. A ratio $R_b = (V_z^0/V_x^0) > 0$ describes the magnitude of buoyancy upwelling rate V_z^0 with respect to the half-spreading rate V_x^0. The location of the deformation may be varied by lateral jumps or by continuous lateral migration. We introduce a deformation migration factor $f_m = V_m/V_x^0$, where V_m is the velocity of which the deformation migrates horizontally at each time step, relative to the half-spreading rate V_x^0.

3.2.3 Material and thermal advection

Lithosphere deformation modes are represented by flow velocity fields $\boldsymbol{V}$, which are used to advect material and temperature. We use a Lagrangian and an Eulerian (x, z) coordinate reference frame system for the material advection and temperature respectively. Grid resolution is 5km horizontally and 2.5km vertically. A time step of 50000yrs is used. The tracker particles nodes of the Lagrangian grid move in space and in time following the flow velocity field $\boldsymbol{V}$. Regridding is required when two nodes are horizontally separated by more than 10km. The evolution of the thinning of continental crust and lithosphere deformation is shown by tracking the Moho and the base of the lithosphere, initially assumed horizontal, which allows the calculation of tectonic subsidence (McKenzie, 1978). Each node characterizes a volume of material with a density ρ, thermal conductivity k and specific heat C_p (see Table 3.1 for the value and references).

Temperature behaviour follows the diffusion-advection equation:

$$\frac{\partial T}{\partial t} = \frac{1}{\rho C_p}\nabla(k\nabla T) - \boldsymbol{V}(\nabla T + h) + \frac{A_0}{\rho C_p} e^{-\frac{z}{a_r}} \qquad (1)$$

where T is temperature and h the adiabatic gradient as described by McKenzie and Bickle (1988). A radiogenic heat production of $A_0 = 2.2e^{-6}$ W.m^{-2} is including for the continental crust with a depth decay length a_r. Radiogenic heat productivity of the gabbroic and basaltic ocean crust is neglected. We set the asthenosphere temperature to 1333°C (in-situ temperature) so it refers to a relatively cold/normal lithosphere (Reston and Morgan, 2004), favoured to explain magma-poor margins. The initial lithosphere thermal structure is assumed to be in thermal equilibrium. The equilibrated oceanic lithosphere thickness is 125km and the initial continental lithosphere 135km thick. The lithosphere thermal structure is compared to an equilibrated oceanic linear geotherm (McKenzie, 1967; Sclater et al., 1980) to calculate thermal load evolution, uplift and subsidence. An initial elevation of ~400m is predicted due to the difference of temperature between these two geotherms.

Table 3.1: Table of constants and physical parameters

Variable	Meaning	value	units
Ak	lithosphere thickness for a linear oceanic geotherm	125	km
At	initial lithosphere thickness	135	km
A_0	heat production	$2.2e^{-6}$	$W.m^{-2}$
a_r	radiogenic layer thickness	$Ct/2$	km
C_p	specific heat	1180	$J.kg^{-1}.K^{-1}$
D_d	brittle seismogenic layer	20	km
D_b	depth buoyancy	-	km
F_{ret}	melt retention	-	%
f_m	migration factor	-	-
g	gravitational acceleration	9.81	$m^2.s^{-1}$
h	adiabatic gradient	-	$°C.km^{-1}$
k_c	reference crustal thermal conductivity	2.6	$W.m^{-1}.K^{-1}$
k_m	reference mantle thermal conductivity	3.14	$W.m^{-1}.K^{-1}$
k	thermal conductivity at (X,Z)	-	$W.m^{-1}.K^{-1}$
LF	latent fusion	400	$kJ.kg^{-1}$
M_{cpx}	weight fraction of clinopyroxene being melted	0.16	%
R_b	buoyancy ratio V_z^0/V_x^0	-	-
$T°$	base lithosphere temperature	1333	°C
T	temperature at (X,Z)	-	°C
t	time	-	Myr
V_x^0	Half-spreading rate	-	$mm.yr^{-1}$
V_z^0	Additional upwelling rate	-	$mm.yr^{-1}$
$\boldsymbol{V}$	local velocity vector at (X,Z)	-	$mm.yr^{-1}$
W	pure-shear width	-	km
X	horizontal coordinate	-	km
Z	vertical coordinate	-	km
α	thermal expansion coefficient	$3.28e^{-5}$	$°C^{-1}$
β	stretching factor	-	-
γ	thinning factor	-	-
γ_{crit}	critical thinning factor	-	-
ρ_c	reference crustal density	2850	$kg.m^{-3}$
ρ_m	reference mantle density	3330	$kg.m^{-3}$
ρ_v	reference volcanic addition density	2850	$kg.m^{-3}$
ρ_w	density of water	1040	$kg.m^{-3}$
ρ	density at (X,Z)	-	$kg.m^{-3}$

*(Parsons & Sclater, 1977; McKenzie, 1978; Sclater et al., 1980; Chapman, 1986; Turcotte & Schubert, 2002)

3.2.4 Timing of melt initiation and melt extraction

During lithosphere thinning, the upwelling asthenospheric mantle results in melt generation (Bown and White, 1995). Decompressional melting is predicted using the parameterization and methodology of Katz et al. (2003). In our modelling melt is extracted directly after its generation, or it can be retained in the mantle until it exceeds a threshold amount of melt fraction F_{ret}. Once the threshold melt fraction is reached, the entire melt is extracted and is evenly distributed within the pure-shear region to form the oceanic crust. Consequently we differentiate the timing of the initiation of decompression melting from when it is extracted to the surface. Before melt extraction, the melt may remain in the mantle (Cannat et al., 2004), or be episodically extracted at the seabed. Buck and Su (1989) showed that retention of melt within the mantle leads to a change of bulk viscosity of the mantle, which would enhance upwelling from buoyancy (Nielsen and Hopper, 2004).

3.2.5 Timing of continental crustal breakup

In the model, pure-shear and passive upwelling deformation stretches and thins the continental crust and lithosphere until it approaches zero thickness. This would not permit mantle exhumation. However, pure-shear represents extensional faulting that would enable mantle exhumation before the Moho defined by tracker particles reaches the surface. Consequently, we need to define a critical crustal thickness after which the continental crust ruptures and separates (i.e. crustal breakup) allowing mantle exhumation. Based on the Iberia-Newfoundland rifted margins observations (Sutra et al., 2013 and references therein), we suggest that the continental crust ruptures and separates after a critical thinning factor $\gamma = 1 - 1/\beta$ between 0.88 and 0.95 (where β is the stretching factor). Therefore, if the initial continental crust is set at 35km thickness, mantle exhumation is supposed to occur when the continental crust is thinned to between 1.75 and 4.2km. We do not exclude that this critical thinning factor may be different between the north and south profiles of Iberia-Newfoundland conjugate rifted margins.

3.2.6 Model limitations

Our model does not incorporate faulting and sedimentation and we are aware that these processes may have a significant impact on the predicted bathymetry. Footwall uplift of normal faults during the extension is not modelled and generates uncertainties in the subsidence history determined from ODP sites. Moreover, mantle density changes due to serpentinization processes are not taken into account in the model prediction.

3.3 Model illustration

The model behaviour may be illustrated through a series of numerical experiments. We test the lithosphere and asthenosphere deformation sensitivity to the pure-shear width, the spreading rate, buoyancy strength and its penetration depth, and the lateral migration of the deformation. We also examine a sequence of lithosphere deformation events. All the model experiments are compared against a reference model that starts with a full pure-shear width of 80km, a full spreading rate of 20mm.yr^{-1} and no buoyancy induced upwelling. Each model is run for 20Myr. We explore the lithosphere deformation by varying one deformation parameter at a time.

3.3.1 Pure-shear width

Lithosphere and asthenosphere deformation sensitivity to pure-shear width is explored in Figure 3.4a. A narrow pure-shear region 20km wide results in localised and fast stretching and thinning. Mantle exhumation is therefore predicted because the continental crust thins faster than the lithosphere. Using a pure-shear 200km wide results in slow regional lithosphere stretching and thinning. The asthenosphere upwelling is therefore slow which delays decompressional melting; however melt is predicted before crustal breakup. The pure-shear width has also an important impact on the rifted margin architecture; the transition from thick to thin continental crust is gentle over a broad region if the pure-shear width is large whereas this transition is sharp if a narrow pure-shear width is used.

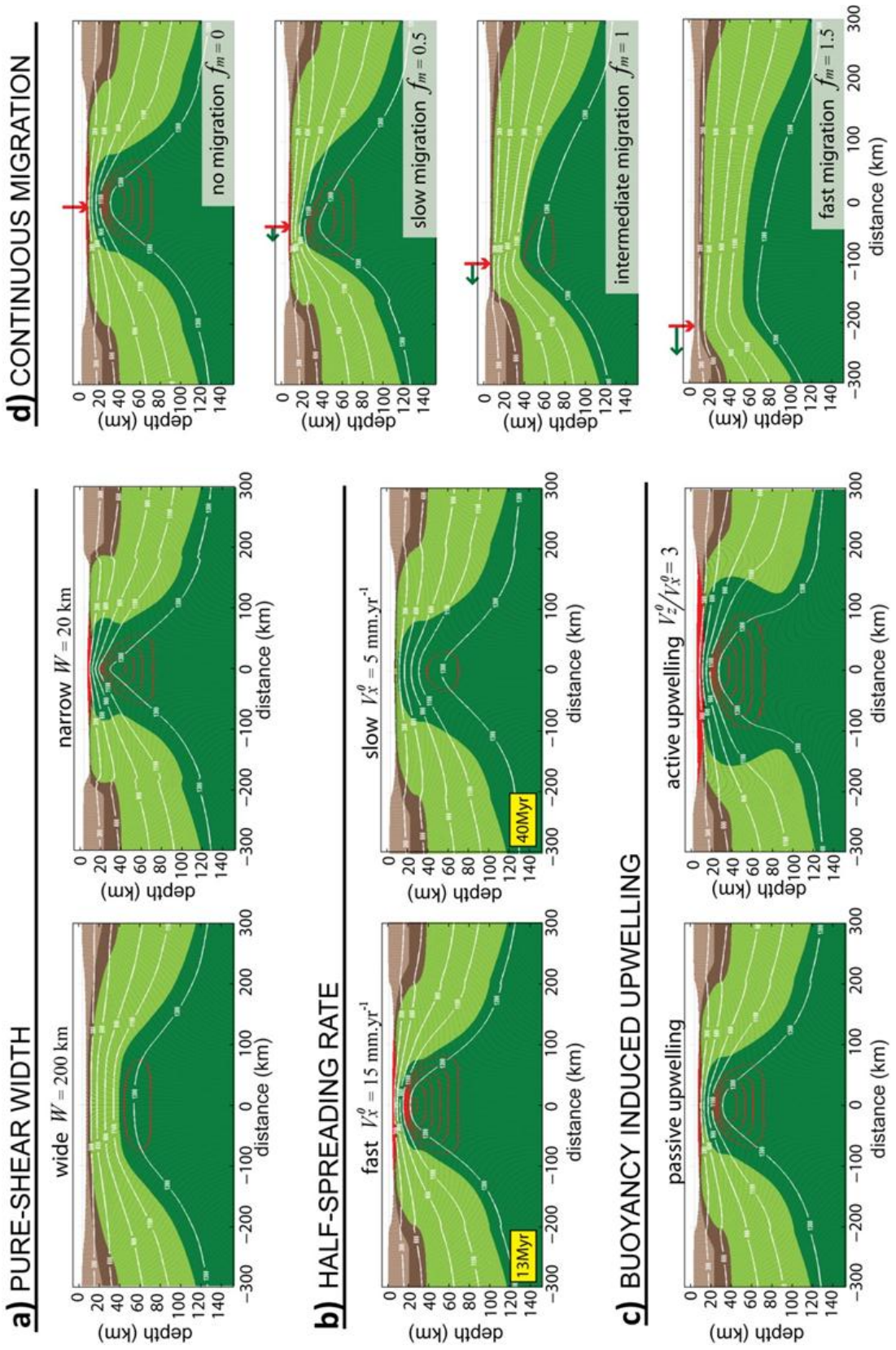
a) PURE-SHEAR WIDTH
wide $W = 200$ km
narrow $W = 20$ km
b) HALF-SPREADING RATE
fast $V_x^0 = 15$ mm.yr^{-1}
slow $V_x^0 = 5$ mm.yr^{-1}
13Myr
40Myr
c) BUOYANCY INDUCED UPWELLING
passive upwelling
active upwelling $V_z^0/V_x^0 = 3$
d) CONTINUOUS MIGRATION
no migration $f_m = 0$
slow migration $f_m = 0.5$
intermediate migration $f_m = 1$
fast migration $f_m = 1.5$
depth (km)
distance (km)

Figure 3.4 *(previous page):* Model sensitivity to **a)** pure-shear width $W = 200$km and 20km, **b)** half-spreading rate $V_x^0 = 5$ and 15 mm.yr-1, **c)** buoyancy strength $R_b = 0$ (passive upwelling) and 3, and **d)** migration of the deformation using no migration, a migration factor $f_m = 0.5$, 1 and 1.5. The deformation axis for each snapshot is indicated by the vertical red arrow. The green horizontal arrow indicates the direction of the migration. Model run time is 20Myr except for the sensitivity to the half-spreading (extension of 200km).

3.3.2 Half-spreading rate

The model sensitivity to the half-spreading rate of 15 and 5 mm.yr^{-1} is shown in Figure 3.4b for the same amount of extension of 40, 120 and 200km. Fast extension rates induce faster lithosphere stretching and thinning and generate significant amount of melt before crustal breakup. Conversely, slow spreading rates allow mantle exhumation with less melting. Breakup of the continental crust occurs at the same amount of extension but mantle exhumation is only possible by using a slow spreading rate.

3.3.3 Buoyancy induced upwelling

The effects of the buoyancy induced upwelling strength are examined in Figure 3.4c. The strength of the additional buoyancy upwelling rate V_z^0 is defined using the ratio $R_b = V_z^0/V_x^0$. We explore the model sensitivity to buoyancy strength $R_b = 3$. Deformation in the upper 20km is not affected by the contribution of buoyancy upwelling. Strong buoyancy induced upwelling gives faster thinning of the lithosphere. Decompression melting is predicted earlier with buoyancy upwelling and the melt production is larger; mantle exhumation is not predicted in any of these particular numerical experiments.

3.3.4 Lateral deformation migration

The horizontal migration of the deformation is defined using a migration factor f_m relative to the half-spreading rate. For the model illustration shown in Figure 3.4d, $f_m = 0$, 0.5, 1 and 1.5, so if the half-spreading rate V_x^0 is 10mm.yr^{-1}, the deformation migrates laterally with a velocity $V_m = 5$, 10 and 15mm.yr^{-1} respectively. Lateral migration of the deformation

has 2 major implications; it generates an asymmetry of the lithosphere and continental crust architecture and it lessens the asthenospheric upwelling which delays decompressional melting. The choice of the migration factor is critically important for crustal breakup; if $f_m > 1$, the deformation migrates faster than the half-spreading rate so that the continental crust never thins to zero thickness. Migrating the lithosphere pure-shear deformation gives a conjugate margin crustal architecture that is not entirely dissimilar to that expected from lithosphere simple shear deformation (Wernicke, 1981).

3.3.5 Sequence of 3 lithosphere deformation events

The kinematic model is illustrated in Figure 3.5 using an evolving sequence of 3 lithosphere deformations events. From 0 to 5Myr, the continental crust and lithosphere are slowly and passively thinned using a wide pure-shear region of 200km and a half-spreading rate of 5mm.yr^{-1}. From 5 to 10Myr, another lithosphere deformation event is applied using a pure-shear region 80km wide and a half-spreading rate of 10mm.yr^{-1}. The axis of new deformation is located 50km eastward of the earlier deformation. The continental crust has thinned by a stretching factor of 2 while the continental lithosphere has only thinned by a factor of 1.2. A third lithosphere deformation event is applied from 10 to 20Myr. The location of this deformation axis is jumped 130km westward of the earlier deformation axis. This event consists of a narrow pure-shear region 40km wide, a half-spreading rate set at 15mm.yr^{-1} and buoyancy upwelling rate of 15mm.yr^{-1} ($R_b = 1$). This results in fast thinning of the continental crust and lithosphere. Melt is generated at 14Myr, but is not extracted immediately because it has not reached the melt fraction threshold set at 9%. Mantle exhumation is therefore possible for a short period of time between 15 and 18Myr before the melt fraction reaches 9%. Oceanic crust forms from 18Myr. The final crustal architecture of the two conjugate margins exhibits an asymmetry due to the jumps of the deformation axes and the narrowing of the pure-shear deformation region.

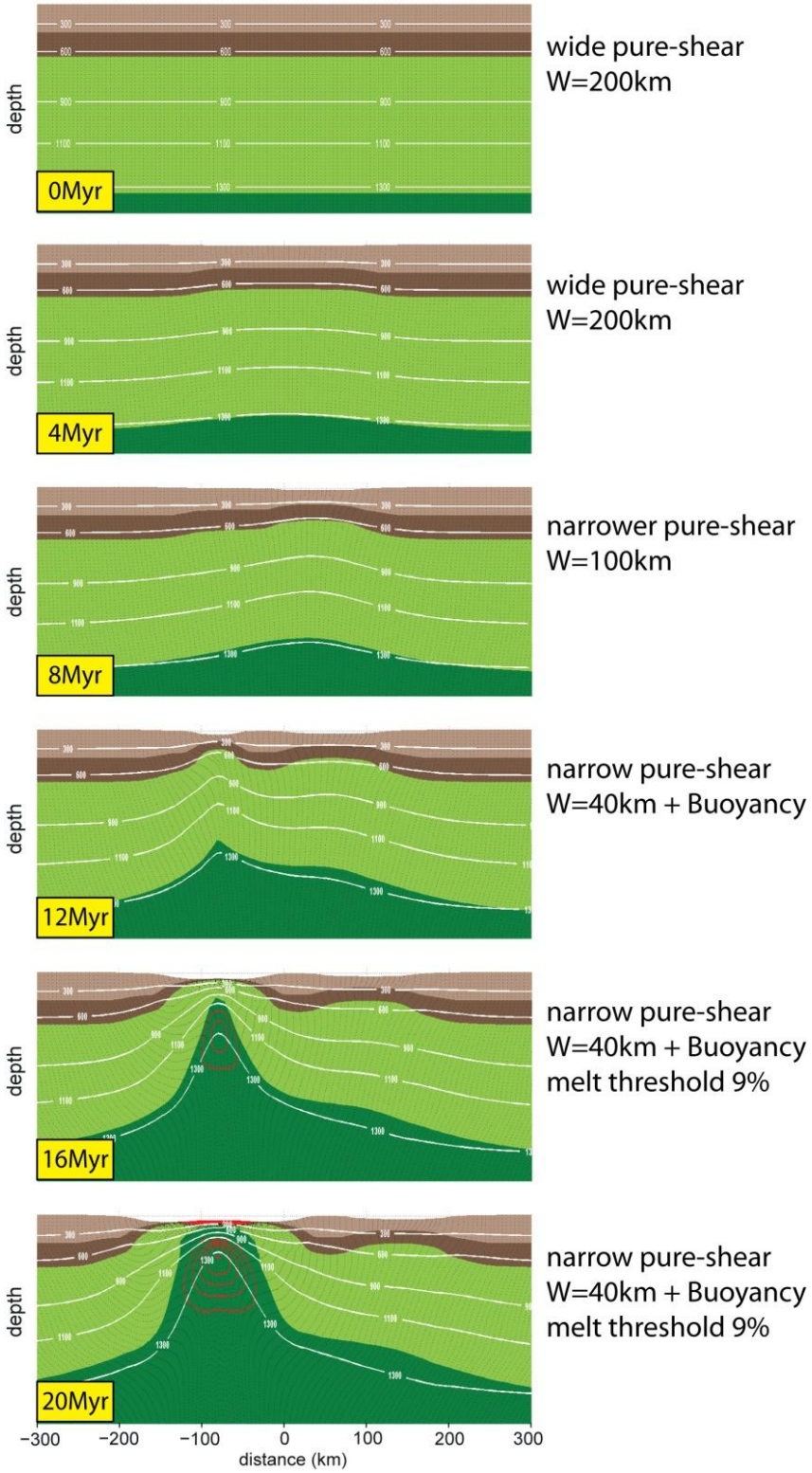

Figure 3.5: Model sensitivity to an evolving sequence of 3 lithosphere deformation events. White lines are isotherms (°C) and red contour lines are melt fraction. Contour interval is 0.03%.

3.4 Modelling constraints for the application to Iberia-Newfoundland margin

The kinematic model of continental rifting, breakup and seafloor spreading initiation has been applied and quantitatively calibrated for two conjugate profiles across the Iberia-Newfoundland rifted margins. The northern conjugate margin profile corresponds to SCREECH 1-ISE01 and the southern profile to SCREECH 2-TGS/LG12. Calibration uses measured present-day water-loaded subsidence and continental crustal thickness, and rifting evolution constraints. The two conjugate cross-sections have been subdivided into distinct domains by Sutra et al. (2013) based on the interpretation of seismic reflection and refraction data for the Newfoundland margins (Funck et al., 2003; Hopper et al., 2004; Hopper et al., 2006; Shillington et al., 2006; Van Avendonk et al., 2006; Eddy et al., 2013) and the Iberia margin (Boillot et al., 1987; Beslier, 1996; Zelt et al., 2003; Reston, 2005; Alves et al., 2006; Sutra et al., 2013). This section summaries the present-day crustal architecture of the Iberia-Newfoundland conjugate margins as shown in Figure 3.6. All geological ages in this paper refers to the timescale of Gradstein et al., (2004).

3.4.1 Present-day water-loaded subsidence

Present-day sediment corrected bathymetry has been calculated using a flexural backstripping model. We have used available seismic refraction and reflection data across the Iberia-Newfoundland rifted margins; the ISE01 line (Zelt et al., 2003; Henning et al., 2004), the LG12 line (Whitmarsh et al., 1990; Beslier, 1996; Krawczyk et al., 1996), the TGS line (Sutra & Manatschal, 2012), the SCREECH line 1 (Funck et al., 2003; Hopper et al., 2004), the SCREECH line 2 (Shipley et al., 2012, public-access Marine Seismic Data Centre of the University of Texas Institute for Geophysics). The flexural backstripping methodology is described in Roberts et al. (2013). Figure 3.6 shows for each profile seabed, top basement and the resulting water-loaded subsidence. We assume that the top basement was at sea-level before the beginning of rifting and that tectonic and thermal subsidence created the

water-loaded subsidence. Present-day bathymetry corrected for sediment-loading is assumed to be equivalent to subsidence.

3.4.2 Present-day crustal thickness

Moho depth and crustal thicknesses for all the Iberia-Newfoundland rifted margin profiles have been determined using a gravity inversion method (see Greenhalgh and Kusznir, 2007; Alvey et al., 2008; Chappell and Kusznir, 2008). Figure 3.6 shows the crustal basement thickness, from gravity inversion, top basement and the Moho depth corrected for sediment-loading. Previous studies identified the Moho depth using seismic tomography analysis (SCREECH 1 - Funck et al, 2003; ISE01 - Zelt et al., 2003) or gravity inversion (SCREECH 2 - Van Avendonk et al., 2009; TGS-LG12 – Cunha, 2008), giving an approximate initial continental crustal thickness of 30-35km. The gravity inversion method used in this study predicts greater initial crustal basement thicknesses and a difference between the Iberia and the Newfoundland margins; 40-42km for the Iberia margins against 35-36.5km for the Newfoundland margins. A limitation of gravity inversion is that the predicted gravity Moho depth does not necessarily fit with the petrological Moho especially in the domain associated with the exhumation of serpentinized mantle

3.4.3 Rifted margin and OCT architecture

Within the Ocean-Continent Transition (OCT), geological observations are necessary to constrain where mantle is exhumed and where the oceanic domain starts. The OCT architecture of the two conjugate margin profiles are illustrated in Figure 3.6 according to the interpretation of Sutra et al. (2013). We use the terminology of Tugend et al. (2014) for the description of magma-poor rifted margins including: (1) a proximal domain of slightly stretched continental crust, (2) a necking zone, (3) a hyper-thinned crust domain which corresponds to a thin (<10km) crust over a wide region, (4) an OCT or Zone of Exhumed Continental Mantle (ZECM, Whitmarsh et al. (2001)) with exhumed mantle and continental crustal slivers, and (5) an oceanic domain.

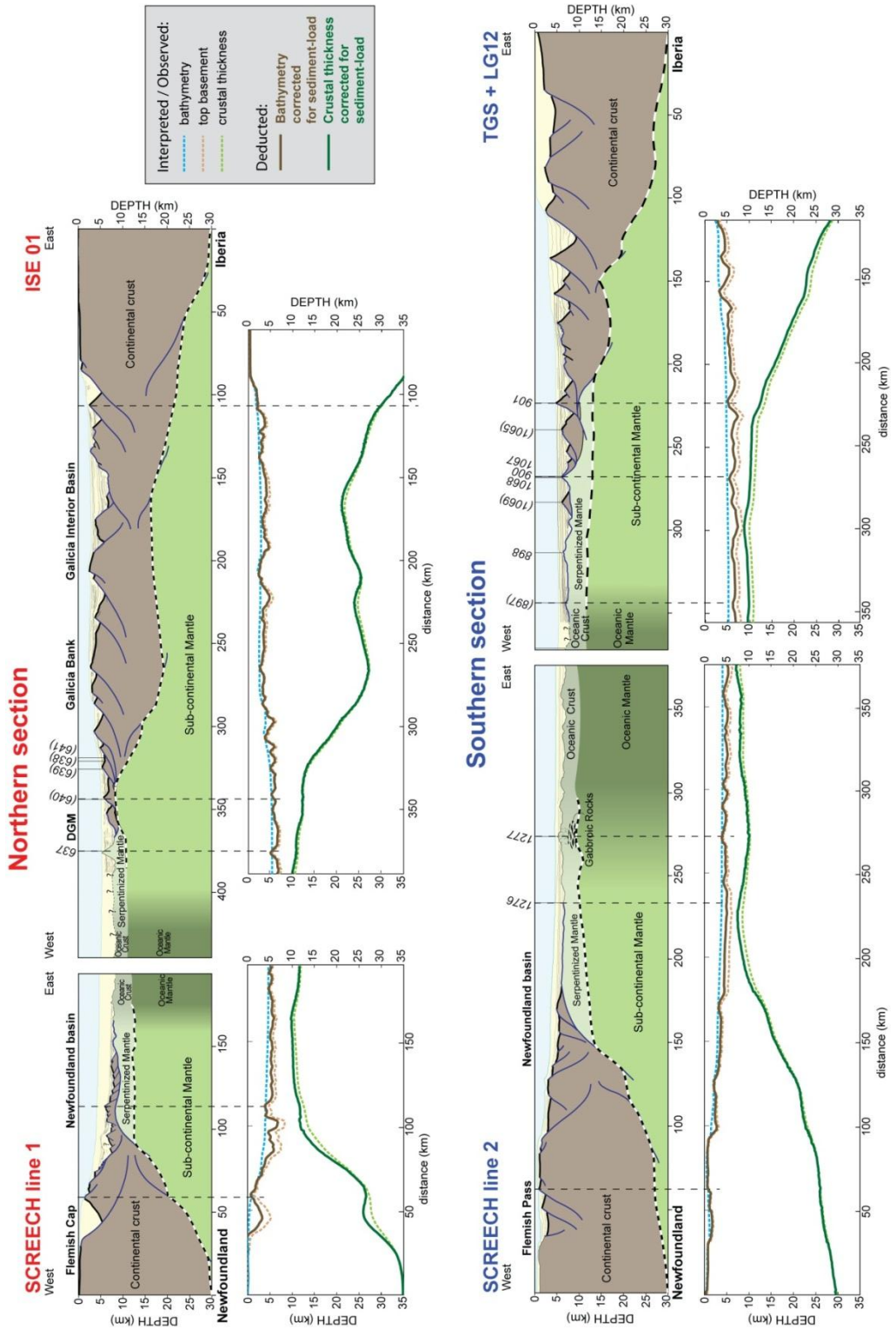

Figure 3.6: Crustal cross-sections for the Iberia-Newfoundland conjugate margins profiles adapted from Sutra et al. (2013), above the observed bathymetry and top basement (from seismic reflection profiles), water-loaded subsidence from flexural backstripping, crustal thickness by gravity inversion.

Northern section

Three major regions are identified on the ISE01 cross-section of the northern transect; the Galicia Interior Basin (GIB), the Galicia Bank (GB) and the Deep Galicia margin (DGM). The GIB is located westward between the Iberian proximal domain and GB (Murillas et al., 1990). The DGM stands westward of Galicia Bank. The transition from GB to DGM comprises a sharp necking zone followed by thin continental crust (Zelt et al., 2003; Ranero and Pérez-Gussinyé, 2010). Evidence for exhumed serpentinized mantle at the seafloor have been reported from ODP Site 637 (Boillot et al., 1987; Sutra and Manatschal, 2012). The conjugate margin SCREECH 1 shows narrow proximal, necking and thin continental crust domains (Funck et al., 2003; Lau et al., 2006). Hopper et al. (2006) and Sutra et al. (2013) interpreted the distal margin as made by hyper-thin continental crust while further outbound the OCT consists of a complex combination of thin continental crust and serpentinized exhumed mantle.

Southern section

In the southern section, SCREECH 2 also exhibits an abrupt transition of continental crust thickness compared to SCREECH 1 (Van Avendonk et al., 2006; Van Avendonk et al., 2009), TGS/LG12 shows a domain over more than 100km width of thinned continental crust with less than 10km thickness outbound of the necking zone (Whitmarsh et al., 1990; Cunha, 2008). The OCT is suggested to be about 80-100km wide on both the Western Iberia and Flemish Pass margins (Péron-Pinvidic and Manatschal, 2009; Sutra et al., 2013). Oceanic crust is interpreted to start eastward of the ODP Site 1277 for the Newfoundland transect (Jagoutz et al., 2007) and westward of ODP Site 897 on the Iberia margin following the interpretation of the ODP Leg 173 Shipboard Scientific Party.

3.4.4 First order constraints on the rifting evolution

The rift evolution of Iberia-Newfoundland rifted margins is reviewed by Péron-Pinvidic et al. (2007); Tucholke et al. (2007); Tucholke & Sibuet (2007); Sutra et al. (2013); where two

major rifting phases are distinguished. The first stage of rifting commenced during Late Triassic to Early Jurassic; the region underwent regional stretching and thinning over a wide region (>500 km) that created large rift basins (e.g. Jeanne d'Arc basin) (Jansa et al., 1988; Moullade et al., 1988). The second stage of rifting, which starts during Late Jurassic, is characterized by localised deformation, and will represent the main focus of this study.

In the north, the GIB may have experienced a first stage of extension during Oxfordian-Kimmeridgian (161Ma) before rifting stopped (Murillas et al., 1990). The GIB experienced its main extensional episode during Berriasian-Valanginian times associated with a significant crustal thinning (β of 3.5-5.5) that led to its present-day configuration (Pérez-Gussinyé et al., 2003). Deformation likely migrated during the Valanginian to Hauterivian times to the west in the DGM. In this domain, the main deformation phase was interpreted as Late Hauterivian to Barremian (Tucholke et al., 2007).

In the south, the Lusitanian Basin underwent its main extensional event during Oxfordian-Kimmeridgian (Wilson, 2008), while the basin remained inactive from the Cretaceous. The main phase of localized stretching and thinning in the distal domains, commenced in the Early Oxfordian (~161 Ma) to Berriasian (~140 Ma) (Boillot et al., 1987; Whitmarsh and Sawyer, 1996; Whitmarsh and Wallace, 2001; Alves et al., 2006). Based on the kinematic inversion of the LG12 section, Manatschal et al. (2001) proposed that extreme thinning of the continental crust in the Southern Iberia Abyssal plain started likely during the Tithonian that led to crustal and mantle exhumation in the Valanginian (~140-136 Ma).

Based on different interpretations, Tucholke et al. (2007) and Bronner et al. (2011) proposed that seafloor spreading initiated during the Albian/Aptian boundary (112Ma). The first suggest that the final breaching of the continental lithosphere is associated with a major change in the stress state visible in seismic sections while the second reinterpret the J-anomaly as an excess magmatic event leading to continental breakup (ODP Site 1277 on

SCREECH 2). We assume in this paper that breakup and seafloor spreading occurred at the same time for both sections.

3.5 Model application to the Iberia-Newfoundland conjugate rifted margins

The kinematic model is applied to the two Iberia-Newfoundland conjugate margin profiles and is constrained using the timing of rifting and the observed final crustal architecture given by their water-loaded subsidence and crustal thickness. We simultaneously model and calibrate both conjugate margins together. We first detail the modelling strategy, and then examine the lithosphere and asthenosphere deformation behaviour, the final crustal architecture of the conjugate margin profile and the relative timing of melt initiation and crustal breakup.

3.5.1 Strategy of modelling, model description, parameterization

Three types of models are examined in order to better understand the key processes of lithosphere deformation: (0) a passive upwelling model where there is no buoyancy and no continuous lateral migration of the deformation, (1a) a passive upwelling model where there is also no buoyancy but including a continuous lateral migration of the deformation, and (1b) an active upwelling model using a high contribution of buoyancy upwelling and which also includes lateral deformation migration. All models share the same parameterization of lithosphere deformation concerning the pure-shear width, half-spreading rate and deformation axis jumps; only the lateral deformation migration factor and the strength of buoyancy are different (Table 3.2). The 3 models have been subjected to the same evolution of extension proposed by Sutra et al. (2013). For these 3 models, melt is assumed to be extracted instantaneously ($F_{ret} = 0$) after its generation to form the oceanic crust.

Table 3.2: Deformation parameterization for models 0, 1a and 1b.

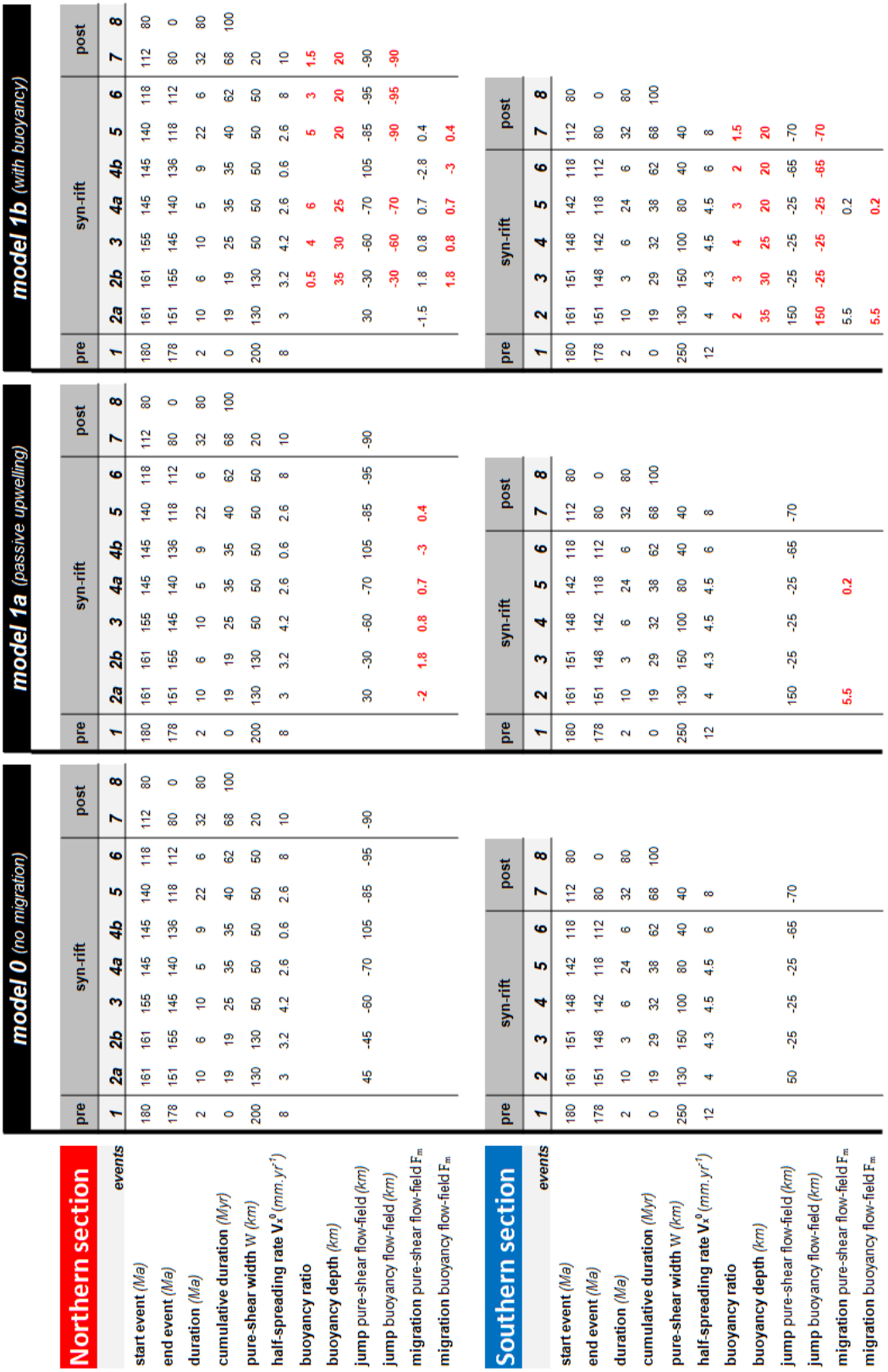

Northern section

events	model 0 (no migration)								model 1a (passive upwelling)								model 1b (with buoyancy)							
	pre	syn-rift						post	pre	syn-rift						post	pre	syn-rift						post
	1	*2a*	*2b*	*3*	*4a*	*4b*	*5*	*6*	*7*	*8*	*1*	*2a*	*2b*	*3*	*4a*	*4b*	*5*	*6*	*7*	*8*	*1*	*2a*	*2b*	*3*	*4a*	*4b*	*5*	*6*	*7*	*8*
start event *(Ma)*	180	161	161	155	145	145	140	118	112	80	180	161	161	155	145	145	140	118	112	80	180	161	161	155	145	145	140	118	112	80
end event *(Ma)*	178	151	155	145	140	136	118	112	80	0	178	151	155	145	140	136	118	112	80	0	178	151	155	145	140	136	118	112	80	0
duration *(Ma)*	2	10	6	10	5	9	22	6	32	80	2	10	6	10	5	9	22	6	32	80	2	10	6	10	5	9	22	6	32	80
cumulative duration *(Myr)*	0	19	19	25	35	35	40	62	68	100	0	19	19	25	35	35	40	62	68	100	0	19	19	25	35	35	40	62	68	100
pure-shear width W *(km)*	200	130	130	50	50	50	50	50	20		200	130	130	50	50	50	50	50	20		200	130	130	50	50	50	50	50	20	
half-spreading rate V_x^0 *(mm.yr^{-1})*	8	3	3.2	4.2	2.6	0.6	2.6	8	10		8	3	3.2	4.2	2.6	0.6	2.6	8	10		8	3	3.2	4.2	2.6	0.6	2.6	8	10	
buoyancy ratio																							0.5	4	6		5	3	1.5	
buoyancy depth *(km)*																							35	30	25		20	20	20	
jump pure-shear flow-field *(km)*		45	-45	-60	-70	105	-85	-95	-90			30	-30	-60	-70	105	-85	-96	-90			30	-30	-60	-70	105	-85	-95	-90	
jump buoyancy flow-field *(km)*																							-30	-60	-70		-90	-95	-90	
migration pure-shear flow-field F_m												-2	1.8	0.8	0.7	-3	0.4					-1.5	1.8	0.8	0.7	-2.8	0.4			
migration buoyancy flow-field F_m																							1.8	0.8	0.7	-3	0.4			

Southern section

events	model 0 (no migration)								model 1a (passive upwelling)								model 1b (with buoyancy)							
	pre	syn-rift						post	pre	syn-rift						post	pre	syn-rift						post
	1	*2*	*3*	*4*	*5*	*6*	*7*	*8*	*1*	*2*	*3*	*4*	*5*	*6*	*7*	*8*	*1*	*2*	*3*	*4*	*5*	*6*	*7*	*8*
start event *(Ma)*	180	161	151	148	142	118	112	80	180	161	151	148	142	118	112	80	180	161	151	148	142	118	112	80
end event *(Ma)*	178	151	148	142	118	112	80	0	178	151	148	142	118	112	80	0	178	151	148	142	118	112	80	0
duration *(Ma)*	2	10	3	6	24	6	32	80	2	10	3	6	24	6	32	80	2	10	3	6	24	6	32	80
cumulative duration *(Myr)*	0	19	29	32	38	62	68	100	0	19	29	32	38	62	68	100	0	19	29	32	38	62	68	100
pure-shear width W *(km)*	250	130	150	100	80	40	40		250	130	150	100	80	40	40		250	130	150	100	80	40	40	
half-spreading rate V_x^0 *(mm.yr^{-1})*	12	4	4.3	4.5	4.5	6	8		12	4	4.3	4.5	4.5	6	8		12	4	4.3	4.5	4.5	6	8	
buoyancy ratio																		2	3	4	3	2	1.5	
buoyancy depth *(km)*																		35	30	25	20	20	20	
jump pure-shear flow-field *(km)*		50	-25	-25	-25	-65	-70			150	-25	-25	-25	-65	-70			150	-25	-25	-25	-65	-70	
jump buoyancy flow-field *(km)*																		150	-25	-25	-25	-65	-70	
migration pure-shear flow-field F_m													5.5		0.2			5.5			0.2			
migration buoyancy flow-field F_m																		5.5			0.2			

3.5.2 Lithosphere and asthenosphere deformation behaviour

The lithosphere and asthenosphere deformation of the 3 models is shown in Figures 3.7 and 3.8 for the northern and the southern section.

Regional stretching and thinning

The first Late Triassic to Early Jurassic stage of rifting, characterized by distributed extension, has not been calibrated. All models 0, 1a and 1b start at 180Ma with a slow event over a wide deformation region, 200km for the north and 250km in the south (Sutra et al., 2013). This event lasts until 161Ma. At this point, the continental crust has slightly thinned by a stretching factor of 1.1-1.2 and is covered by shallow-water. The lithosphere remains 130-135km thick.

Localised stretching and thinning leading to mantle exhumation

In our modelling, the localisation of the deformation commences at 161Ma for both sections. Pure-shear widths are sequentially narrowed from 250km to 20km which results in stronger thinning of the continental crust and lithosphere for both conjugate pairs. The GIB and the DGM are created in the north, and a single rift basin is formed in the south. In passive upwelling models 0 and 1a, continental crust is thinned more than $\gamma = 0.88/0.95$ before the initiation of melt decompression (113Ma), thus predicting mantle exhumation. Crustal breakup starts between 149Ma and 143Ma in the north and between 139Ma and 134Ma in the south. Model 1b which includes buoyant upwelling results in fast thinning of the lithosphere. Decompression melting is initiated at 146Ma hindering mantle exhumation.

Figure 3.7 & 3.8 (next pages): Model lithosphere and asthenosphere behaviour for models 0, 1a and 1b applied to the northern and southern evolution of Iberia-Newfoundland. The 3 models have been calibrated using the extension rate of Sutra et al., 2013. Their deformation parameterization is shown in Table 2a. All models start at 180Ma and run to present-day. 5 snapshots for each model are shown at 161, 150, 140, 120 and 100Ma. Melt extraction is instantaneous after its generation. White lines are isotherms (°C) and red contour lines are melt fraction. Contour interval is 0.03%.

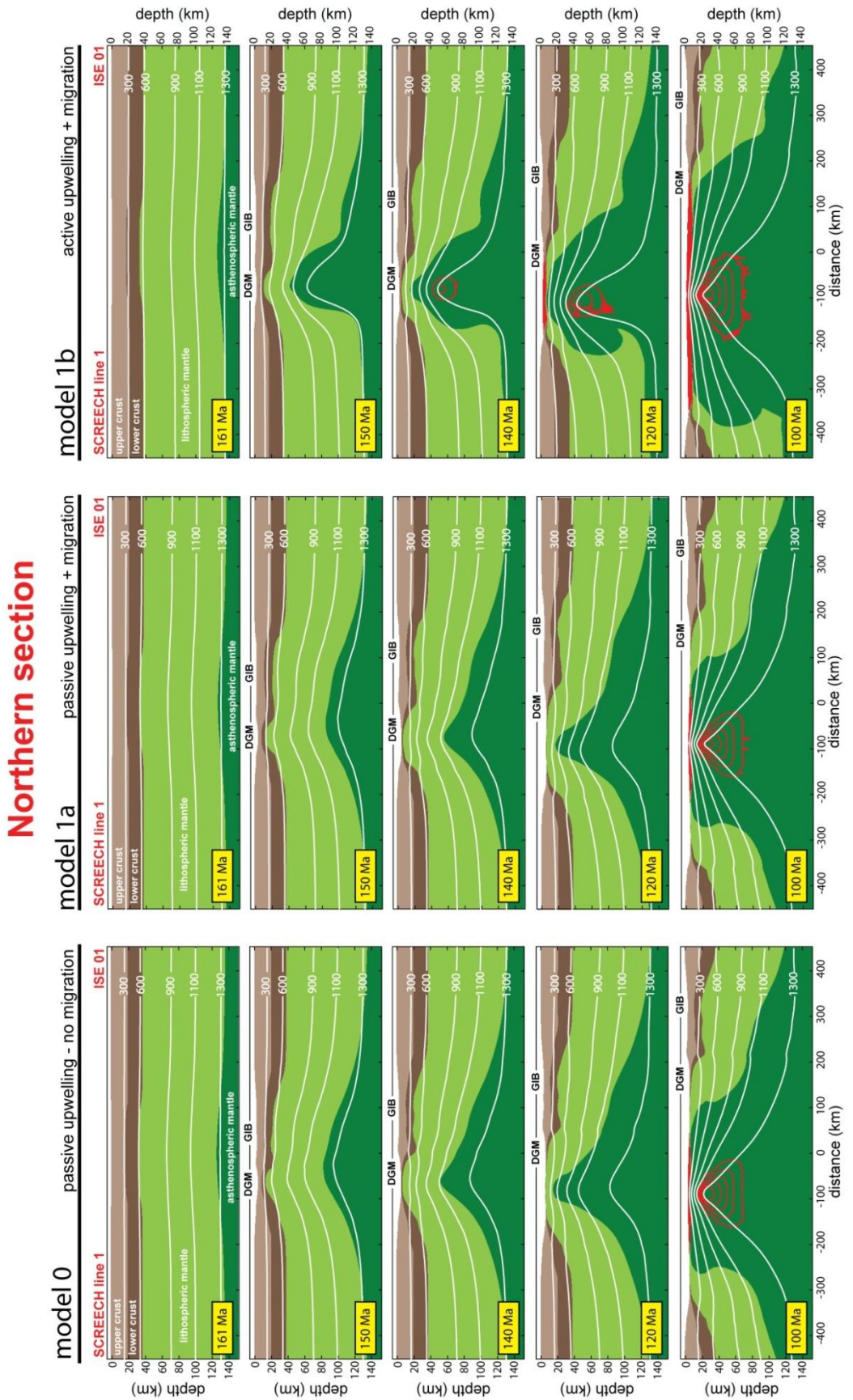
Northern section
model 0
passive upwelling - no migration
model 1a
passive upwelling + migration
model 1b
active upwelling + migration
SCREECH line 1
ISE 01
upper crust
lower crust
lithospheric mantle
asthenospheric mantle
DGM
GIB
161 Ma
150 Ma
140 Ma
120 Ma
100 Ma
depth (km)
distance (km)

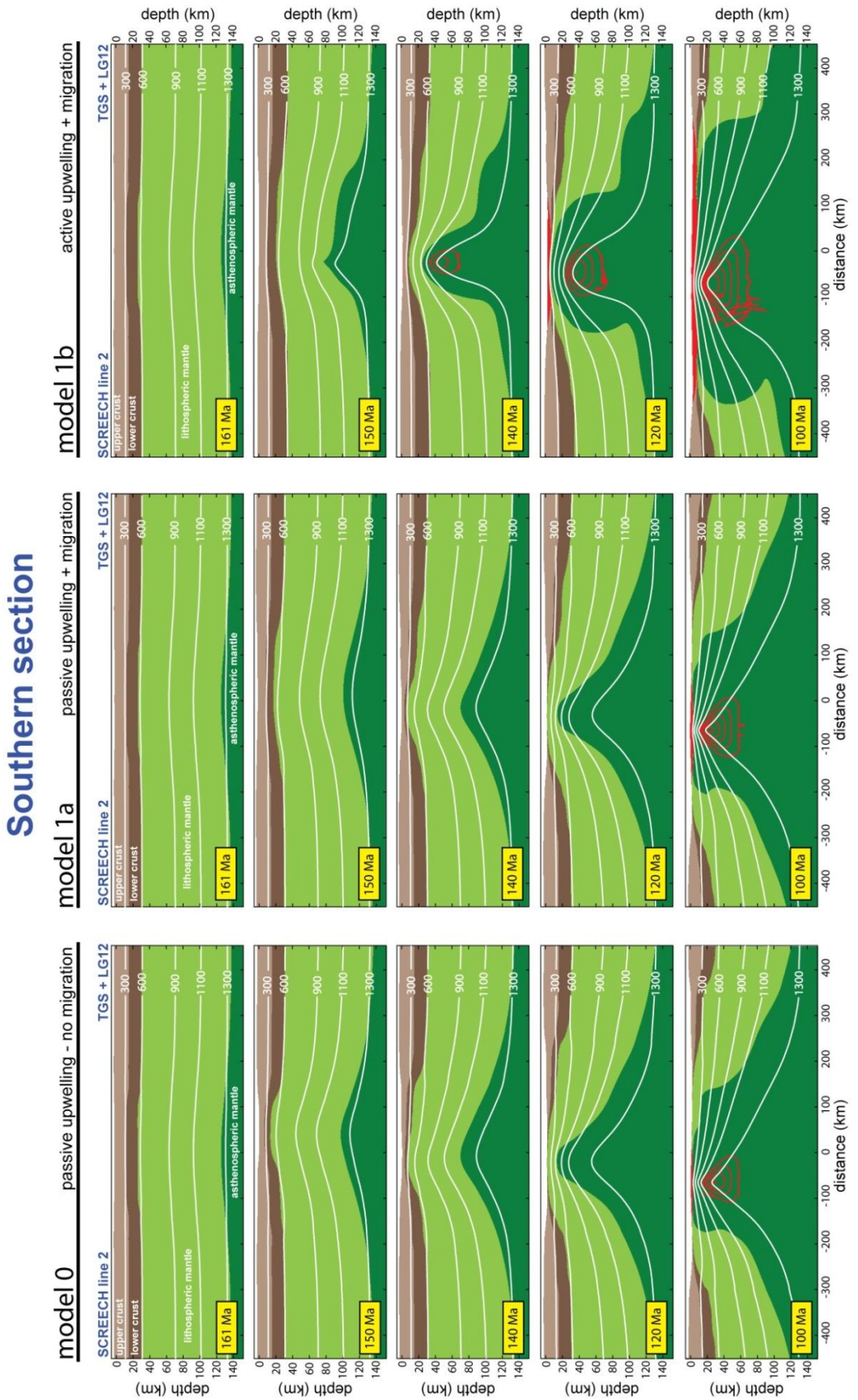
Southern section
model 0
passive upwelling - no migration
model 1a
passive upwelling + migration
model 1b
active upwelling + migration
SCREECH line 2
TGS + LG12
upper crust
lower crust
lithospheric mantle
asthenospheric mantle
depth (km)
distance (km)
161 Ma
150 Ma
140 Ma
120 Ma
100 Ma

Breakup and seafloor spreading

Breakup is prescribed at 112Ma by increasing the spreading rate and narrowing the deformation width. Seafloor spreading follows using a pure-shear deformation width of 20km and constant full extension rate of 20mm.yr^{-1} (Minshull et al., 2001) for the north and using a deformation width of 40km and extension rate of 16mm.yr^{-1} for the south. The lower spreading rate for the southern section gives a better fit with the observed oceanic crustal thickness; however we do not exclude the possibility that the spreading rate later increases to similar values as in the north.

5.3 Present-day model calibration

The bathymetry and crustal architecture predictions from the 3 model applications 0, 1a and 1b are compared in Figure 3.7 and 3.8 with the observed water loaded subsidence, crustal thickness and OCT architecture. We have tested the sensitivity of the model to the initial thickness of the continental crust with values of 35, 37.5 and 40km. The Newfoundland SCREECH lines 1&2 are better calibrated using an initial continental crustal thickness of 36.5 and 35km respectively, while an initial continental crustal thickness of 40km gives a better match to the observed Moho depth for the two Iberia margins profiles.

The final crustal architecture of the two conjugate margins sections resulting from the passive upwelling model (model 0) shows some mismatches with the observed Moho depth (Figure 3.9a). The observed necking transition of the continental crustal thickness within the DGM is steeper for the model prediction and is also slightly gentler for its conjugate margin SCREECH 1. The continuous lateral deformation migration of model 1a corrects the observed necking mismatches, as shown in Figure 3.9b, but the absence of predictions of magmatism on SCREECH 1 and 2 suggest that passive upwelling alone does not produce enough magma. However, thinning of the continental crust until crustal breakup is permitted, matching the observed mantle exhumation. In model 1b, buoyancy induced upwelling, which is applied from 161Ma, has a strong effect on the OCT architecture (Figure

3.9c); the mantle cannot be exhumed because of the early decompression melt. Moreover, buoyancy induced upwelling increases the rate of melt production, thus exceeding the thickness of the observed oceanic crust.

3.5.4 Synthesis calibration of the Iberia-Newfoundland margins

The model applications described above are end-members models showing the relative contribution of the timing of events, pure-shear width, half-spreading rate and migration of the deformation in controlling the crustal architecture of the margin. Other processes including buoyancy upwelling cannot be constrained only by the presence or absence of exhumed mantle and oceanic crust in the observed OCT; a passive model cannot produce enough melt while an active model including buoyancy upwelling predicts too early melt. Further observations related to the melting history are therefore necessary to constrain the strength of buoyancy induced upwelling. Moreover, the extension rate history used in these 3 models reveals a paradox. Following the extension rate given by Sutra et al. (2013), our modelling shows that the continental crustal breakup propagated southward, while it has been suggested that the North Atlantic opened from the south towards the north (Sibuet et al., 2007; Sibuet et al., 2012).

Figure 3.9 (next page): Comparison and calibration of the predicted rifted margin crustal architecture for **a)** model 0, **b)** model 1a and **c)** model 1b, for the northern and southern section against water-loaded subsidence and crustal basement thickness. Sensitivity tests to the initial continental crustal thickness of 35, 37.5 and 40km are shown.

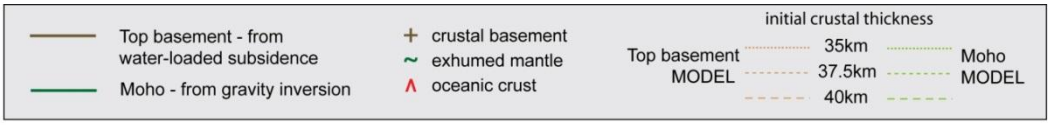
Top basement - from water-loaded subsidence
Moho - from gravity inversion
crustal basement
exhumed mantle
oceanic crust
initial crustal thickness
Top basement MODEL
35km
37.5km
40km
Moho MODEL

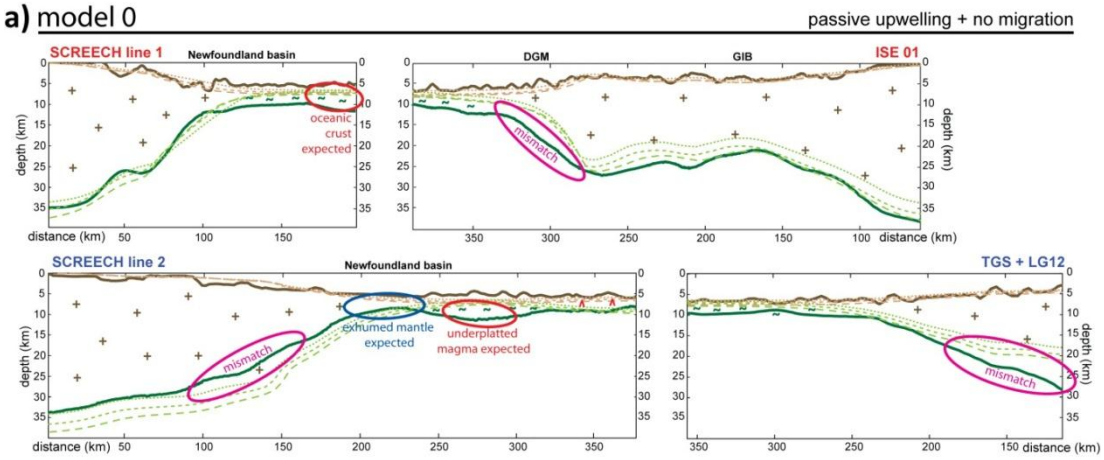
a) model 0
passive upwelling + no migration
SCREECH line 1
Newfoundland basin
DGM
GIB
ISE 01
oceanic crust expected
mismatch
SCREECH line 2
exhumed mantle expected
underplatted magma expected
TGS + LG12
depth (km)
distance (km)

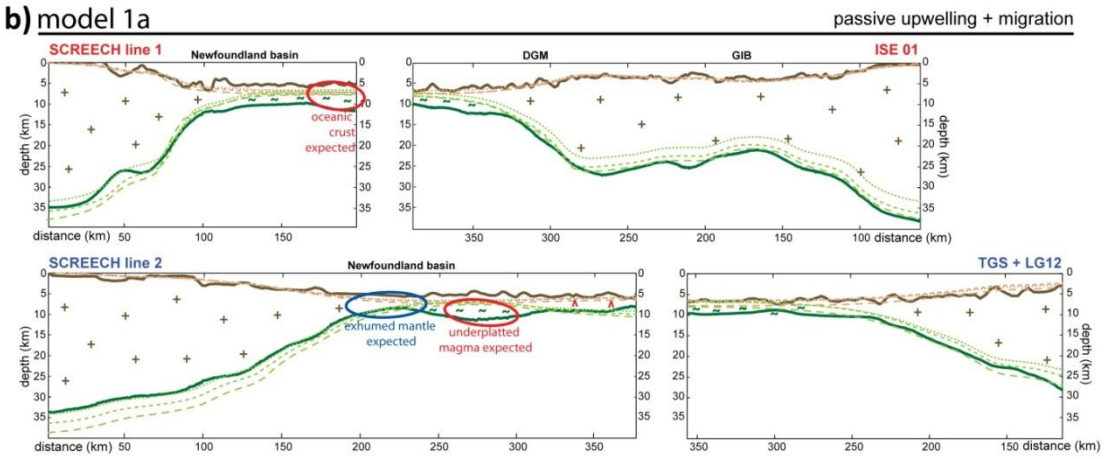
b) model 1a
passive upwelling + migration
SCREECH line 1
Newfoundland basin
DGM
GIB
ISE 01
oceanic crust expected
SCREECH line 2
exhumed mantle expected
underplatted magma expected
TGS + LG12
depth (km)
distance (km)

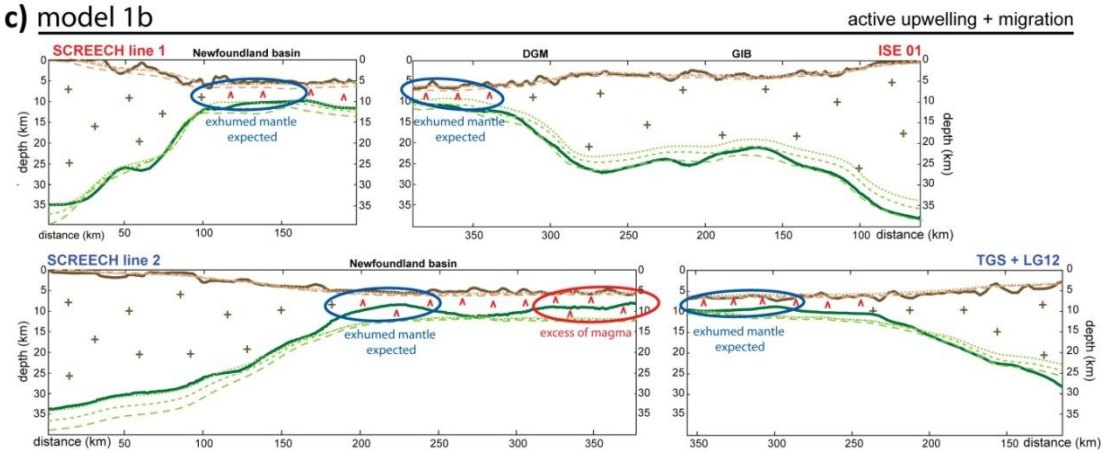
c) model 1b
active upwelling + migration
SCREECH line 1
Newfoundland basin
DGM
GIB
ISE 01
exhumed mantle expected
SCREECH line 2
excess of magma
TGS + LG12
depth (km)
distance (km)

3.6 Additional constraints on lithosphere deformation evolution from subsidence and melting histories

While dynamic modelling uses rheological properties to shape rifted margins into a particular and unique crustal architecture, determined by model initial conditions, the deformation evolution of kinematic models is prescribed in order to get the observed end-product. Determining the evolution of lithosphere deformation for the Iberia-Newfoundland margins requires additional constraints. These constraints are the observed subsidence history and age of magmatism. Because there are no reliable observations related to the paleobathymetry during the early stage of rifting in the southern section drilling sites, we focus our investigation on subsidence history for the northern section based on drilling results of ODP Sites 638-639 (Boillot et al., 1987). The relative timing of melt generation and continental crustal breakup that controls mantle exhumation is nevertheless well constrained for both sections (Schärer et al., 2000; Manatschal et al., 2001; Jagoutz et al., 2007).

3.6.1 Subsidence history at the ODP Sites 638-639

During the Tithonian (150-145Ma), a shallow-water shelf platform occupied the region (see Boillot et al. (1988) and references therein) and resulted in deposition of neritic sediments (Wilson et al., 2001). Early to middle Valanginian, hemipelagic limestones are deposited suggesting a bathymetry up to 600-1000m depth (Moullade et al., 1987) by 140-135Ma. Shortly afterwards during late Valanginian and Hauterivian (135-130Ma), the Galicia margin subsided rapidly to deep water (2000-3000m), indicated by the presence of turbidite sands and reworked neritic/infrabathyal foraminifers. Boillot et al. (1987) suggest that the deepening of the margin is due to extreme thinning of the continental crust. The present-day top basement at the ODP Site 638 is located at 5200m depth. Local crustal thickness is between 6.5km (Boillot & Winterer, 1988) and 10km (Zelt et al., 2003).

3.6.2 Timing of melt generation, melt extraction and crustal breakup

The occurrence of exhumed mantle provides useful information to constrain lithosphere deformation modes. Thanks to ODP legs 103, 149, 173 and 210 and geophysical surveys, the timing and localization of exhumed mantle domains are relatively well constrained.

In the northern section, extreme thinning of the continental crust as interpreted by Boillot et al. (1987) may suggest that continental crustal breakup occurred during or after the Hauterivian (133Ma - onward). Based on U-Pb dating from zircons on meta-gabbros, Schärer et al. (2000) dated the age of the oldest magmatism at ~122Ma.

In the southern section, Manatschal et al. (2001) suggest an age of mantle exhumation between 140 and 136Ma, based on $^{40}Ar/^{39}Ar$ detachment fault datation. Serpentinized exhumed mantle on the seafloor is observed to be accompanied by gabbroic intrusions, the oldest of which have been dated at 128-127Ma at the ODP Site 1277 (Jagoutz et al., 2007) and 1070 (Beard et al., 2002). This early magmatic event, prior to breakup and the formation of an oceanic crust 4-7km thick (Wang et al., 2011), does not give the minimum age of melt generation. Melt generation might have started earlier but, depending on the rate of melt production, it could have been retained in the mantle. Within the Lusitanian basin, Grange et al. (2008) dated first alkaline magmatism at about 145Ma and suggested that it was generated during a phase of maximum lithospheric thinning. Consequently, melt generation is likely to have started earlier than 128Ma at least in the southern section.

3.7 Calibration of the rifting evolution

The new observational constraints describing the evolution of subsidence and magmatism are used to quantitatively calibrate our models. In addition to model 0, 1a and 1b, two new models 2 and 3 are investigated in this section. These two models are differentiated by a specific extension rate history compared to Sutra et al. (2013). The parameterization of

each lithosphere deformation events is shown in Table 3.3. All the models share the same pre- and post-rift deformation parameterization. The total extension for the 3 extension rate histories is the same, but their extensional evolution during the main phase of rifting (from 161 to 112Ma) differs; model 2 has slower early extension rates than model 1. Model 3 has a slow initial extensional rifting phase from 161 to 140Ma, before it speeds up for 10Myr and then slows again at 130Ma. A summary of the extension evolution is shown in Figure 3.10 which illustrates that the same amount of total extension can be distributed in time in different ways. We also show the uncertainty range of extension with time given by Sutra et al. (2013). Alternatively Figure 3.11 recapitulates the characteristics of each model, including model predictions and our preferred model.

Each of the two extension rate histories 2 and 3 is applied to both passive upwelling models (models 2a and 3a) and active upwelling models (models 2b and 3b). The crustal margin architecture predicted all from these models is consistent with the observed Iberia-Newfoundland conjugate margins architecture (appendix B) and calibrates well against the observed water-loaded subsidence and the crustal basement thickness. No melt retention is applied in these models, indicating that the initiation of melting also corresponds to its extraction.

The subsidence history is determined for ODP leg 103 at Sites 638-639 which are located on the northern section (profile ISE01). Figure 3.12 shows the model prediction of subsidence for a continental crust that has thinned to 8km thick. We have tested the subsidence sensitivity to an initial crustal thickness of 30km (as suggested by Boillot et al., 1987; Zelt et al., 2003) and 35km and 40km (as suggested from gravity inversion for the Newfoundland and Iberia margins respectively). The relative timing of melt initiation (and therefore its extraction) and continental crustal breakup is examined for each model and compared to timing based on geophysical/geological data (Figure 3.13).

Table 3.3: Deformation parameterization for passive or active upwelling models 2 and 3. See Table 2 for deformation parameterization of models 1.

model 2a *(passive upwelling)*

Northern section

events	pre	syn-rift							post	
	1	*2*	*3*	*4a*	*4b*	*5*	*6*	*7*	*8*	*9*
start event *(Ma)*	180	161	151	145	145	140	136	118	112	80
end event *(Ma)*	178	151	145	140	136	136	118	112	80	0
duration *(Ma)*	2	10	6	5	9	4	18	6	32	80
cumulative duration *(Myr)*	0	19	29	35	35	40	44	62	68	100
pure-shear width W *(km)*	200	100	130	100	50	50	40	40	20	
half-spreading rate V_x^0 *(mm.yr^{-1})*	0.8	2.3	3.2	1.4	2.8	0.6	4.2	8	10	
buoyancy ratio								2.5	0.8	
buoyancy depth *(km)*								20	20	
jump pure-shear flow-field *(km)*		45	-50	25	-65	80	-85	-90	-90	
jump buoyancy flow-field *(km)*								-90	-90	
migration pure-shear flow-field F_m			0.2	-1.2	1	-1.4	0.2			
migration buoyancy flow-field F_m										

Southern section

events	pre	syn-rift						post	
	1	*2*	*3*	*4*	*5*	*6*	*7*	*8*	
start event *(Ma)*	180	161	151	145	140	118	112	80	
end event *(Ma)*	178	151	145	140	118	112	80	0	
duration *(Ma)*	2	10	6	5	22	6	32	80	
cumulative duration *(Myr)*	0	19	29	35	40	62	68	100	
pure-shear width W *(km)*	250	100	150	100	80	40	40		
half-spreading rate V_x^0 *(mm.yr^{-1})*	1.2	1.7	3.5	4.5	5.2	6	10		
buoyancy ratio						3	1.2		
buoyancy depth *(km)*						20	20		
jump pure-shear flow-field *(km)*		150	-25	-25	-15	-65	-70		
jump buoyancy flow-field *(km)*									
migration pure-shear flow-field F_m		5.5			0.2				
migration buoyancy flow-field F_m									

model 2b *(active upwelling)*

events	pre	syn-rift							post	
	1	*2*	*3*	*4a*	*4b*	*5*	*6*	*7*	*8*	*9*
start event *(Ma)*	180	161	151	145	145	140	136	118	112	80
end event *(Ma)*	178	151	145	140	136	136	118	112	80	0
duration *(Ma)*	2	10	6	5	9	4	18	6	32	80
cumulative duration *(Myr)*	0	19	29	35	35	40	44	62	68	100
pure-shear width W *(km)*	200	100	130	100	50	50	40	40	20	
half-spreading rate V_x^0 *(mm.yr^{-1})*	0.8	2.3	3.2	1.4	2.8	0.6	4.2	8	10	
buoyancy ratio			6		10		4	2.5	0.8	
buoyancy depth *(km)*			35		25		20	20	20	
jump pure-shear flow-field *(km)*		45	-50	25	-65	80	-85	-90	-90	
jump buoyancy flow-field *(km)*			-50		-60		-90	-90	-90	
migration pure-shear flow-field F_m			0.2	-1.2	1	-1.4	0.2			
migration buoyancy flow-field F_m			0.2		1		0.2			

Southern section

events	pre	syn-rift						post	
	1	*2*	*3*	*4*	*5*	*6*	*7*	*8*	
start event *(Ma)*	180	161	151	145	140	118	112	80	
end event *(Ma)*	178	151	145	140	118	112	80	0	
duration *(Ma)*	2	10	6	5	22	6	32	80	
cumulative duration *(Myr)*	0	19	29	35	40	62	68	100	
pure-shear width W *(km)*	250	100	150	100	80	40	40		
half-spreading rate V_x^0 *(mm.yr^{-1})*	1.2	1.7	3.5	4.5	5.2	6	10		
buoyancy ratio		4	4	4	3.5	3	1.2		
buoyancy depth *(km)*		35	30	25	20	20	20		
jump pure-shear flow-field *(km)*		150	-25	-25	-15	-65	-70		
jump buoyancy flow-field *(km)*		150	-25	-25	-15	-65	-70		
migration pure-shear flow-field F_m		5.5			0.2				
migration buoyancy flow-field F_m		5.5			0.2				

model 3a *(passive upwelling)*

Northern section

events	pre	syn-rift								post	
	1	*2*	*3*	*4a*	*4b*	*5a*	*5b*	*6*	*7*	*8*	*9*
start event *(Ma)*	180	161	151	140	140	136	136	130	118	112	80
end event *(Ma)*	178	151	140	136	136	133	130	118	112	80	0
duration *(Ma)*	2	10	11	4	4	3	6	12	6	32	80
cumulative duration *(Myr)*	0	19	29	40	40	44	44	50	62	68	100
pure-shear width W *(km)*	200	100	130	130	50	50	50	50	40	20	
half-spreading rate V_x^0 *(mm.yr^{-1})*	0.8	1.2	1.7	3.5	1	2	7.5	4	8	10	
buoyancy ratio								1	2	0.8	
buoyancy depth *(km)*								20	20	20	
jump pure-shear flow-field *(km)*		35	-57	40	-57	60	-82	-95	-95	-95	
jump buoyancy flow-field *(km)*								-95	-95	-95	
migration pure-shear flow-field F_m			0.4	-1.6	1.7	-1.4	0.4				
migration buoyancy flow-field F_m											

Southern section

events	pre	syn-rift						post	
	1	*2*	*3*	*4*	*5*	*6*	*7*	*8*	*9*
start event *(Ma)*	180	161	151	140	136	130	118	112	80
end event *(Ma)*	178	151	140	136	130	118	112	80	0
duration *(Ma)*	2	10	11	4	6	12	6	32	80
cumulative duration *(Myr)*	0	19	29	40	44	50	62	68	100
pure-shear width W *(km)*	250	100	150	100	80	50	50	40	
half-spreading rate V_x^0 *(mm.yr^{-1})*	1.2	1.4	2.2	5	13	2	8	10	
buoyancy ratio						4	1.5	1.2	
buoyancy depth *(km)*						20	20	20	
jump pure-shear flow-field *(km)*		35	-5	-12	-8	-40	-60	-60	
jump buoyancy flow-field *(km)*						-40	-45	-60	
migration pure-shear flow-field F_m					0.3				
migration buoyancy flow-field F_m									

model 3b *(active upwelling)*

events	pre	syn-rift								post	
	1	*2*	*3*	*4a*	*4b*	*5a*	*5b*	*6*	*7*	*8*	*9*
start event *(Ma)*	180	161	151	140	140	136	136	130	118	112	80
end event *(Ma)*	178	151	140	136	136	133	130	118	112	80	0
duration *(Ma)*	2	10	11	4	4	3	6	12	6	32	80
cumulative duration *(Myr)*	0	19	29	40	40	44	44	50	62	68	100
pure-shear width W *(km)*	200	100	130	130	50	50	50	50	40	20	
half-spreading rate V_x^0 *(mm.yr^{-1})*	0.8	1.2	1.7	3.5	1	2	7.5	4	8	10	
buoyancy ratio			6		20		2	4	2	0.8	
buoyancy depth *(km)*			35		30		25	20	20	20	
jump pure-shear flow-field *(km)*		35	-57	40	-57	60	-82	-95	-95	-95	
jump buoyancy flow-field *(km)*			-57		-57		-82	-95	-95	-95	
migration pure-shear flow-field F_m			0.4	-1.6	1.7	-1.4	0.4				
migration buoyancy flow-field F_m			0.4		1.7		0.4				

Southern section

events	pre	syn-rift						post	
	1	*2*	*3*	*4*	*5*	*6*	*7*	*8*	*9*
start event *(Ma)*	180	161	151	140	136	130	118	112	80
end event *(Ma)*	178	151	140	136	130	118	112	80	0
duration *(Ma)*	2	10	11	4	6	12	6	32	80
cumulative duration *(Myr)*	0	19	29	40	44	50	62	68	100
pure-shear width W *(km)*	250	100	150	100	80	50	50	40	
half-spreading rate V_x^0 *(mm.yr^{-1})*	1.2	1.4	2.2	5	13	2	8	10	
buoyancy ratio			5	6	0	4	1.5	1.2	
buoyancy depth *(km)*			35	30	25	20	20	20	
jump pure-shear flow-field *(km)*		35	-5	-12	-8	-40	-60	-60	
jump buoyancy flow-field *(km)*			-12	-12	-8	-40	-45	-60	
migration pure-shear flow-field F_m					0.3				
migration buoyancy flow-field F_m					0.3				

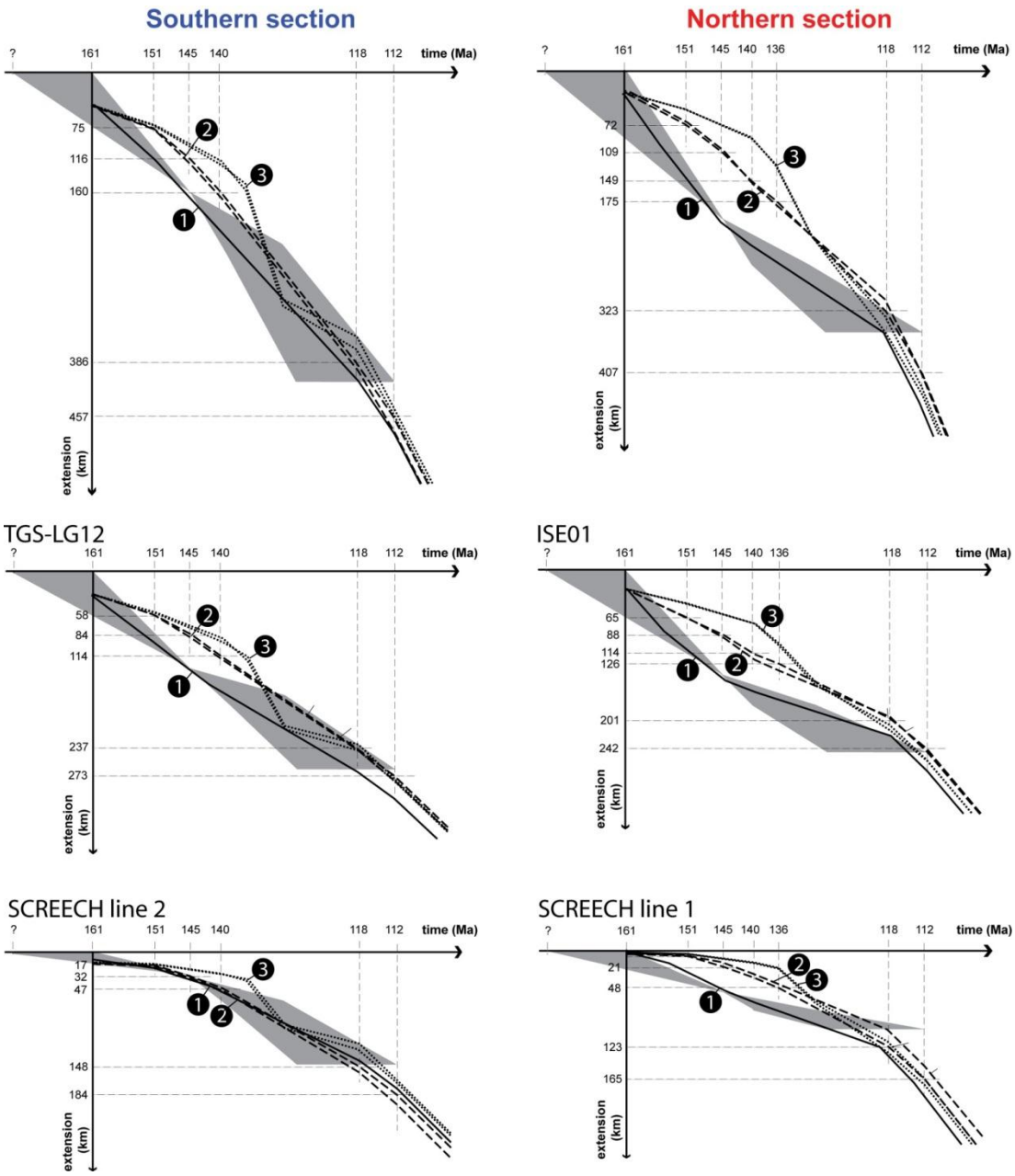

F*igure 3.10:* Possible evolution for extension history of models 1, 2 and 3 for both the southern and northern full sections. Model 1 follows the extension evolution given by Sutra et al., 2013 and including the error bar (grey surface).

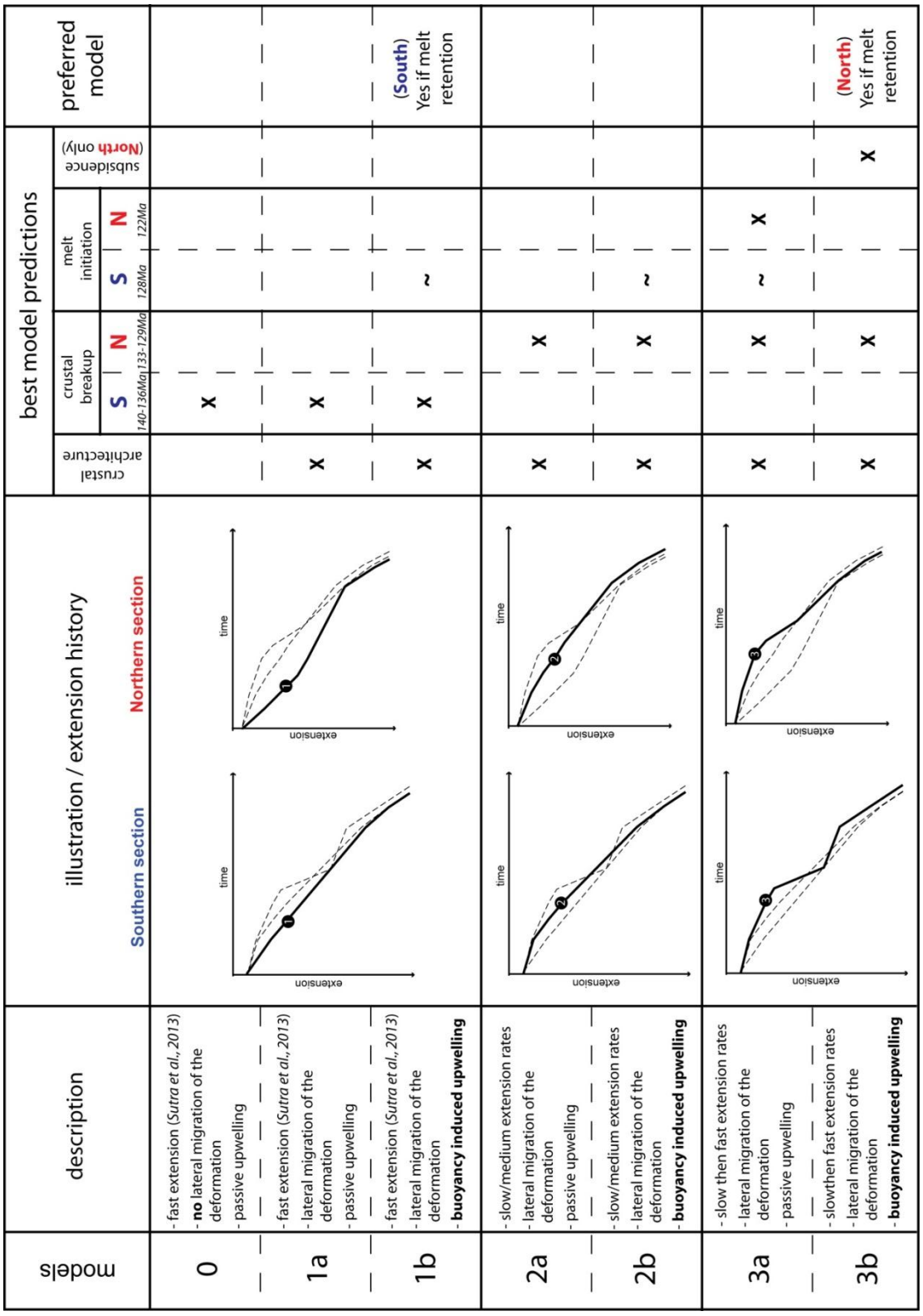

F***igure 3.11:*** recapitulation table with each model's characteristics

The 6 model predictions are investigated and discussed in order to pick which model has the best match with the observations:

Models 1a+1b: While the observed continental crustal breakup was estimated at 140-136Ma in the south (Manatschal et al., 2001) and 133-130Ma in the north (Boillot et al., 1987), the model 1 based on the extension rate of Sutra et al. (2013) predicts crustal breakup in the north at 149-143Ma, prior to the south at 136-130.5Ma. This result is incompatible with the idea of a migration of rifting towards the north (Tucholke et al., 2007; Mohn et al., 2015). In addition, the subsidence history for the northern section using this extension rate history shows that extreme thinning of the continental crust associated with the deposition of shallow marine sediments (Péron-Pinvidic and Manatschal, 2009) is not predicted by our models, even with the highest buoyancy contribution beneath the deformation (model 1b); bathymetries greater than 2000m are predicted at 145Ma while the continental crust is 8km thick. These results suggest that the extension rates used for the northern section are too fast and those used for the southern section are slightly too slow. Moreover for both northern and southern profiles, this extension rate history predicts either late melt initiation at ~113Ma for the passive upwelling model 1a or too early melting at 145Ma for the active upwelling model 1b.

Models 2a+2b: Using a progressive increase in extension rate, these models predict the exhumation of mantle at similar time for the northern and southern sections. If these models satisfy crustal breakup during the Hauterivian in the north, these predictions do not match the timing of mantle exhumation in the south. In addition, the predicted subsidence history is different from the observed subsidence in the north. Without buoyancy induced upwelling, models 2a predict basins ca. 3000m deep at 140Ma, suggesting that the

extension rate was too fast. Although the subsidence from crustal thinning is better compensated by thermal uplift with strong buoyancy induced upwelling (model 2b), the subsidence target is weakly satisfied. A difference greater than 1000m with the observed bathymetry is predicted if the initial continental crust is 35 or 40km. In addition, the contribution of buoyancy upwelling (model 2b) initiates decompressional melting too early in the north (137Ma) and the south (140Ma) and before mantle exhumation, while passive upwelling model 2a predicts too late melting at 118Ma and 122Ma for the north and the south respectively.

Models 3a+3b: Model 3 extension rate history start with a slower spreading rate than used for model 2 extension rate history. The spreading rate is increased at 136Ma before it is slightly decreased from 130Ma because the model is constrained by the total extension and the final width of the conjugate rifted margins profile. This extension rate history predicts the northward rifting propagation with crustal breakup between 132-130Ma in the north and 135-133Ma in the south. However in the south, mantle exhumation would still be predicted about 5Myr later than suggested by geophysical and geological data. In the north, the subsidence history predicted by model 3b gives the best match to observations especially using an initial continental crustal thickness of 35-37.5km. However for both sections, melt is initiated too early at 134-135Ma with strong buoyancy upwelling (model 3b), hindering mantle exhumation, while the timing is perfect for the passive upwelling model 3a.

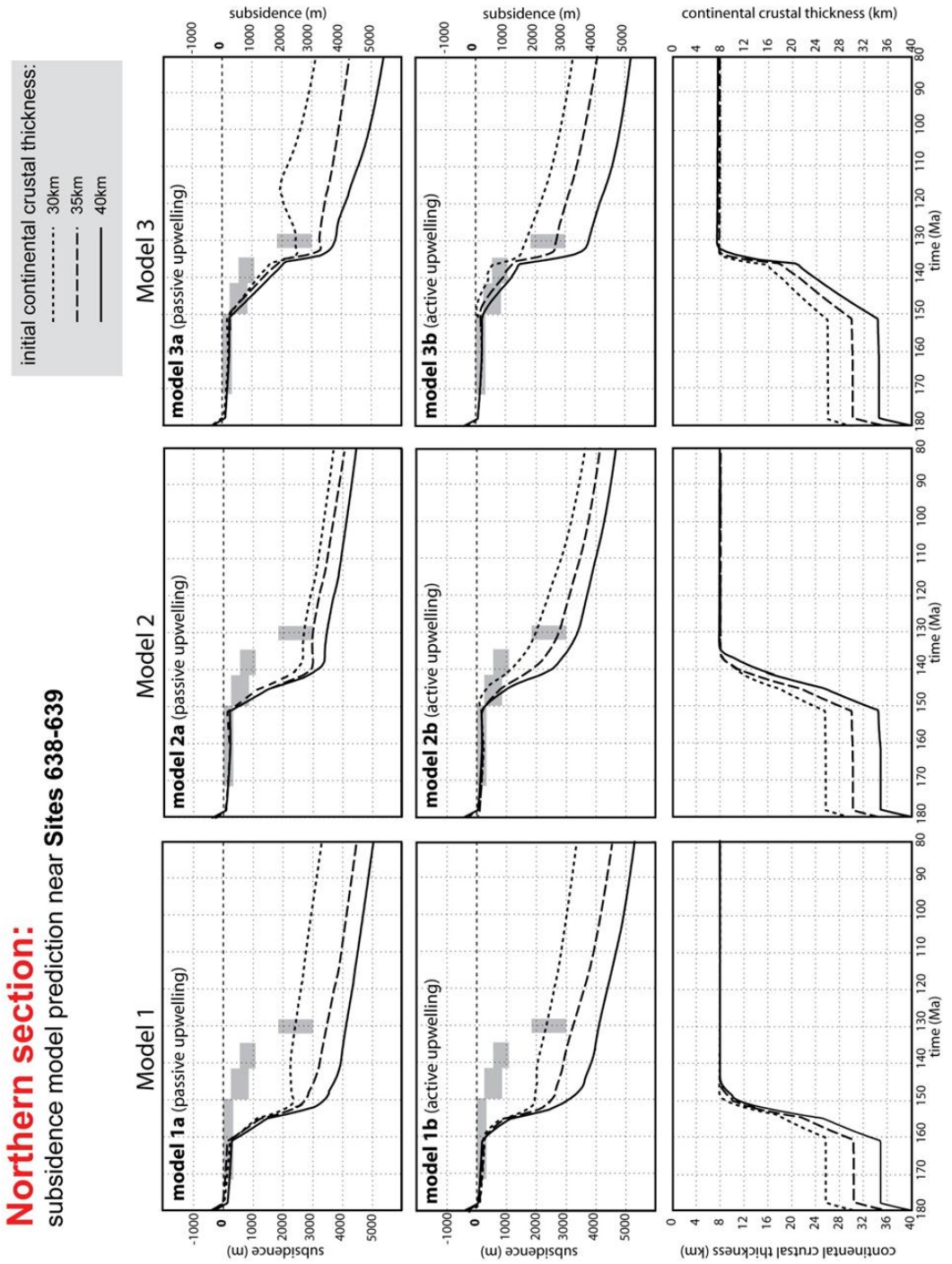

Figure 3.12: Predicted subsidence and crustal basement thickness model development with time at ODP Sites 638-639 on Iberia rifted margins of the northern section for model extension history 1, 2 and 3. The two upper panels show the subsidence predictions for all the passive and active models, while the lower panel show the evolution of the continental crustal thickness predicted at ODP Sites 638-639. Sensitivity to the initial continental crustal thickness of 30, 35 and 40km are shown. Grey areas are the subsidence targets established by Boillot & Winterer (1988).

A key observation from Figure 3.12 concerns the melt initiation relationship to the half-spreading and buoyancy upwelling rates. Predicted melt generation times are different for all the passive upwelling models (1a, 2a and 3a); melt is initiated earlier in model 3a for both the north and the south than for model 1a (122 and 131.5Ma against 112.5 and 113.5Ma respectively). This is due to the different extension rate evolution between these models; the spreading rate of model 1a starts fast before it slows, which delays the generation of melt. Conversely in model 2a and 3a, the spreading rate, after it started slowly, increases continuously with time initiating melt earlier.

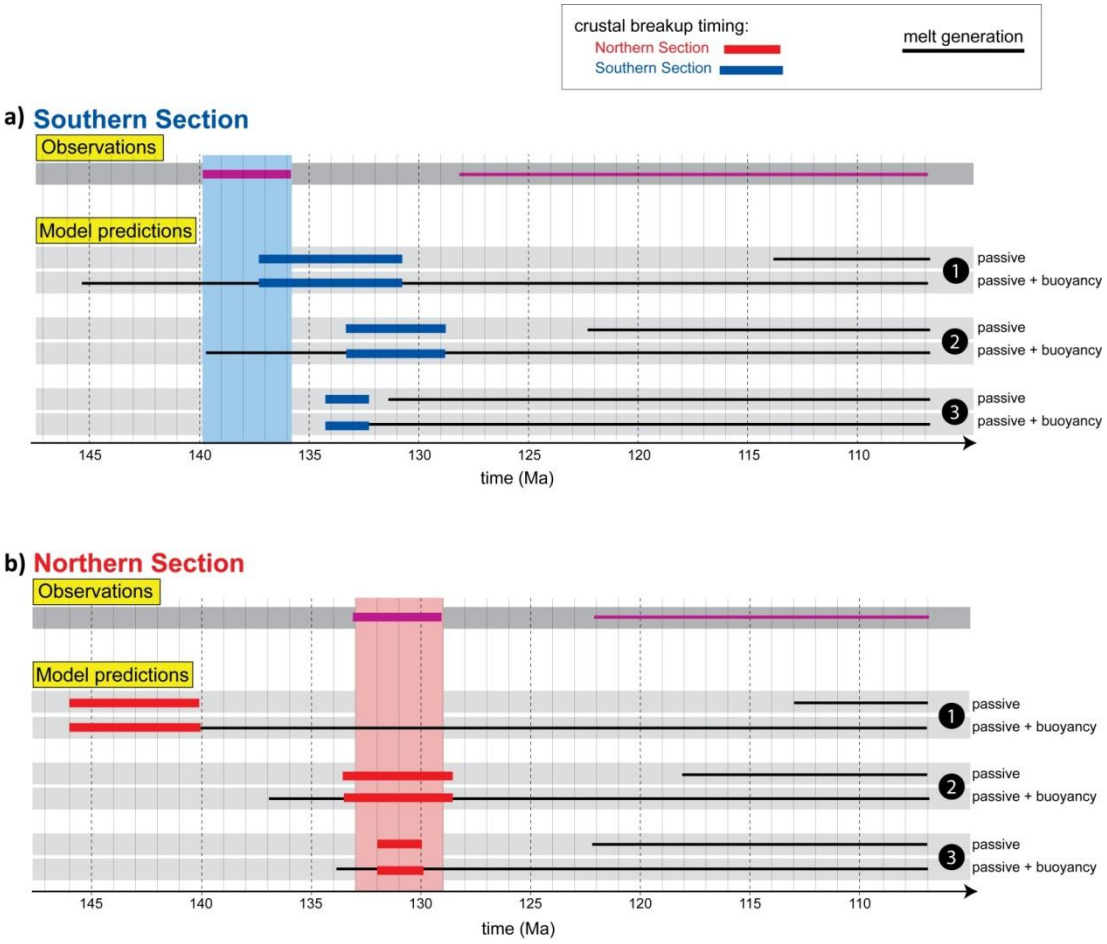

Figure 3.13: Relative timing of melt initiation and crustal breakup for the model extension history 1, 2 and 3 for the northern and southern sections. On the right side is shown the observed timing of crustal breakup and melt generation. For each model, the northern section is on the right, and the southern section on the left.

From this summary of these 6 models predictions, it appears that the north and the south must have followed a different lithosphere deformation evolution. In the north, according to the subsidence records described in section 3.6.1, none of the passive or active upwelling models 1 and 2 match the observed bathymetry, the best extension rate history fitting to observations in the north is model 3. In contrast in the south, none of the models 1, 2 or 3 satisfies the observed timing for the onset of mantle exhumation between 140 and 136Ma. The closest extension rate history for the southern section is model 1, but rifting must have started earlier or with a faster spreading rate that would increase the thinning rate, bringing forward crustal breakup.

One of the important questions related to the opening of the Iberia-Newfoundland concerns the rift opening propagation from the south to the north (Tucholke et al., 2007; Mohn et al., 2015). Two general ideas of how the rift may have propagated are:

> ***Synchronism:*** Both north and south transects underwent extreme thinning of the continental crust and lithosphere at the same time, but the south went faster than the north. Only models 2 and 3 were synchronous; the start and end times of each lithosphere deformation events for the north and the south are similar. Although the spreading rate used for the south are faster than for the north, these models do not predict the opening of the south before the north.
>
> ***Diachronism:*** The main phase of rifting in the south and the north occur at different time. Although that in all models localised rifting starts at 161Ma, only model 1 is diachronous. Eventually, our two preferred models, model 3 for the northern and model 1 for the southern profiles, are diachronous: extreme thinning of the continental crust leading to mantle exhumation is applied from 145Ma in the south and from 136Ma in the north.

3.8 Discussion

The aim of this study was to understand how the lithosphere and asthenosphere deform during continental rifting, breakup and seafloor spreading initiation. Using a kinematic finite-element model, we showed how the lithosphere deformation was controlled by deformation width, the half-spreading rate, the contribution of buoyancy and lateral deformation migration. We illustrated the importance of each of these parameters and varied them to produce a sequence of evolving lithosphere deformation events prescribed kinematically. Thus, our model could produce complex rifted margin architectures and be applied to particular 2D margin cross-sections. It also allowed quantitative calibration. The model was applied for two conjugate sections across the Iberia-Newfoundland rifted margins. The lithosphere deformation events were constrained during rifting, continental breakup and seafloor spreading initiation using present-day water-loaded subsidence obtained from flexural backstripping, crustal thickness from gravity inversion, subsidence history, the relative timing of crustal breakup and melt initiation, and oceanic accretion.

3.8.1 Passive versus active upwelling models

The importance of buoyancy upwelling has been demonstrated at slow spreading ocean ridges (e.g. Braun et al., 2000) and is therefore likely to also be significant during the formation of magma-poor rifted margins. However, the exact timing of buoyancy induced upwelling initiation remains unclear. We examined 3 rift-to-breakup extension rate histories leading to a similar Iberia-Newfoundland rifted margin crustal architecture (models 1, 2 and 3). For each of the 3 extension rate histories, we investigate both passive upwelling models (1a, 2a and 3a) and active upwelling models (1b, 2b and 3b). In the last case, buoyancy induced upwelling was added during the onset of the localised deformation.

Passive or active upwelling models seem to play an important role for the occurrence of exhumed mantle domain and the initiation of melting. The OCT's of the 4 conjugate

profiles of the Iberia-Newfoundland rifted margins show serpentinized exhumed mantle (Boillot et al., 1987; Chian et al., 1999; Whitmarsh et al., 2001; Péron-Pinvidic et al., 2007). All passive upwelling models predict mantle exhumation as observed. However the preferred passive upwelling models (i.e. section 3.7), model 1a in the south and model 3a in the north, show other mismatches with observations. In the south, model 1a predicts melt initiation at 110 Ma which is ca. 20 Myr later than observed. In the north, model 3a predicts a bathymetry greater than 1500m at the end of the Valanginian compared with the observation of less than 1000m. In contrast none of the active upwelling models predict mantle exhumation while the prediction of melt initiation seems to be coherent with observation.

How can we explain or reconcile these contradictions between observation and model prediction? In the south, buoyancy induced upwelling may have occurred later or weaker than proposed in model 1b; this could have brought forward melt initiation in time but still allowed mantle exhumation. In the north either the extreme thinning of the lithosphere is delayed or there is a contribution from buoyancy induced upwelling but delayed compared with model 3b. Because the extension rate is constrained by the observed total extension and the timing of mantle exhumation, if the extreme thinning is initially delayed, then the subsequent later full extension rate must be greater than 20mm.yr^{-1}, which would inevitably bring forward the time of melt initiation prior to that observed at 122 Ma.

An alternative way of reconciling the contradictions between observations and model predictions, and the apparent paradox that buoyancy induced upwelling is necessary despite that it brings forward melting initiation, is to add melt retention in our modelling. In previous models (1b, 2b, 3b) buoyancy induced upwelling brought forward melt initiation leading to a discrepancy between model prediction and geological data. We suggest that the melt initiated may be retained within the mantle, which delays its

extraction and therefore allows mantle exhumation. Müntener & Manatschal (2006) proposed that melt impregnation may occur during rifting of the Iberia-Newfoundland margins. In addition, based on the ophiolitic remnants of the Alpine Tethys, Müntener et al. (2010) suggested that up to 12% of an oceanic ridge-type melt may remain in the asthenospheric mantle. In our modelling, Figure 13 shows when the melt is generated and when it reaches a 12% threshold melt fraction. If the melt is retained within the mantle until it reaches 12% melt fraction, melt extraction starts after 115Ma in all models.

Melt retention may be an important process at the early stage of rifting during the formation of magma-poor rifted margin. Although there is no doubt that melt extraction properties are related to the permeability and porosity of the mantle (Morgan, 1987; White and McKenzie, 1989), their relation to the mode of lithosphere deformation remains obscure. The critical melt fraction may be dependent on the pure-shear width as already proposed by Cannat et al. (2004); during the early phase of continental rifting, the deformation occurs over a broad region, so that the passive flows beneath the rift are slow and distributed, leading the melt to remain in the upper mantle (Buck and Su, 1989). As the rift evolves to seafloor spreading, the pure-shear region focuses to narrower widths so that more melt is efficiently extracted.

3.8.2 Localisation and migration of the deformation during rifting

The models were constrained using the conjugate crustal architecture of the Iberia-Newfoundland rifted margins using a minimum number of lithosphere deformation events. This exercise revealed that the final crustal configuration of the conjugate margins predicted by modelling is dependent on 1) the evolving width of the pure-shear deformation and 2) lateral migration and/or jumps of the deformation (illustrated with model 0).

The predicted migration of the deformation in our modelling is consistent in all the models 1, 2 and 3. In the case of the Iberia-Newfoundland rifted margins, the deformation width

commenced wide and ended narrow, as illustrated in Figure 3.14. The first stage of rifting starts with a wide pure-shear deformation region (>200km). This distributed extension event is slow and precedes the onset of rifting with the focussing of the deformation sequentially from 150-130 to 50-40km. Post-rifting is marked by breakup and seafloor spreading initiation with complete focussing of the deformation width to 40 20km wide. The focussing of the deformation may have various origins. Hirth and Kohlstedt (1996) showed that the onset of melting decreases the viscosity of the mantle, further to which Minshull (2002) also proposed that, at magma-poor rifted margin, the onset of melting results in the increase of upwelling rate that narrows the deformation region.

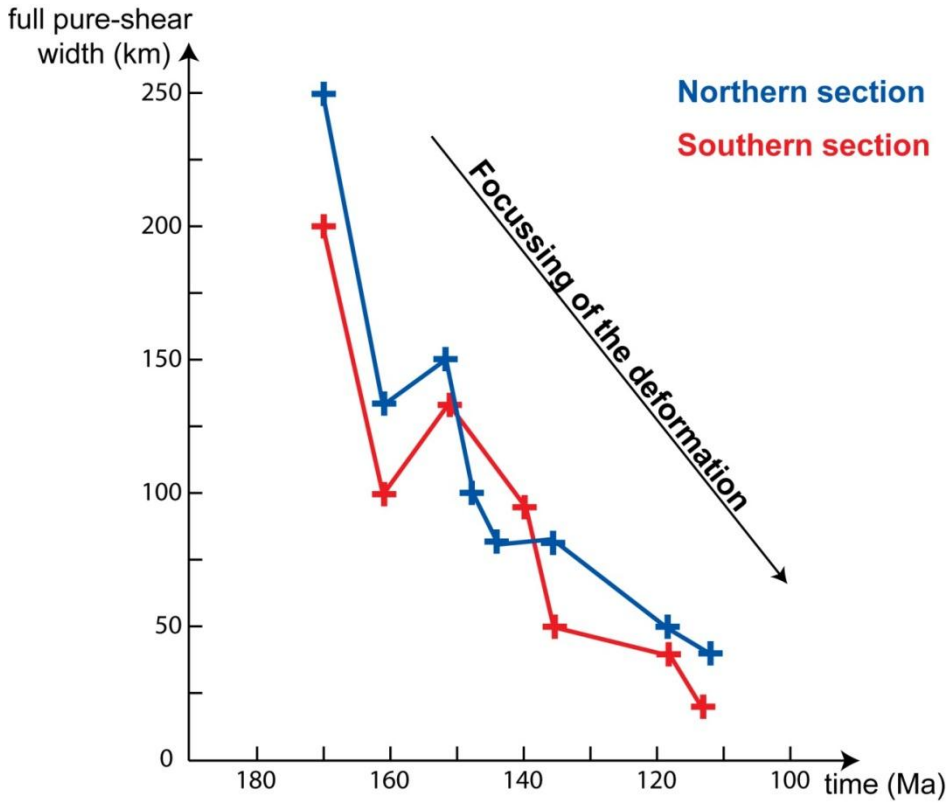

Figure 3.14: predicted evolution of the full pure-shear width in function of time for the northern and southern sections

Our modelling schemes revealed the importance of lateral jump and migration leading to the localization of the extensional deformation in the future distal margins. Jump and continuous migration of the deformation mimic two different geological processes occurring at different scale. A jump may occur when the deformation stopped in a specific region and "jumped" (>~100km) onto another area. This situation is suggested for the jump of the extensional deformation from the GIB to the DGM. Conversely, continuous migration is a progressive displacement of the deformation and may mimic simple shear deformation (Wernicke, 1981).

The exact processes controlling the jump and eventually the locus of breakup remain still in debate. Notably the rifting of the Iberia-Newfoundland rifted margins occur in a complex geologic setting at the limit between the Caledonian/Acadian orogeny, preserved mainly in the Newfoundland margin and mainly the Variscan orogeny, preserved in the Iberia margin. Furthermore, this region is characterized by the collage of several micro-continents and continents separated by oceanic sutures (e.g. Matte, 2001). Therefore, such geodynamic setting may explain the different crustal thickness revealed by our gravity inversion results (35 km for the Newfoundland margin and 40 km for the Iberia margin) and eventually the jump and the localization of the extensional deformation towards the future hyper-extended domains. Indeed, Pascal et al. (2002) suggest that contrast in continental crustal thicknesses may control the localization of rifting.

Continuous lateral migration of the deformation produces an asymmetry of the conjugate rifted margins (Brune et al., 2014). Reston (2009) suggested that the migration of the rift axis would only occur after that the entire crust become brittle, which would enhance a detachment fault system permitting crustal and mantle exhumation (Pérez-Gussinyé and Reston, 2001). In our modelling, a migration factor is used to 1) calibrate the crustal basement structure of Iberia Newfoundland conjugate margins and 2) correct the interference of extension created during simultaneous rift events. Conversely to what

proposed Reston (2009), a lateral migration rate of the deformation is used at early stage of rifting in our modelling where the crust is not entirely brittle. However, this migration is rather insignificant with a factor $f_m = V_m/V_x^0$ less than 0.4.

3.8.3 Geodynamic evolution of the Iberia-Newfoundland rifted margins

Following the reasoning above, we propose a preferred scenario for the Iberia-Newfoundland rifted margins formation. Its evolution is illustrated by the lithosphere and asthenosphere deformation sequence shown in Figure 3.15, and the relative timing of melt generation and crustal breakup summarized in Figure 3.16. Lithosphere deformation parameters for the two preferred models are defined in Table3. 4.

Table 3.4: Deformation parameterization for our preferred models

Northern section	pre	syn-rift							post	
events	*1*	*2*	*3*	*4a*	*4b*	*5a*	*5b*	*6*	*7*	*8*	*9*
start event *(Ma)*	180	161	151	140	140	136	136	130	118	112	80
end event *(Ma)*	161	151	140	136	136	133	130	118	112	80	
duration *(Ma)*	2	10	11	4	4	3	6	12	6	12	80
cumulative duration *(Myr)*	0	19	29	40	40	44	44	50	62	68	180
pure-shear width W *(km)*	100	50	65	65	25	25	25	25	20	10	
half-spreading rate V_x^0 *($mm.yr^{-1}$)*	0.8	1.2	1.7	3.5	1	2	7.5	4	8	10	
buoyancy ratio			4		16			2	1.8	0.8	
buoyancy depth *(km)*			35		30			20	20	20	
jump pure-shear flow-field *(km)*		35	-57	40	-57	60	-82	-95	-95	-95	
jump buoyancy flow-field *(km)*			-57		-57			-95	-95	-95	
migration pure-shear flow-field F_m			0.4	-1.6	1.7	-1.4	0.4				
migration buoyancy flow-field F_m			0.4		1.7						

Southern section	pre	syn-rift						post	
events	*1*	*2*	*3*	*4*	*5*	*6*	*7*	*8*	*9*
start event *(Ma)*	180	161	152	148	145	136	118	112	80
end event *(Ma)*	161	152	148	145	136	118	112	80	
duration *(Ma)*	2	9	4	3	9	18	6	32	80
cumulative duration *(Myr)*	0	19	28	32	35	44	62	68	180
pure-shear width W *(km)*	125	65	75	50	40	40	25	20	
half-spreading rate V_x^0 *($mm.yr^{-1}$)*	1.2	4.5	4.5	4.5	6	2.5	6	10	
buoyancy ratio		0.5	0.5	0.5	0.5	6	3	1.2	
buoyancy depth *(km)*		35	30	25	20	20	20	20	
jump pure-shear flow-field *(km)*		60	-35	-25	-25	-40	-65	-70	
jump buoyancy flow-field *(km)*		60	-35	-25	-30	-45	-60	-70	
migration pure-shear flow-field F_m		2			0.2				
migration buoyancy flow-field F_m		2			1	0.4			

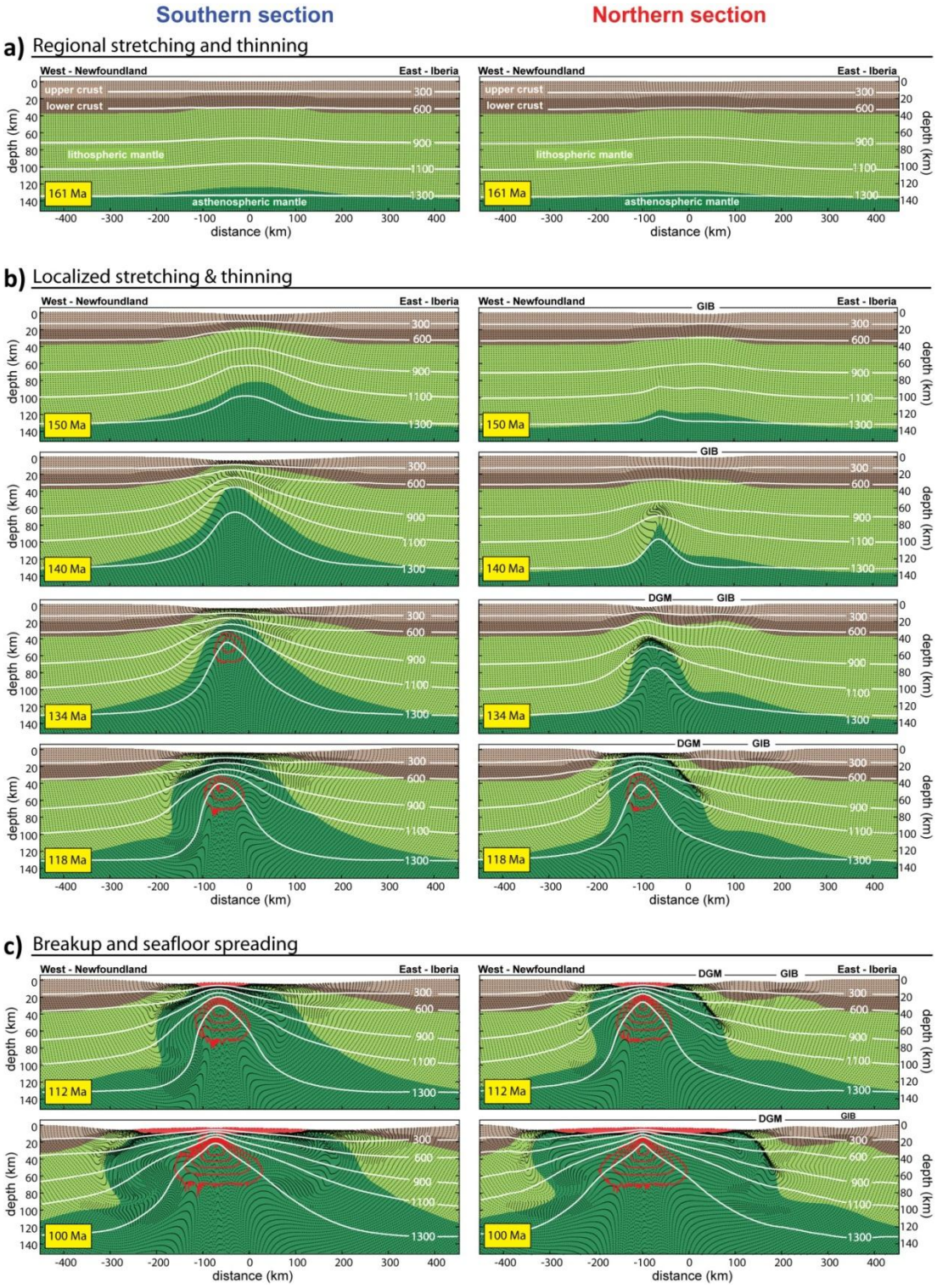
Southern section
Northern section
a) Regional stretching and thinning
b) Localized stretching & thinning
c) Breakup and seafloor spreading
West - Newfoundland
East - Iberia
upper crust
lower crust
lithospheric mantle
asthenospheric mantle
GIB
DGM
161 Ma
150 Ma
140 Ma
134 Ma
118 Ma
112 Ma
100 Ma
depth (km)
distance (km)

Figure 3.15 (previous page): Modelled lithosphere and asthenosphere deformation history for a preferred sequence of lithosphere deformation events, for both the southern and northern sections of the Iberia-Newfoundland conjugate rifted margins. The figure is divided into three stages of rifting: **a)** regional stretching and thinning, **b)** localized stretching and thinning and **c)** continental breakup followed by sea-floor spreading. Melt extraction is assumed to occur after it reaches a melt fraction threshold of 6%. White lines are isotherms (°C) and red contour lines are melt fraction. Contour interval is 0.03%.

After initial Late Triassic - Early Jurassic distributed stretching and thinning, the deformation occurred over a wide region more than 200km. In agreement with our previous modelling (models 1, 2, 3), we suggest that the northern and southern section underwent a different deformation evolution. In the south, the extension is faster from 161Ma than used in model 1 (Sutra et al. (2013) extension rate history), while in the north, model 3 extension rate history is preferred. In the south, the succession of deformation events are short and use a full spreading rate of 9mm.yr^{-1} whereas in the north, the deformation events last longer with slower spreading rates of 2.4-3.4mm.yr^{-1}. These two different lithosphere deformation evolution imply that at 150Ma, while the continental crust of the southern section has thinned by β =2.5, the continental crust in the north remains thicker ($\beta = 1.4$). The deformation during extreme thinning of the continental crust and lithosphere is brought forward of few Myr in the south in order to allow crustal breakup in the Valanginian (142-137Ma). In the north, extreme thinning of the continental crust and lithosphere occurs within the DGM from 136Ma to 130Ma leading to mantle exhumation from 133-130Ma.

As discussed earlier, buoyancy induced upwelling is better applied during the onset of the localised deformation from 161Ma in the south and from 151Ma in the north. However, the contribution of buoyancy induced upwelling is set weaker ($R_b = V_z^0/V_x^0 = 0.5$ in the south and 4 in the north) than that used in model 1b and 3b ($R_b = 6$ for both sections), in order to delay melt initiation but also to maintain shallow water condition in the north. In this

case, the onset of decompression melting is delayed to 135Ma in the south and to 128Ma in the north. Melt generation occurs therefore after mantle exhumation in both cases. In addition, we apply in these preferred models melt retention F_{ret} in order to delay melt extraction until a certain amount is generated. Melt retention threshold is set at 6%, although this value is arbitrary and may be highly variable due to mantle heterogeneities. In our preferred models, complete melt extraction occurs at 118Ma after an acceleration of the spreading rate coupled with a final buoyancy contribution (Bronner et al., 2011). This short event initiates seafloor spreading at 112Ma and the formation of an oceanic crust 6-7km thick at 110Ma for the northern and southern sections.

3.8.5 Conclusion

We developed a kinematic finite-element model in order to investigate the mode of deformation of continental lithosphere during rifting and the formation of magma-poor rifted margins. The model has been successfully applied to the Iberia-Newfoundland rifted margins by testing the importance of the extension rate history, buoyancy induced upwelling and the migration of the deformation. The quantitative calibration gave important insights on lithosphere deformation processes and also on the evolution of the Iberia-Newfoundland rifting.

1) Our modelling of the two conjugate profiles of Iberia-Newfoundland rifted margins shows that lithosphere deformation modes must evolve during continental breakup. We showed that using a sequence of lithosphere deformation events can better produce complex crustal margin architecture, and also give flexibility into the deformation history.

2) In the case of the formation of the Iberia-Newfoundland rifted margins, the lithosphere deformation evolves from wide to narrow pure-shear widths, and it must include, jumps and continuous lateral migration of the deformation.

3) Buoyancy induced upwelling has an important role early during rifting because it brings forward melt initiation and permits greater thinning of the lithosphere while maintaining weaker subsidence.

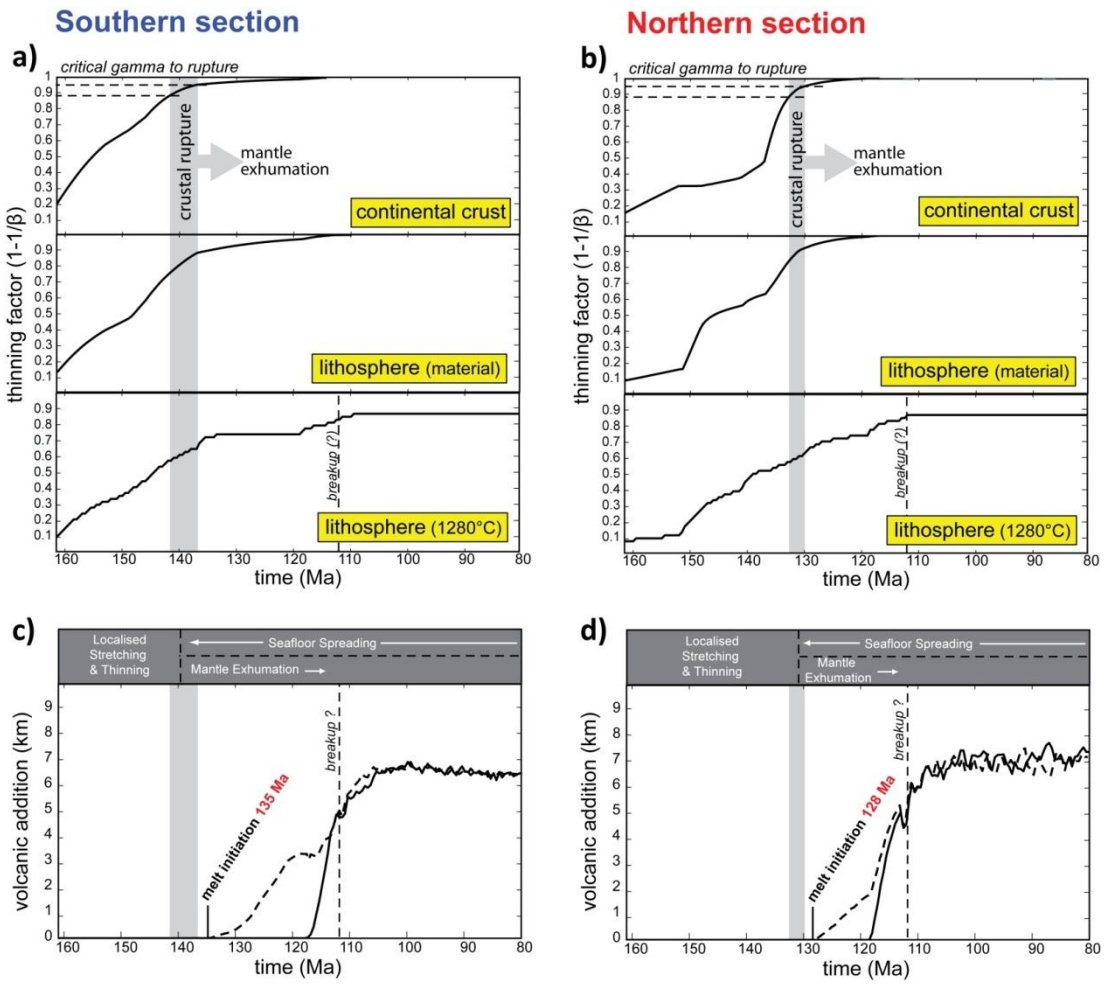

Figure 3.16: Relative timing of melt initiation, its extraction and crustal breakup for **a)** the northern and **b)** southern sections. The evolution of the thinning of the lithosphere (temperature and initial material tracking) and the continental crust is shown from 161Ma to 80Ma. The critical thinning factor is set between 0.88 and 0.95 and is shown on the upper panel. The lower panels also show the presume timing of breakup at 112Ma. **c)** and **d)** evolution of the volcanic addition thiskness from 161Ma to 80Ma. The grey area shows the timing for crustal breakup. The dash line represents the oceanic crustal thickness if there was no melt retention. The solid line represents the oceanic crustal thickness if the melt is extracted after it exceeds a threshold melt fraction of 6%.

4) While buoyancy induced upwelling is applied early during rifting, melt retention is therefore necessary for the formation of magma-poor rifted margins. We have shown that melt extraction can be delayed to allow mantle exhumation over long period of times. However, melt retention was poorly constrained.

5) Our modelling results suggest that the northern and southern sections have undergone a different lithosphere deformation evolution with the propagation of continental rifting towards the north.

ACKNOWLEDGMENT

We acknowledge the MM3 (Margin Modelling Phase 3) industry partners (BP, ConocoPhillips, HESS, BR Petrobras, Statoil, Shell, TOTAL, BG Group, BHP-Billiton) for financial support and discussions.

REFERENCES

Alves, T. M., Moita, C., Sandnes, F., Cunha, T., Monteiro, J. H., & Pinheiro, L. M. (2006). Mesozoic–Cenozoic evolution of North Atlantic continental-slope basins: The Peniche basin, western Iberian margin. *AAPG Bulletin*, *90*(1), 31–60.

Alvey, A., C. Gaina, N. J. Kusznir, and T. H. Torsvik, 2008, Integrated crustal thickness mapping and plate reconstructions for the high Arctic: Earth and Planetary Science Letters, v. 274, p. 310-321.

Beard, J. S., P. D. Fullagar, and A. K. Sinha, 2002, Gabbroic pegmatite intrusions, Iberia Abyssal Plain, ODP Leg 173, Site 1070: Magmatism during a transition from non-volcanic rifting to sea-floor spreading: Journal of Petrology, v. 43, p. 885-905.

Beaumont, C., Keen, C. E., & Boutilier, R. (1982). On the evolution of rifted continental margins: comparison of models and observations for the Nova Scotian margin (Canada). *Geophysical Journal*, *70*, 667–715.

Beslier, M.-O. (1996). 48. DATA REPORT: SEISMIC LINE LG12 IN THE IBERIA ABYSSAL PLAIN.

Boillot, G., & Winterer, E. L. (1988). 41. Rifting of the Galicia margin: crustal thinning and emplacement of mantle rocks on the sea-floor. *Proceedings of the Ocean Drilling Program, Scientific Results*, *103: Colle*.

Boillot, G., Winterer, E. L., & Meyer, A. W. (1987). Leg 103. In *Proc. Ocean Drill. Program, Initial Reports* (Vol. 103, p. 663).

Bown, J. W., and R. S. White, 1995, Effect of finite extension rate on melt generation at rifted continental margins: Journal of Geophysical Research: Solid Earth (1978–2012), v. 100, p. 18011-18029.

Braun, M. G., G. Hirth, and E. M. Parmentier, 2000, The effects of deep damp melting on mantle flow and melt generation beneath mid-ocean ridges: Earth and Planetary Science Letters, v. 176, p. 339-356.

Bronner, A., D. Sauter, G. Manatschal, G. Péron-Pinvidic, and M. Munschy, 2011, Magmatic breakup as an explanation for magnetic anomalies at magma-poor rifted margins: Nature Geoscience, v. 4, p. 549-553.

Brun, J., and M. Beslier, 1996, Mantle exhumation at passive margins: Earth and Planetary Science Letters, v. 142, p. 161-173.

Brune, S., C. Heine, M. Pérez-Gussinyé, and S. V. Sobolev, 2014, Rift migration explains continental margin asymmetry and crustal hyper-extension: Nat Commun, v. 5.

Buck, W. R., and W. Su, 1989, Focused mantle upwelling below mid-ocean ridges due to feedback between viscosity and melting: Geophysical Research Letters, v. 16, p. 641-644.

Cannat, M., J. Cann, and J. Maclennan, 2004, Some hard rock constraints on the supply of heat to mid-ocean ridges: Geophysical Monograph Series, v. 148, p. 111-149.

Cannat, M., G. Manatschal, D. Sauter, and G. Peron-Pinvidic, 2009, Assessing the conditions of continental breakup at magma-poor rifted margins: What can we learn from slow spreading mid-ocean ridges?: Comptes Rendus Geoscience, v. 341, p. 406-427.

Chapman, D. S. (1986). Thermal gradients in the continental crust. *Geological Society, London, Special Publications*, *24*(1), 63–70.

Chappell, A. R., and N. J. Kusznir, 2008, Three-dimensional gravity inversion for Moho depth at rifted continental margins incorporating a lithosphere thermal gravity anomaly correction: Geophysical Journal International, v. 174, p. 1-13.

Chian, D., Louden, K. E., Minshull, T. A., & Whitmarsh, R. B. (1999). Deep structure of the ocean-continent transition in the southern Iberia Abyssal Plain from seismic refraction profiles : Ocean Drilling Program (Legs 149 and 173) transect Deping Chian seismic refraction of an 80x40 of the southern reflection / refracti, *104*, 7443–7462.

Contrucci, I., F. Klingelhöfer, J. Perrot, R. Bartolome, M. A. Gutscher, M. Sahabi, J. Malod, and J. P. Rehault, 2004, The crustal structure of the NW Moroccan continental margin from wide-angle and reflection seismic data: Geophysical Journal International, v. 159, p. 117-128.

Cunha, T., 2008, Gravity Inversion, flexure, and the thermal and mechanical evolution of the West Iberia margin and its conjugate of Newfoundland: Ph.D. thesis.

Eddy, D. R., H. J. Van Avendonk, and D. J. Shillington, 2013, Compressional and shear-wave velocity structure of the continent-ocean transition zone at the eastern Grand Banks, Newfoundland: Geophysical Research Letters, v. 40, p. 3014-3020.

Fernàndez, M., & Ranalli, G. (1997). The role of rheology in extensional basin formation modelling. *Tectonophysics*, *282*, 129–145.

Fletcher, R., N. Kusznir, and M. Cheadle, 2009, Melt initiation and mantle exhumation at the Iberian rifted margin: Comparison of pure–shear and upwelling-divergent flow models of continental breakup: Comptes Rendus Geoscience, v. 341, p. 394-405.

Forsyth, D. W., D. S. Scheirer, S. C. Webb, L. M. Dorman, J. A. Orcutt, A. J. Harding, D. K. Blackman, J. P. Morgan, R. S. Detrick, Y. Shen, C. J. Wolfe, J. P. Canales, D. R. Toomey, A. F. Sheehan, S. C.

Solomon, and W. S. D. Wilcock, 1998, Imaging the deep seismic structure beneath a mid-ocean ridge : The MELT experiment: Science, v. 280, p. 1215-1218.

Funck, T., J. R. Hopper, H. C. Larsen, K. E. Louden, B. E. Tucholke, and W. S. Holbrook, 2003, Crustal structure of the ocean-continent transition at Flemish Cap: Seismic refraction results: Journal of Geophysical Research: Solid Earth (1978–2012), v. 108.

Gradstein, F. M., J. G. Ogg, and A. G. Smith, 2004, A geologic time scale 2004, v. 86, Cambridge University Press.

Grange, M., U. Schärer, G. Cornen, and J. Girardeau, 2008, First alkaline magmatism during Iberia–Newfoundland rifting: Terra Nova, v. 20, p. 494-503.

Greenhalgh, E. E., and N. J. Kusznir, 2007, Evidence for thin oceanic crust on the extinct Aegir Ridge, Norwegian Basin, NE Atlantic derived from satellite gravity inversion: Geophysical Research Letters, v. 34.

Harry, D. L., and S. Grandell, 2007, A dynamic model of rifting between Galicia Bank and Flemish Cap during the opening of the North Atlantic Ocean: Geological Society, London, Special Publications, v. 282, p. 157-172.

Henning, A. T., Sawyer, D. S., & Templeton, D. C. (2004). Exhumed upper mantle within the ocean-continent transition on the northern West Iberia margin: Evidence from prestack depth migration and total tectonic subsidence analyses. *Journal of Geophysical Research: Solid Earth (1978–2012)*, *109*(B5).

Hirth, G., and D. L. Kohlstedt, 1996, Water in the oceanic upper mantle: Implications for rheology, melt extraction and the evolution of the lithosphere: Earth and Planetary Science Letters, v. 144, p. 93-108.

Hopper, J. R., Funck, T., Tucholke, B. E., Larsen, H. C., Holbrook, W. S., Louden, K. E., … Lau, H. (2004). Continental breakup and the onset of ultraslow seafloor spreading off Flemish Cap on the Newfoundland rifted margin. *Geology*, *32*(1), 93–96.

Hopper, J. R., T. Funck, B. E. Tucholke, K. E. Louden, W. S. Holbrook, and H. Christian Larsen, 2006, A deep seismic investigation of the Flemish Cap margin: implications for the origin of deep reflectivity and evidence for asymmetric break-up between Newfoundland and Iberia: Geophysical Journal International, v. 164, p. 501-515.

Huismans, R., and C. Beaumont, 2011, Depth-dependent extension, two-stage breakup and cratonic underplating at rifted margins: Nature, v. 473, p. 74-78.

Jagoutz, O., Müntener, O., Manatschal, G., Rubatto, D., Péron-Pinvidic, G., Turrin, B. D., & Villa, I. M. (2007). The rift-to-drift transition in the North Atlantic: A stuttering start of the MORB machine? *Geology*, *35*(12), 1087–1090.

Katz, R. F., M. Spiegelman, and C. H. Langmuir, 2003, A new parameterization of hydrous mantle melting: Geochemistry Geophysics Geosystems, v. 4.

Krawczyk C M, T. J. R. M. O. B. G. B. (1996). 38. EVIDENCE FOR DETACHMENT TECTONICS ON THE IBERIA ABYSSAL PLAIN RIFTED MARGIN, *149*, 1–13.

Kusznir, N. J., & Karner, G. D. (2007). Continental lithospheric thinning and breakup in response to upwelling divergent mantle flow: application to the Woodlark, Newfoundland and Iberia margins. *Geological Society, London, Special Publications*, *282*(1), 389–419.

Lau, K. H., K. E. Louden, T. Funck, B. E. Tucholke, W. S. Holbrook, J. R. Hopper, and H. C. Larsen, 2006, Crustal structure across the Grand Banks—Newfoundland Basin Continental Margin—I. Results from a seismic refraction profile: Geophysical Journal International, v. 167, p. 127-156.

Lavier, L. L., and G. Manatschal, 2006, A mechanism to thin the continental lithosphere at magma-poor margins: Nature, v. 440, p. 324-328.

Leg, O., and S. S. Party, 1998, Drilling reveals transition from continental breakup to early magmatic crust: Eos, v. 79.

Manatschal, G., Froitzheim, N., Rubenach, M., & Turrin, B. D. (2001). The role of detachment faulting in the formation of an ocean-continent transition: Insights from the Iberia Abyssal Plain. *Geological Society, London, Special Publications*, *187*(1), 405–428.

Manatschal, G., 2004, New models for evolution of magma-poor rifted margins based on a review of data and concepts from West Iberia and the Alps: International Journal of Earth Sciences, v. 93, p. 432-466.

Matte, P. (2001). The Variscan collage and orogeny (480-290 Ma) and the tectonic definition of the Armorica microplate: A review. *Terra Nova*, *13*(1997), 122–128.

McKenzie, D., 1978, Some remarks on the development of sedimentary basins: Earth and Planetary Science Letters, v. 40, p. 25-32.

McKenzie, D., and M. J. Bickle, 1988, The Volume and Composition of Melt Generated by Extension of the Lithosphere: Journal of Petrology, v. 29, p. 625-679.

McKenzie, D. P., 1967, Some remarks on heat flow and gravity anomalies: Journal of Geophysical Research, v. 72, p. 6261-6273.

Minshull, T. A., 2002, The break-up of continents and the formation of new ocean basins: Philosophical Transactions of the Royal Society of London. Series A: Mathematical, Physical and Engineering Sciences, v. 360, p. 2839-2852.

Minshull, T. A., S. M. Dean, R. S. White, and R. B. Whitmarsh, 2001, Anomalous melt production after continental break-up in the southern Iberia Abyssal Plain: Geological Society, London, Special Publications, v. 187, p. 537-550.

Mohn, G., G. Manatschal, M. Beltrando, E. Masini, and N. Kusznir, 2012, Necking of continental crust in magma-poor rifted margins: Evidence from the fossil Alpine Tethys margins: Tectonics, v. 31.

Mohn G, Karner G.D. Manatschal G., Johnson C.A.. Structural and stratigraphic evolution of the Iberia-Newfoundland hyper-extended rifted margin: A quantitative modeling approach. In Gibson G.M., Roure F., Manatschal M., (eds), Sedimentary Basins and Crustal Porcesses at Continental Margins: From Modern Hyper-extended Margins to Deformed Ancient Analogues, accepted

Morgan, J. P., 1987, Melt migration beneath mid-ocean spreading centers: Geophysical Research Letters, v. 14, p. 1238-1241.

Müntener, O., & Manatschal, G. (2006). High degrees of melt extraction recorded by spinel harzburgite of the Newfoundland margin: The role of inheritance and consequences for the evolution of the southern North Atlantic. *Earth and Planetary Science Letters*, *252*(3–4), 437–452

Müntener, O., G. Manatschal, L. Desmurs, and T. Pettke, 2010, Plagioclase peridotites in ocean–continent transitions: refertilized mantle domains generated by melt stagnation in the shallow mantle lithosphere: Journal of Petrology, v. 51, p. 255-294.

Murillas, J., D. Mougenot, G. Boulot, M. C. Comas, E. Banda, and A. Mauffret, 1990, Structure and evolution of the Galicia Interior Basin (Atlantic western Iberian continental margin): Tectonophysics, v. 184, p. 297-319.

Nielsen, T. K., and J. R. Hopper, 2004, From rift to drift: Mantle melting during continental breakup: Geochemistry, Geophysics, Geosystems, v. 5.

Parsons, B., & Sclater, J. G. (1977). An analysis of the variation of ocean floor bathymetry and heat flow with age. *Journal of Geophysical Research*, *82*(5), 803–827.

Pascal, C., J. W. Van Wijk, S. Cloetingh, and G. R. Davies, 2002, Effect of lithosphere thickness heterogeneities in controlling rift localization: numerical modeling of the Oslo Graben: Geophysical Research Letters, v. 29, p. 69-1-69-4.

Pérez-Gussinyé, M., C. Ranero, T. J. Reston, and D. Sawyer, 2003, Mechanisms of extension at nonvolcanic margins: Evidence from the Galicia interior basin, west of Iberia: Journal of Geophysical Research: Solid Earth (1978–2012), v. 108.

Pérez-Gussinyé, M., and T. J. Reston, 2001, Rheological evolution during extension at nonvolcanic rifted margins: onset of serpentinization and development of detachments leading to continental breakup: Journal of Geophysical Research: Solid Earth (1978–2012), v. 106, p. 3961-3975.

Péron-Pinvidic, G., and G. Manatschal, 2009, The final rifting evolution at deep magma-poor passive margins from Iberia-Newfoundland: a new point of view: International Journal of Earth Sciences, v. 98, p. 1581-1597.

Péron-Pinvidic, G., G. Manatschal, T. A. Minshull, and D. S. Sawyer, 2007, Tectonosedimentary evolution of the deep Iberia-Newfoundland margins: Evidence for a complex breakup history: Tectonics, v. 26.

Ranero, C. R., and M. Pérez-Gussinyé, 2010, Sequential faulting explains the asymmetry and extension discrepancy of conjugate margins: Nature, v. 468, p. 294-299.

Reid, I. D., 1994, Crustal structure of a nonvolcanic rifted margin east of Newfoundland: Journal of Geophysical Research: Solid Earth (1978–2012), v. 99, p. 15161-15180.

Reston, T., 2009, The structure, evolution and symmetry of the magma-poor rifted margins of the North and Central Atlantic: a synthesis: Tectonophysics, v. 468, p. 6-27.

Reston, T., C. M. Krawczyk, and D. Klaeschen, 1996, The S reflector west of Galicia (Spain): Evidence from prestack depth migration for detachment faulting during continental breakup: Journal of Geophysical Research: Solid Earth (1978–2012), v. 101, p. 8075-8091.

Reston, T. J., and K. G. McDermott, 2011, Successive detachment faults and mantle unroofing at magma-poor rifted margins: Geology, v. 39, p. 1071-1074.

Reston, T. J., and J. P. Morgan, 2004, Continental geotherm and the evolution of rifted margins: Geology, v. 32, p. 133-136.

Reston, T. J. (2005). Polyphase faulting during the development of the west Galicia rifted margin. *Earth and Planetary Science Letters*, *237*(3), 561–576.

Schmeling, H., 2010, Dynamic models of continental rifting with melt generation: Tectonophysics, v. 480, p. 33-47.

Sclater, J., C. Jaupart, and D. Galson, 1980, The heat flow through oceanic and continental crust and the heat loss of the Earth: Reviews of Geophysics, v. 18, p. 269-311.

Shillington, D. J., W. S. Holbrook, H. J. Van Avendonk, B. E. Tucholke, J. R. Hopper, K. E. Louden, H. C. Larsen, and G. T. Nunes, 2006, Evidence for asymmetric nonvolcanic rifting and slow incipient oceanic accretion from seismic reflection data on the Newfoundland margin: Journal of Geophysical Research: Solid Earth (1978–2012), v. 111.

Sibuet, J.-C., S. Rouzo, and S. Srivastava, 2012, Plate tectonic reconstructions and paleogeographic maps of the central and North Atlantic oceans1,2 1This article is one of a series of papers published in this CJES Special Issue on the theme of Mesozoic–Cenozoic geology of the Scotian Basin. 2Earth Sciences Sector Contribution 20120172: Canadian Journal of Earth Sciences, v. 49, p. 1395-1415.

Sibuet, J. C., S. P. Srivastava, M. Enachescu, and G. D. Karner, 2007, Early Cretaceous motion of Flemish Cap with respect to North America: implications on the formation of Orphan Basin and SE Flemish Cap–Galicia Bank conjugate margins: Geological Society, London, Special Publications, v. 282, p. 63-76.

Spiegelman, M., and J. R. Reynolds, 1999, Combined dynamic and geochemical evidence for convergent melt flow beneath the East Pacific Rise: Nature, v. 402, p. 282-285.

Sutra, E., & Manatschal, G. (2012). How does the continental crust thin in a hyperextended rifted margin? Insights from the Iberia margin. *Geology*, *40*(2), 139–142.

Sutra, E., Manatschal, G., Mohn, G., & Unternehr, P. (2013). Quantification and restoration of extensional deformation along the Western Iberia and Newfoundland rifted margins. *Geochemistry, Geophysics, Geosystems*, *14*(8), 2575–2597.

Tucholke, B. E., Sawyer, D. S., & Sibuet, J. C. (2007). Breakup of the Newfoundland–Iberia rift. *Geological Society, London, Special Publications*, *282*(1), 9–46.

Tucholke, B. E., & Sibuet, J.-C. (2007). Leg 210 synthesis: Tectonic, magmatic, and sedimentary evolution of the Newfoundland-Iberia rift. In *Proceedings of the Ocean Drilling Program, scientific results* (Vol. 210, pp. 1–56).Tucholke, B. E., D. S. Sawyer, and J. C. Sibuet, 2007, Breakup of the Newfoundland–Iberia rift: Geological Society, London, Special Publications, v. 282, p. 9-46.

Turcotte, D. L., & Schubert, G. (2002). *Geodynamics*. University Press. Retrieved from

Van Avendonk, H. J. A., W. S. Holbrook, G. T. Nunes, D. J. Shillington, B. E. Tucholke, K. E. Louden, H. C. Larsen, and J. R. Hopper, 2006, Seismic velocity structure of the rifted margin of the eastern Grand Banks of Newfoundland, Canada: Journal of Geophysical Research: Solid Earth (1978–2012), v. 111.

Van Avendonk, H. J. A., L. L. Lavier, D. J. Shillington, and G. Manatschal, 2009, Extension of continental crust at the margin of the eastern Grand Banks, Newfoundland: Tectonophysics, v. 468, p. 131-148.

Wang, T., J. Lin, B. Tucholke, and Y. J. Chen, 2011, Crustal thickness anomalies in the North Atlantic Ocean basin from gravity analysis: Geochemistry, Geophysics, Geosystems, v. 12, p. Q0AE02.

Wernicke, B., 1981, Low-angle normal faults in the Basin and Range province: Nappe tectonics in an extending orogen: Nature, v. 291, p. 645-648.

White, R., and D. McKenzie, 1989, Magmatism at rift zones: the generation of volcanic continental margins and flood basalts: Journal of Geophysical Research: Solid Earth (1978–2012), v. 94, p. 7685-7729.

Whitmarsh, R., P. Miles, and A. Mauffret, 1990, The ocean-continent boundary off the western continental margin of Iberia—I. Crustal structure at 40° 30′ N: Geophysical Journal International, v. 103, p. 509-531.

Whitmarsh, R. B., G. Manatschal, and T. A. Minshull, 2001, Evolution of magma-poor continental margins from rifting to seafloor spreading: Nature, v. 413, p. 150-154.

Whitmarsh, R. B., and D. S. Sawyer, 1996, The ocean/continent transition beneath the Iberia Abyssal Plain and continental-rifting to seafloor-spreading processes: PROCEEDINGS-OCEAN DRILLING PROGRAM SCIENTIFIC RESULTS, p. 713-736.

Whitmarsh, R. B., and P. J. Wallace, 2001, The rift-to-drift development of the West Iberia non-volcanic continental margin; a review of the contribution of Ocean Drilling Program Leg 173.

Wilson, B. M., 1989, Igneous petrogenesis a global tectonic approach, Springer.

Wilson, R. C. L., 2008, A reconnaissance study of Upper Jurassic sediments of the Lusitanian Basin: Ciências da Terra, v. 5.

Wilson, R. C. L., G. Manatschal, and S. Wise, 2001, Rifting along non-volcanic passive margins: stratigraphic and seismic evidence from the Mesozoic successions of the Alps and western Iberia: Geological Society, London, Special Publications, v. 187, p. 429-452.

Zelt, C. A., Sain, K., Naumenko, J. V, & Sawyer, D. S. (2003). Assessment of crustal velocity models using seismic refraction and reflection tomography. *Geophysical Journal International*, *153*(3), 609–626.

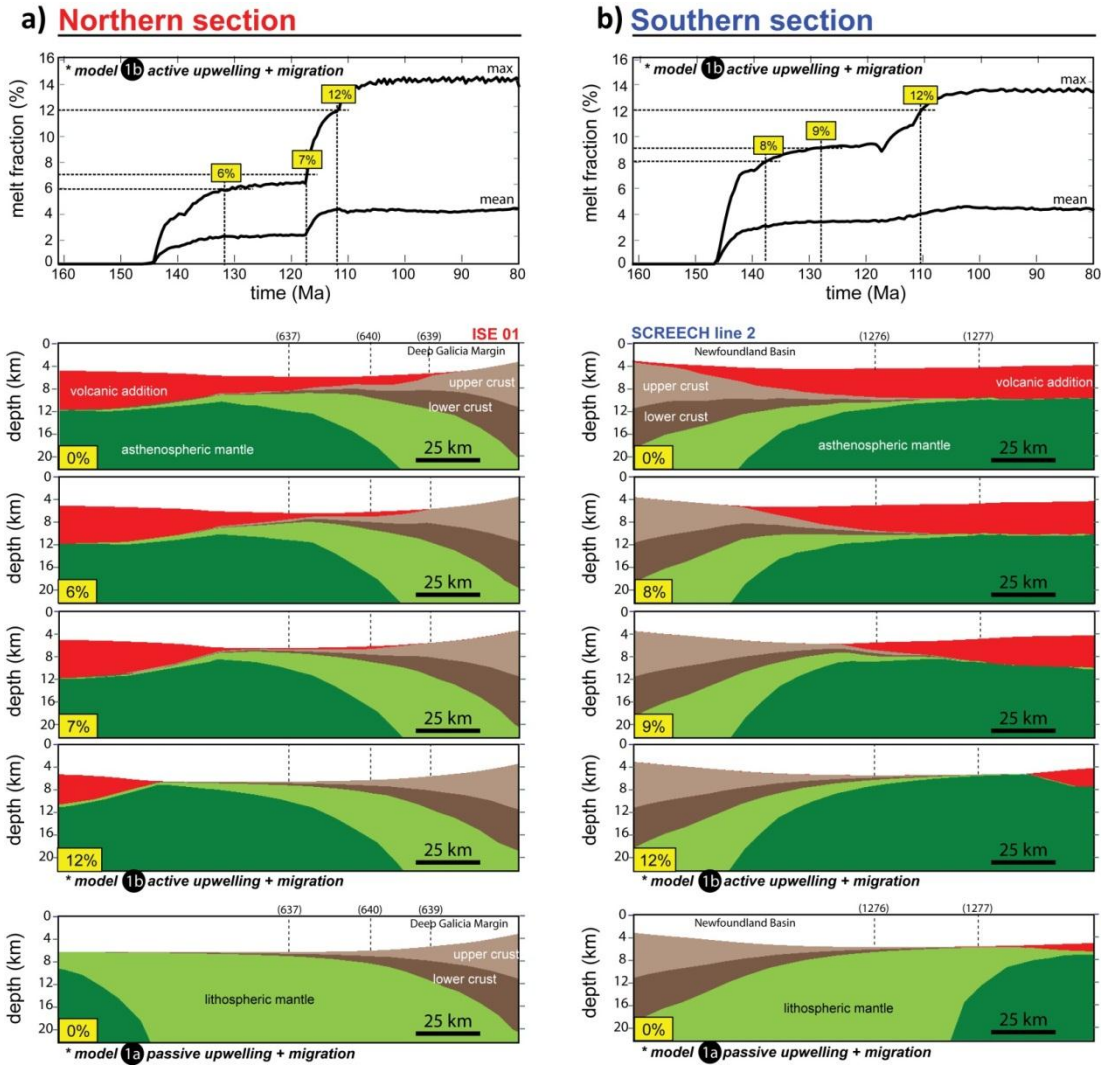

Appendix 3.1: OCT architecture sensitivity to melt retention **a)** for the northern section (ISE01) and **b)** for the southern section (SCREECH line 2). The upper panel shows the evolution of melt fraction from 161Ma to 80Ma for model 1b. The 4 middle panels illustrate the OCT architecture sensitivity to melt retention. The bottom panel show the OCT architecture for the passive model 1a model.

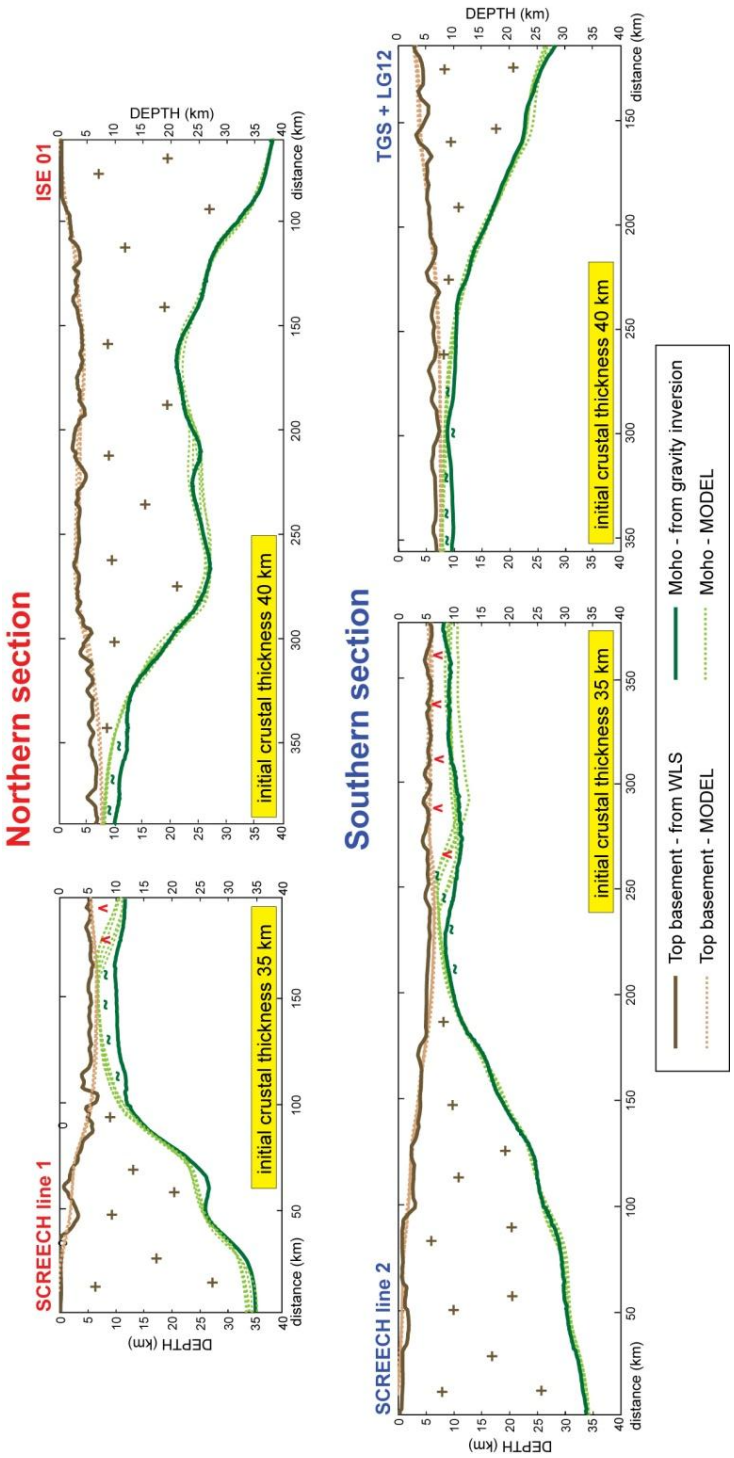

Appendix 3.2: Comparison of the rifted margin calibration of the model predictions for all models 1-3 for the northern and southern section against water-loaded subsidence and crustal basement thickness. Note that all models match the observed water-loaded subsidence and crustal basement thickness if the initial continental crust for the Iberia margin was 40km and 35km for the conjugate Newfoundland margins.

Chapter 4

Numerical experiments of the formation of the Alpine Tethys rifted margins: implications for the uplift and subsidence history of the Briançonnais domain

Preface

This chapter is a paper format and is aim to be submitted to the Journal of the Geological Society.

Numerical experiments of the formation of the Alpine Tethys rifted margins; implications for the uplift and subsidence history of the Briançonnais domain

Ludovic Jeanniot[1], Nick Kusznir[1], Geoffroy Mohn[2], Gianreto Manatschal[3] and Marco Beltrando[4]

[1]Department of Earth, Ocean and Ecological Sciences, University of Liverpool, Liverpool, L69 3GP, UK

[2]Department of Geosciences and Environmental Sciences, Université de Cergy-Pontoise, Cergy-Pontoise, France

[3]IPGS-EOST, UDS-CNRS, Strasbourg, France

[4]Dipartemento di Scienze della Terra, Universita di Torino, Via Valperga Caluso 35, 10125 Torino, Italy

ABSTRACT

We apply a 2D kinematic finite-element model of lithosphere and asthenosphere deformation for the temporal and spatial development of the Alpine Tethys. Lithosphere deformation modes use pure-shear and passive upwelling and/or buoyancy induced upwelling. The model can predict subsidence, melting and P-T-t histories and is quantitatively calibrated against observations from the vertical motion of the Briançonnais domain, a continental ribbon between two hyper-extended rift basins. Taking into account the documented stratigraphic records and the range of conceptual models already

proposed for the evolution of this rift system, 10 different model scenarios for the Alpine Tethys formation are generated. We explore the sensitivity of the Briançonnais uplift (and emergence) and subsidence to the formation of a single or two simultaneous rift basins and their mode of migration. Additionally, the influence of the initial continental crustal thickness, the buoyancy upwelling strength and its penetration depth are explored. The emergence of the Briançonnais requires buoyancy induced upwelling which also satisfies the high geothermal gradient and early melting history inferred from geological data. Using an initial continental crustal thickness of 32.5km, uplift is achieved if buoyancy is active only for a penetration depth >20km. We demonstrate that thermal subsidence alone cannot explain the rapid post-uplift subsidence observed in some area of the Briançonnais and that crustal thinning (possibly depth-dependent) is also necessary. Lateral migration of the deformation is necessary to generate a hyper-extended domain on the conjugate Adriatic margin (Err, Bernina).

4.1 Introduction

The evolution of lithosphere deformation modes during continental breakup leading to seafloor spreading initiation are fundamental to understanding the formation processes of present-day and fossil rifted margins. Their evolution controls the thinning of the continental crust and lithosphere, subsidence, thermal and melting histories. While considerable amount of data regarding the crustal and stratigraphic architecture (e.g. seismic, drilling, gravity) have been collected at present-day rifted margins, fossil rifted margins enable direct access to an extensive stratigraphic record. Remnants of the Alpine Tethys exposed in the European Alps provide the opportunity to study distal margins in one of the most studied orogens in the world.

The Alpine Tethys, as shown in Figure 4.1 results from Late Triassic to Middle Jurassic rifting and separation of the European and Adriatic plates during the late Middle to the early Late Jurassic (Frisch, 1979; Ricou, 1994). In detail, the Alpine Tethys consists of two main

separate basins, labeled the Valais and Piemonte-Liguria basins, separated by a continental ribbon referred to as the Briançonnais domain (Trümpy, 1960; Frisch, 1979; Stampfli, 1993). Both basins were floored by hyper-extended lithosphere (Florineth and Froitzheim, 1994; Manatschal and Nievergelt, 1997; Dal Piaz, 1999; Beltrando et al., 2010; Mohn et al., 2010; Beltrando et al., 2012), with partial evidence for an ultra-slow spreading ridge within the Piemonte-Liguria basin (Manatschal et al., 2011; Sanfilippo et al., 2014).

In the context of this Jurassic rifting, the vertical motion of the Briançonnais is of particular interest showing uplift during the main thinning episode of the Alpine Tethys and eventually followed by rapid subsidence (Bourbon, 1980; Lemoine and Trümpy, 1987; Stampfli, 1993; Mohn et al., 2010 and reference therein) at the period of lithospheric breakup. Several processes have been proposed to account for this paleobathymetric evolution including; (1) the simultaneous formation of the two basins (i.e. Valais and Piemonte Liguria) causing the in-between domain to be uplifted isostatically by lithosphere thinning, and/or (2) the presence of major normal faults in the Briançonnais leading to footwall uplift and possible emergence and/or (3) the presence of a thermal anomaly due to buoyancy upwelling beneath the Briançonnais. Because the lower crustal basement of the Briançonnais continental ribbon is not outcropping and has likely disappeared during Tertiary subduction/collision, its pre-orogenic crustal thickness history and isostatic consequences remains unknown. Additionally, uncertainties remain concerning the evolution of the Valais basin during rifting and breakup, as hyper-extension has been alternatively attributed to Jurassic rifting (Manatschal and Müntener, 2009) or to Cretaceous rifting, related to the opening of the Bay of Biscay (Frisch, 1979; Stampfli, 1993). In this paper we examine the isostatic response of the Briançonnais domain to rift dynamics. Several different scenarios are considered, accounting for the range of uncertainties in the geological record. Therefore, we test different hypothesis regarding the formation of the Valais basin and investigate how it may have impacted the subsidence history of the Briançonnais domain.

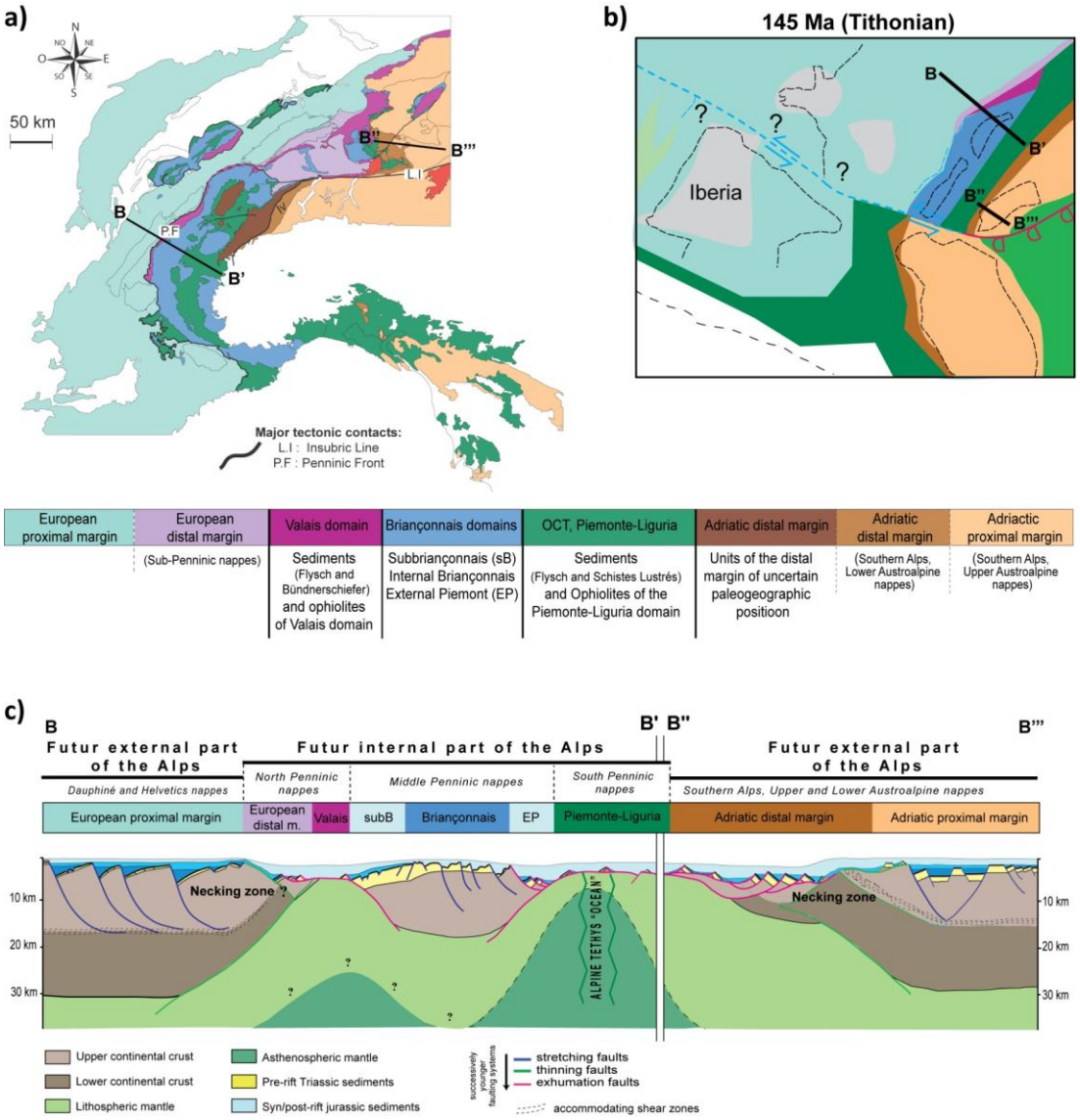

Figure 4.1: **a)** Tectonic map of the Central and Western Alps showing the distribution of 5 major paleogeographic units: European margin, Valais domain, Briançonnais domain, Piemonte-Liguria and Adriatic margin. **b)** Paleogeography of the Alpine domain at the end of Jurassic (Tithonian 145Ma). **c)** Cross-section during the late Jurassic illustrating the Alpine Tethys crustal rifted margins architecture. The cross-section presented here is a montage from two cross-sections as presented in **a)** and **b)**. Modified from Mohn et al. (2010) (and reference therein)

This study aims to (1) investigate the modes and evolution of lithosphere deformation during the formation of the Alpine Tethys and (2) explore the different mechanisms that can generate the observed isostatic response recorded in the stratigraphic evolution of the Briançonnais. In order to address these questions, we use a kinematic finite-element model of continental rifting, breakup and seafloor spreading initiation. Geological observations regarding the nature and composition of sedimentary, crustal and mantle rocks as well as conceptual models permit the elaboration of 10 model scenarios for the evolution of lithosphere deformation modes. We examine the complex thermal and isostastic evolution of the Briançonnais domain from intracontinental rifting leading to mantle exhumation and seafloor spreading using a series of numerical experiments.

Our kinematic finite-element model uses two main lithosphere deformation modes: (1) upper lithosphere pure-shear inducing passive upwelling below, and (2) buoyancy-induced active upwelling. A kinematic control of these two end-member deformation modes allows an application of this model to the Alpine Tethys. The quantitative calibration of the model takes advantage of the wealth of geological constraints on the evolution of the Alpine Tethys rifted margins. As the architecture of the Alpine Tethys rifted margins has been significantly reworked during the Alpine orogenesis, our models are calibrated against constraints arising from the stratigraphic record and the P-T-t history of the basement rocks observed in the Alps preserving the record of pre-Alpine events. An interpretative 2D profile of the post-rift margin architecture of the Alpine Tethys (Figure 4.1c) is taken as reference for testing the modelling results.

4.2 Geological overview

An overview of the main paleogeographic domains sampled in the tectono-stratigraphic units of the European Alps is provided in this section. These units sampled different portions of the Alpine Tethys (Figure 4.1) during Cretaceous-Tertiary inversion, thus providing information on the timing of the main rift events and subsidence history. The key

steps of the stratigraphic and structural evolution of the Alpine Tethys are summarized in section 4.2.1. This synthesis, which is referred to the profile marked in Figure 4.1c, is by no means intended to account for all second-order signals and for the significant along-strike variations. The complex vertical motion history of the Briançonnais domain is only described in section 4.2.3.

4.2.1 Description of the paleogeographic domains preserved in the Alps

The Alpine Tethys resulted from the separation of the European and Adriatic plates during the Late Middle Jurassic. Remnants of the former margin are now found throughout the European Alps, stretching over 1200km from France to Slovenia, as a result of the subsequent convergence of the Eurasian and Adriatic plates (Trümpy, 1960; Frisch, 1979; Tricart, 1984; Haas et al., 1995; Stampfli et al., 2001). The Alpine orogeny beneficed of numerous studies enabling a detailed description of the Mesozoic stratigraphic record, structural data and tectono-metamorphic evolution that resulted in the recognition of distinctively different paleogeographical domains that, on a NW-SE section (Figure 4.1a) range from the European margin to the Valais basin, Briançonnais domain, Piemonte-Liguria basin and the Adriatic margin. A qualitative restoration of the Alpine belt in the Tithonian is shown in Figure 1b and 1c (Mohn et al., 2010). The main features of the Valais basin, Piemonte-Liguria basin and Briançonnais domain are summarized hereafter.

The Piemonte-Liguria basin

The presence of ophiolites associated with post-rift and Flysch deposits has long permitted the identification of the Alpine Tethys basins as an oceanic domain (Elter, 1972; Elter and Decndia, Frisch, 1979; Trümpy and Homewood, 1980; Lemoine et al., 1987; Stampfli, 1993; Manatschal et al., 2006). More recent studies have subsequently documented that both the Valais and Piemonte-Liguria basins were largely floored by exhumed sub-continental mantle, locally capped by continental allochtones (Florineth and Froitzheim, 1994;

Manatschal and Nievergelt, 1997; Dal Piaz, 1999; Manatschal et al., 2006; Beltrando et al., 2010; Beltrando et al., 2012; Beltrando et al., 2014). The Piemonte-Liguria basin may exhibit asymmetric conjugate rifted margins (Lemoine and Trümpy, 1987). The Adriatic margin is characterized by the occurrence of extensional detachment systems within a hyper-extended domain (<10km thick), while the European margins may show a more abrupt transition (Figure 1c) (Mohn et al., 2010) and reference therein).

The Valais domain

Mantle exhumation within the Valaisan domain has been documented both in the Eastern (Florineth and Frotzheim, 1994; manatschal et al., 2006) and Western Alps (Beltrando et al., 2012). However, the timing of hyper-extension within this domain is still controversial; complete crustal excision has been alternatively placed in the Jurassic (Beltrando et al., 2012; Manatschal et al., 2006) or in the Cretaceous (e.g. Frisch, 1979; Trümpy and Homewood, 1980; Stampfli, 1993). Despite this controversy, existing studies agree on the overall geometry of this basin, which is considered to be linked with the Piemonte-Liguria basin to the NE, while it tapers out to the SW (Frisch, 1979; Trümpy and Homewood, 1980; Cannat et al., 2006; Hebert and Montési, 2010; Mohn et al., 2010).

The Briançonnais domain

The Briançonnais has been the subject of long standing debates regarding its paleographic affinity (Stampfli (1993) and reference therein) and its subsidence history (discussed in section 4.2.3). The Briançonnais domain stands between the Valais and Piemonte-Liguria basins and is subdivided into 3 zones: the Sub-Briançonnais, located next to the Valais basin, the External Piemont (or Prepiemont) next to the Piemonte-Liguria basin, and the Internal Briançonnais in-between. The Briançonnais domain was interpreted to have originated from a 'H'-block standing between the proximal European and Adriatic margins (Lavier and Manatschal, 2006), which narrows and disappears in the NE whereas it merges with the European plate in the SW (Trümpy and Homewood, 1980; Lemoine et al., 1986).

4.2.2 Timing of the main rift events

The stratigraphic record documenting the evolution of the Alpine Tethys margins enables to define 4 rift stages (Figure 4.2):

Distributed extension

The eastern part of the Alpine realm underwent a first episode of rifting during the Trias related to the opening of the Neo-Tethys along the eastern border of Adria (Dercourt, 2000). This event resulted in the deposition of thick Triassic carbonate platforms (~1-2km) documented in the Briançonnais and Austroalpine domains (Stampfli and Marchant, 1997). The wide spread Triassic platform was interpreted as resulting from post-rift thermal subsidence related to the Neo-Tethys (Manatschal and Bernoulli, 1999). Platform sediments suggest a shallow marine depositional environment (≤100m). A second wide spread rifting started at the end of Trias to early Jurassic marking the onset of rifting leading to the formation of the Alpine Tethys.

Localised extension

From the Toarcian onward extension migrated and localised in the future distal domains, causing major thinning of the continental lithosphere which led to the development of the Valais and the Piemonte-Liguria basins separated by the Briançonnais domain (Bertotti et al., 1993; Mohn et al., 2010) and reference therein). This stage is indicated by (1) the onset of gravity-driven deeper water sedimentation (i.e. breccias, claystones, marls) in the European distal margin, Sub-Briançonnais, the External Piemonte and the Adriatic distal margin (Dumont, 1984; Decarlis and Lualdi, 2011) and (2) top-basement detachment faults initiation from 185Ma to 165Ma (Frotzheim and Eberli, 1990; Manatschal and Nievergelt, 1997; Niu, 1997; Masini et al., 2011; Mohn et al., 2012). Mantle decompression melting may be initiated around 180Ma, as indicated by melt infiltration within the lithospheric mantle and crustal basement (Müntener et al., 2010). This early melting stage may result from an extreme thinning of the lithosphere.

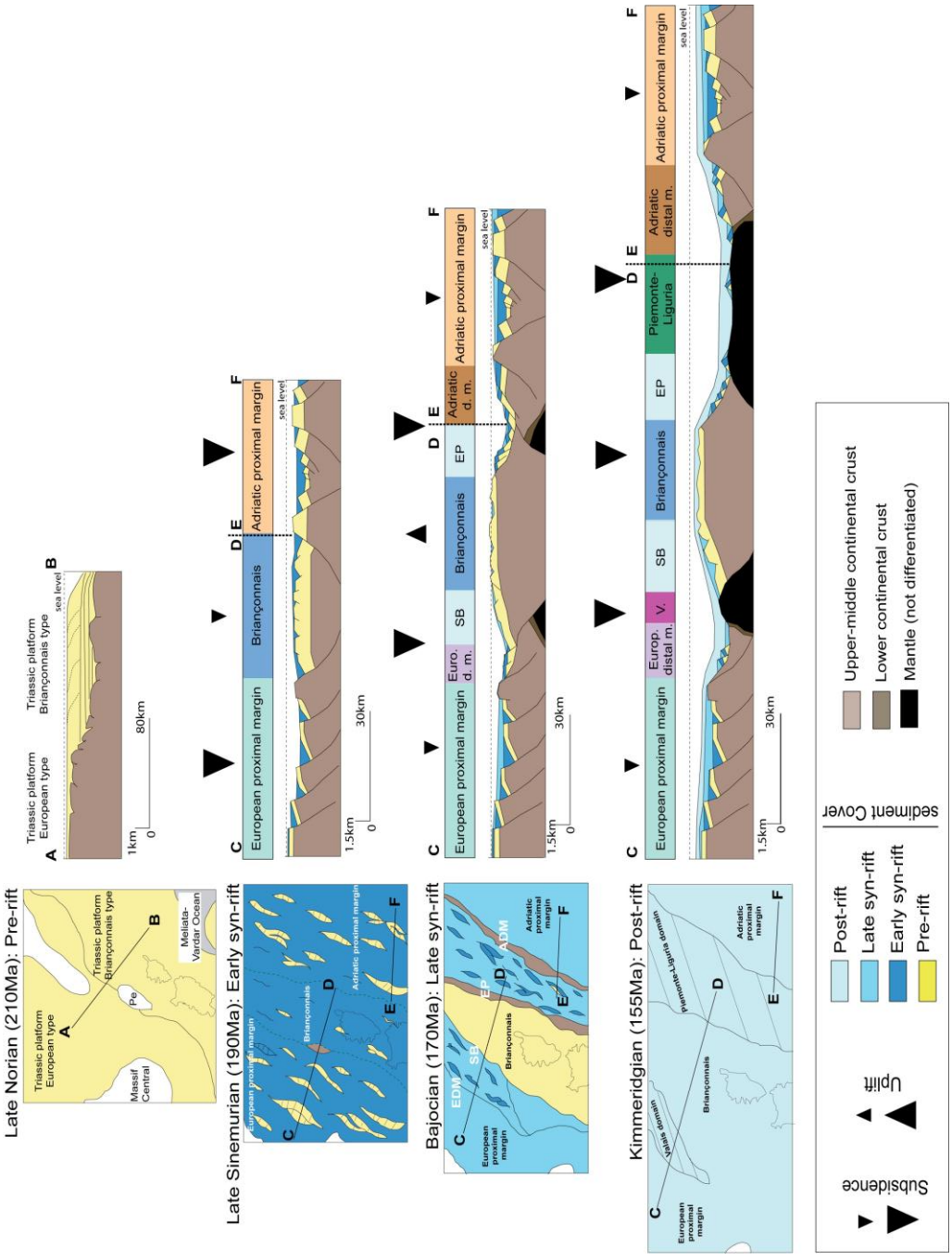

Figure 4.2: Simplified stratigraphic record logs from the major paleogeographic units of the Alpine Tethys and their location (Mohn et al. (2010). Zooms on the European proximal margin (modified after Lemoine et al., 1986), the Briançonnais domains (modified from Baud et Septfontaine, 1980) and Adriatic distal margins (modified from Mohn et al. (2010)) show detailed sediment and faults architecture. Abbreviations: M, Mantle; B, Basement; LT, MT, UT, Lower, Middle, Upper Triassic; LJ, MJ, UJ, Lower, Middle, Upper Jurassic; A-A; LC, Lower Cretaceous; A-A, Aptian-Albian. Vertical scale is exaggerated.

Onset of mantle exhumation

Top-basement detachments faults initiated during the localised extension phase and eventually led to mantle exhumation during late stage rifting. Deposition of radiolarian cherts over the exhumed mantle within the Piemonte-Liguria domain (e.g. Platta nappe) suggests an exhumation in Bathonian to Callovian times (Bill et al., 2001; Desmurs et al, 2001). No biostratigraphic age is available to constrain mantle exhumation in the Valais basin. Based on Ar-Ar step-heating of phlogopite from a spinel websterite within the exhumed sub-continental mantle, (Manatschal et al., 2006) proposed similar ages (169Ma – onward) for mantle exhumation at the Tasna nappe. As a result, those authors suggested that complete crustal excision in both Valais and Piemonte-Liguria basins was achieved at the same time. Conversely, based on U-Pb dating of zircons from mafic rocks found within the complex nappe stack in the Central and Western Alps, (Liati et al., 2003) suggests that the Valais opened during a second stage of rifting in the Early Cretaceous (Stampfli et al., 1998; Handy et al., 2010). However, as noted by the same authors, several Alpine tectonometamorphic units that originated from the Valais basin also host evidence of mafic magmatism in the Middle to Upper Jurassic (Liati et al., 2005).

Seafloor spreading initiation

The magmatic history provides further insights on the rifting evolution, especially regarding the latest stages of tectonic activity recorded along the margins of the Alpine Tethys. Gabbroic intrusions associated with tholeiitic pillow lavas and basaltic flow in the Piemonte-Liguria Ocean were largely emplaced in the mantle peridotite during the Middle Jurassic (165-160Ma) (Schaltegger et al., 2002; Manatschal and Müntener, 2009; Li et al., 2013). Based on zircon U-Pb and O-Hf isotopes from the Chenaillet ophiolites, Li et al. (2013) suggest that spreading of the Piemonte-Liguria Ocean lasted 11Myr. The same authors proposed that the final width of the Alpine Tethys Ocean was about 300km assuming a full

spreading rate less than 30mm.yr^{-1} for slow spreading ridges (Cannat et al., 2009). No available data permits to estimate the duration and width of the Valais spreading.

4.2.3 Uplift and subsidence history of the Briançonnais domain

The vertical motion of the Briançonnais domain is summarized in Figure 4.2. The Briançonnais domain resided a shallow water depth during the Triassic-Early Jurassic, where thick carbonate platforms were deposited (Stampfli and Marchant, 1997). Notably during the Toarcian to Aalenian (~185-170Ma), corresponding to the period of major lithospheric thinning, the Briançonnais records an initial uplift leading to emergence indicated by karstification of the carbonate platform (Lemoine et al., 1986; Claudel and Dumont, 1999). Erosion, from a few tens of meters up to 300m (Franke, 2013) of the original carbonate platform is observed within the karsts and the basins around the Briançonnais, suggesting that the top of the domain was just above sea-level. The uplift and occasional emergence is followed by subsidence at variable rate in different parts of the Briançonnais domain. Slow subsidence up to Late Bathonian (165Ma), coupled with the deposition of a carbonate platform, was locally followed by rapid drowning to depths below the Carbonate Compensation Depth (CCD), as indicated by radiolarian cherts (Bourbon, 1980). However, the same author pointed out an uncertainty about the rapid subsidence and advised that the CCD may change through time and may depend on the paleomorphology and paleogeography of continents, so that it cannot be used as a paleodepth indicator. Other parts of the Internal Briançonnais, instead, still resided at shallow water conditions in the Late Jurassic (Baud and Septfontaine, 1980).

4.3 Model formulation and illustration

This section presents the numerical model which is applied to the formation of the Alpine Tethys Ocean. The model uses a sequence of lithosphere deformation events to deform lithosphere and asthenosphere during intracontinental rifting leading to breakup and seafloor spreading initiation. Each lithosphere deformation event is represented by a flow-

field generated by a finite-element viscous flow model. The flow-fields are generated using a Newtonian layered viscosity structure as illustrated in Figure 4.3.

4.3.1 Lithosphere deformation modes

The lithosphere deformation model uses two deformation modes; upper lithosphere pure-shear model with passive upwelling and buoyancy induced upwelling.

Pure-shear + passive upwelling

The pure-shear deformation mode describes the lithosphere deformation occurring during intracontinental rifting (McKenzie, 1978). The pure-shear deformation is controlled by the rate of extension V_x^0 for the topmost seismogenic brittle layer that imposes passive upwelling beneath the deformation region. We show in Figure 4.3a all the boundary conditions of the finite-element viscous flow model and the resulting flow vectors. The strong viscosity layer imposes divergence and generates localized pure-shear deformation within the low viscosity layer and passive upwelling beneath that region. The pure-shear inducing passive upwelling is the primary deformation mode.

Buoyancy induced upwelling

The importance of buoyancy during rifting processes leading to continental lithosphere breakup has been suggested by several studies (Forsyth et al., 1998; Spiegelman and Reynolds, 1999; Braun et al., 2000; Nielsen and Hopper, 2004). An active upwelling rate V_z^0 is set at the flow axis below a buoyancy penetration depth D_b, as shown in Figure 4.3b. The penetration depth below which buoyancy induces upwelling can be varied; in the models, the upwelling rate V_z^0 applied to material points located >20km beneath depth D_b. The buoyancy induced upwelling flow field is added to the pure-shear and passive upwelling flow vectors. The buoyancy contribution induces small-scale convection upwelling beneath the brittle upper lithosphere. Buoyancy induced upwelling is a secondary deformation mode that accompanies continental rifting and serves to amplify lithosphere thinning.

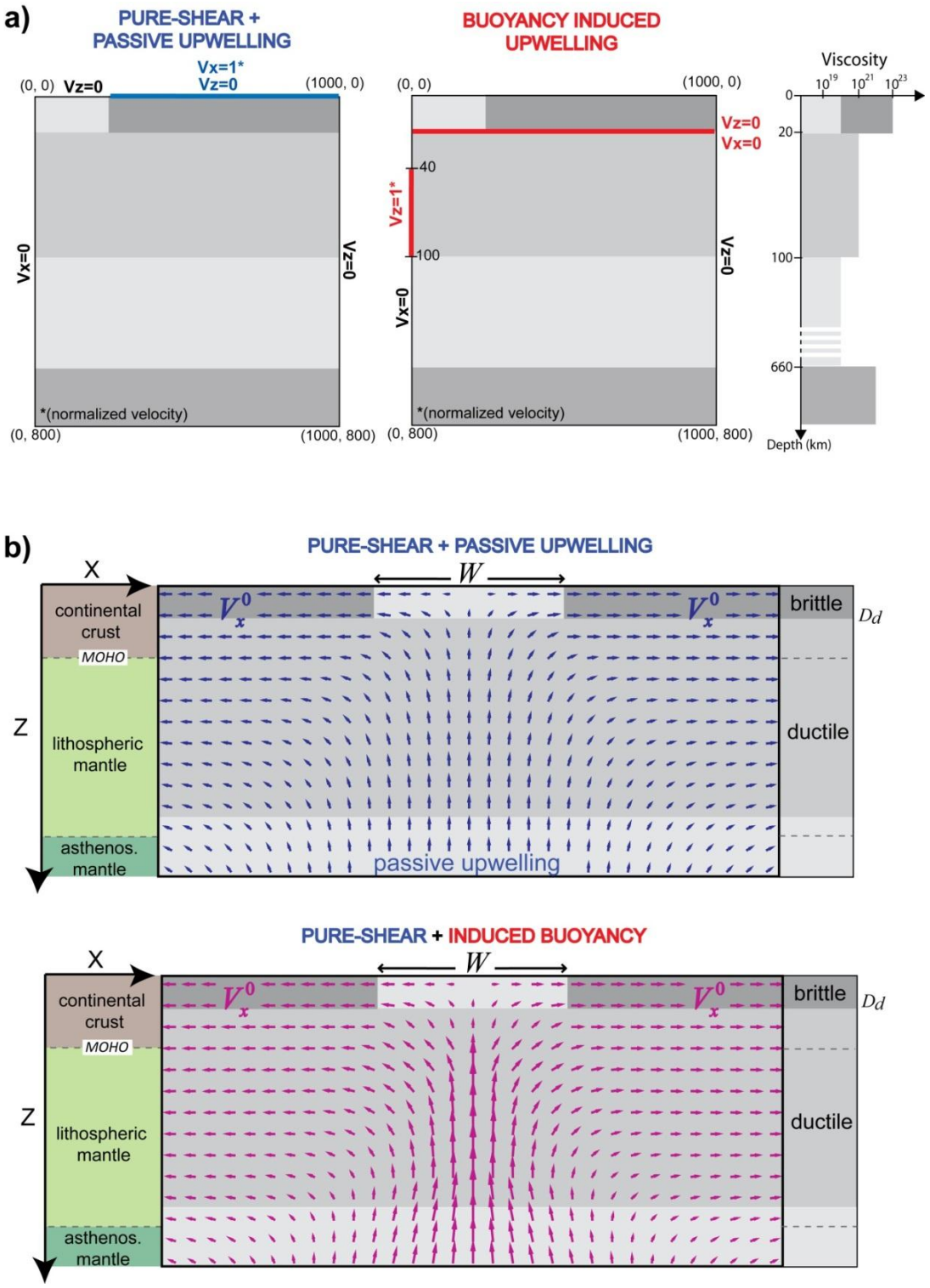

Figure 4.3: Boundary conditions of the 2D finite-element viscous flow model using a Newtonian layered viscosity structure and their resulting flow vectors for **a)** pure-shear + passive upwelling and **b)** buoyancy induced upwelling. W is the pure-shear deformation width. D_d is the decoupling depth between the upper brittle seismogenic layer and the ductile lithosphere and asthenosphere below.

4.3.2 Material and temperature advection

Vectors from buoyancy induced upwelling added to the pure-shear and passive upwelling define a deformation flow-field $\boldsymbol{V}$, which is used to advect material and temperature. Temperature advection uses a Eulerian (x, z) coordinate reference frame system whereas material advection uses Lagrangian. Resolution for both grids is 5km horizontally and 2.5km vertically. Time steps of 50000yrs are used. Regridding of the Lagrangian material grid is required when the horizontal distance between two nodes exceeds 10km. The Moho and the base of the lithosphere are assumed to be initially horizontal. Tracking these boundaries is important to follow the evolution of the continental crust and lithosphere. We identify in our modelling two lithosphere evolutions; the evolution of the isotherm 1280°C and the evolution of the initial base of the lithosphere, which is a passive marker specified by the material boundary (Figure 1c – boundary between the light and dark green domains). Each node characterizes a volume of material, parameterized with a density ρ, thermal conductivity k and specific heat C_p either for the continental crust or the mantle (see Table 4.1 for the value and references).

Temperature behaviour follows the diffusion-advection equation:

$$\frac{\partial T}{\partial t} = \frac{1}{\rho C_p}\nabla(k\nabla T) - \boldsymbol{V}(\nabla T + h) + \frac{A_0}{\rho C_p} e^{-\frac{z}{a_r}} \qquad (1)$$

where T is temperature and h the adiabatic gradient as described by McKenzie and Bickle (1988). Radiogenic heat productivity for the upper half of the continental crust a_r is included using a radiogenic heat production $A_0 = 2.2e^{-6}$ W.m^{-2}. Radiogenic heat productivity of the gabbroic and basaltic ocean crust is neglected. We set the asthenosphere temperature to 1333°C. The initial lithosphere thermal structure is assumed to be in thermal equilibrium. The temperature difference within the lithosphere is compared against an equilibrated oceanic linear thermal structure (McKenzie, 1967; Sclater et al., 1980) to calculate thermal load evolution uplift and subsidence. An initial surface

elevation of approximately 400m is predicted due to the difference of temperature between the initial continental geotherm and the oceanic reference geotherm.

Table 3.1: Table of constants and physical parameters

Variable	Meaning	value	units
Ak	lithosphere thickness for a linear oceanic geotherm	125	km
At	initial lithosphere thickness	135	km
A_0	heat production	$2.2e^{-6}$	$W.m^{-2}$
a_r	radiogenic layer thickness	$Ct/2$	km
C_p	specific heat	1180	$J.kg^{-1}.K^{-1}$
D_d	brittle seismogenic layer	20	km
D_b	depth buoyancy	-	km
F_{ret}	melt retention	-	%
f_m	migration factor	-	-
g	gravitational acceleration	9.81	$m^2.s^{-1}$
h	adiabatic gradient	-	$°C.km^{-1}$
k_c	reference crustal thermal conductivity	2.6	$W.m^{-1}.K^{-1}$
k_m	reference mantle thermal conductivity	3.14	$W.m^{-1}.K^{-1}$
k	thermal conductivity at (X,Z)	-	$W.m^{-1}.K^{-1}$
LF	latent fusion	400	$kJ.kg^{-1}$
M_{cpx}	weight fraction of clinopyroxene being melted	0.16	%
R_b	buoyancy ratio V_z^0/V_x^0	-	-
$T°$	base lithosphere temperature	1333	°C
T	temperature at (X,Z)	-	°C
t	time	-	Myr
V_x^0	Half-spreading rate	-	$mm.yr^{-1}$
V_z^0	Additional upwelling rate	-	$mm.yr^{-1}$
$\boldsymbol{V}$	local velocity vector at (X,Z)	-	$mm.yr^{-1}$
W	pure-shear width	-	km
X	horizontal coordinate	-	km
Z	vertical coordinate	-	km
α	thermal expansion coefficient	$3.28e^{-5}$	$°C^{-1}$
β	stretching factor	-	-
γ	thinning factor	-	-
γ_{crit}	critical thinning factor	-	-
ρ_c	reference crustal density	2850	$kg.m^{-3}$
ρ_m	reference mantle density	3330	$kg.m^{-3}$
ρ_v	reference volcanic addition density	2850	$kg.m^{-3}$
ρ_w	density of water	1040	$kg.m^{-3}$
ρ	density at (X,Z)	-	$kg.m^{-3}$

*(Parsons & Sclater, 1977; McKenzie, 1978; Sclater et al., 1980; Chapman, 1986; Turcotte & Schubert, 2002)

4.3.3 Relative timing of melt generation and crustal breakup

The relative timing of crustal breakup and decompressional melt initiation controls whether mantle exhumation may occur. However, due to the absence of faulting in our model, in the pure-shear and passive upwelling, continental crust is stretched and thinned until the Moho approaches zero depth. Within this context, mantle exhumation would therefore not be possible. We define a critical crustal thickness threshold value after which the continental crust ruptures and separates (i.e. crustal breakup). The critical continental crustal thinning factor ($\gamma = 1 - 1/\beta$) ranges between 0.88 ($\beta = 8.3$) and 0.95 ($\beta = 20$).

The parameterization and methodology of Katz et al. (2003) are used to predict decompressional melting. Melt is generated when the continental lithosphere geotherm crosses the solidus of dry peridotite, but is only extracted after it exceeds a threshold amount of melt fraction F_{ret}. Once the threshold amount of melt fraction F_{ret} is reached, all the melt is extracted and is evenly distributed within the pure-shear region to form the oceanic crust. Consequently the timing of melt production and extraction/migration to the surface are differentiated in the models. During that transient phase before its extraction, the melt may infiltrate the mantle (Cannat et al., 2004; Müntener et al., 2010). Melt retention within the mantle lithosphere may have a considerable importance in explaining mantle exhumation over a wide region at magma-poor rifted margins, as well as providing a viable mechanism for the onset of deformation and buoyancy upwelling (Buck and Su, 1989). In this study, melt retention is set at 6%, unless stated.

4.3.4 Sequence of lithosphere deformation events

The extension of the continental lithosphere leading to continental breakup and seafloor spreading results in complex and polyphase rift evolution, as documented in several rift systems worldwide. Therefore, as shown by several existing numerical and conceptual models (Lavier and Manatschal, 2006; Péron-Pinvidic and Manatschal, 2009), a single lithosphere deformation stage cannot explain the complex rifted margin architecture

commonly imaged (Zelt et al., 2003; Van Avendonk et al., 2009). In the context of the numerical models developed here, deformation events can be applied sequentially by changing the pure-shear deformation width, the half-spreading rate and buoyancy induced upwelling at any time of the sequence. Furthermore, the deformation axis can be displaced by lateral jumps or through continuous lateral migration. Simultaneous rift events are also possible, with important implications for the applicability of our modelling approach to the formation of the Valais and Piemonte-Liguria basins. Therefore, kinematic model can be parameterized in a variety of ways, thus enabling to track the evolution of rifting

4.3.5 Model illustration

The sensitivity of the lithosphere deformation as well as rifted margin architecture to variations of the pure-shear deformation width, the half-spreading rate, buoyancy upwelling strength and the lateral continuous migration of the deformation is illustrated in detail in this section. Each model runs 20Myr.

Pure-shear width

Figure 4.4a explores the sensitivity of the lithosphere and asthenosphere evolution to variations in pure-shear width: a wide (200km) and narrow (20km) pure-shear width are used for illustration. Distributed pure-shear deformations over a wide area result in slow passive upwelling. Decompressional melting is delayed and a small amount of melt is produced. Conversely, narrow pure-shear deformation widths accelerate the passive upwelling and generate melt earlier. The rifted margin crustal architecture exhibits markedly different shapes: a wide pure-shear region results in an elongated margin, with small gradients in both Moho and top basement morphology, while the OCT is sharper if using a narrower pure-shear width. These results indicate that the pure-shear width used in lithosphere deformation modes can be constrained by the observed crustal architecture of rifted margins. Based on the observations at present-day rifted margins (e.g. Iberia-Newfoundland, Péron-Pinvidic and Manatschal, 2009) and slow-spreading ocean ridges

(e.g. Southwest Indian Ridge, Cannat et al., 2009), domains width affected by deformation evolves from broad at the beginning of rifting to narrow during seafloor spreading**.**

Half-spreading rate

We investigate in Figure 4.4b the lithosphere deformation model sensitivity to a half-spreading of 15mm.yr^{-1} and a slower half-spreading rate of 5mm.yr^{-1}. For the same amount of extension, a high spreading rate results in fast passive upwelling, inducing faster thinning of the lithosphere and continental crust with respect to the model runs when a slower spreading rate is used. Melt is also generated earlier and with a higher production rate for fast spreading rates. These results indicate that crustal breakup prior the onset of melting can be achieved only for low half-spreading rates. Therefore, the half-spreading rate is one of the main parameters that may control the presence or absence of mantle exhumation at magma-poor rifted margins. This outcome is consistent with the results from White et al. (2001). As apparent from this section, constraints on the half-spreading rate depend on accurate information on the timing on regional events ranging from basin formation initiation, age of mantle exhumation and melt initiation.

Buoyancy upwelling strength

An additional buoyancy induced upwelling rate V_z^0 is defined using the buoyancy ratio $R_b = V_z^0/V_x^0$. We show in Figure 4.4c that the contribution of buoyancy ($R_b = 3$, $V_x^0 = 10$) enhances fast lithospheric thinning which in turn leads to earlier melting with respect to the model runs involving only passive upwelling. More melt is therefore produced. Buoyancy upwelling is not only important to produce earlier and more voluminous melting, but also to explain lower subsidence or strong uplift during rifting (i.e. mantle plume - Afar rift (Schilling, 1973)). It is possible to constrain the presence or absence of buoyancy at magma-poor rifted margin using melting and subsidence histories.

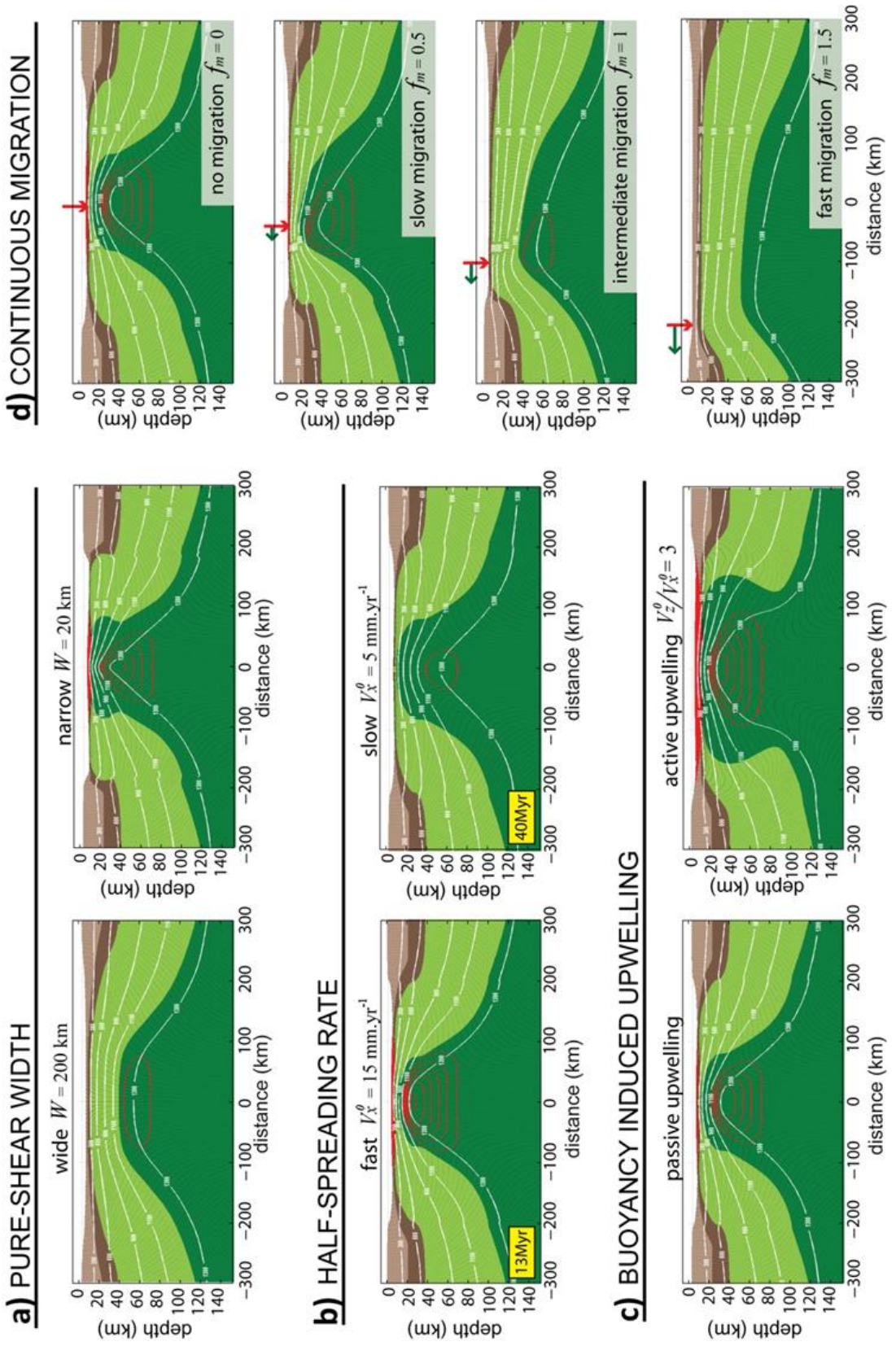
a) PURE-SHEAR WIDTH
wide $W = 200$ km
narrow $W = 20$ km
b) HALF-SPREADING RATE
fast $V_x^0 = 15$ mm.yr^{-1}
slow $V_x^0 = 5$ mm.yr^{-1}
13Myr
40Myr
c) BUOYANCY INDUCED UPWELLING
passive upwelling
active upwelling $V_z^0/V_x^0 = 3$
d) CONTINUOUS MIGRATION
no migration $f_m = 0$
slow migration $f_m = 0.5$
intermediate migration $f_m = 1$
fast migration $f_m = 1.5$
depth (km)
distance (km)

Figure 4.4 *(previous page):* Model sensitivity to **a)** pure-shear width $W = 200$km and 20km, **b)** half-spreading rate $V_x^0 = 5$ and 15 mm.yr-1, **c)** buoyancy strength $R_b = 0$ (passive upwelling) and 3, and **d)** migration of the deformation using no migration, a migration factor $f_m = 0.5$, 1 and 1.5. The deformation axis for each snapshot is indicated by the vertical red arrow. The green horizontal arrow indicates the direction of the migration. Model run time is 20Myr except for the sensitivity to the half-spreading (extension of 200km).

Continuous lateral migration of the deformation

The lateral migration of the deformation is defined as a migration factor f_m relative to the half-spreading rate. Model illustration in Figure 4.4d shows 4 model examples where $f_m =$ 0, 0.5, 1 and 1.5, which, for the half-spreading rate of $V_x^0 = 10$ mm.yr^{-1}, imply a velocity of migration of deformation $V_m = 0$, 5, 10 or 15mm.yr^{-1}, respectively. The horizontal deformation migration generates an asymmetry of the lithosphere and continental crust architecture (see also Sparks and Parmentier (1991)) and it lowers the upwelling rate which in turn delays decompressional melting. The choice of the migration factor is critically important for crustal breakup: if $f_m > 1$, deformation migrates faster than the half-spreading rate, hindering complete excision of the continental crust. In the work described in this paper, which is focussed on the Mesozoic Alpine Tethys, the continuous lateral migration is important because the Valais and Piemonte-Liguria basins may be formed simultaneously; the two rift events consists of adding two flow-fields one to each other so that the half-spreading rate used for one basin interferes with the other basin. This migration interference of the deformation generates an asymmetry of the two basins margins. The asymmetry of one basin is proportional to the half-spreading rate used for the other basin, and it can be avoided by prescribing the corresponding migration factor.

4.3.6 Model limitation and philosophy

The kinematic model presented here is affected by a range of limitations; faulting, sedimentation and erosion are not included. These processes are all known to affect the

subsidence history during rifting; sedimentation attenuates the amount of subsidence and uplift, while footwall uplift of normal faults results in topographic highs that affect the depositional environment. The lack of erosion, sedimentation and faulting may result in deviations of the modeled subsidence history with respect to the actual values. Despite these limitations, we wish to stress that our model is primarily used to investigate the first order deformation of the lithosphere and asthenosphere. The application of the kinematic model to the Alpine Tethys margins aims to investigate the impact exerted by the parameters discussed in section 4.3.4. We test the first order sensitivity of the Internal Briançonnais subsidence history and the evolution of the Alpine Tethys to a single deformation event, two simultaneous rift events and their respective lateral migration and buoyancy induced upwelling.

4.4 Model applications to the Alpine Tethys margins

We examine in this section 10 different models (A to J) for the formation of the Alpine Tethys margins. The 10 model descriptions are schematically shown in Figure 4.5. The first set of models (**A** to **E**) only uses passive lithosphere stretching and thinning while the second set (**F** to **J**) includes buoyancy induced upwelling early during the rifting, from 185 to 170Ma, corresponding to the main thinning phase of the continental lithosphere in the Alpine Tethys. The subsidence history of the Briançonnais domain for each model will be examined in section 4.4.5. We group the 10 models into 4 case experiments: (1) Models **A** and **F** explore a scenario without the formation of the Valais basin, with or without buoyancy induced upwelling; (2) models **B** to **E** examine the importance of the rift migration of both the Valais and Piemont-Liguria basins; (3) models **G** and **H** investigate scenarios with a different duration, timing and speed of the Valais basin; and (4) models **I** and **J** explore the effect of the location of the buoyancy axis, ranging from a single buoyancy upwelling beneath the Briançonnais to double buoyancy upwelling beneath each rift basin.

Figure 4.5 *(previous page):* Schematic description of 10 models scenarios. 2D-cross sections represent the Valais and Piemonte-Liguria basins, their continuous migration and the presence of buoyancy.

4.4.1 Parameterization of the model applications

The lithosphere deformation event parameterization for the 10 models is shown in Table 4.2. They all share the same pre- and post- lithosphere deformation events. All models start with an initial continental crustal thickness of 32.5km and an initial lithosphere thickness of 135km. The initial crustal thickness was constrained following the work of Müntener et al. (2000). These authors suggest that the continental crust had a minimum thickness of 30km at the initiation of the Jurassic rifting based on the estimated depth of crystallization of a mafic intrusion emplaced at the crust-mantle transition during the Permian.

This paper aims to model the uplift and emergence of the Briançonnais domain after its initial subsidence due to a pre/syn-rift event leading to the deposition of the thick Triassic carbonate platform. Consequently, the model starts with the Jurassic rifting at 185Ma with a basin 200km wide and 400m deep. This first deformation event is characterized by the localization of extensional deformation within the Valais and Piemonte-Liguria basins. The Valais basin forms within a width of $W =$ 20-40km (unless inexistent – model **A** and **F**) and the Piemonte-Liguria basin within a width of $W =$ 40-50km. The two deformation axes are initially located 70km apart. The values of the deformation width are arbitrary, but they better describe the narrow rifting evolution of the Piemonte-Liguria (~300km, Li et al., 2013), the Briançonnais domains (~60km, e.g. Lemoine et al., 1986) and, although not well constrained, of the Valais domain (arbitrary ~100km, Stampfli et al., 2002; Handy et al., 2010). Both basins are formed using a half-spreading rate of $V_x^0 = 1.5$mm.yr^{-1} until 170Ma. Between 170 and 165Ma, the half-spreading increases for both basins. However, because the model is constrained using the final width of the Alpine Tethys, their extension rates are different, slower for the Valais than for the Piemonte-Liguria.

Table 4.2: Deformation parameterization for models **A-J.**

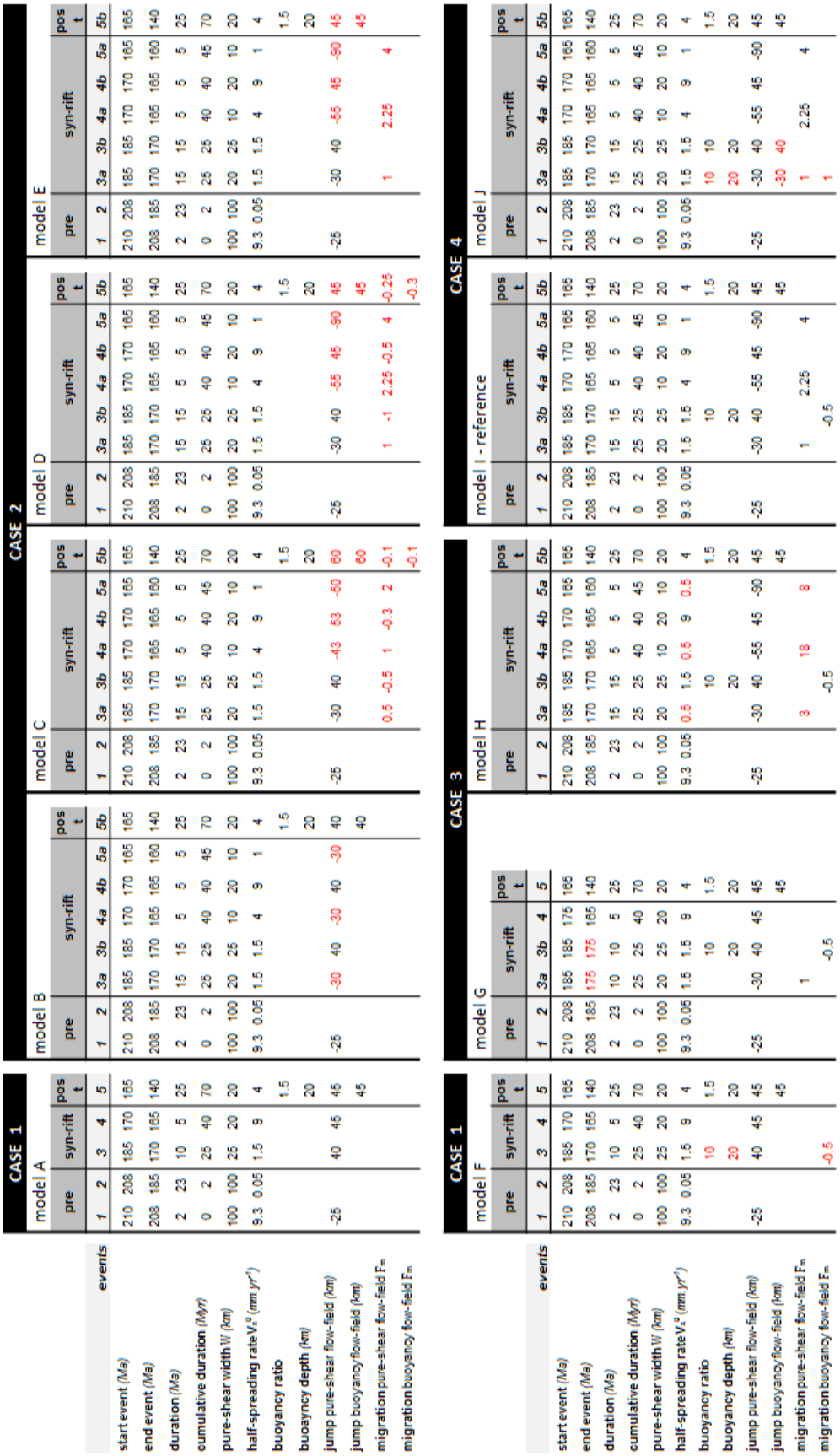

events	CASE 1						CASE 2																	
	model A						model B						model C						model D					
	pre		syn-rift			pos t	pre		syn-rift			pos t	pre		syn-rift			pos t	pre		syn-rift			pos t
	1	2	3	4	5		1	2	3a	3b	4a	4b	5a	5b	1	2	3a	3b	4a	4b	5a	5b	1	2	3a	3b	4a	4b	5a	5b
start event (Ma)	210	208	185	170	165		210	208	185	185	170	170	165	165	210	208	185	185	170	170	165	165	210	208	185	185	170	170	165	165
end event (Ma)	208	185	170	165	140		208	185	170	170	165	165	160	140	208	185	170	170	165	165	160	140	208	185	170	170	165	165	160	140
duration (Ma)	2	23	10	5	25		2	23	15	15	5	5	5	25	2	23	15	15	5	5	5	25	2	23	15	15	5	5	5	25
cumulative duration (Myr)	0	2	25	40	70		0	2	25	25	40	40	45	70	0	2	25	25	40	40	45	70	0	2	25	25	40	40	45	70
pure-shear width W (km)	100	100	25	20	20		100	100	20	25	10	20	10	20	100	100	20	25	10	20	10	20	100	100	20	25	10	20	10	20
half-spreading rate V_x^a (mm.yr^{-1})	9.3	0.05	1.5	9	4		9.3	0.05	1.5	1.5	4	9	1	4	9.3	0.05	1.5	1.5	4	9	1	4	9.3	0.05	1.5	1.5	4	9	1	4
buoyancy ratio					1.5									1.5								1.5								1.5
buoayncy depth (km)					20									20								20								20
jump pure-shear flow-field (km)	-25		40	45	45		-25		-30	40	-30	40	-30	40	-25		-30	40	-43	53	-50	60	-25		-30	40	-55	45	-90	45
jump buoyancy/flow-field (km)					45									40								60								45
migration pure-shear flow-field F_m													0.5	-0.1								-0.1			1		2.25		4	
migration buoyancy flow-field F_m														-0.1								-0.1								-0.3

events	CASE 1						CASE 3																	
	model F						model G						model H						model I - reference					
	pre		syn-rift			pos t	pre		syn-rift			pos t	pre		syn-rift			pos t	pre		syn-rift			pos t
	1	2	3	4	5		1	2	3a	3b	4	5	1	2	3a	3b	4a	4b	5a	5b	1	2	3a	3b	4a	4b	5a	5b
start event (Ma)	210	208	185	170	165		210	208	185	185	175	165	210	208	185	185	170	170	165	165	210	208	185	185	170	170	165	165
end event (Ma)	208	185	170	165	140		208	185	175	175	165	140	208	185	170	170	165	165	160	140	208	185	170	170	165	165	160	140
duration (Ma)	2	23	10	5	25		2	23	10	10	5	25	2	23	15	15	5	5	5	25	2	23	15	15	5	5	5	25
cumulative duration (Myr)	0	2	25	40	70		0	2	25	25	40	70	0	2	25	25	40	40	45	70	0	2	25	25	40	40	45	70
pure-shear width W (km)	100	100	25	20	20		100	100	20	25	20	20	100	100	20	25	10	20	10	20	100	100	20	25	10	20	10	20
half-spreading rate V_x^a (mm.yr^{-1})	9.3	0.05	1.5	9	4		9.3	0.05	1.5	1.5	9	4	9.3	0.05	0.5	1.5	0.5	9	0.5	4	9.3	0.05	1.5	1.5	4	9	1	4
buoyancy ratio			10		1.5					10		1.5								1.5				10				1.5
buoyancy depth (km)			20		20					20		20				20				20				20				20
jump pure-shear flow-field (km)	-25		40	45	45		-25		-30	40	45	45	-25		-30	40	-55	45	-90	45	-25		-30	40	-55	45	-90	45
jump buoyancy/flow-field (km)					45							45								45				40				45
migration pure-shear flow-field F_m									1						3		18		8				1		2.25		4	
migration buoyancy flow-field F_m			-0.5							-0.5						-0.5								-0.5				

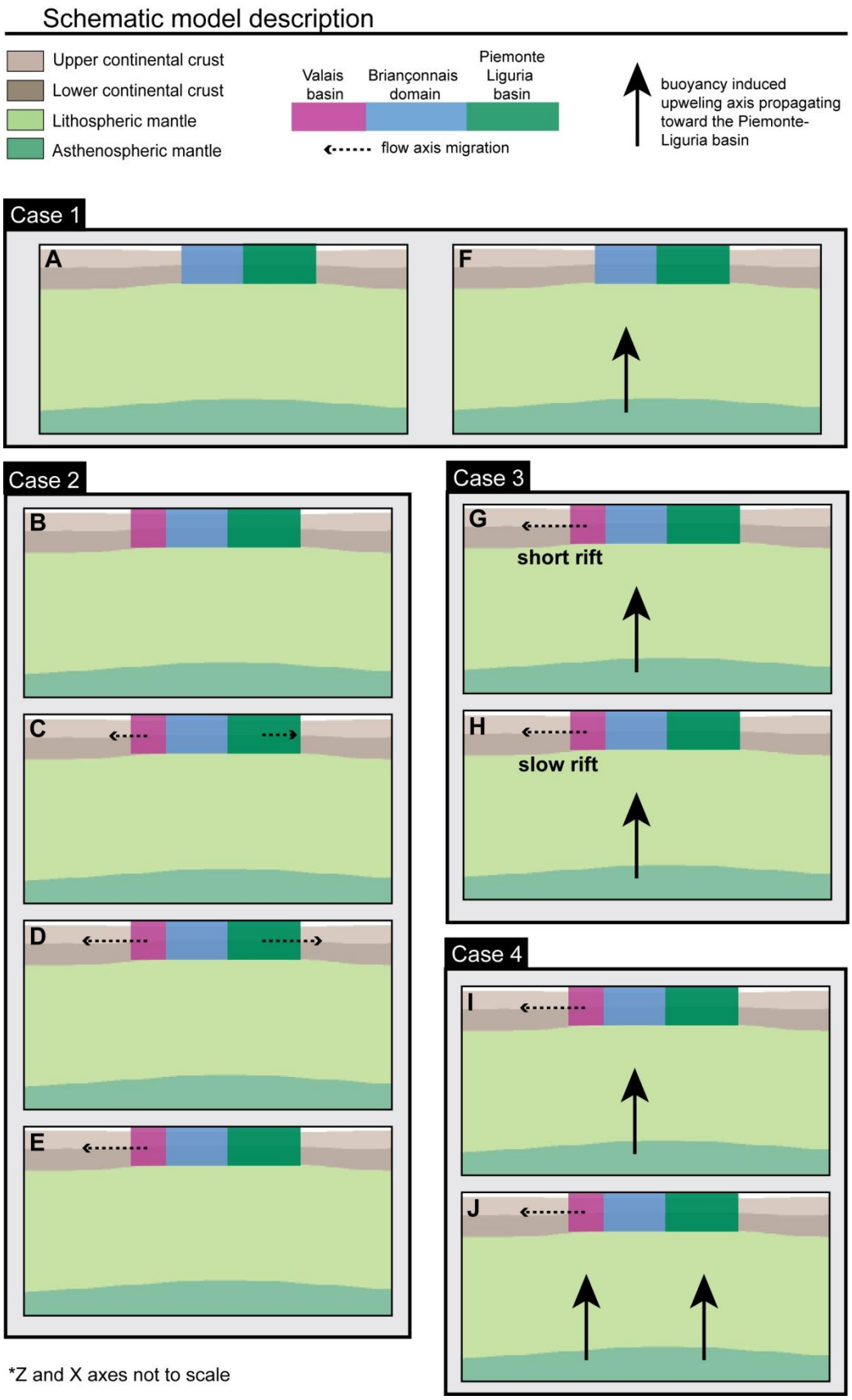
Schematic model description
Upper continental crust
Lower continental crust
Lithospheric mantle
Asthenospheric mantle
Valais basin
Briançonnais domain
Piemonte Liguria basin
flow axis migration
buoyancy induced upweling axis propagating toward the Piemonte-Liguria basin
Case 1
A
F
Case 2
B
C
D
E
Case 3
G
short rift
H
slow rift
Case 4
I
J
*Z and X axes not to scale

Case 1 – Sensitivity to a single rift event

We test the idea that the Valais opened during the second stage of rifting in the Cretaceous as proposed by Frisch (1979), Trümpy and Homewood (1980) and Stampfli (1993). Thus, we explore the model sensitivity to a single rift event leading to the opening of the Piemonte-Liguria basin alone during the Jurassic. Because the model runs to the end of Jurassic, the second stage of rifting of the Valais during the Cretaceous has not been included.

Model A: We explore a single deformation rift event to form the Piemonte-Liguria basin.

Model F: In addition to the formation of the Piemonte-Liguria basin, we impose buoyancy upwelling beneath the future Briançonnais domain at a penetration depth of 20km. This buoyancy upwelling axis migrates slowly toward the Piemonte-Liguria basin until 170Ma.

Case 2 – Sensitivity to lateral migration of two simultaneous rift basins

Two rift events simultaneously form the Valais and the Piemonte-Liguria basins from 185Ma to 160Ma.

Model B: We investigate the lithosphere deformation of the Valais and Piemonte-Liguria basin formation in the case of stable rift axes (no migration).

Model C: The Valais and Piemonte-Liguria basins migrate away from each other at half speed of the half-spreading velocity of the other basin.

Model D: The Valais and Piemonte-Liguria basins migrate away from each other at full speed of the half-spreading velocity of the other basin.

Model E: Only the Valais basin migrates at the same speed as the half-spreading rate of the Piemonte-Liguria. The Piemonte-Liguria basin stays at its original location during all stages of rifting.

Case 3 –Sensitivity to a short duration and slow extension of the Valais basin

Model G: We test the idea of the formation of the Valais basin in the Jurassic during a short period of time from 185 to 175Ma. Buoyancy upwelling, which is applied beneath the Briançonnais domain at a penetration depth of 20km only during the formation of the Valais, migrates laterally toward the Piemonte-Liguria basin.

Model H: Extension in the Valais basin persists for 25Myr at ultra-slow half-spreading rate V_x^0 =0.5mm.yr^{-1}. Buoyancy, which is also applied beneath the Briançonnais domain from 185 to 170Ma, migrates laterally toward the Piemonte-Liguria basin.

Case 4 – Sensitivity to a single and double buoyancy upwelling

Model I: A single buoyancy upwelling is applied at penetration depth 20km beneath the Briançonnais domain from 185 to 170Ma. The buoyancy axis laterally migrates toward the Piemonte-Liguria basin. The Valais basin migrates at the same speed than the half-spreading rate of the Piemonte-Liguria, which is kept stationary (similar to model **E**).

Model J: Two buoyancy upwelling are applied beneath he Valais and Piemonte-Liguria basins from 185 to 170Ma. Lateral migration of the Valais occurs at the same speed than for the Piemonte-Liguria, which is also kept stationary (similar to model **E**).

Breakup and seafloor spreading in the Piemonte-Liguria Ocean are initiated at 165Ma and lasts 25Myr until the modelling ends at 140Ma. An ultra-slow half-spreading rate of 4mm.yr^{-1} is used.

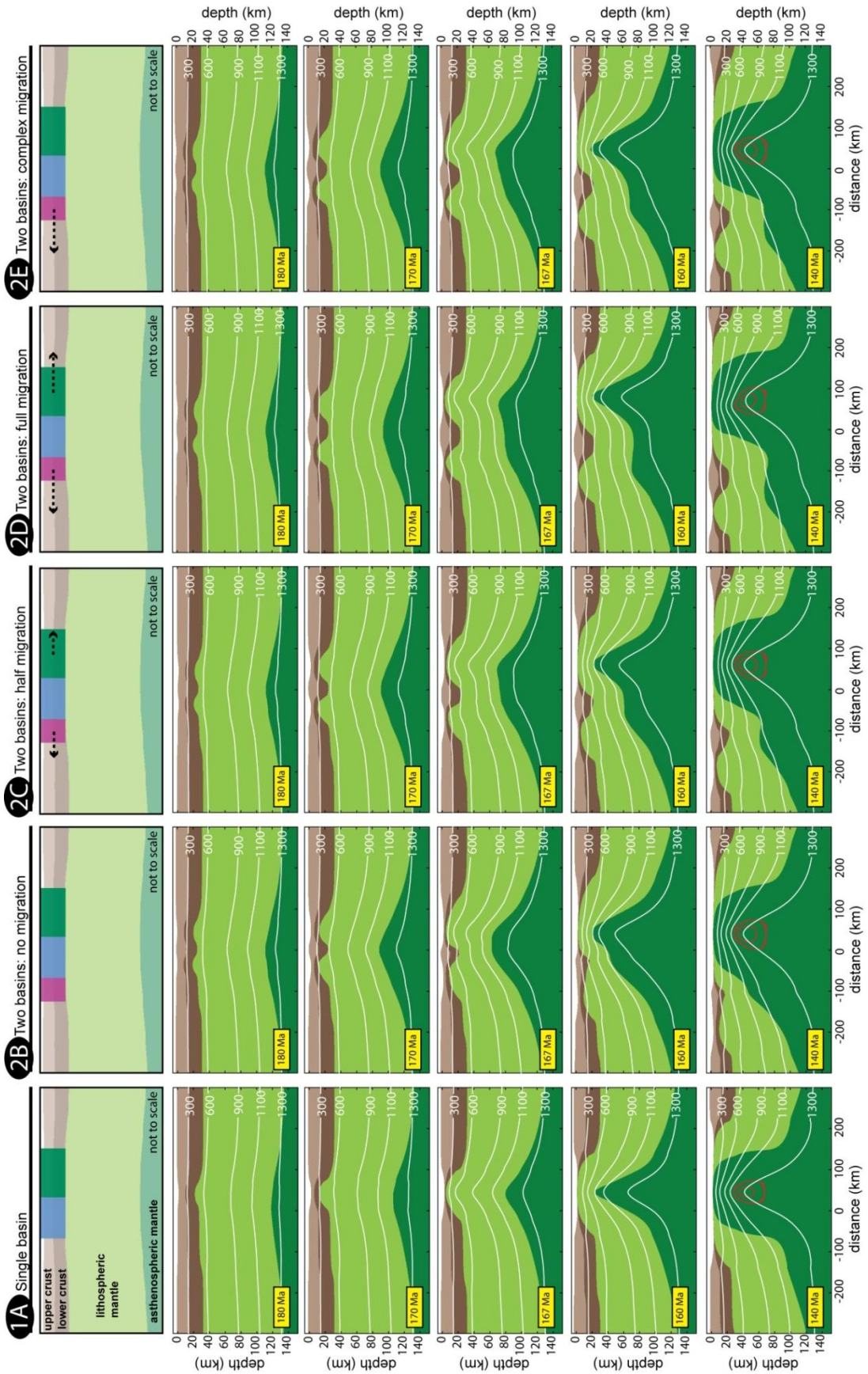
1A Single basin
2B Two basins: no migration
2C Two basins: half migration
2D Two basins: full migration
2E Two basins: complex migration
upper crust
lower crust
lithospheric mantle
asthenospheric mantle
not to scale
depth (km)
distance (km)
180 Ma
170 Ma
167 Ma
160 Ma
140 Ma

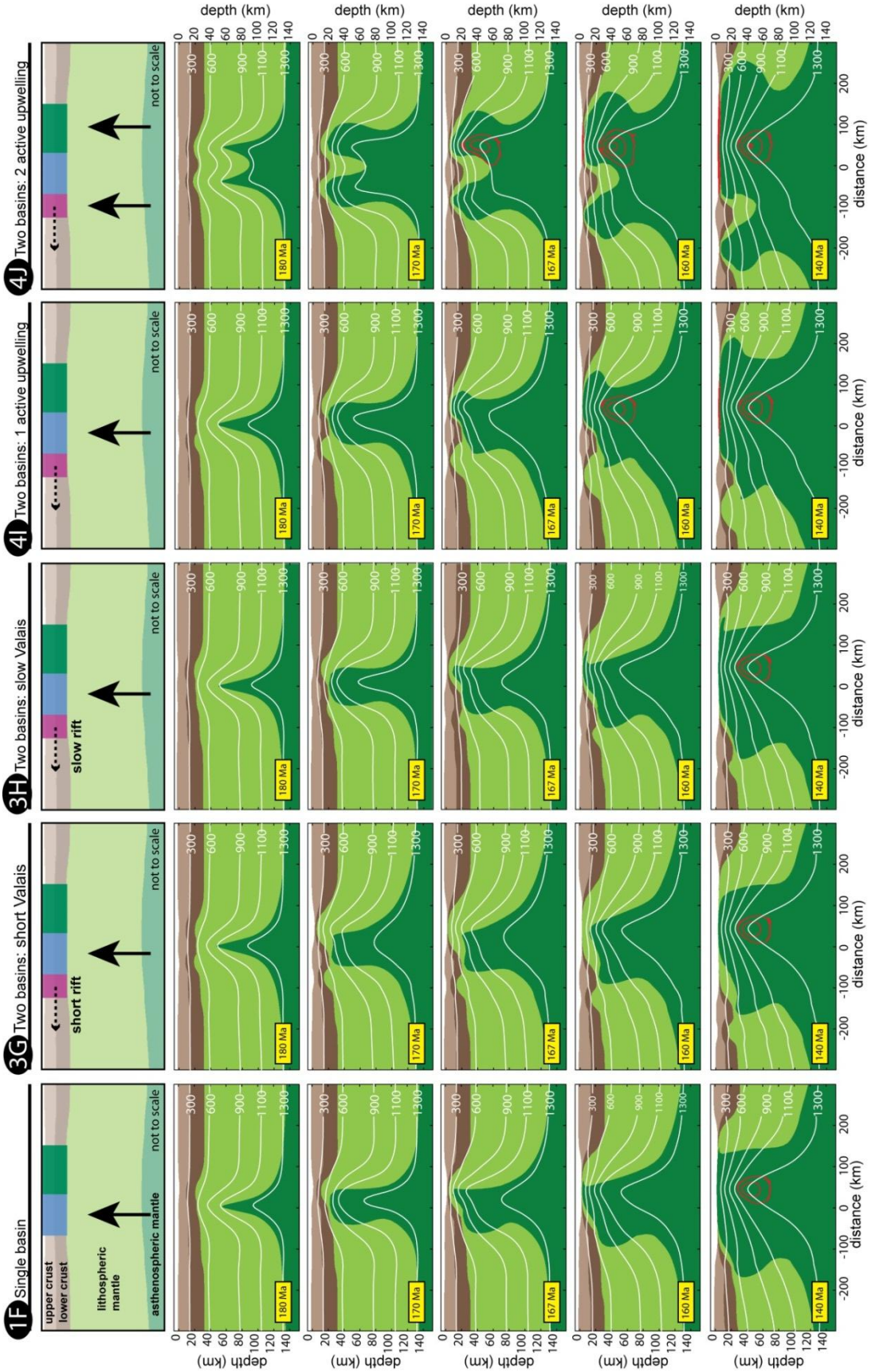
1F Single basin
3G Two basins: short Valais
3H Two basins: slow Valais
4I Two basins: 1 active upwelling
4J Two basins: 2 active upwelling
upper crust
lower crust
lithospheric mantle
asthenospheric mantle
short rift
slow rift
not to scale
depth (km)
distance (km)
180 Ma
170 Ma
167 Ma
160 Ma
140 Ma

Figure 4.6 and ***Figure 4.7*** *(previous pages):* Model lithosphere and asthenosphere behaviour for passive upwelling models **A**-**E** and active upwelling models **F**-**J**. See text for models details. We show 6 snapshots for each model scenarios at 180, 175, 170, 167 and 160 and 140Ma. Melt extraction is instantaneous after its generation. White lines are isotherms (°C) and red contour lines are melt fraction. Contour interval is 0.03%.

4.4.2 Lithosphere deformation model behaviour

The evolution of lithosphere and asthenosphere deformation is shown for each model at 180, 170, 167, 160 and 140Ma in Figure 4.6 (model **A**-**E**) and in Figure 4.7 (model **F**-**J**). Following the distributed extensional event (not showed), which is imposed to achieve a shallow marine environment, the continental crust is thinned from 32.5 to 28km while the lithosphere remains approximately 130-135km thick.

Passive upwelling VS active upwelling

The continental crust is stretched and thinned slowly to form the Piemonte-Liguria basin in all models. From 185 to 170Ma, thinning of lithosphere occurs slowly for passive upwelling models (**A**-**E**). From 170Ma, the lithosphere and continental crust of models **A**-**E** are thinned faster when the extension increases in the Piemonte-Liguria basin, eventually leading to mantle exhumation at about 167Ma and to the first melt around 164-157Ma. Continental crust and lithosphere in the models using buoyancy thin more rapidly (**F**-**J**). These models predict the same timing of mantle exhumation, and earlier melt initiation at 174-163Ma. In models using a single buoyancy upwelling applied below a penetration depth of 20km (**F**-**I**), the Briançonnais domain is thinned by removal of its lower crustal basement. Model **J** explores double buoyancy upwelling: the Briançonnais crust remains thick and this model predicts the earliest melting initiation age (174Ma). Another prediction concerns the type of exhumed mantle, which is asthenospheric, except for all passive models and model **G**.

Sensitivity to the lateral migration of the Valais and Piemonte-Liguria basins

The sensitivity of the model deformation behaviour to lateral migration of two simultaneous lithosphere deformation events is explored in models **B**-**E** (Figure 6). Lithosphere thinning occurs faster in models **B** where the two rift axes remain close to each other, and it also leads to earlier melting at 165Ma. On the other hand, thinning of the lithosphere is slower in models **C**-**E** because rift axes migrates away from each other, thus attenuating passive upwelling flows. Melting in these models is initiated at 160Ma. Model **B** generates a strong asymmetry between the four rifted margins due to migration interference: the spreading rate during the Valais basin formation interferes with that of Piemonte-Liguria basin. Model **E** also predicts the asymmetry but only for the Piemonte-Liguria basin with hyper-extension occurring in the Adriatic distal margin and a sharper necking zone for the Briançonnais conjugate margin. Also in models **B** and **E**, the Briançonnais basement undergoes greater and prolonged thinning. Mantle exhumation within the Valais domain is achieved at ca. 165Ma only if the Valais basin migrates at the same speed as the half-spreading rate set for the Piemonte-Liguria (models **C**-**E**). In model **E** the Valais thins faster than the Piemonte-Liguria domain because its active lateral migration suppresses the effect of the Piemonte-Liguria opening rate.

Sensitivity to the Valais development

No Valais basin results from models **A** and **F**. In models **G** and **H,** the Valais basin is poorly developed due to its short duration (model **G**) or slow spreading rate (model **H**) of rifting. The continental basement flooring the Valais basin is thinned with a stretching factor of 2, so that none of them predicts mantle exhumation. All these models **A**, **F**, **G** and **H** predict slower passive upwelling which delay melting until 165-160Ma, despite that buoyancy upwelling is applied.

4.5 Lithosphere deformation modes constraints from the vertical motion of the Briançonnais

We investigate the complex vertical motion of the Briançonnais domain during rifting to gain insights on the lithosphere deformation modes and highlight the geodynamic evolution of the Alpine Tethys. The Briançonnais domain records uplift in the order of a few hundred meters resulting in emergence from 185 to 170Ma, followed by rapid subsidence to a neritic or a pelagic environment depending the location (Baud and Septfontaine, 1980; Bourbon, 1980). The mechanisms responsible for this subsidence history are explored in this section, which is focused on the predicted model bathymetry of the internal Briançonnais for models **A** to **J**. Further numerical experiments test the uplift/subsidence sensitivity to the initial continental crustal thickness, buoyancy strength and depth and an additional extension event. Model **I** serves as a reference model for comparison.

4.5.1 Briançonnais uplift and subsidence sensitivity to lithosphere deformation

The vertical motion and continental crustal thickness evolution of the Briançonnais domain is explored from 200 to 140Ma. Models start at 185Ma after a first stage of rifting, thinning the continental crust from 32.5km to 28km. This event resulted in the formation of a broad region underlying a water environment ~400m at the beginning of Toarcian (185Ma).

Case 1 – Sensitivity to a single rift event

The sensitivity of Internal Briançonnais subsidence history to a single deformation event leading to the opening of the Piemonte-Liguria alone, either passively (model **A**) or actively with buoyancy upwelling (model **F**) is illustrated in Figure 4.8a. Model **A** does not match the observed uplift/subsidence history of the Briançonnais; it results in little uplift from 185 to 170Ma that keeps the domain underwater. This prediction reflects the too slow passive upwelling to permit rift shoulder uplift. Including buoyancy upwelling to a minimum

penetration depth of 20km beneath the Briançonnais domain as shown by model **F** predicts faster uplift that can possibly lead to its emergence. The continental crust of the Briançonnais remains 27km thick in model **A** while it thins to approximately 20km in model **F**. Fast thermal subsidence of 500m in 10Myr follows the Briançonnais uplift in model **F**, which matches the observations better than model **A**, where the Briançonnais domain remains in water depth ~300m until the model ends. This results from buoyancy induced upwelling beneath the Briançonnais domain which has caused early great lower crustal excision (up to 20km) during the uplift stage.

Case 2 – Sensitivity to lateral migration of two simultaneous rift basins

The predicted bathymetry sensitivity of the Briançonnais domain to the rate of continuous lateral migration of the Valais and Piemonte-Liguria basins in models **B**-**E** is shown in Figure 4.8b. These models do not include any buoyancy. All models predict low uplift from 185Ma to 170Ma with a slow uplift rate of 20m.Myr^{-1}. Emergence of the Briançonnais domain is accomplished but is delayed with respect to the 185-170Ma interval defined from field observations, being initiated at 170Ma. The relationship between the migration of deformation and the interference spreading rates with the resulting vertical motion of the Briançonnais domain is discussed:

(1) ***No migration of the two rift axes:*** This process, illustrated by model **B**, results in a continuous thinning of the Briançonnais crustal basement from 27 to 15km, and in short-lived emersion (2Myr) prior to drowning to depths >1000m in only 5Myr. This successful rapid subsidence is caused upon increasing both rift spreading rates; a faster half-spreading rate for the Piemonte-Liguria basin than for the Valais basin results in displacing the Briançonnais domain toward the initial Valais rift axis. As a consequence, the Briançonnais domain is thinned, leading to rapid subsidence, and the initial Valais basin has stopped spreading.

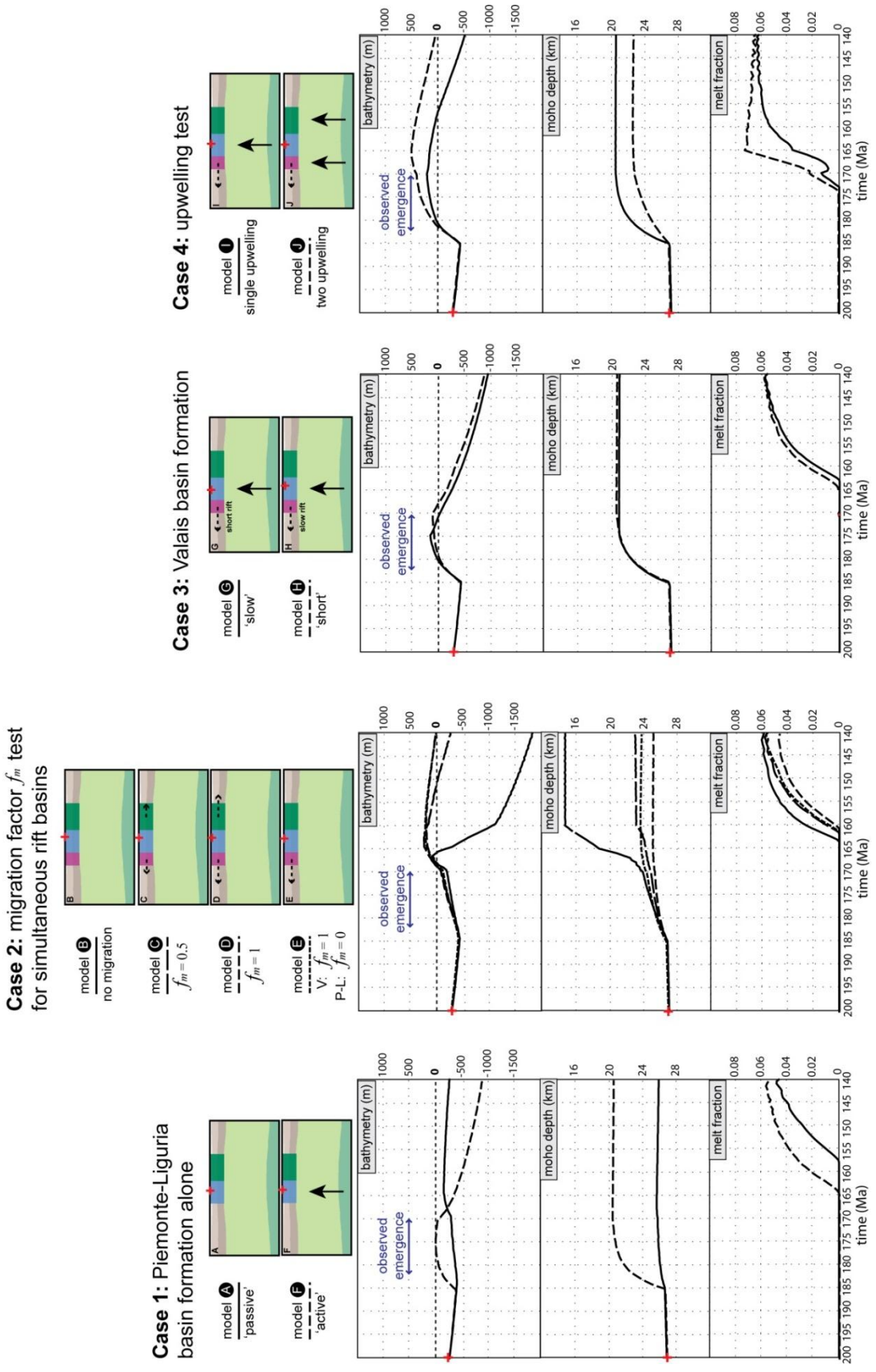
Case 1: Piemonte-Liguria basin formation alone
model A 'passive'
model F 'active'
Case 2: migration factor f_m test for simultaneous rift basins
model B no migration
model C $f_m = 0.5$
model D $f_m = 1$
model E V: $f_m = 1$ P-L: $f_m = 0$
Case 3: Valais basin formation
model G 'slow'
model H 'short'
short rift
slow rift
Case 4: upwelling test
model I single upwelling
model J two upwelling
bathymetry (m)
moho depth (km)
melt fraction
observed emergence
time (Ma)

Figure 4.8 *(previous page):* Vertical motion history of the internal Briançonnais domain for the 4 cases models. The upper panel shows the bathymetry evolution of the Briançonnais, the middle panel shows its crustal thickness evolution and the lower panel melt fraction.

(2) ***Migration of the two rift axes:*** in models **C** and **D**, the crustal thickness is thinned to 25km and 23km respectively because the two basin axes migrate away to each other attenuating the interference of their prescribed spreading rates. This inevitably prevents subsequent rapid subsidence of the Briançonnais domain and therefore predicts a longer lived emersion. The maximum amplitude of emergence is 250m above sea-level. Duration of emergence and final thickness of the Briançonnais basement are related to the migration rate of the Valais and Piemonte-Liguria basins; The thermal subsidence starts at 165Ma and plunges the Briançonnais below sea-level from 150Ma (model **C**) or 140Ma (models **D**).

(3) ***Migration of the Valais basin only:*** In model **E**, the Briançonnais vertical motion predicts similar results than to model **D**. This result shows that the migration of the deformation has little impact on the subsidence history of the Briançonnais domain, but that the spreading rate controls the overall passive upwelling, especially beneath the Briançonnais, in case of simultaneous basins formation.

Case 3 – Sensitivity to a short duration and slow extension of the Valais basin

Models **G** and **H** explore a short and slow Valais basin formation respectively. Both models follow a similar behaviour as shown in Figure 4.8c, which match the observed emergence and subsidence of the Briançonnais; Briançonnais uplift and emergence up to 100m above sea-level is predicted from 180 to 170Ma prior to sink below 500m in 15Myr. The fast uplift and emergence is due to buoyant upwelling prescribe beneath the Briançonnais domain so that the continental crust thinned from 28km to 20km. The results from both models **G** and

H are similar to those from model **F**, where no Valais basin is prescribed. Therefore, rapid post-uplift subsidence of the Briançonnais domain is equally achieved if rifting in the Valais basin post-dated the Piemonte-Liguria basin formation (model **F**) or was contemporary, either at slow extension rate (model **G**) or for short duration of rifting (model **H**). These similar consequences arising from widely different model setups are best explained due to the fact that the Valais basin remains a cold region, thus allowing thermal equilibration and faster subsidence of the Briançonnais domain.

Case 4 – Sensitivity to a single and double buoyancy upwelling

The sensitivity of the predicted Briançonnais vertical motion to a single (model **I**) and double (model **J**) buoyancy upwelling is shown in Figure 4.8d. Both models predict fast uplift leading to the emergence of the Briançonnais domain rapidly after the onset of the two simultaneous rift events at 185Ma. In model **I** (single upwelling), sub-aerial elevation of ~250m is achieved and emersion lasts for 25Myr. Double upwelling (model **J**) results in greater uplift, reaching up to 500m above sea-level, and long-lived emersion, lasting until early Cretaceous (140Ma). This is because in model **I** the Valais basin is active until 160Ma so that the Briançonnais remains close to the upwelling. The lower crust of the Briançonnais is removed by buoyancy induced upwelling in both models; resulting in a final thickness of the Briançonnais domain of 21km and 23km for model **I** and **J** respectively. Subsidence starts from 170Ma in model I, where the Briançonnais reached submarine condition at 155Ma. Model **J** prediction displays the same subsidence rate than in model **I**. However, due to its preceding high altitude, the Briançonnais domain does not plunge below sea-level within the time allocated by the model.

Summary

Uplift and emergence of the Briançonnais domain is accomplished, in the context of passive lithospheric thinning, only in case of contemporaneous rifting of the Valais and Piemonte-Liguria basins (models **B**-**E**). However, our modelling results suggest that the thermal uplift

related to passive upwelling is too slow to permit emergence of the Internal Briançonnais at 180Ma (models **A**-**E**). We can presume that the emergence of the Briançonnais domain may be possible by passive upwelling alone if its initial bathymetry was close to sea-level (<100m). The rate of passive upwelling may also be increased by using extension rates >3mm.yr^{-1}. However, such high rates are inconsistent with the timing of rifting (~185Ma), mantle exhumation (~167-onward) and seafloor spreading (~160Ma) for the Alpine Tethys.

There is no doubt that a single or double buoyancy upwelling can generate the emergence of the internal Briançonnais, and especially in the presence of the simultaneous formation of the Valais and Piemonte-Liguria basins. However, the emergence lasts too long in all models including buoyancy induced upwelling. The duration of emergence is dependent on the location of buoyancy upwelling axis and on the predicted Valais basin development; a poorly developed Valais basin, unless inexistent, results in faster subsidence of the Briançonnais domain. Consequently, further numerical experiments need to be carrying out to improve the results of uplift and subsidence of the Briançonnais domain.

4.5.2 Briançonnais uplift and subsidence sensitivity to initial continental crustal thickness, buoyancy strength and buoyancy penetration depth

The sensitivity of vertical motion to the initial continental crustal thickness, the rate of buoyancy upwelling and the penetration depth below which buoyancy is applied, are dealt with in detail in this section. Model **I**, with an initial crustal thickness of 32.5km and buoyancy upwelling rate of $V_z^0 = 15$mm.yr^{-1}, is used as reference. Only one parameter is changed at a time in each numerical experiment.

Sensitivity to initial continental crustal thickness

We examine in Figure 4.9a the sensitivity of the predicted vertical motion of the Briançonnais domain to an initial continental crustal thickness of 30, 32.5 and 35km.

Significant uplift is achieved only for a relatively thin initial continental crust (<35km), while no emergence is predicted for an initial continental crust >35km. Uplift of the Briançonnais of 500m above sea-level is achieved for an initial crustal thickness of 30km. In this case, submarine conditions are attained again after a relatively long interval, at 145Ma.

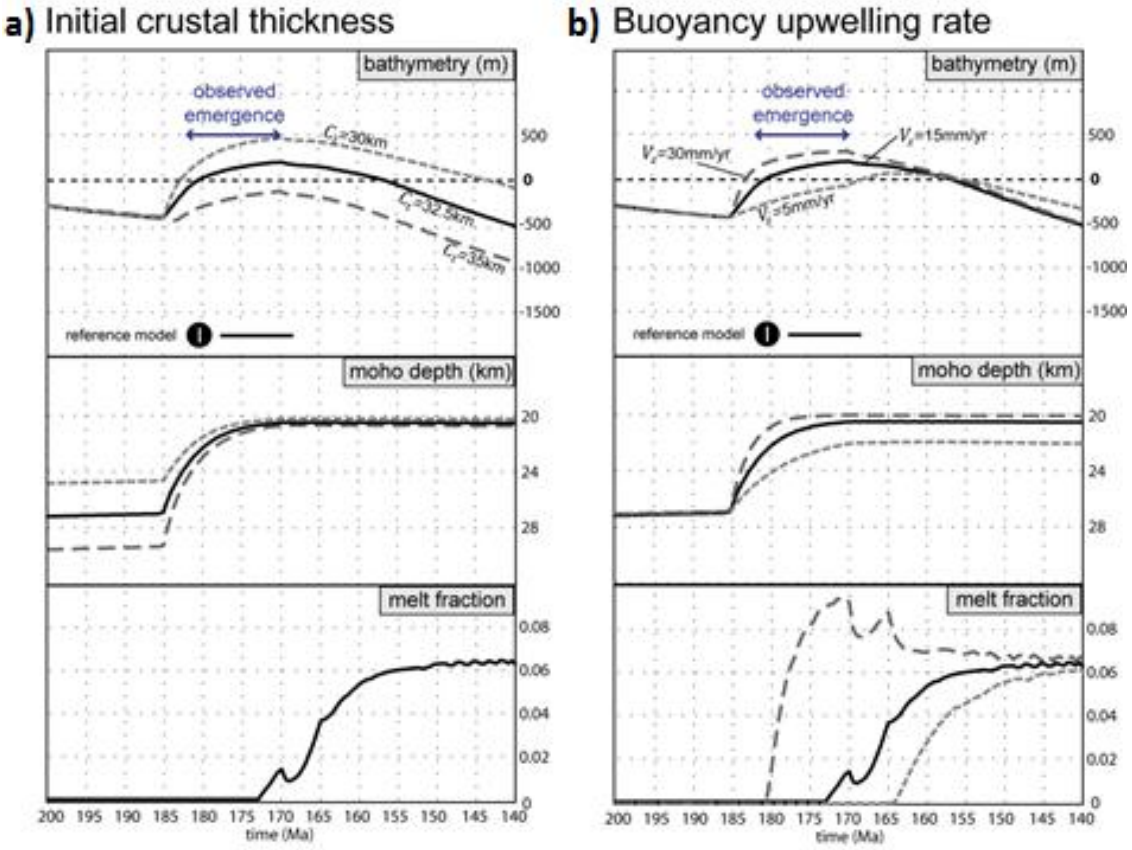

Figure 4.9: Model **I** Briançonnais vertical motion, crustal basement thickness and melt fraction sensitivity to **a)** initial continental crustal thickness of 30, 32.5 and 35 km and **b)** the buoyancy upwelling rate $V_x^0 = 5$, 15 and 30mm.yr^{-1}.

Sensitivity to buoyancy upwelling rate

In Figure 9b buoyancy strength is examined using an upwelling rate ranging from $V_z^0 = 30$mm.yr^{-1} ($R_b = 20$) to $V_z^0 = 5$mm.yr^{-1} ($R_b = \sim 3$). A single and weak buoyancy upwelling

beneath the Briançonnais does not permit its emergence between 185 and 170Ma. Weak buoyancy upwelling rate of $V_z^0 = 5\text{mm.yr}^{-1}$ results in slow uplift at the beginning of the localization of the deformation from 185 to 170Ma, followed by the increase of the uplift rate. This second uplift, due to the increase of the extension rate in adjacent Valais and Piemonte-Liguria basins, results in the emergence of the Briançonnais. In addition, a weak contribution of buoyancy results in thinning of Briançonnais crustal basement to 22km, thus predicting little post-uplift subsidence. Conversely, strong buoyancy upwelling rate of $V_z^0 = 30\text{mm.yr}^{-1}$ results in faster uplift rates and higher elevation. However, strong buoyant upwelling does not particularly change the trend of the post-uplift subsidence because the Briançonnais need longer time to thermally cool down.

Sensitivity to buoyancy penetration depth

Buoyancy driven upwelling equates to small-scale convection occurring in the middle/lower lithosphere, but the shallowest lithospheric depths involved in this process may vary. The influence of variable buoyancy upwelling penetration depths of 10, 20 and 30km on the crustal architecture of the Briançonnais is explored in Figure 10a. Figure 10b shows the resulting subsidence history for the internal Briançonnais. A buoyancy depth of 10km results in thinning of the continental crust of the Briançonnais domain to ~8km, leading to strong subsidence (bathymetry of ~2800m). For a 30km buoyancy depth, crustal thinning to ~24km in the Briançonnais is exclusively due to the formation of the two adjacent basins; emergence is possible, but post-uplift thermal subsidence is slow so that the domain remains emerged until the end of the model. Therefore, as apparent from this section, the choice of the buoyancy penetration depth exerts a major influence on the resulting uplift and subsidence; shallow depth implies no uplift and strong subsidence and deep penetration depth leads to emergence and slow subsidence.

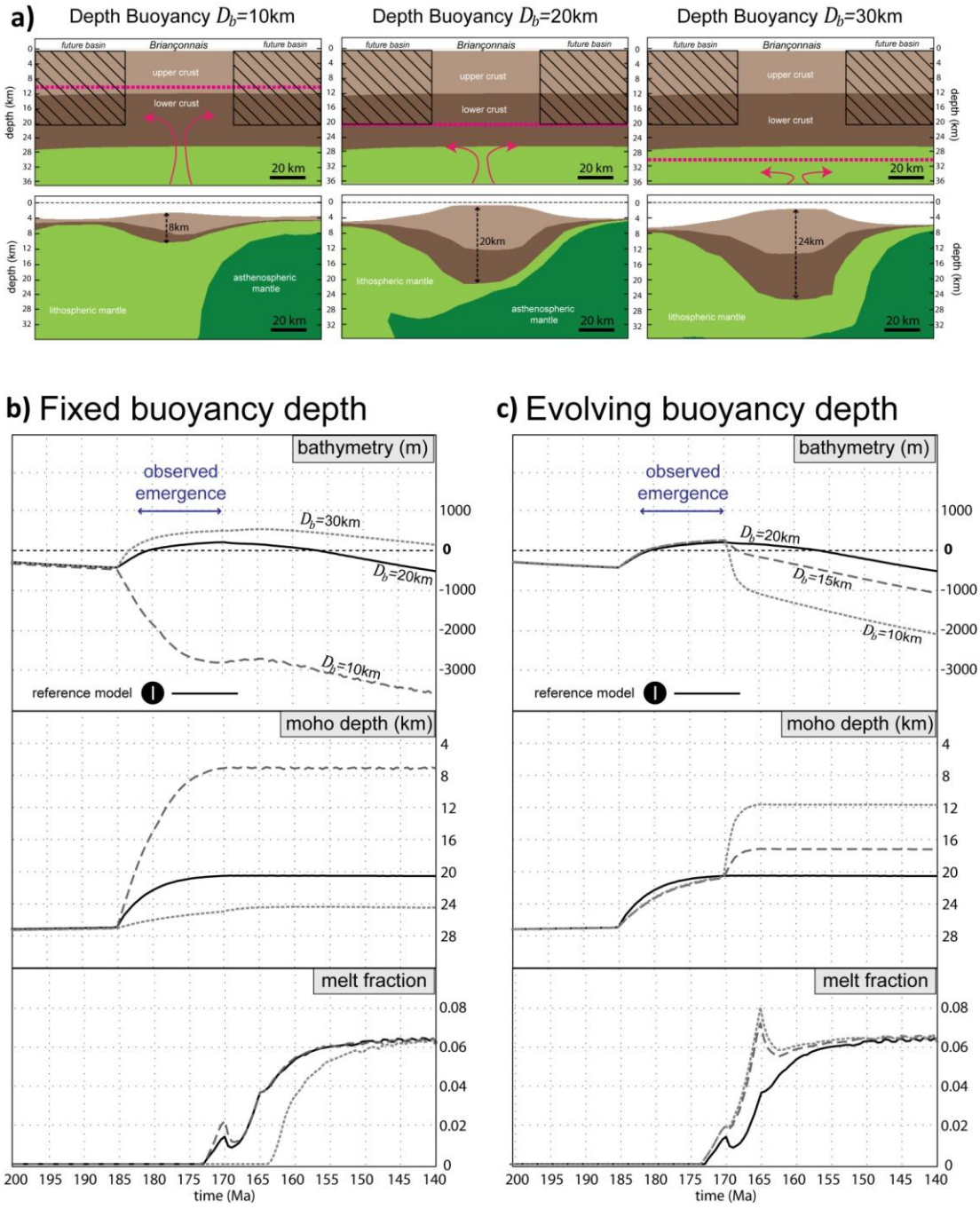

Figure 4.10: **a)** Snapshots illustrating the resulting crustal architecture of the Briançonnais domain due to deep or shallow buoyancy upwelling penetration depths. **b)** Model **I** Briançonnais vertical motion, crustal basement thickness and melt fraction sensitivity to the buoyancy upwelling penetration depth $D_b = 10$, 20 and 30km. **c)** Sensitivity test to an evolving buoyancy upwelling penetration depth from $D_b = 20$km (up to 170Ma) to 15 or 10km for 5Myr (from 170 to 165Ma).

4.5.3 Additional subsidence

In our modelling, the predicted slow post-uplift subsidence is not consistent with the stratigraphic evolution of the SW Briançonnais domain indicating fast subsidence, locally reaching deep water conditions (Bourbon, 1980). As shown in the previous section, changes in the buoyancy penetration depth lead to results that, while matching some key features of the Briançonnais subsidence history, fail to predict others. More specifically, the penetration depth of buoyancy upwelling should be ≥20km in order to permit the emergence of the Briançonnais domain. In contrast, the buoyancy depth must be shallower than 20km in order to reach greater depth subsidence. However, this parameter choice subsequently prevents sufficient subsidence. Therefore, we propose a model using an evolving buoyancy penetration depth, starting at 20km in the 185-170Ma interval, and then ascending to 15 or 10km for 5Myr, as shown in Figure 10c. This scenario implies that buoyancy induced upwelling continues until 165Ma. As apparent from Figure 4.10, a buoyancy depth to 10km from 170Ma results in very fast subsidence from 200m above sea-level to -1000m at 167Ma, followed by slower thermal subsidence to -2000m by the end of Jurassic.

While the penetration depth below which buoyancy induced upwelling is applied permits to remove the lower crustal basement of the Briançonnais domain, and also to control its subsidence, another process may be involved. Although no subsequent extensional event is recorded in the internal Briançonnais, we explore in Figure 4.11 the post-uplift subsidence sensitivity to an extensional event affecting the Briançonnais basement. This new test is similar to model **B** where the Valais and Piemonte-Liguria basin remained at their initial location during rifting. In this previous model, the Briançonnais domain was moving toward the Valais deformation region upon increasing of the spreading rate in the Piemonte-Liguria basin (Figure 4.11a), resulting in its thinning. As an illustration in Figure 4.11b, we test the model at different extension rate, $V_x^0 = 0.5$, 1, 1.5 and 2mm.yr^{-1}. This event last 10Myr

from 175 to 165Ma, and results in thinning of the Briançonnais domain that plunges the domain rapidly to great depth. Using an extensional rate of 2mm.yr^{-1} leads the Briançonnais crust to thin unto 12km and predicts a bathymetry of -2000m.

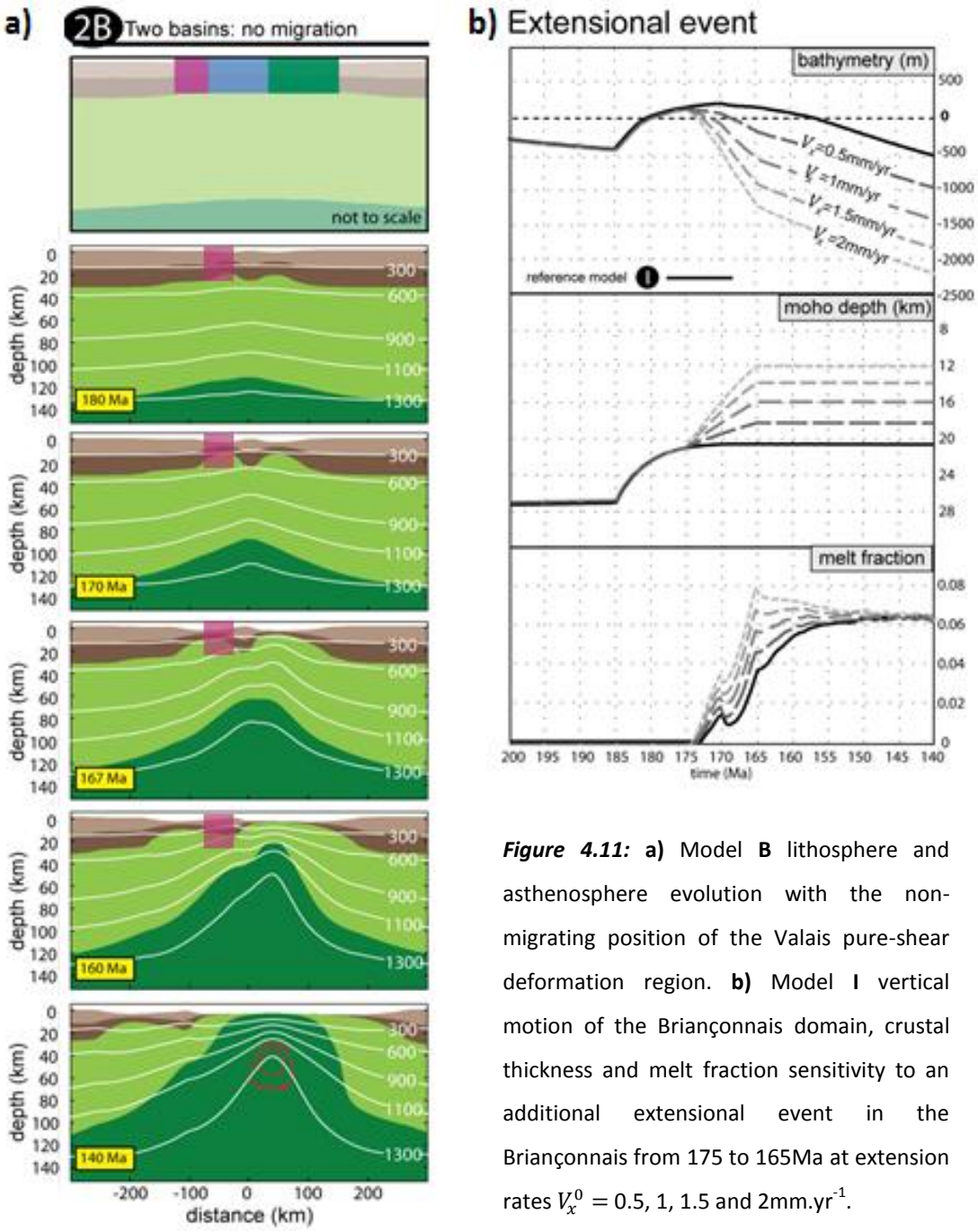

Figure 4.11: **a)** Model **B** lithosphere and asthenosphere evolution with the non-migrating position of the Valais pure-shear deformation region. **b)** Model **I** vertical motion of the Briançonnais domain, crustal thickness and melt fraction sensitivity to an additional extensional event in the Briançonnais from 175 to 165Ma at extension rates V_x^0 = 0.5, 1, 1.5 and 2mm.yr^{-1}.

4.5.4 Summary of the model results

We have explored the sensitivity of the models to the lateral migration of deformation, passive and active upwelling, the Jurassic or Cretaceous opening of the Valais basin, and short duration or slow extension of the Valais opening. In this section the best parameterization of the lithosphere deformation modes predicting the emergence of the Briançonnais domain from 180-170Ma and its post-uplift fast or slow subsidence is summarised. The results and parameterization of all models are summarized in Figure 4.12.

Regardless geodynamic implications, models **B** (if buoyancy also induces upwelling beneath the Briançonnais domain), **F**, **G**, **H**, **I** and **J** give predictions which may likely match the observed uplift and emergence. Buoyancy induced upwelling play the most important role to cause the emergence of the Briançonnais domain. Migration of the buoyancy upwelling axis toward the Piemonte-Liguria domain was introduced in order to move the Briançonnais away from the thermal upwelling (models **G**, **H** and **I**), but this process resulted in less than 500m of thermal subsidence in 10Myr, thus failing to explain the rapid subsidence

Emergence of the Briançonnais domain is successfully achieved with a depth of buoyancy >20km during the first stage of rifting from 185 to 170Ma; for values <20km, the thermal uplift cannot compensate the subsidence resulting from the increased crustal thinning. However, a final thickness of the Briançonnais crust in order of 20km thick prevents rapid post-tectonic subsidence. We thus propose that tectonic thinning of the continental crust, rather than thermal equilibration, is the main process explaining fast subsidence. An evolving buoyancy depth from 20km to shallower depth permits the Briançonnais to subside rapidly. Therefore, if the depth of buoyancy shallows gradually from 20 to 10km (from 170 to 160Ma) fast subsidence is achieved, thus matching geological data. An upward-propagating penetration depth of buoyancy beneath the Briançonnais may be the main process causing the initial uplift and emergence of the Briançonnais domain (penetration depth of ~30-25km) before it subsides when the penetration depth shallows.

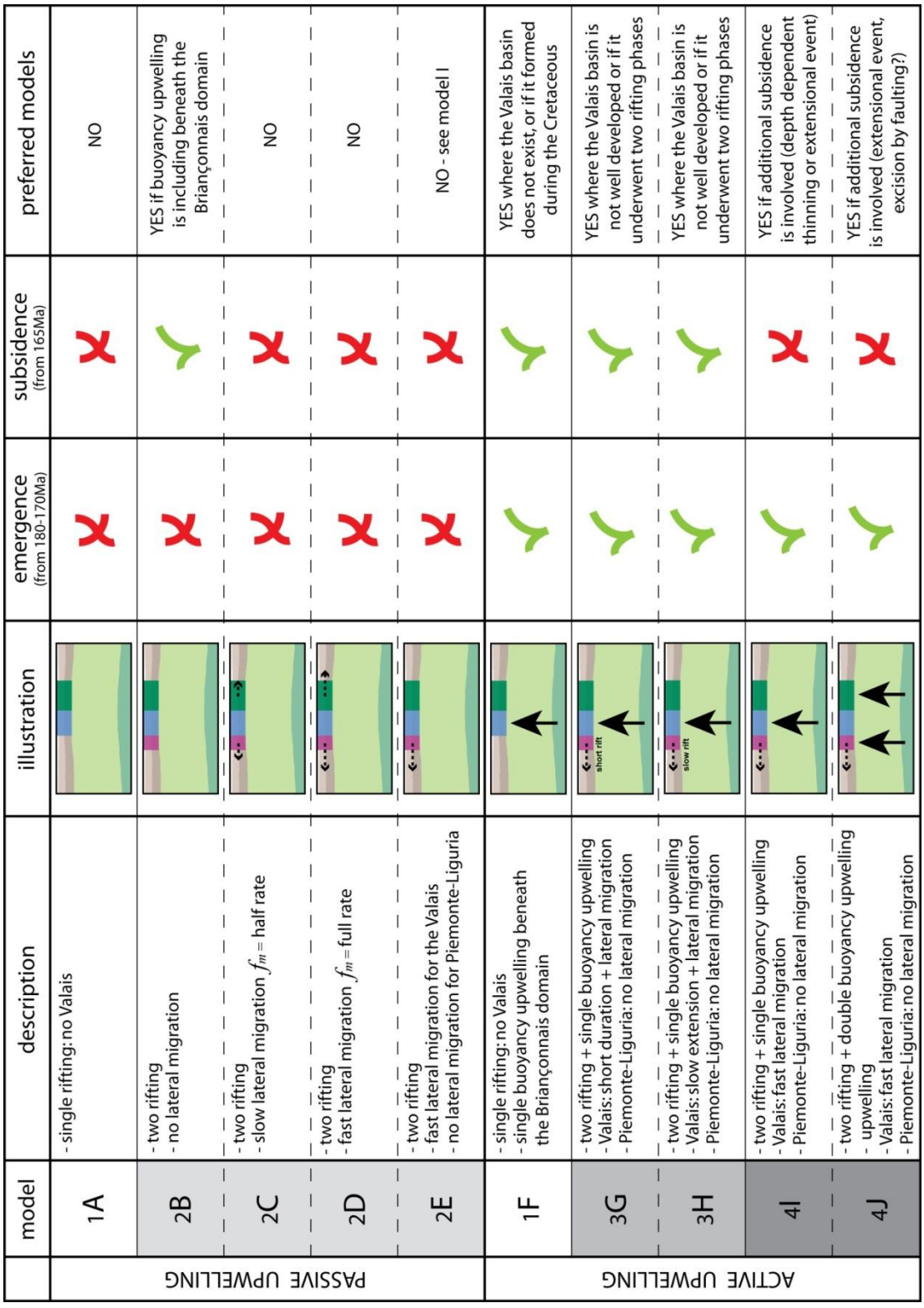

Figure 4.12: Summarization of models **A**-**J**

4.6 Discussion

The aim of the paper was to (1) investigate the lithosphere deformation during intracontinental rifting leading to breakup that formed the Alpine Tethys and (2) to unravel the tectonic processes responsible for the complex uplift and subsidence history record of the Briançonnais domain during rifting. We have examined 10 models using a kinematic model of lithosphere deformation. These models have been quantitatively calibrated using available geological data observed in the Alps. In this section the geodynamic implications for the evolution of the Alpine Tethys is discussed according to the Briançonnais uplift and subsidence results. A summary of the evolution of the Alpine Tethys is also proposed using model **I** and P-T-t predictions for this model.

4.6.1 Geodynamic implications for the evolution of the Alpine Tethys

Models **B**, **F**, **G**, **H I** and **J** were selected to satisfy uplift and subsidence of the Briançonnais domain, despite any geodynamic consideration on their applicability to the specific case of the Alpine Tethys. In this section, geodynamic implications of these models are tested against the first order observations and controversies concerning the Alpine Tethys history.

Timing evolution of the Alpine Tethys

The possibility that the Valaisan opening post-dated rifting in the Piemonte-Liguria basin is modelled in model **F**. Within this geodynamic scenario localized rifting occurs first for the Piemonte-Liguria domain, from Pliensbachian (185Ma) onward, followed by re-rifting during the Early Cretaceous of the Alpine Tethys domain due to plates tectonic re-organization (i.e. the north-propagating opening of the Atlantic North) which led to the formation of the Valais basin westward of the Briançonnais domain (Liati et al., 2005). In this case, the Briançonnais domain can uplift and emerge due to buoyancy upwelling. In addition, it is also possible that a poorly developed Valais basin was created

contemporaneously to the Piemonte-Liguria basin but the extension did not persist to the entire opening, until it re-rifted during the Cretaceous (Liati et al., 2005). Models **B**, **G** and **H**, illustrating this scenario, predict uplift and emergence of the Briançonnais domain only with buoyancy induced upwelling. Our modelling shows that earlier the Valais rifting stops (model **G**) or the most slowly it opens (model **H**), in deeper water the Briançonnais sinks.

The other scenario suggests that the opening of the Valais is contemporaneous with the Piemonte-Liguria during the Jurassic. The simultaneous formation of the Piemonte-Liguria and Valais basins causes the Briançonnais to remain close to the heat source. This results in uplift of the Briançonnais and its emergence with buoyancy upwelling as shown with models **I** and **J**. Melting initiation for these models is consistent with the observed early melting due to high passive upwelling rate in addition to buoyancy upwelling. However, fast subsidence is unlikely by thermal subsidence only, unless there is an additional subsidence process, such as faulting or depth dependent thinning (ascending buoyancy depth).

Spatial evolution of the Alpine Tethys

Marked along strike variations of the architecture of the European margin, with the Valais basin progressively widening to the NE where it merges with the Piemonte-Liguria Ocean (Frisch, 1979; Trümpy and Homewood, 1980; Lemoine et al., 1986; Bertotti et al., 1993), should also be taken into account. This lateral variation may be due to different opening rates (or the presence of a rotation pole) from SW to NE which would suggest that models **B**, **F**, **G** or **H** may be applicable for the SW end of the basin, while models **I** or **J** may work for the NE. We illustrate in Figure 4.13 this lateral variation of the deformation with two example scenarios using 3 models evolution; model **F** is used further the SW end of the Valaisan basin, model **H** where the Valais basin is poorly developed, and either model **I** (scenario 1 – single buoyancy upwelling) or model **J** (scenario 2 – double buoyancy upwelling) where the Valais rifting leads to mantle exhumation. In both example scenarios, we want to illustrate from 180Ma to 140Ma the faster opening of the Valais basin in the NE.

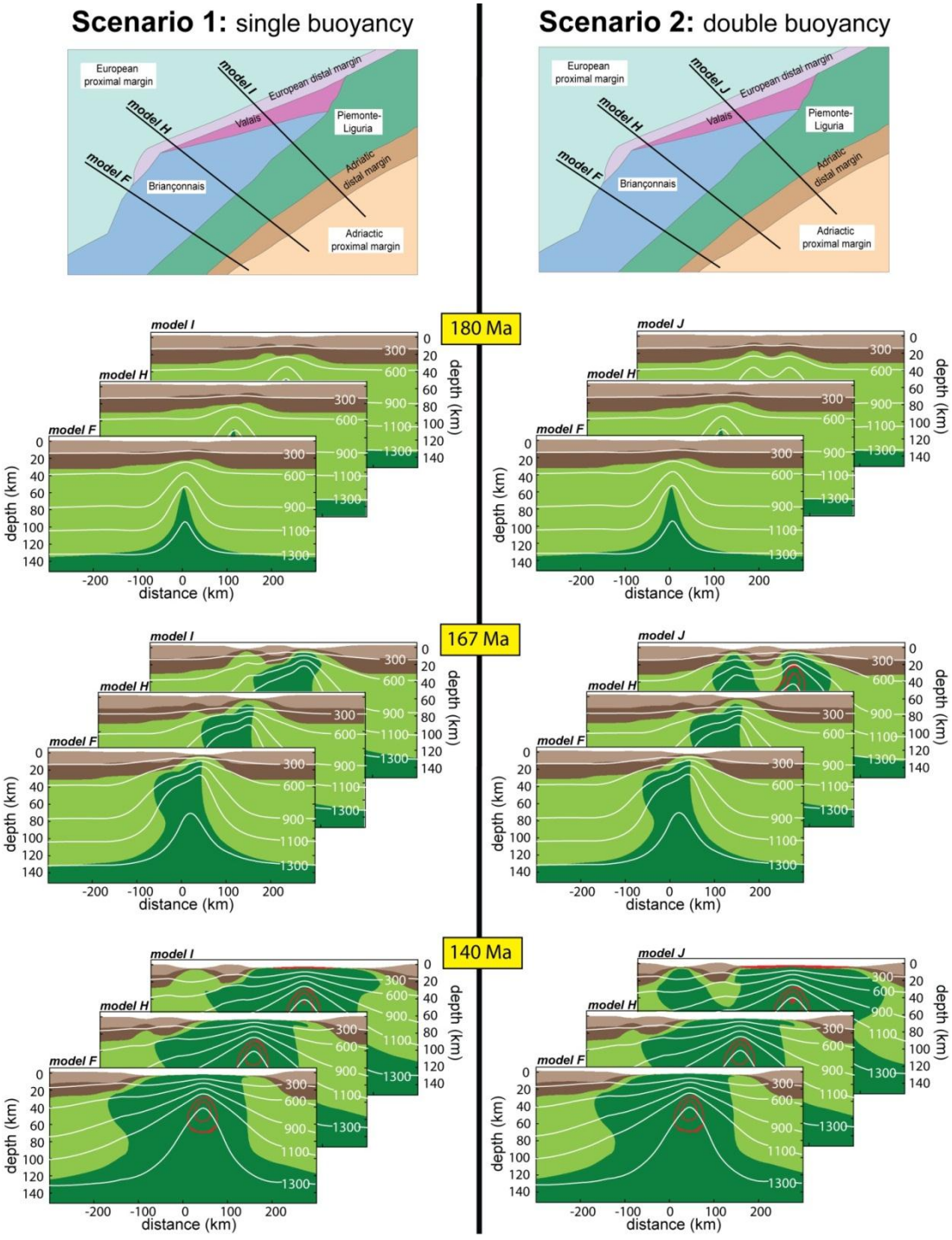

Figure 4.13: Two possible geodynamic scenarios illustrating the spatial variation evolution of the Alpine Tethys at 180, 167 and 140Ma. In scenario 1, a single buoyancy upwelling (model I) is used in the NE, while double buoyancy upwelling (model J) is used in scenario 2. For the southern regions, model H and F are used to describe the poorly developed Valais basin formation and its non-existence respectively.

4.6.2 Evolution and discussion summary of the formation of the Alpine Tethys rifted margins

As apparent from this study, no unique geodynamic model can be proposed for the evolution of the whole Alpine Tethys, yet, especially considering the lack of faulting and sedimentation in our coupled kinematic model. As a review and discussion, we show in Figure 4.14 the evolution of one section of the Alpine Tethys, corresponding to model **I**, where both Valais and Piemonte-Liguria basin successfully lead to mantle exhumation during the Jurassic. The key timing of deformation snapshots, together with the stratigraphic evidence and kinematic conceptual models of Mohn et al. (2010) illustrate the review and discussion. In addition, the tracking of 3 material points A, B and C are predicted and discussed.

Distributed stretching and thinning

A first phase of rifting associated with the Meliata/Vardar post-rifting thermal subsidence affected a wide region, which subsequently hosted the Alpine Tethys, during the Trias-Early Jurassic. As a result, a shallow marine environment was established regionally, (Figure 14a). The stratigraphic observations show thick carbonate platforms on the Sub-Briançonnais, Briançonnais and External Piemonte domain, and a thin sequence for the European proximal margin. Material points A, B and C are originally located within the Briançonnais crustal basement (A), or within the subcontinental mantle beneath the Briançonnais domain (B and C), at depths 15, 40 and 55km respectively.

The formation of the Valais and Piemonte-Liguria basins

Starting in the Toarcian, localised lithosphere stretching and thinning resulted in the simultaneously formation of the Valais and Piemonte-Liguria basins, leaving the Briançonnais domain in between (Figure 14b). Two important processes, lateral migration of the deformation and buoyancy induced upwelling, are discussed:

(1) ***Lateral migration of deformation:*** As discussed in section 4.5.1, the migration of deformation prescribed during the simultaneous formation of two basins has little impact on the resulting vertical motion of the in-between domain. However, the Piemonte-Liguria deformation axis should remain close to the Briançonnais domain, in order to generate the asymmetry of the conjugate OCT architecture (Mohn et al., 2010) and reference therein). The formation of the Valais generates velocity interference with the Piemonte-Liguria basin, leading to the asymmetry of the basin without prescribing a migration of deformation; the Adriatic distal margin shows hyper-extension while the Briançonnais show a more abrupt OCT. Conversely, the Valais must migrate laterally, moving away from the Piemonte-Liguria basin which generates strong velocity interference. According to the numerical experiment of lateral migration of deformation illustrated in Figure 1.4d, the strong spreading interference of the Piemonte-Liguria would generate a migration factor $f_m \geq 1$ in the Valais, thus hindering mantle exhumation. Therefore, the assumption of the Valais migrating and the Piemonte-Liguria deformation axis remaining static, as presented in model **I**, seems adequate.

(2) ***Buoyancy induced upwelling:*** This study demonstrated that buoyancy induced upwelling is critically important to allow the uplift and emergence of the Briançonnais domain from 185 to 170Ma. However, we favour the presence of a single buoyancy upwelling, rather than double, because of the formation of a conjugate normal fault system with the Briançonnais domains acting as a hanging 'H'-block between the European and Adriatic plates (Lavier and Manatschal, 2006). In this scenario, the continental crust and lithosphere beneath the Briançonnais domain thins considerably, compared to the adjacent basins.

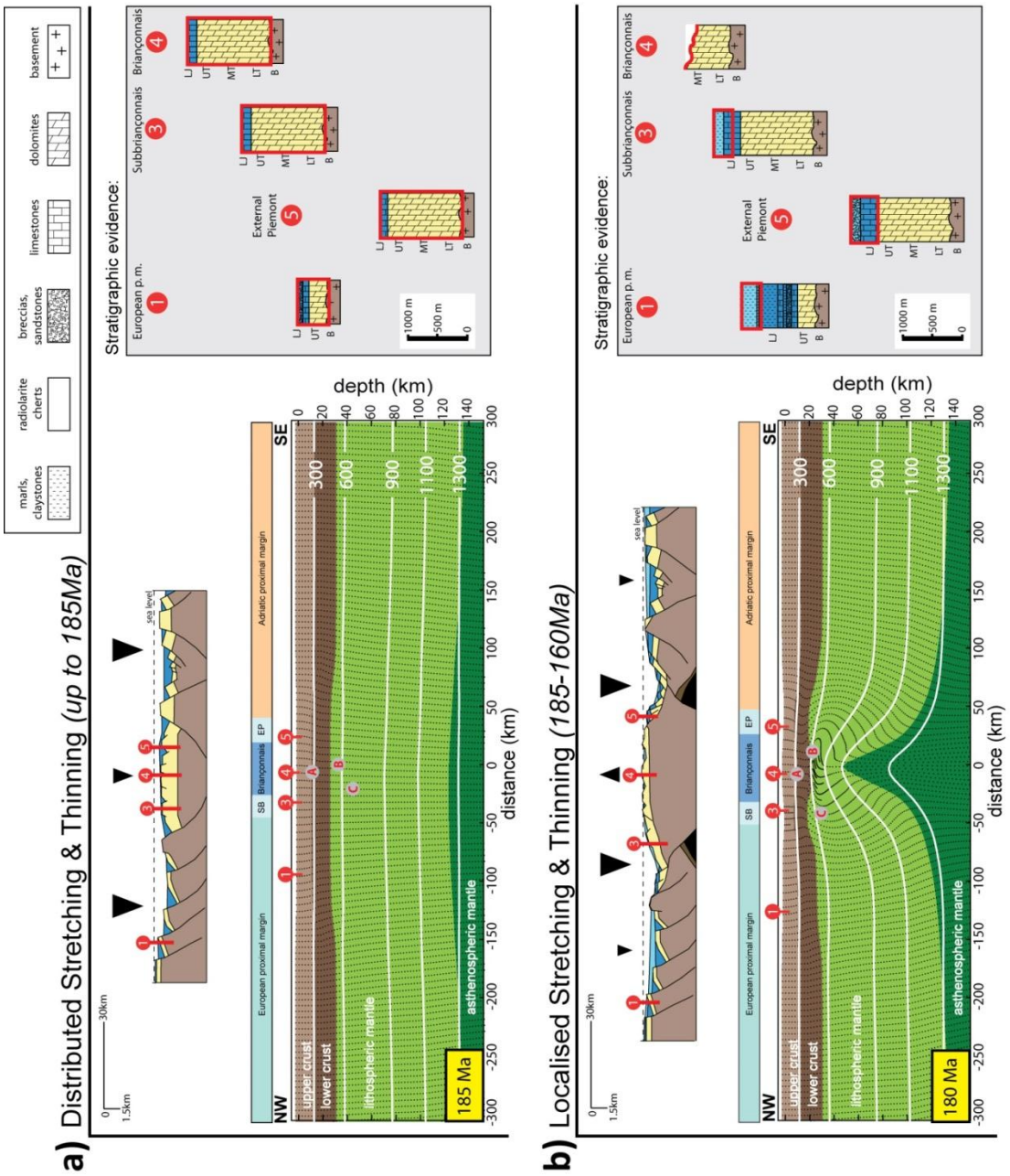

Figure 4.14: Model **I** lithosphere and asthenosphere deformation behaviour snapshots illustrating **a)** regional stretching and thinning (185Ma) and **b)** localised stretching and thinning including buoyancy beneath the Briançonnais (180Ma). Each snapshot is documented with the hypothetic stratigraphic evidence of the major paleogeographic areas of the Alpine domains and the conceptual kinematic model evolution according to Mohn et al., (2010). We also show the tracking evolution of 3 rocks at depth A-15km, B-40km and C-55km Melt extraction occurs after it exceeds a melt fraction threshold of 6%. White lines are isotherms (°C) and red contour lines are melt fraction. Contour interval is 0.03%.

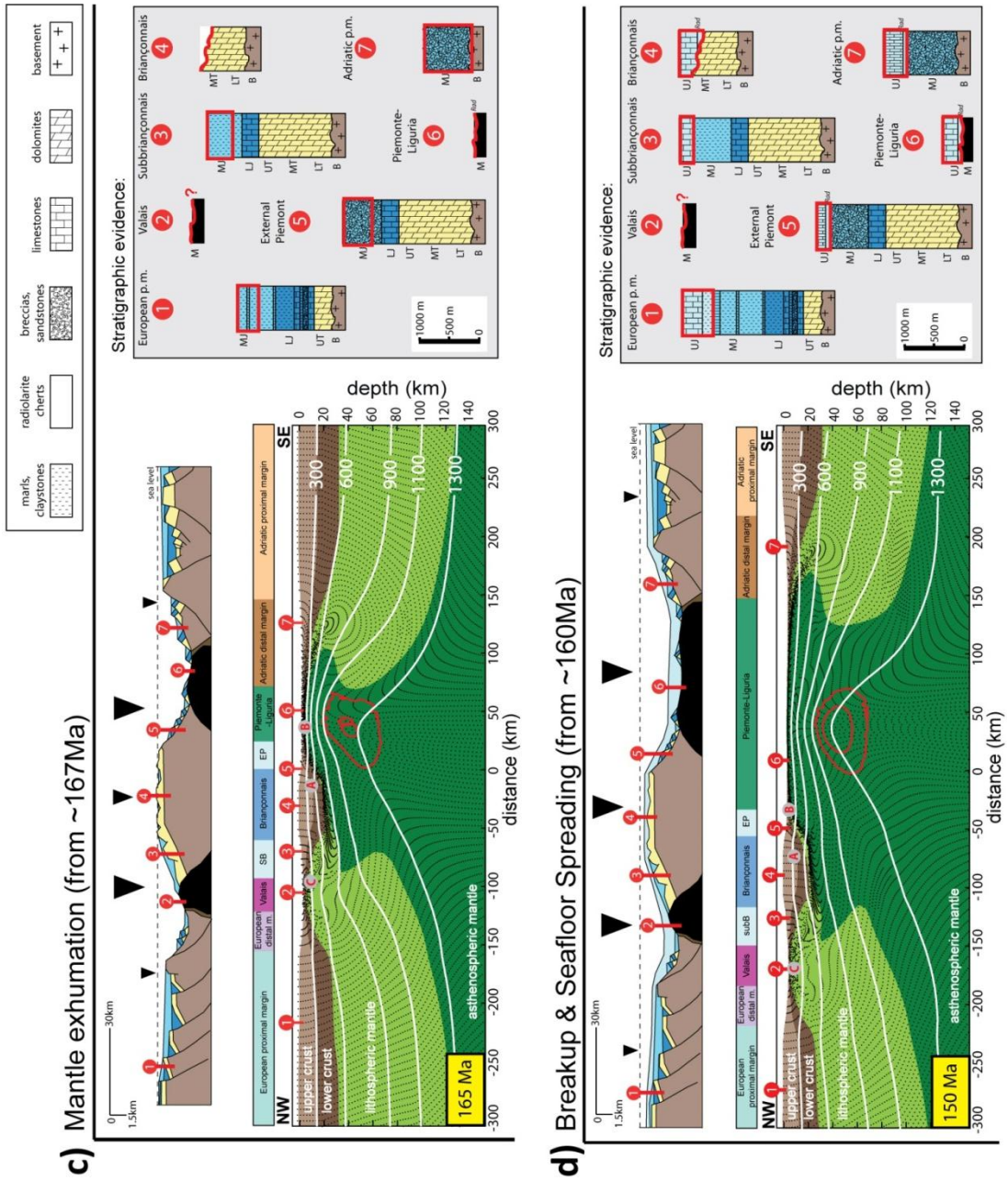

Figure 4.14: Model **I** lithosphere and asthenosphere deformation behaviour snapshots illustrating, **c)** mantle exhumation and initiation of melting (165Ma) and **d)** breakup and seafloor spreading (150Ma). Each snapshot is documented with the hypothetic stratigraphic evidence of the major paleogeographic areas of the Alpine domains and the conceptual kinematic model evolution according to Mohn et al., (2010). We also show the tracking evolution of 3 rocks at depth A-15km, B-40km and C-55km Melt extraction occurs after it exceeds a melt fraction threshold of 6%. White lines are isotherms (°C) and red contour lines are melt fraction. Contour interval is 0.03%.

As a result from the discussion above, an additional upwelling rate more than 15mm.yr^{-1} from buoyancy is suggested beneath the Briançonnais domain. Buoyancy induced upwelling is applied below a penetration depth of 20km, resulting in initial lower crustal removal by depth-dependant thinning. A shallower penetration depth would not permit the Briançonnais domain to uplift and emerge. Strong thermal uplift compensates lower continental crustal thinning, leading to emergence of the Internal Briançonnais. Meanwhile, material points B and C ascend from the sub-continental mantle toward the base of the continental crust. This evolution can only occur in the presence of shear zones or deep faults allowing deeper mantle to be in contact with the continental crust (e.g. detachment fault initiation, Peron-Pinvidic and Manatschal, 2008).

Earlier melting is initiated at 174Ma, which is consistent with early melt infiltration within the mantle suggested by Müntener et al. (2010). In our modelling, melt is not extracted to the surface and is therefore retained in the mantle until it exceeds an arbitrary melt fraction threshold of 6%. We suggest that melt migration to the surface is difficult beneath the Briançonnais due to the 20km of crust above it. The melt would rather spread toward the adjacent permeability channels generated by the formation of the two adjacent basins, thus delaying its extraction.

Mantle exhumation

Mantle exhumation is predicted in our model from ~167Ma in the Piemonte-Liguria and Valais basins (Figure 4.14c). It is during this stage that the penetration depth of buoyancy induced upwelling may evolve to shallower depth because the thermal anomaly migrates toward the Piemonte-Liguria domain. The evolution of the buoyancy upwelling depth to a shallower penetration depth removes the lower crustal basement of the Briançonnais resulting in rapid subsidence, in addition to that from thermal subsidence. These conditions would therefore favour the deposition of radiolarian cherts in the Briançonnais domain (Bourbon, 1980).

According to model **I**, the predicted exhumed mantle exposed within the Piemonte-Liguria Ocean is primarily asthenospheric (dark green material), although the material point B is also exhumed, squeezed between the surface and asthenospheric material. Conversely the mantle exposed in the Valais is primarily lithospheric (light green material). This is due to strong and early buoyancy induced upwelling bringing asthenospheric material quickly toward the surface. However, it has been established that ophiolites within the Piemonte-Liguria Ocean are characterized by exhumed sub-continental peridotite (Piccardo, 1976; Desmurs et al., 2002). These evidence of primarily exposed sub-continental mantle is also found in the Iberia-Newfoundland OCT (Whitmarsh et al., 2001), after which Piccardo et al. (2009) suggested that these sub-continental mantle exposure were a charachteric of exhumed mantle at magma-poor rifted margins.

One way to allow sub-continental mantle to be exhumed on the seafloor would be to decrease the upwelling rate of buoyancy induced upwelling, initially assumed at 15mm.yr^{-1}. However, decreasing this velocity affect the uplift of the Briançonnais domain and prevent its emergence. An other solution is the prescription of an initially thinner continental crust (~30km). In this case, our numerical experiments showed that the upwelling rate from buoyancy would not need to be as fast as presented in model **I**, although melt initiation would be delayed.

Breakup and seafloor spreading initiation

Seafloor spreading may be initiated after that mantle is exhumed (~165Ma) (Figure 4.14d). The Briançonnais domain thermally subsides from 165Ma until the model ends at 140Ma. Because the melting does not exceed the melt fraction threshold of 6%, melt is retained in the mantle where it can be episodically extracted to seabed. Episodic extraction of melt is consistent with the few isolated magmatic rocks exposed in the Alps (ref). However, their geochemical evolution reveals another incompatibility with our modelling predictions. Desmurs et al., 2002 showed that the gabbros exposed on the Platta nappe indicate an

oceanward evolution from T-MORB's to N-MORB's, linked to increasing degrees of melting; related to continuous thinning of the sub-continental mantle during rifting, mantle exhumation until breakup (also see Piccardo et al., 2009). In this context, the exhumed and partially melted sub-continental mantle reveals a paradox between geological data and modelling approaches.

4.6.3 P-T-t history prediction

We have predicted two sets of P-T-t history describing the evolution of material points (rocks) using the reference model **I**. The first set is composed of rocks A, B and C, initially located beneath the surface of the Briançonnais domain at depth 15, 40 and 55km respectively (see their all evolution track in Figure 4.14). Rock A remains stationary within the Briançonnais crust during rifting, while B and C are exhumed within the Piemonte-Liguria and the Valais basins respectively (Figure 4.15a). The second set of rocks D, D', D'' and D''', which is showed in Figure 4.15b at the end of rifting, were all located initially at Moho depth (32.5km) beneath the Briançonnais domain at a horizontal distance of 5km from each other. As a result, at the end of rifting D is located deep beneath the Briançonnais, while D''' is exhumed at the seafloor. Both sets of P-T-t paths show the evolution of the temperature and geothermal gradients as a function of time.

As the models predict an initial temperature of the Moho of 500°C which is about 100-150°C less than suggested by Müntener et al. (2000) for the Alpine Tethys realm, these results should be considered as qualitative only. P-T-t paths show that the Briançonnais is strongly heated from 185Ma onwards (rocks A, D and D'). Beltrando et al., (in prep) show that the basement of the Briançonnais underwent a strong heating which is consistent with the model prediction only if we include an additional buoyant upwelling beneath the Briançonnais. Rock A was initially located at depth 15km with a temperature of 300°C, and has been warmed to ~530°C. The rocks that are exhumed at the surface do not necessarily become hotter although they experience a strong geothermal gradient (rocks B, D'' and

D'''); higher geothermal gradients only occurs at the time when the half-spreading rate is set faster from 170Ma which accelerate lithosphere thinning leading to mantle exhumation. The temperature of these rocks reaches approximately 750°C at this time.

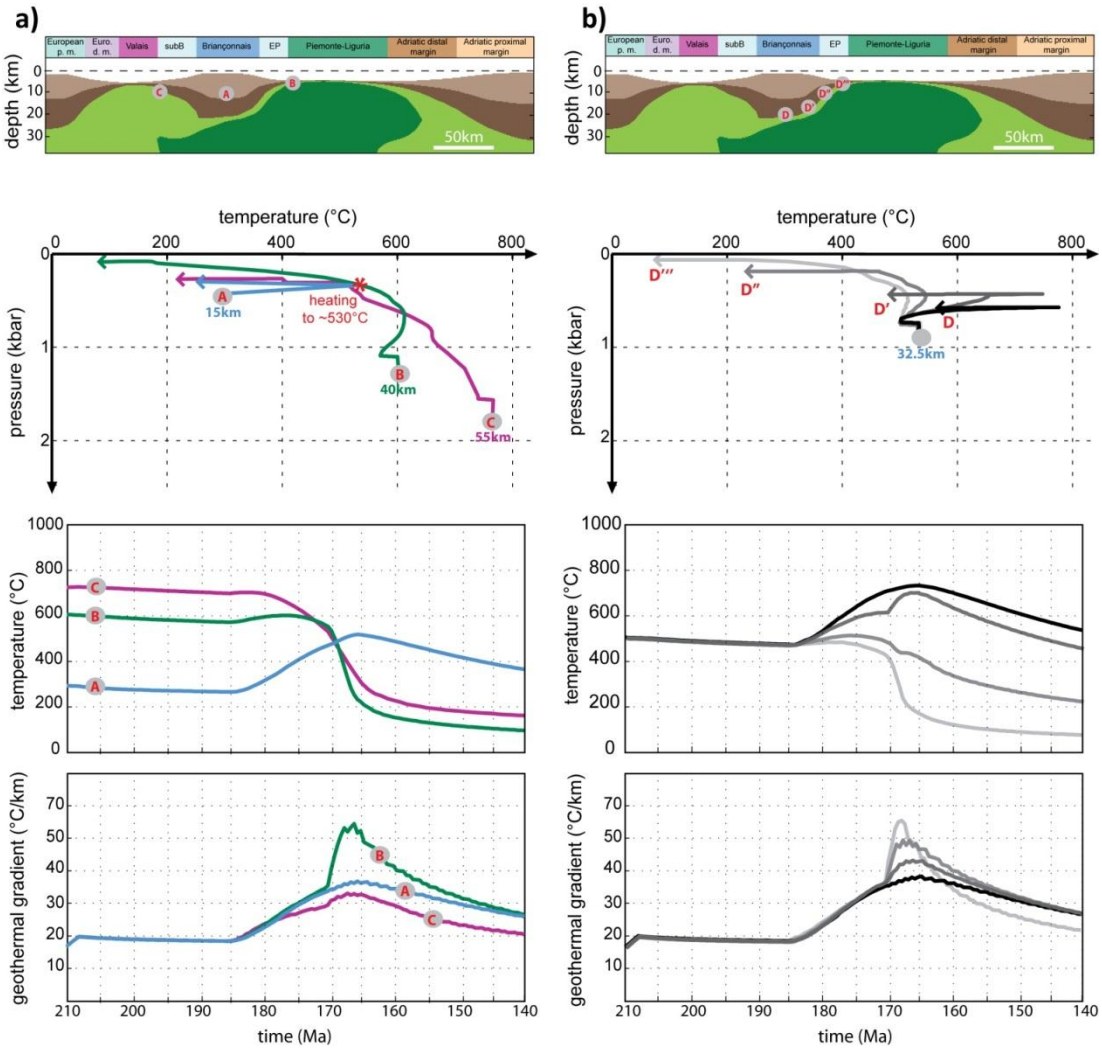

Figure 4.18: P-T-t histories, temperature and geothermal gradient evolution for two sets of hypothetic rocks: **a)** rocks A, B and C, and **b)** rocks D, D', D'', D'''. See text for their initial location. The upper panel is a snapshot with the final position of the two sets of rock at 150Ma.

4.6.4 Conclusion

Thanks to strong stratigraphic dataset documented in the Alps, the vertical motion of the Briançonnais domain helped to successfully model the Jurassic formation of the Alpine Tethys. We used a kinematic lithosphere deformation model to generate 10 different models applied to the Alpine Tethys in order to reveal the optimal condition of lithosphere deformation permitting the uplift, emergence and the subsequent rapid subsidence of the Briançonnais domain. Defining a sequence of lithosphere deformation events controlled by the timing and duration of the event, half-spreading rate, deformation width, buoyancy upwelling and lateral deformation migration, is required to create simultaneously the Valais and Piemonte-Liguria basin, and also investigate different geodynamical scenarios for the Alpine Tethys formation.

We demonstrated the importance of buoyancy induced upwelling in order to allow the uplift and emergence of the Briançonnais domain. The penetration depth beneath which buoyancy induced upwelling occur should not be shallower than 20km to permit the emergence of the Briançonnais domain. The upwelling rate also must not be too weak (>15mm.yr^{-1}) to generate faster uplift. However, fast subsidence of the Briançonnais domain can only be determined using an evolving penetration depth (depth-dependent thinning to shallower depth (~10km)), with an extensional event affecting the Briançonnais domain, or if the Valais rifted during the Cretaceous.

A single model of lithosphere deformation applied the Alpine Tethys formation cannot be used due to the lateral and temporal variations of the Alpine Tethys paleogeographic domains evolution. However, modelling the Alpine Tethys rifted margins gives insight about the formation of magma-poor rifted margins. One of the major result is the initiation of buoyancy induced upwelling early during intracontinental rifting. Buoyancy upwelling initiation remains poorly understood, but further investigations about the initial conditions

of the continental crust and mantle lithosphere before the Alpine Tethys formation may give some answers.

ACKNOWLEDGMENT

This research was financed and supported by the MM3 (Margin Modelling Phase 3) partners (BP, ConocoPhillips, HESS, BR Petrobras, Statoil, Shell, TOTAL, BG Group, BHP-Billiton). We are thankful for the numerous discussions that took place during field excursions all over the Alps.

REFERENCES

Baud, A., and M. Septfontaine, 1980, Présentation d'un profil palinspastique de la nappe des Préalpes médianes en Suisse occidentale: Eclogae Geol. Helv, v. 73, p. 651-600.

Beltrando, M., R. Compagnoni, and B. Lombardo, 2010, (Ultra-) High-pressure metamorphism and orogenesis: An Alpine perspective: Gondwana Research, v. 18, p. 147-166.

Beltrando, M., G. Frasca, R. Compagnoni, and A. Vitale-Brovarone, 2012, The Valaisan controversy revisited: Multi-stage folding of a Mesozoic hyper-extended margin in the Petit St. Bernard pass area (Western Alps): Tectonophysics, v. 579, p. 17-36.

Beltrando, M., G. Manatschal, G. Mohn, G. V. Dal Piaz, A. Vitale Brovarone, and E. Masini, 2014, Recognizing remnants of magma-poor rifted margins in high-pressure orogenic belts: The Alpine case study: Earth-Science Reviews, v. 131, p. 88-115.

Bernoulli, D., 1964, Zur Geologie des Monte Generoso Lombardische Alpen.

Bertotti, G., V. Picotti, D. Bernoulli, and A. Castellarin, 1993, From rifting to drifting: tectonic evolution of the South-Alpine upper crust from the Triassic to the Early Cretaceous: Sedimentary Geology, v. 86, p. 53-76.

Bill, M., L. O'Dogherty, J. Guex, P. O. Baumgartner, and H. Masson, 2001, Radiolarite ages in Alpine-Mediterranean ophiolites: Constraints on the oceanic spreading and the Tethys-Atlantic connection: Geological society of America bulletin, v. 113, p. 129-143.

Bourbon, M., 1980, Evolution d'un secteur de la marge nord-téthysienne en milieu pélagique: la zone briançonnaise près de Briançon entre le début du Malm et l'Eocène inférieur, Université Louis Pasteur-Strasbourg I.

Braun, M. G., G. Hirth, and E. M. Parmentier, 2000, The effects of deep damp melting on mantle flow and melt generation beneath mid-ocean ridges: Earth and Planetary Science Letters, v. 176, p. 339-356.

Buck, W. R., and W. Su, 1989, Focused mantle upwelling below mid-ocean ridges due to feedback between viscosity and melting: Geophysical Research Letters, v. 16, p. 641-644.

Cannat, M., J. Cann, and J. Maclennan, 2004, Some hard rock constraints on the supply of heat to mid-ocean ridges: Geophysical Monograph Series, v. 148, p. 111-149.

Cannat, M., G. Manatschal, D. Sauter, and G. Peron-Pinvidic, 2009, Assessing the conditions of continental breakup at magma-poor rifted margins: What can we learn from slow spreading mid-ocean ridges?: Comptes Rendus Geoscience, v. 341, p. 406-427.

Cannat, M., D. Sauter, V. Mendel, E. Ruellan, K. Okino, J. Escartin, V. Combier, and M. Baala, 2006, Modes of seafloor generation at a melt-poor ultraslow-spreading ridge: Geology, v. 34, p. 605-608.

Claudel, M. E., and T. Dumont, 1999, A record of multistage continental break-up on the Briançonnais marginal plateau (Western Alps): Early and Middle-Late Jurassic rifting: Eclogae Geologicae Helvetiae, v. 92, p. 45-61.

Connolly, J. A. D., M. W. Schmidt, G. Solferino, and N. Bagdassarov, 2009, Permeability of asthenospheric mantle and melt extraction rates at mid-ocean ridges: Nature, v. 462, p. 209-212.

Dal Piaz, G. V., 1999, The Austroalpine-Piedmont nappe stack and the puzzle of Alpine Tethys: Memorie di Scienze Geologiche, v. 51, p. 155-176.

Decarlis, A., and A. Lualdi, 2011, Synrift sedimentation on the northern Tethys margin: an example from the Ligurian Alps (Upper Triassic to Lower Cretaceous, Prepiedmont domain, Italy): International Journal of Earth Sciences, v. 100, p. 1589-1604.

Dercourt, J., 2000, Atlas Peri-Tethys Palaeogeographical Maps, CCGM/CGMW.

Desmurs, L., Müntener, O., & Manatschal, G. (2002). Onset of magmatic accretion within a magma-poor rifted margin: a case study from the Platta ocean-continent transition, eastern Switzerland. *Contributions to Mineralogy and Petrology*, *144*(2002), 365–382.Dumont, T., 1984, Le Rhétien et le Lias inférieur prépiémontais: enregistrement sédimentaire du passage des carbonates de plate-forme triasiques au Jurassique hémipélagique lors du début du rifting téthysien: Géologie Alpine, v. 60, p. 13-25.

Florineth, D., and N. Froitzheim, 1994, TRANSITION FROM CONTINENTAL TO OCEANIC BASEMENT IN THE TASNA NAPPE (ENGADINE WINDOW, GRAUBUNDEN, SWITZERLAND)-EVIDENCE FOR EARLY CRETACEOUS OPENING OF THE VALAIS OCEAN: Schweizerische Mineralogische und Petrographische Mitteilungen, v. 74, p. 437-448.

Forsyth, D. W., D. S. Scheirer, S. C. Webb, L. M. Dorman, J. A. Orcutt, A. J. Harding, D. K. Blackman, J. P. Morgan, R. S. Detrick, Y. Shen, C. J. Wolfe, J. P. Canales, D. R. Toomey, A. F. Sheehan, S. C. Solomon, and W. S. D. Wilcock, 1998, Imaging the deep seismic structure beneath a mid-ocean ridge : The MELT experiment: Science, v. 280, p. 1215-1218.

Franke, D., 2013, Rifting, lithosphere breakup and volcanism: Comparison of magma-poor and volcanic rifted margins: Marine and Petroleum Geology, v. 43, p. 63-87.

Frisch, W., 1979, Tectonic progradation and plate tectonic evolution of the Alps: Tectonophysics, v. 60, p. 121-139.

Haas, J., S. Kovács, L. Krystyn, and R. Lein, 1995, Significance of Late Permian-Triassic facies zones in terrane reconstructions in the Alpine-North Pannonian domain: Tectonophysics, v. 242, p. 19-40.

Handy, M. R., S. M Schmid, R. Bousquet, E. Kissling, and D. Bernoulli, 2010, Reconciling plate-tectonic reconstructions of Alpine Tethys with the geological–geophysical record of spreading and subduction in the Alps: Earth-Science Reviews, v. 102, p. 121-158.

Hebert, L. B., and L. G. J. Montési, 2010, Generation of permeability barriers during melt extraction at mid-ocean ridges: Geochemistry, Geophysics, Geosystems, v. 11.

Katz, R. F., M. Spiegelman, and C. H. Langmuir, 2003, A new parameterization of hydrous mantle melting: Geochemistry Geophysics Geosystems, v. 4.

Lavier, L. L., and G. Manatschal, 2006, A mechanism to thin the continental lithosphere at magma-poor margins: Nature, v. 440, p. 324-328.

Lemoine, M., T. Bas, A. Arnaud-Vanneau, H. Arnaud, T. Dumont, M. Gidon, M. Bourbon, P.-C. de Graciansky, J.-L. Rudkiewicz, and J. Megard-Galli, 1986, The continental margin of the Mesozoic Tethys in the Western Alps: Marine and Petroleum Geology, v. 3, p. 179-199.

Lemoine, M., and R. Trümpy, 1987, Pre-oceanic rifting in the Alps: Tectonophysics, v. 133, p. 305-320.

Li, X.-H., M. Faure, W. Lin, and G. Manatschal, 2013, New isotopic constraints on age and magma genesis of an embryonic oceanic crust: The Chenaillet Ophiolite in the Western Alps: Lithos, v. 160, p. 283-291.

Liati, A., N. Froitzheim, and C. M. Fanning, 2005, Jurassic ophiolites within the Valais domain of the Western and Central Alps: geochronological evidence for re-rifting of oceanic crust: Contributions to Mineralogy and Petrology, v. 149, p. 446-461.

Liati, A., D. Gebauer, and C. M. Fanning, 2003, The youngest basic oceanic magmatism in the Alps (Late Cretaceous; Chiavenna unit, Central Alps): geochronological constraints and geodynamic significance: Contributions to Mineralogy and Petrology, v. 146, p. 144-158.

Lizarralde, D., G. J. Axen, H. E. Brown, J. M. Fletcher, A. González-Fernández, A. J. Harding, W. S. Holbrook, G. M. Kent, P. Paramo, and F. Sutherland, 2007, Variation in styles of rifting in the Gulf of California: Nature, v. 448, p. 466-469.

Manatschal, G., 2004, New models for evolution of magma-poor rifted margins based on a review of data and concepts from West Iberia and the Alps: International Journal of Earth Sciences, v. 93, p. 432-466.

Manatschal, G., and D. Bernoulli, 1999, Architecture and tectonic evolution of nonvolcanic margins: Present-day Galicia and ancient Adria: Tectonics, v. 18, p. 1099-1119.

Manatschal, G., A. Engström, L. Desmurs, U. Schaltegger, M. Cosca, O. Müntener, and D. Bernoulli, 2006, What is the tectono-metamorphic evolution of continental break-up: the example of the Tasna Ocean–Continent Transition: Journal of Structural Geology, v. 28, p. 1849-1869.

Manatschal, G., and O. Müntener, 2009, A type sequence across an ancient magma-poor ocean–continent transition: the example of the western Alpine Tethys ophiolites: Tectonophysics, v. 473, p. 4-19.

Manatschal, G., and P. Nievergelt, 1997, A continent-ocean transition recorded in the Err and Platta nappes (Eastern Switzerland): Eclogae Geologicae Helvetiae, v. 90, p. 3-27.

Manatschal, G., D. Sauter, A. M. Karpoff, E. Masini, G. Mohn, and Y. Lagabrielle, 2011, The Chenaillet Ophiolite in the French/Italian Alps: An ancient analogue for an Oceanic Core Complex?: Lithos, v. 124, p. 169-184.

Masini, E., G. Manatschal, G. Mohn, J. F. Ghienne, and F. Lafont, 2011, The tectono-sedimentary evolution of a supra-detachment rift basin at a deep-water magma-poor rifted margin: the example of the Samedan Basin preserved in the Err nappe in SE Switzerland: Basin Research, v. 23, p. 652-677.

McKenzie, D., 1978, Some remarks on the development of sedimentary basins: Earth and Planetary Science Letters, v. 40, p. 25-32.

McKenzie, D., and M. J. Bickle, 1988, The Volume and Composition of Melt Generated by Extension of the Lithosphere: Journal of Petrology, v. 29, p. 625-679.

McKenzie, D. P., 1967, Some remarks on heat flow and gravity anomalies: Journal of Geophysical Research, v. 72, p. 6261-6273.

Mohn, G., G. Manatschal, M. Beltrando, E. Masini, and N. Kusznir, 2012, Necking of continental crust in magma-poor rifted margins: Evidence from the fossil Alpine Tethys margins: Tectonics, v. 31.

Mohn, G., G. Manatschal, O. Müntener, M. Beltrando, and E. Masini, 2010, Unravelling the interaction between tectonic and sedimentary processes during lithospheric thinning in the Alpine Tethys margins: International Journal of Earth Sciences, v. 99, p. 75-101.

Müntener, O., J. Hermann, and V. Trommsdorff, 2000, Cooling History and Exhumation of Lower-Crustal Granulite and Upper Mantle (Malenco, Eastern Central Alps): Journal of Petrology, v. 41, p. 175-200.

Müntener, O., G. Manatschal, L. Desmurs, and T. Pettke, 2010, Plagioclase peridotites in ocean–continent transitions: refertilized mantle domains generated by melt stagnation in the shallow mantle lithosphere: Journal of Petrology, v. 51, p. 255-294.

Nielsen, T. K., and J. R. Hopper, 2004, From rift to drift: Mantle melting during continental breakup: Geochemistry, Geophysics, Geosystems, v. 5.

Niu, Y., 1997, Mantle melting and melt extraction processes beneath ocean ridges: evidence from abyssal peridotites: Journal of Petrology, v. 38, p. 1047-1074.

Péron-Pinvidic, G., and G. Manatschal, 2009, The final rifting evolution at deep magma-poor passive margins from Iberia-Newfoundland: a new point of view: International Journal of Earth Sciences, v. 98, p. 1581-1597.

Piccardo, G. B. (1976). Petrologia del massiccio lherzolitico di Suvero (La Spezia). *Ofioliti*, *1*, 279–317.

Piccardo, G. B., Vannucci, R., & Guarnieri, L. (2009). Evolution of the lithospheric mantle in an extensional setting: Insights from ophiolitic peridotites. *Lithosphere*, *1*, 81–87.

Ricou, L. E., 1994, Tethys Reconstructed-Plates, Continental Fragments and Their Boundaries since 260-Ma from Central-America to South-Eastern Asia: Geodinamica Acta, v. 7, p. 169-218.

Sanfilippo, A., R. Tribuzio, and M. Tiepolo, 2014, Mantle–crust interactions in the oceanic lithosphere: Constraints from minor and trace elements in olivine: Geochimica et Cosmochimica Acta, v. 141, p. 423-439.

Schaltegger, U., L. Desmurs, G. Manatschal, O. Müntener, M. Meier, M. Frank, and D. Bernoulli, 2002, The transition from rifting to sea-floor spreading within a magma-poor rifted margin: field and isotopic constraints: Terra Nova, v. 14, p. 156-162.

Schilling, J. G., 1973, Afar mantle plume: rare earth evidence: Nature, v. 242, p. 2-5.

Schmid, S. M., B. Fügenschuh, E. Kissling, and R. Schuster, 2004, Tectonic map and overall architecture of the Alpine orogen: Eclogae Geologicae Helvetiae, v. 97, p. 93-117.

Sclater, J., C. Jaupart, and D. Galson, 1980, The heat flow through oceanic and continental crust and the heat loss of the Earth: Reviews of Geophysics, v. 18, p. 269-311.

Shillington, D. J., C. L. Scott, T. A. Minshull, R. A. Edwards, P. J. Brown, and N. White, 2009, Abrupt transition from magma-starved to magma-rich rifting in the eastern Black Sea: Geology, v. 37, p. 7-10.

Sparks, D. W., and E. M. Parmentier, 1991, Melt extraction from the mantle beneath spreading centers: Earth and Planetary Science Letters, v. 105, p. 368-377.

Spiegelman, M., and J. R. Reynolds, 1999, Combined dynamic and geochemical evidence for convergent melt flow beneath the East Pacific Rise: Nature, v. 402, p. 282-285.

Stampfli, G., and R. Marchant, 1997, Geodynamic evolution of the Tethyan margins of the Western Alps: Deep structure of the Swiss Alps: results of NRP, v. 20, p. 223-239.

Stampfli, G. M., 1993, Le Briançonnais, terrain exotique dans les Alpes?: Eclogae Geologicae Helvetiae, v. 86, p. 1-45.

Stampfli, G. M., J. Mosar, P. Favre, A. Pillevuit, and J.-C. Vannay, 2001, Permo-Mesozoic evolution of the western Tethys realm: The Neo-Tethys east Mediterranean basin connection: Mémoires du Muséum national d'histoire naturelle, v. 186, p. 51-108.

Stampfli, G. M., J. Mosar, D. Marquer, R. Marchant, T. Baudin, and G. Borel, 1998, Subduction and obduction processes in the Swiss Alps: Tectonophysics, v. 296, p. 159-204.

Tricart, P., 1984, From passive margin to continental collision; a tectonic scenario for the Western Alps: American Journal of Science, v. 284, p. 97-120.

Trümpy, R., 1960, Paleotectonic evolution of the Central and Western Alps: Geological society of America bulletin, v. 71, p. 843-907.

Trümpy, R., and P. Homewood, 1980, Geology of Switzerland: a guide-book, Wepf and Company.

White, R. S., T. A. Minshull, M. J. Bickle, and C. J. Robinson, 2001, Melt generation at very slow-spreading oceanic ridges: Constraints from geochemical and geophysical data: Journal of Petrology, v. 42, p. 1171-1196.

Whitmarsh, R. B., Manatschal, G., & Minshull, T. A. (2001). Evolution of magma-poor continental margins from rifting to seafloor spreading. *Nature*, *413*(6852), 150–154.

Chapter 5

Discussion and Conclusions

5.1 Introduction

The aim of the thesis was to investigate the lithosphere and asthenosphere deformation during intracontinental rifting leading to breakup and seafloor spreading initiation. Lithosphere and asthenosphere deformation has been modelled using a parameterization consisting of distinct modes, or pattern, of deformation. These distinct deformation modes are subject to several important questions:

(1) What are these distinct modes of lithosphere deformation that can be used to represent lithosphere and asthenosphere deformation during rifting leading to continental breakup?

(2) How do these modes control rifted margin architecture and explain the occurrence or absence of exhumed mantle within an Ocean-Continent Transition (OCT)?

(3) How do they control subsidence and melting histories? How can subsidence and melting histories be used to constrain lithosphere deformation modes?

The formation of rifted margin is characterised by the stretching and thinning of the continental crust and lithosphere resulting in asthenosphere upwelling which lead to decompression melting. Therefore, other important questions concern the melting history and the evolution of the lithosphere thermal structure.

(4) How does melting by mantle decompression control rheology, lithosphere deformation modes and the resulting continental rifted margin architecture?
(5) When is the melt extracted to the surface and what are the implications of melt retention for lithosphere deformation modes?
(6) What is the thermal structure evolution during the formation of magma-poor rifted margins and can it be quantitatively described?

The strategy to answer these questions was to develop a geodynamic model that may provide insight on lithosphere deformation modes. Ultimately, this model was used to relate lithosphere deformation history and observations at magma-poor rifted margins. The study focused on non-volcanic margins because they show important features that allow the deformation history to be constrained and also because these are direct observations from rifting and continental breakup. These observations include the architecture of magma-poor rifted margins with the presence of a zone of exhumed continental mantle within the OCT, continental ribbons and embryonic oceanic crust suggesting complex deformation, thermal and subsidence histories (Boillot et al., 1987; Jagoutz et al., 2008; Péron-Pinvidic and Manatschal, 2009; and references therein). Coupling numerical

modelling and observations have permitted to investigate the thermal evolution and to compare it with the interpretation of Cannat et al. (2009).

I first summarize the results of each of the three main chapters before discussing them together. A comparison between magma-poor and volcanic rifted margins is proposed and also between the thermal predictions from our models with the Cannat et al. (2009) thermal structure evolution interpretation. I finally suggest future work.

5.2 How does the lithosphere deformation mode during continental breakup affect mantle exhumation?

In chapter 2, a series of numerical experiments was carried out to explore the relative timing of melt initiation and crustal breakup in order to predict under which conditions mantle exhumation may occur. I used a hybrid analytical model, as suggested by Cannat (1996), based on two combined lithosphere deformation modes; a pure-shear deformation mode for the topmost 15-20km lithosphere where extensional faulting is dominant, above an upwelling divergent flow for the remaining lithosphere and asthenosphere. Each parameter controlling the behaviour of the model was examined individually. These parameters included the decoupling depth between the pure-shear and upwelling divergent flow deformation modes, the pure-shear deformation region width, the half-spreading rate, the rate of buoyant upwelling, the asthenosphere temperature, crustal and lithosphere thicknesses, and melt retention.

Investigations of the model behaviour show that mantle exhumation is possible but only under particular conditions of slow spreading rate, narrow pure-shear region, passive upwelling (no buoyancy), shallow decoupling depth or cold asthenosphere temperature.

However, all numerical experiments predict a short period of exhumation lasting a maximum of 2Myr, while observations on magma-poor rifted margins show a longer period of mantle exhumation often lasting more than 10Myr (Li et al., 2013; Sibuet et al., 2007; Whitmarsh and Wallace, 2001). We therefore suggest that mantle exhumation can persist for a long period of time only by using a combination of slow spreading rate, narrow pure-shear region width, shallow decoupling depth, passive upwelling and/or cold asthenosphere temperature. Also melt retention within the mantle plays an important role as it can delay melt extraction and therefore allow mantle exhumation over a longer period of time.

The modelling methodology used in this chapter shows its main limitations in modelling the more complex architecture of magma-poor rifted margins. In our model predictions does not predict a proximal margin, hyper-extended crust and asymmetry. Application of a non-evolving lithosphere deformation mode to natural laboratories is therefore too simplistic.

5.3 Constraining lithosphere deformation modes during continental breakup for the Iberia-Newfoundland conjugate margins

Chapter 3 aimed to understand lithosphere deformation modes during continental breakup using a kinematic finite-element model. The finite-element mode, named FE-margin, uses an evolving sequence of lithosphere deformation modes kinematically driven. The model can therefore be applied to specific continental rifted margins and be quantitatively calibrated using their observations. FE-Margin uses two deformation flow-fields consisting of (1) pure-shear induces passive upwelling and (2) an additional upwelling due to buoyancy (Braun et al., 2000; Forsyth et al., 1998; Nielsen and Hopper, 2004; Spiegelman and

Reynolds, 1999). The pure-shear and passive upwelling deformation of FE-Margin is not dissimilar to the hybrid deformation mode described in chapter 2, but is calculated using finite-element. While the pure-shear deformation end-member mode in chapter 2 focuses the passive upwelling beneath the deformation width only, this calculation has the advantage to refine the flow-field solution and attenuate the passive upwelling rate in depth. Each lithosphere deformation event is kinematically controlled by the duration of the event, a pure-shear deformation width, a half-spreading rate, buoyancy upwelling contribution and its penetration depth and lateral migration by jumps and/or continuous migration of the deformation.

The model has been applied to the formation of 2pairs of the Iberia-Newfoundland conjugate rifted margins, southern and northern section, during late Jurassic to mid Cretaceous (~180-112Ma). The quantitative calibration consisted of matching the predicted conjugate rifted margin architecture to that observed. In detail, that involves matching the continental crustal thickness determined from gravity inversion and water-loaded subsidence from flexural backstripping. We constrain our models using the extensional evolution given by Sutra et al. (2013). This calibration revealed that the pure-shear deformation width and the lateral migration of the deformation flow-field by jumps and/or continuous migration were the two main parameters required by the model to fit the observations. However, a similar rifted margins crustal architecture can be obtained by different deformation histories using different timing, duration and half-spreading rates. Thus, the evolution of the lithosphere deformation was further constrained using observations of the onset of melting, the duration of mantle exhumation and subsidence history. The evolution of the northward rift-opening propagation of the Iberia-Newfoundland rifted margins was also examined. The calibration of the lithosphere

deformation history suggests a diachronic evolution of the two conjugate margin profiles; the south opened more rapidly and earlier than the north.

Chapter 3 provided information on the evolution of the deformation region width; it evolved from broad (>200km) at the beginning of rifting when deformation is regional, to narrow during localized stretching and thinning (150-50km) and even narrower (<40km) after continental lithosphere breakup. The evolution of extension followed different paths in the north and the south; the continental crust and lithosphere of the southern section thinned more quickly and earlier than in the northern section. Buoyancy upwelling is required early during rifting on both conjugate profiles in order to predict subsidence and melting histories compatible with the observations. However, the strength of buoyancy induced upwelling contribution is less constrained during the evolution of Iberia-Newfoundland and its relationship with melt retention, melt extraction and focussing of the deformation remain obscure. Melt retention (6 to 12%) within the mantle is required to allow mantle exhumation over a long period of time.

5.4 Numerical experiments of the formation of the Alpine Tethys rifted margins: implications for the uplift and subsidence history of the Briançonnais

FE-Margin was applied to a fossil analogue rifted margin, the Alpine Tethys, exposed in the European Alps. The study particularly provided insights on the complex vertical motion of the Briançonnais domain, a continental ribbon between two hyper-extended basins, the Valais and Piemonte-Liguria. The domain showed initial subsidence before it uplifted leading to the emergence of its internal part. This was followed by rapid subsidence which affected the Briançonnais domain but 3D variations exist between the SW and the NE. The

quantitative calibration of the Alpine Tethys is not possible due to the lack of quantitative observations. The formation of the Valais basin remains also obscure in time, with its formation of the Valais basin either during the Jurassic or Cretaceous.

10 different models were examined to explain the complex subsidence and uplift history of the Briançonnais domain. I also discussed their geodynamic implications for the more regional Alpine Tethys formation. These 10 models were grouped together into 4 cases:

(1) Two models examined how the lithosphere deformation was affected by the absence of the Valais rifting with or without buoyant upwelling beneath the Briançonnais domain.
(2) Two models examined the consequences of a short duration or slow extension rate for the Jurassic rifting of the Valais.
(3) Four models behaviour examined the effect of the lateral migration of the Valais and Piemont-Liguria basins.
(4) Two models behaviour examined the consequences of either a single or double buoyancy upwelling, one each beneath the Valais and Piemonte-Liguria basins.

The results showed that the emergence of the Briançonnais domain was possible by passive upwelling if its initial bathymetry was close to sea-level (<100m) but was more likely possible if buoyant upwelling occurred beneath it. Rapid post-uplift subsidence was shown to be not possible by thermal subsidence only. However, the Briançonnais domain subsidence sensitivity to different evolution scenarios of the Valais rifting predicted more rapid post-uplift subsidence if the Valais was poorly developed during the Jurassic or if it rifted during the Cretaceous. In order to accelerate this post-rift subsidence, another

process including depth-dependent thinning may have occurred. The depth below which buoyancy upwelling is active might have become shallower with time so that the lower crustal basement of the Briançonnais was removed leading to fast tectonic subsidence. P-T-t histories also predicted the heating of the Briançonnais crustal basement.

5.5 General conclusions

5.5.1 Modelling approach

FE-Margin is the modelling tool I have developed to deform lithosphere and asthenosphere and advect temperature and material. The model has evolved from a purely kinematic model, using single end-members deformation modes consisting of pure-shear and upwelling divergent flow, to an evolving kinematic model which uses a sequence of lithosphere deformation mode events. Pure dynamic models may include real rheological properties and show how lithosphere deformation evolves during intra-continental rifting leading to breakup and seafloor spreading initiation. However, dynamic models are difficult to apply to real scenarios and therefore difficult to quantitatively calibrate.

Applying the kinematic model to the formation of Iberia-Newfoundland and the Alpine Tethys rifted margins has given important insight on the main rifting lithosphere deformation modes and their evolution. This insight includes the duration of each deformation mode, pure-shear deformation width, extension rate, buoyancy upwelling strength and its penetration depth, and lateral deformation migration.

5.5.2 Regional to localised stretching and thinning leading to mantle exhumation, breakup and seafloor spreading initiation

I show in Figure 5.1 a hypothetical evolution of lithosphere deformation for the formation of a magma-poor rifted margin, using what I have learnt from chapters 2, 3 and 4. This example illustration uses a sequence of 4 lithosphere deformation events that show the 4 main polyphase stages occurring during intracontinental rifting leading to breakup and seafloor spreading initiation.

Distributed stretching and thinning

Already suggested by many observations and conceptual models, the calibration of FE-Margin to Iberia-Newfoundland and the Alpine Tethys confirmed that regional stretching and thinning over a wide region (>200km) precedes localised deformation that later lead to mantle exhumation and continental breakup. Regional rifting deformation is a slow process of lithosphere stretching and thinning where the continental crust thins to a stretching factor of approximately 1.1-1.2 as shown in Figure 5.1a. This stage in the model illustration lasts 20Myr at ultra-slow extension rate (~1mm.yr^{-1}). Slow extensional tectonic of faults are initiated over a wide region resulting in minor crustal and lithosphere thinning. During this stage, the base of lithosphere remains deep. Thermal subsidence may accompany these extensional events that result the top basement subsiding to form a shallow marine environment. This stage of rifting forms the proximal margin domain according to the description of Mohn et al. (2012).

Localized stretching and thinning

Regional deformation is followed by localised stretching and thinning with deformation ranging between 150 and 40km wide. Because narrowing the pure-shear deformation

width increases the passive upwelling rate, continental crust and lithosphere in this model thin more rapidly. Half-spreading rates suggested for magma-poor rifted margins and used for the Iberia-Newfoundland and the Alpine Tethys modelling suggest that extension is slow less than 5mm.yr^{-1}. Chapters 3 and 4 also suggested that buoyancy induced upwelling was an important component even for magma-poor rifted margin, and speeds up lithosphere thinning. Buoyancy upwelling is initiated below a penetration depth of 30km for Iberia-Newfoundland margins so that it does not significantly thin the continental crust. Continuous migration or jumps of the extensional deformation not only generates the asymmetry seen at conjugate rifted margins but also slows down the thinning process of lithosphere and continental crust that mantle exhumation and melt initiation are delayed. For the illustration in Figure 5.1b, the deformation has migrated to -40km. Péron-Pinvidic and Manatschal (2009) proposed that it is during this stage of localised stretching and thinning that detachment faults are initiated to accommodate crustal or mantle exhumation beneath a 'Hanging' H-block (i.e. Briançonnais?). This stage leads to the formation of a necking zone at continental rifted margins. The active upwelling may also initiate an exhumation fault in the mantle.

Mantle exhumation

During localised lithosphere stretching and thinning, exhumation and detachment faults pull out subcontinental mantle to the surface (Péron-Pinvidic and Manatschal, 2009) as illustrated in Figure 5.1c. Based on the model predictions of the Iberia-Newfoundland or the Alpine Tethys rifted margin formation, mantle exhumation generally occurs at magma-poor rifted margins when the deformation region width narrows to 40-80km. It also appears that the half-spreading rate speeds up during crustal breakup before the extension rate decreases. Boillot et al. (1987) suggested from ODP Sites 638/639 that the subsidence

rapidly increases from shallow to deep water prior to mantle exhumation. The question remains open if this process is true or not, but it may be an artefact of our models due to the absence of faulting. If an acceleration of the extension occurred, it would initiate decompression melting too early and prevent the persistence of mantle exhumation over a long period of time. For the case illustration in Figure 5.1c, the half-spreading rate decreases and the buoyancy ratio increases in order to keep a consistent upwelling rate (see annex A).

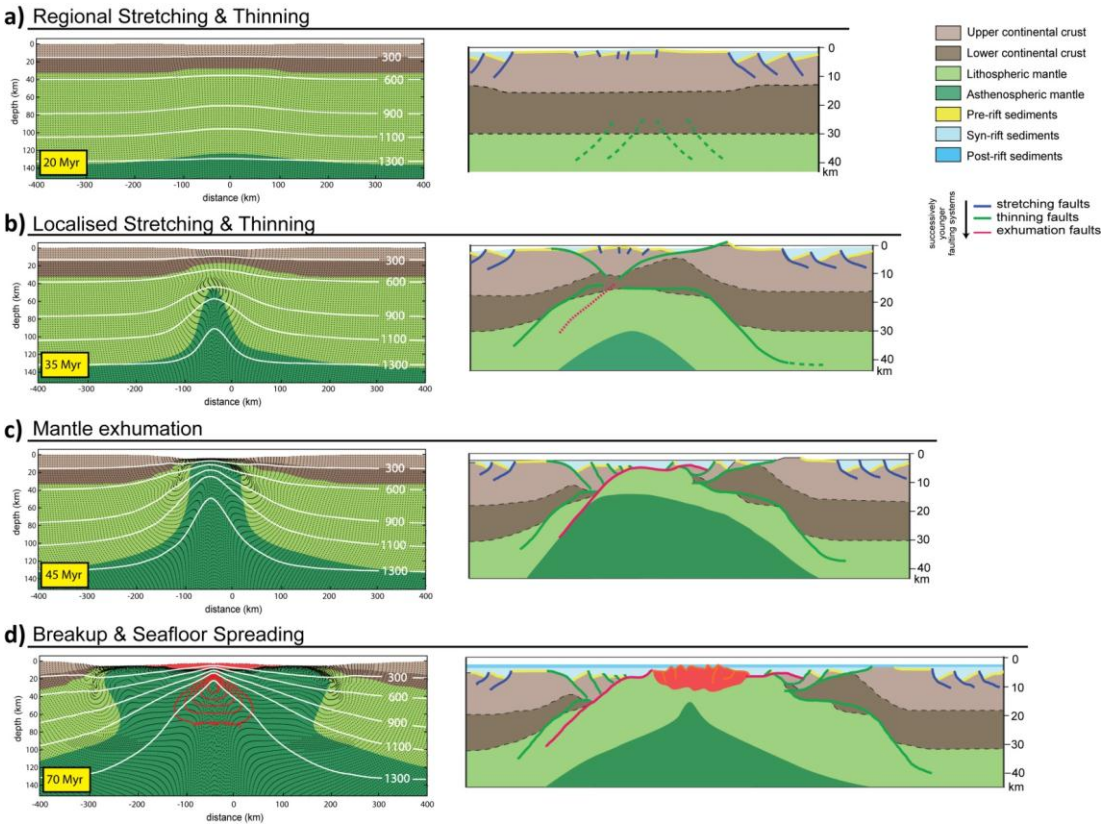

Figure 5.1: Hypothetical modelled and observed polyphase evolution of lithosphere deformation during rifting leading to continental breakup and seafloor spreading initiation. (Legend: light brown, upper crust; dark brown, lower crust; light green, lithospheric mantle; dark green, asthenospheric mantle; red, volcanic addition

Continental breakup and seafloor spreading

During mantle exhumation, melting may be generated but is not extracted to the surface. The melt is probably retained within the mantle until it reaches a threshold melt fraction after which melt is extracted to the surface. Some extraction of melt is not excluded below the melt threshold (i.e. embryonic oceanic crust and dyking). In Figure 5.1d, this threshold melt fraction is set at 6%; melt is initiated at ~50Myr but is not extracted to the surface so that mantle exhumation can persist until 60Myr. Then at 60Myr the focussing of the deformation (<20km width) occurs which gives a faster half-spreading rate that increases the upwelling. Because more melt is generated, the melt fraction reaches the critical threshold. Melt is finally extracted to form a new oceanic crust. This stage is called breakup after which seafloor spreading occurs. I will discuss what may happen during that latent phase of melt retention in a further section.

From these conclusions, it seems that a relationship exists between the pure-shear width and the half-spreading rate for magma-poor rifted margins formation. Regional stretching and thinning is used with slow spreading rate and localised deformation is used with increasing half-spreading rates.

5.5.3 Buoyancy induced upwelling

Buoyancy induced upwelling plays an important role during slow rifting. It is applied during localised stretching and thinning in order to speed up lithosphere thinning. In chapter 3 for the Iberia-Newfoundland rifted margins formation, buoyancy induced upwelling was used to predict early melt initiation while for the Alpine Tethys rifted margins formation in chapter 4, it was used to predict the uplift, emergence and the rapid post-uplift subsidence of the Briançonnais domain.

Initiation of buoyancy upwelling

During the Alpine Tethys formation, if the Valais and Liguria-Piemonte basins are formed simultaneously, then the main passive upwelling rate occurs beneath the Briançonnais domain, which may result in buoyancy induced upwelling there. For the Iberia-Newfoundland rifted margins formation, buoyancy upwelling is initiated beneath the future Atlantic. However, what enhances the localisation of the deformation from regional to localised stretching and thinning? Does the acceleration of extension increase the passive upwelling that generates buoyancy upwelling or does early buoyancy upwelling localise the deformation? During the first stage of regional stretching and thinning, mantle inheritance (e.g. hydrated mantle, depleted/fertile mantle) or crustal thickness anomalies (e.g. Iberia-Newfoundland - Pascal et al., 2002)) may initiate a beginning of buoyancy upwelling.

On the other hand, if buoyancy upwelling is important early during rifting, what makes the difference between volcanic and non-volcanic margin? Figure 5.2 shows two generic models, one for a slow margin and the other one for a fast margin. I have reused the polyphase stages of Figure 5.1 that showed regional stretching and thinning first, then localisation of the deformation leading to breakup and seafloor spreading initiation. For a fast margin, the OCT does not exhibit exhumed mantle on seafloor. Fast spreading rate induces fast passive upwelling and need less buoyant upwelling to initiate melting early during rifting. Using a slow spreading rate would need a strong buoyancy upwelling. There may be other ways to generate a volcanic margin; I have only show a model where the main reason is a fast spreading rate. A hot geotherm or asthenospheric temperature may also be involved. A mantle plume beneath the mid-oceanic ridge accelerates large-scale convection; does this process lead to extension driven by buoyancy upwelling? It is not

possible to model this with FE-Margin because buoyancy upwelling is assumed to not affect the horizontal displacement of the brittle seismogenic layer.

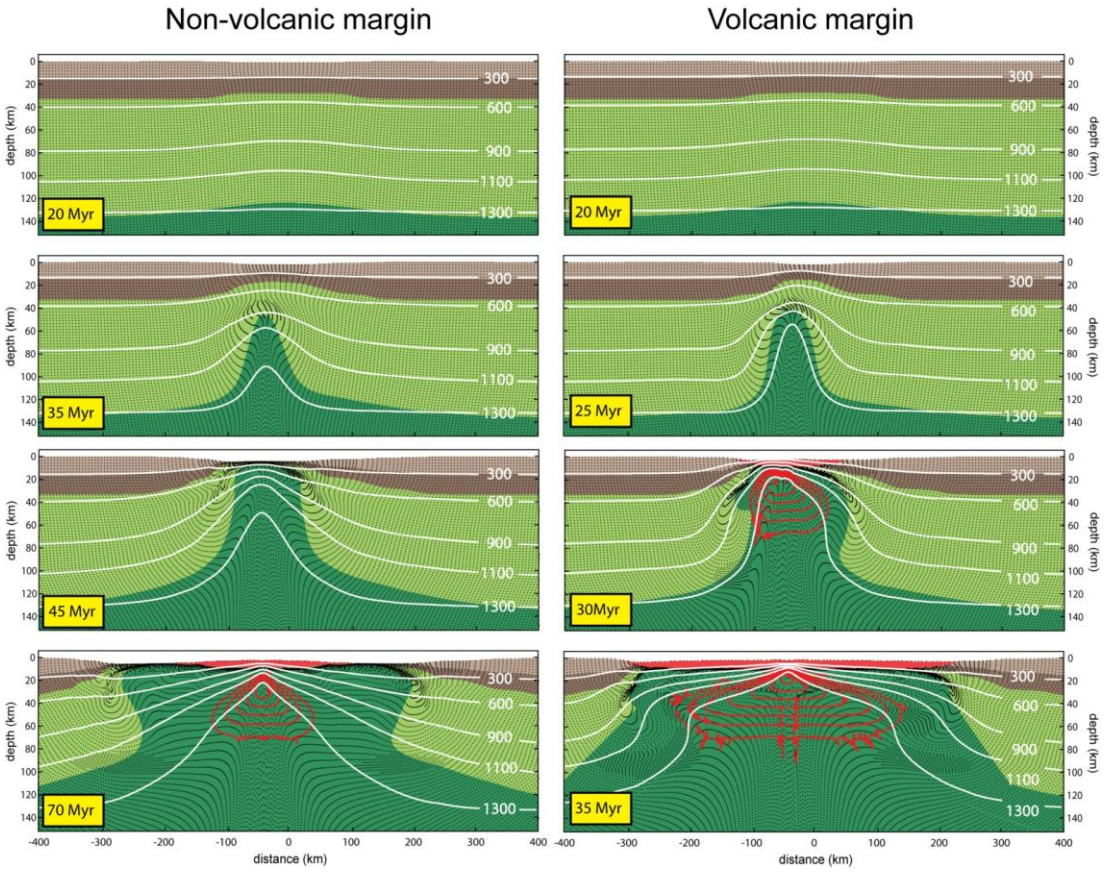

Figure 5.2: Non-volcanic vs. volcanic margins lithosphere deformation prediction using FE-Margin. The non-volcanic model runs for 70Myr and was described in Figure 5.1. The volcanic margin model uses faster spreading rates, shorter lithosphere deformation events and runs for 35Myr. (Legend: light brown, upper crust; dark brown, lower crust; light green, lithospheric mantle; dark green, asthenospheric mantle; red, volcanic addition

Buoyancy upwelling strength

I defined the strength of buoyancy induced upwelling by the ratio V_z^0/V_x^0 where V_x^0 is half-spreading rate and V_z^0 is the active upwelling rate generated by buoyancy. The relative strength of buoyancy is dependent on the half-spreading rate. The quantitative calibration of the Iberia-Newfoundland and the Alpine Tethys rifted margins suggested that the contribution of buoyancy was high early during rifting in order to speed up lithosphere thinning and predict strong thermal uplift and earlier melting. The relative strength of buoyancy then decreases when the half-spreading rate increases. Therefore, it seems that the increase of half-spreading rate during rifting amplifies passive upwelling which attenuates the contribution of buoyant upwelling (annex A). These results are consistent with those in Braun et al. (2000). However the distinction between two buoyancy upwelling effects needs to be clarified:

(1) Thermal buoyancy may be generated during early intracontinental rifting due to the initial heterogeneities within the mantle or more localised deformation. This may initiate melt at some point

(2) The melt then lowers the viscosity if it is retained in the mantle. It results in the increase of buoyant upwelling rate leading to more melting. Melt extraction follows at some point with focussing of the deformation region to form a mid-ocean ridge.

These two effects may be summarized in Figure 5.3. The first increase of buoyancy upwelling from regional to localised stretching and thinning is followed by the possible attenuation of the contribution of buoyancy upwelling because the extension has accelerated during mantle exhumation. Then buoyancy upwelling increase again due to melt retention (Nielsen and Hopper, 2004). The half-spreading extension rate remains the

same until melting reaches a critical threshold melt fraction (Buck and Su, 1989) leading to its extraction.

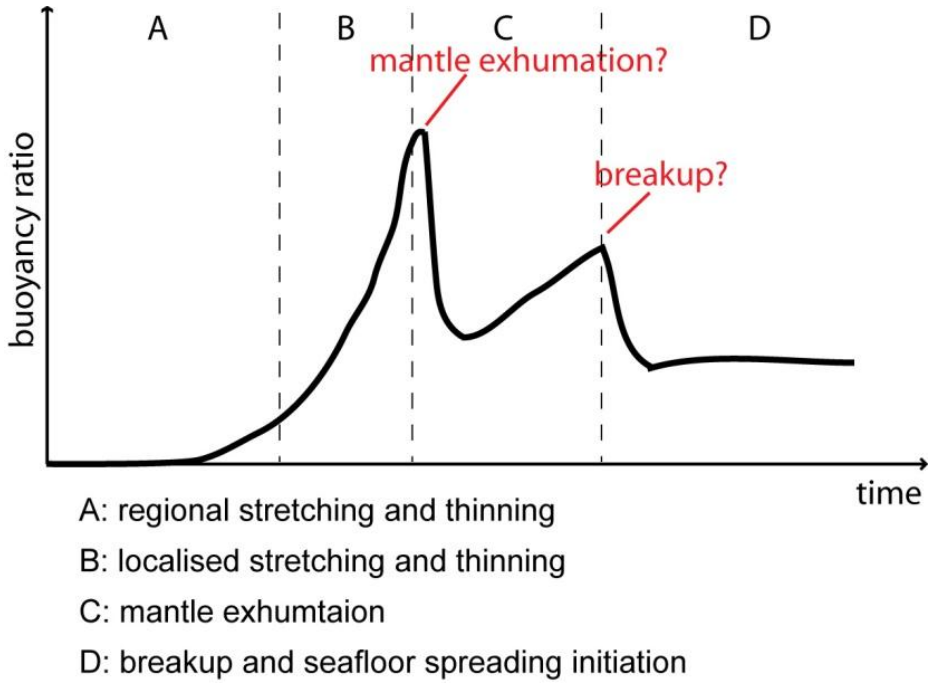

Figure 5.3: Suggested buoyancy upwelling ratio evolution during the formation of magma-poor rifted margins.

Buoyancy upwelling depth evolution

In chapter 3 for the Iberia-Newfoundland rifted margins formation, the depth below which buoyancy induced upwelling is applied is set to not thin the continental crust. The penetration depth of buoyancy upwelling may therefore evolve from >30km to shallower depth, and may be enhanced by stronger passive upwelling during localised stretching and thinning. This upward-propagation of the buoyancy penetration depth is essential to predict the rapid post-uplift subsidence of the Briançonnais domain for the formation of the Alpine Tethys rifted margins in chapter 4, as it removes the lower crustal basement.

Despite good calibration using Iberia-Newfoundland and the Alpine Tethys rifted margins observations, the initiation of buoyancy upwelling, its strength and penetration depth remain difficult to precisely quantify using only melting and subsidence history as constraints.

5.5.4 Melt retention

Buoyancy induced upwelling early during rifting generates earlier decompression melting; therefore melt retention is necessary to produce wide zones of exhumed mantle as proposed at magma-poor rifted margins (Boillot et al., 1987; Péron-Pinvidic et al., 2007). Quantifying melt retention would bring important insight not only into the understanding to the formation of magma-poor rifted margins, but also into how the lithosphere deform during intracontinental rifting leading to breakup and seafloor spreading.

Definitions

Melt retention during continental rifting and at slow-spreading ocean ridges has previously been proposed. Müntener & Manatschal (2006) suggested that melt impregnation occurs during the formation of the Iberia-Newfoundland rifted margins. Furthermore, Müntener et al. (2010) proposed that up to 12% of an oceanic ridge-type melt remains in the asthenospheric mantle, based on ophiolitic remnants of the Alpine Tethys. These aspects led me to consider melt retention as an important parameter. I distinguished in chapter 2 two processes for melt retention:

(1) ***Threshold melt fraction:*** The melt is only extracted after a critical threshold melt fraction is reached.

(2) ***Efficiency:*** During the process of melt extraction, only a percentage is extracted to the surface and the rest remains in the mantle.

The occurrence of scattered embryonic oceanic crust and dykes accompanying serpentinized exhumed mantle within the OCT of magma-poor rifted margins specifies the characterization of melt retention. The initiation of melting may be followed by its instantaneous extraction to the surface but with an evolving efficiency from high retention of melt to low retention. Also the melt may be episodically extracted. The increase of melt fraction, which is retained in the mantle, increases the strength of buoyancy induced upwelling (Buck and Su, 1989). More melt is therefore produced until it reaches a threshold melt fraction. Melt extraction then become more efficient and focuses the deformation to a width 10-20km around the ridge axis. This event results in continental breakup and the onset of seafloor spreading.

Modelling predictions of melt retention

Our modelling results from chapter 2 showed how melt retention was likely to occur to permit mantle exhumation. The calibration of the Iberia-Newfoundland and the Alpine Tethys rifted margins formation in chapter 3 and 4 suggested that melt may be retained within the mantle until it reaches a threshold melt fraction between 6 to 12% before melt is more efficiently extracted. However, these predictions are difficult to compare to nature because there are only few studies that aimed to quantify melt retention. As said previously, Müntener et al. (2010) suggested that up to 12% of an oceanic ridge-type melt remains in the asthenospheric mantle, but using a kinematic modelling approach is a limitation to further quantifying melt retention due to its complicated relationships with the rheology.

Processes involving melt retention

The physics of melt extraction has been investigated (Morgan, 1987; Spiegelman, 1993). There is no doubt that pressure gradients and buoyancy-driven convection are involved in the focussing of the deformation (Buck and Su, 1989; Faul, 2001; Scott and Stevenson, 1989), but its relationship with the mode of lithosphere, the pure-shear deformation width, passive (half-spreading rate (Lizarralde et al., 2004)) or active (buoyancy) upwelling rate remain obscure. How the efficiency of melt extraction evolves according to the mode of lithosphere deformation is a key question for the quantitative calibration of kinematic models. We can only speculate from the results of chapter 3 and 4. I have seen that the half-spreading rate is proportionally related to the pure-shear width; slow spreading rates are used with a wide pure-shear deformation region and conversely faster spreading rates are used with a narrow pure-shear width. Cannat et al. (2004) already suggested than more melt was extracted to form an oceanic crust if the pure-shear deformation width was narrow. Even if the flow-lines of the deformation control the porosity and permeability of the mantle and therefore melt migration to the surface, no existing studies permit the quantification of the critical threshold melt fraction before melt is extracted. Also how this critical threshold melt fraction evolves in function of the lithosphere deformation mode? These questions are critically important for the rifted margin community, but our modelling approach remain a limitation to quantifying melt retention.

5.5.4 Thermal structure evolution during continental rifting leading to breakup and seafloor spreading initiation

The thermal evolution during intracontinental rifting leading to breakup and seafloor spreading initiation was the main question that addresses this thesis to better understand

processes of lithosphere deformation. Cannat et al. (2009) proposed that the lithosphere thermal structure during continental breakup evolves (cf. Figure 1.6). At the beginning of rifting, the base of the lithosphere remains deep close to its original depth, then it shallows rapidly leading to decompressional melting, and finally it stabilizes at shallow depth. The onset of ridge type mantle upwelling defines the breakup. Then the lithosphere thickness becomes controlled by active heat balance; this is seafloor spreading.

I have examined in chapter 2, 3 and 4 the thermal evolution of our final preferred models for a long duration of mantle exhumation and for the Iberia-Newfoundland and the Alpine Tethys rifted margins formation. The comparison of the thermal structure evolution (isotherm 1280°C) and initial lithosphere-asthenosphere material boundary from the model prediction with the Cannat et al. (2009) lithosphere evolution is described as follows:

(1) In chapter 2, I used a single lithosphere deformation mode to demonstrate how mantle exhumation may persist under certain conditions over a long period of time. I show in Figure 5.4 that it is difficult to match the predicted evolution of the isotherm 1280°C and original lithosphere-asthenosphere boundary together with the Cannat et al. (2009) thermal structure evolution. In addition, continental breakup could have not been defined as specified by Cannat et al. (2009) by the installation of a ridge-type thermal regime (or active heat balance).

(2) I compare in Figure 5.5 the thermal evolution prediction of the Iberia-Newfoundland rifted margins application from our preferred model with the Cannat et al. (2009) model. There is a good fit between these. The only difference is that decompressional melting occurs after the mantle

exhumation for both the northern and southern Iberia-Newfoundland rifted margin profiles and at shallower depth. Both the evolution of the original lithosphere-asthenosphere material boundary and the isotherm 1280°C are similar for both model predictions.

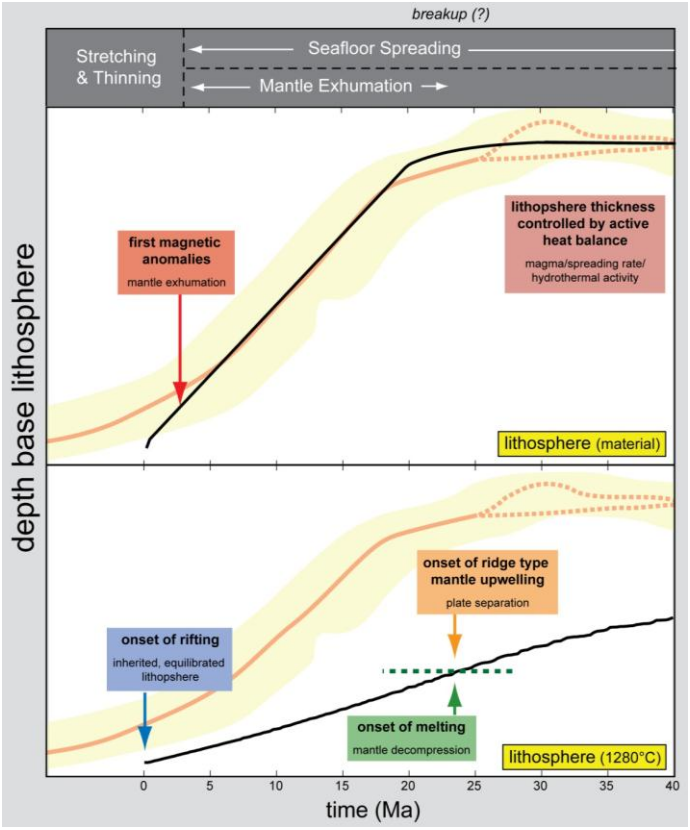

Figure 5.4: Lithosphere thermal structure evolution predicted from our preferred model in chapter 2. Both lithosphere thermal structure evolution predictions are compared with the Cannat et al. (2009) thermal evolution (orange and yellow trends).

(3) Figure 5.6 show the comparison of the thermal structure and original lithosphere-asthenosphere boundary evolutions between the preferred model of the Alpine Tethys rifted margins formation and the Cannat et al. (2009) thermal structure evolution. The results are similar to those from the

Iberia-Newfoundland rifted margin application; there is a good fit between the predicted and suggested thermal structure evolution, and decompressional melting occurs when the base of the lithosphere is already too shallow. Additionally, both evolutions of the base of the lithosphere and the original lithosphere-asthenosphere material boundary have a similar trend. However, the initiation of melting precedes mantle exhumation.

These preferred thermal evolution predictions result from two distinct applications, a present-day and a fossil analogue rifted margins, and both show notable similar results. The observations of these 3 thermal predictions validate the necessity of using evolving lithosphere deformation modes and also including buoyancy induced upwelling early during rifting. However, an important question remains; during the extreme thinning phase of rifting that leads to mantle exhumation, what is the relationship between melt generation and the initiation of mantle exhumation? Melt is initiated before mantle exhumation during the Alpine Tethys formation, while for the Iberia-Newfoundland application, crustal breakup occurs prior to the onset of melting. It does not seem that melt generation controls when mantle exhumation will occur. However, both these two model predictions together with the Cannat et al. (2009) thermal evolution suggest that mantle exhumation occurs when the base of the lithosphere is relatively shallow.

Figure 5.5 *(next page):* Lithosphere thermal structure evolution predicted from our models preferred for the formation of the Iberia-Newfoundland conjugate rifted margins in chapter 3. Both lithosphere thermal structure evolution predictions are compared with the Cannat et al. (2009) thermal evolution (orange and yellow trends).

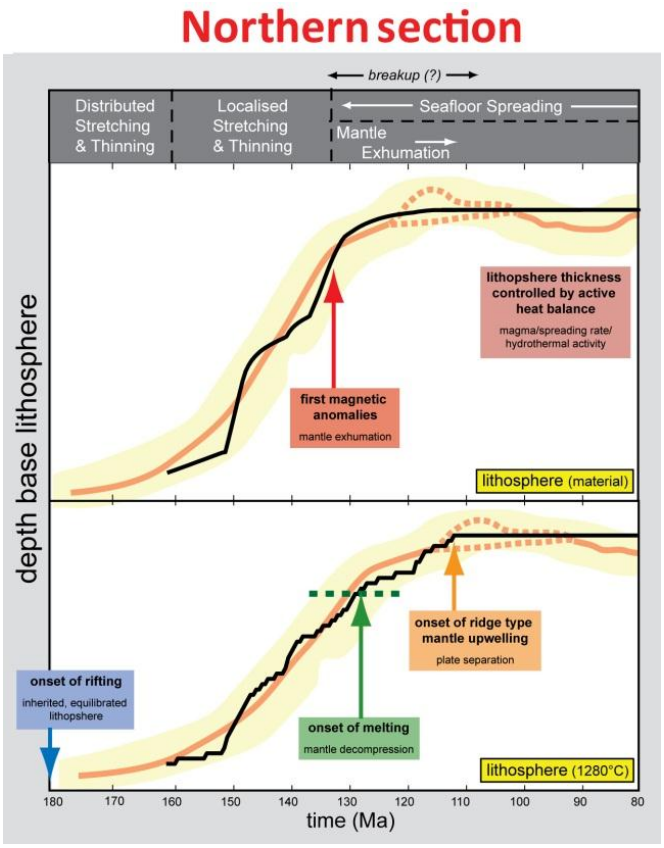
Northern section
breakup (?)
Distributed Stretching & Thinning
Localised Stretching & Thinning
Seafloor Spreading
Mantle Exhumation
depth base lithosphere
lithopshere thickness controlled by active heat balance
magma/spreading rate/ hydrothermal activity
first magnetic anomalies
mantle exhumation
lithosphere (material)
onset of ridge type mantle upwelling
plate separation
onset of rifting
inherited, equilibrated lithopshere
onset of melting
mantle decompression
lithosphere (1280°C)
180 170 160 150 140 130 120 110 100 90 80
time (Ma)

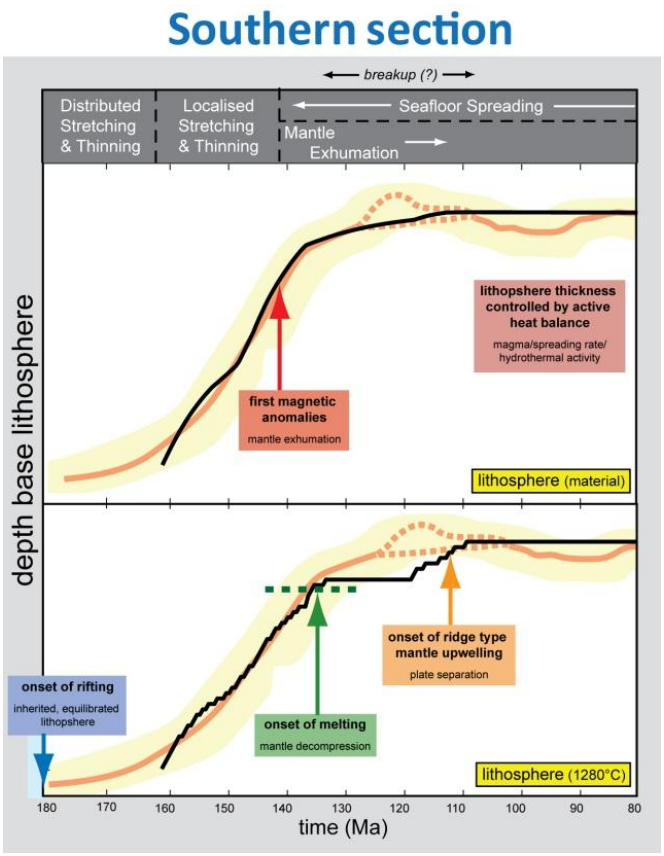
Southern section
breakup (?)
Distributed Stretching & Thinning
Localised Stretching & Thinning
Seafloor Spreading
Mantle Exhumation
depth base lithosphere
lithopshere thickness controlled by active heat balance
magma/spreading rate/ hydrothermal activity
first magnetic anomalies
mantle exhumation
lithosphere (material)
onset of ridge type mantle upwelling
plate separation
onset of rifting
inherited, equilibrated lithopshere
onset of melting
mantle decompression
lithosphere (1280°C)
180 170 160 150 140 130 120 110 100 90 80
time (Ma)

However, in both cases melt is generated during mantle exhumation. Mantle exhumation can therefore not be defined using the relative timing of melt initiation and crustal breakup, but as the relative timing of melt extraction and crustal breakup. Melt retention must be taken into account in the definition of mantle exhumation. Additionally, the first melt being extracted cannot be defined as oceanic accretion, reserved for post-continental breakup melt extraction, but as volcanic addition, which can be related in the nature to embryonic oceanic crust (Reid, 1994; Jagoutz et al., 2007; Bronner et al., 2011). However, melt retention cannot give further insight about the definition of continental breakup because melt retention cannot be quantifed using our current kinematic model.

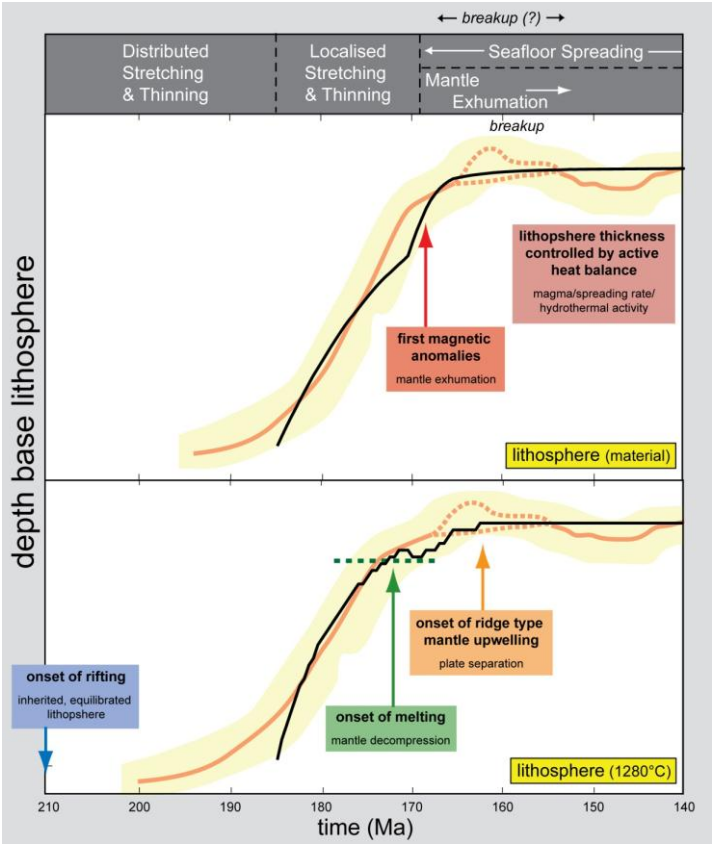

Figure 5.6: Lithosphere thermal structure evolution predicted from our reference model **I** for the formation of the Alpine Tethys rifted margin in chapter 4. Both lithosphere thermal structure evolution predictions are compared with the Cannat et al. (2009) thermal evolution (orange and yellow trends).

5.6 Further work

The quantitative calibration of the lithosphere deformation model applied to natural laboratories was a key point of my PhD because it gives insights on natural processes of lithosphere deformation, but also allows the prediction of thermal and subsidence history on particular rifted margins that may be of application the oil industry. Several modifications to the kinematic model FE-Margin that I developed during my PhD are required:

(1) The calibration of the rifting evolution using subsidence history cannot easily and precisely be predicted if the model does not include faulting, sedimentation and erosion. These processes affect the subsidence history during rifting; sedimentation modifies the amount of subsidence and uplift, while footwall uplift of normal faults result in topographic highs that considerably affect the depositional environment and subsidence analysis. Also the sediment cover affects heat flow predictions.

(2) Melt generation by mantle decompression may also be improved by including mantle inheritance such as the presence of hydrated, depleted or fertile mantle. Because melting evolves from initial alkaline magmatism to localised MORB (occasionally replaced by continuing alkaline events), the calibration of bulk chemistry of predicted magma would significantly improve the precision of the model, and also give insights on melt retention.

(3) Another improvement of FE-Margin concerns the rheology. I calculated the lithosphere deformation flow-fields using a unique viscosity structure. It would be therefore interesting to couple the calculation of flow-fields with a control of (a) the viscosity structure by a temperature constraint, and (b)

lateral migration by jumps or continuous migration. Further work would also relate these controls to the inheritance of the mantle, continental crust and especially melt retention.

This last point, however, has to be carefully introduced to FE-Margin in order to avoid transforming the model into a purely dynamic model and therefore less amenable to quantitative calibration. The strength of this study is the kinematic component of FE-Margin that allows the control of the lithosphere deformation mode parameters and location. As a consequence I was able to quantitatively calibrate this kinematic model using observational data in order to interrogate natural laboratories and reveal their lithosphere deformation histories.

REFERENCES

Boillot, G., E. L. Winterer, and A. W. Meyer, 1987, Leg 103: Proc. Ocean Drill. Program, Initial Reports, p. 663.

Braun, M. G., G. Hirth, and E. M. Parmentier, 2000, The effects of deep damp melting on mantle flow and melt generation beneath mid-ocean ridges: Earth and Planetary Science Letters, v. 176, p. 339-356.

Bronner, A., D. Sauter, G. Manatschal, G. Péron-Pinvidic, and M. Munschy, 2011, Magmatic breakup as an explanation for magnetic anomalies at magma-poor rifted margins: Nature Geoscience, v. 4, p. 549-553.

Buck, W. R., and W. Su, 1989, Focused mantle upwelling below mid-ocean ridges due to feedback between viscosity and melting: Geophysical Research Letters, v. 16, p. 641-644.

Cannat, M., 1996, How thick is the magmatic crust at slow spreading oceanic ridges?: Journal of Geophysical Research: Solid Earth, v. 101, p. 2847-2857.

Cannat, M., J. Cann, and J. Maclennan, 2004, Some hard rock constraints on the supply of heat to mid-ocean ridges: Geophysical Monograph Series, v. 148, p. 111-149.

Cannat, M., G. Manatschal, D. Sauter, and G. Peron-Pinvidic, 2009, Assessing the conditions of continental breakup at magma-poor rifted margins: What can we learn from slow spreading mid-ocean ridges?: Comptes Rendus Geoscience, v. 341, p. 406-427.

Faul, U. H., 2001, Melt retention and segregation beneath mid-ocean ridges: Nature, v. 410, p. 920-923.

Forsyth, D. W., D. S. Scheirer, S. C. Webb, L. M. Dorman, J. A. Orcutt, A. J. Harding, D. K. Blackman, J. P. Morgan, R. S. Detrick, Y. Shen, C. J. Wolfe, J. P. Canales, D. R. Toomey, A. F. Sheehan, S. C.

Solomon, and W. S. D. Wilcock, 1998, Imaging the deep seismic structure beneath a mid-ocean ridge : The MELT experiment: Science, v. 280, p. 1215-1218.

Jagoutz, O., Müntener, O., Manatschal, G., Rubatto, D., Péron-Pinvidic, G., Turrin, B. D., & Villa, I. M. (2007). The rift-to-drift transition in the North Atlantic: A stuttering start of the MORB machine? *Geology*, *35*(12), 1087–1090.

Li, X.-H., M. Faure, W. Lin, and G. Manatschal, 2013, New isotopic constraints on age and magma genesis of an embryonic oceanic crust: The Chenaillet Ophiolite in the Western Alps: Lithos, v. 160, p. 283-291.

Lizarralde, D., J. B. Gaherty, J. A. Collins, G. Hirth, and S. D. Kim, 2004, Spreading-rate dependence of melt extraction at mid-ocean ridges from mantle seismic refraction data: Nature, v. 432, p. 744-747.

Mohn, G., G. Manatschal, M. Beltrando, E. Masini, and N. Kusznir, 2012, Necking of continental crust in magma-poor rifted margins: Evidence from the fossil Alpine Tethys margins: Tectonics, v. 31.

Morgan, J. P., 1987, Melt migration beneath mid-ocean spreading centers: Geophysical Research Letters, v. 14, p. 1238-1241.

Müntener, O., & Manatschal, G. (2006). High degrees of melt extraction recorded by spinel harzburgite of the Newfoundland margin: The role of inheritance and consequences for the evolution of the southern North Atlantic. *Earth and Planetary Science Letters*, *252*(3–4), 437–452.

Müntener, O., G. Manatschal, L. Desmurs, and T. Pettke, 2010, Plagioclase peridotites in ocean–continent transitions: refertilized mantle domains generated by melt stagnation in the shallow mantle lithosphere: Journal of Petrology, v. 51, p. 255-294.Nielsen, T. K., and J. R. Hopper, 2004, From rift to drift: Mantle melting during continental breakup: Geochemistry, Geophysics, Geosystems, v. 5.

Pascal, C., J. W. Van Wijk, S. Cloetingh, and G. R. Davies, 2002, Effect of lithosphere thickness heterogeneities in controlling rift localization: numerical modeling of the Oslo Graben: Geophysical Research Letters, v. 29, p. 69-1-69-4.

Péron-Pinvidic, G., and G. Manatschal, 2009, The final rifting evolution at deep magma-poor passive margins from Iberia-Newfoundland: a new point of view: International Journal of Earth Sciences, v. 98, p. 1581-1597.

Péron-Pinvidic, G., G. Manatschal, T. A. Minshull, and D. S. Sawyer, 2007, Tectonosedimentary evolution of the deep Iberia-Newfoundland margins: Evidence for a complex breakup history: Tectonics, v. 26.

Reid, I. D., 1994, Crustal structure of a nonvolcanic rifted margin east of Newfoundland: Journal of Geophysical Research: Solid Earth (1978–2012), v. 99, p. 15161-15180.

Scott, D. R., and D. J. Stevenson, 1989, A self-consistent model of melting, magma migration and buoyancy-driven circulation beneath mid-ocean ridges: Journal of Geophysical Research: Solid Earth (1978–2012), v. 94, p. 2973-2988.

Sibuet, J. C., S. P. Srivastava, M. Enachescu, and G. D. Karner, 2007, Early Cretaceous motion of Flemish Cap with respect to North America: implications on the formation of Orphan Basin and SE Flemish Cap–Galicia Bank conjugate margins: Geological Society, London, Special Publications, v. 282, p. 63-76.

Spiegelman, M., 1993, Physics of melt extraction: Theory, implications and applications: Philosophical Transactions of the Royal Society of London. Series A: Physical and Engineering Sciences, v. 342, p. 23-41.

Spiegelman, M., and J. R. Reynolds, 1999, Combined dynamic and geochemical evidence for convergent melt flow beneath the East Pacific Rise: Nature, v. 402, p. 282-285.

Sutra, E., G. Manatschal, G. Mohn, and P. Unternehr, 2013, Quantification and restoration of extensional deformation along the Western Iberia and Newfoundland rifted margins: Geochemistry, Geophysics, Geosystems, v. 14, p. 2575-2597.

Whitmarsh, R. B., and P. J. Wallace, 2001, The rift-to-drift development of the West Iberia non-volcanic continental margin; a review of the contribution of Ocean Drilling Program Leg 173.

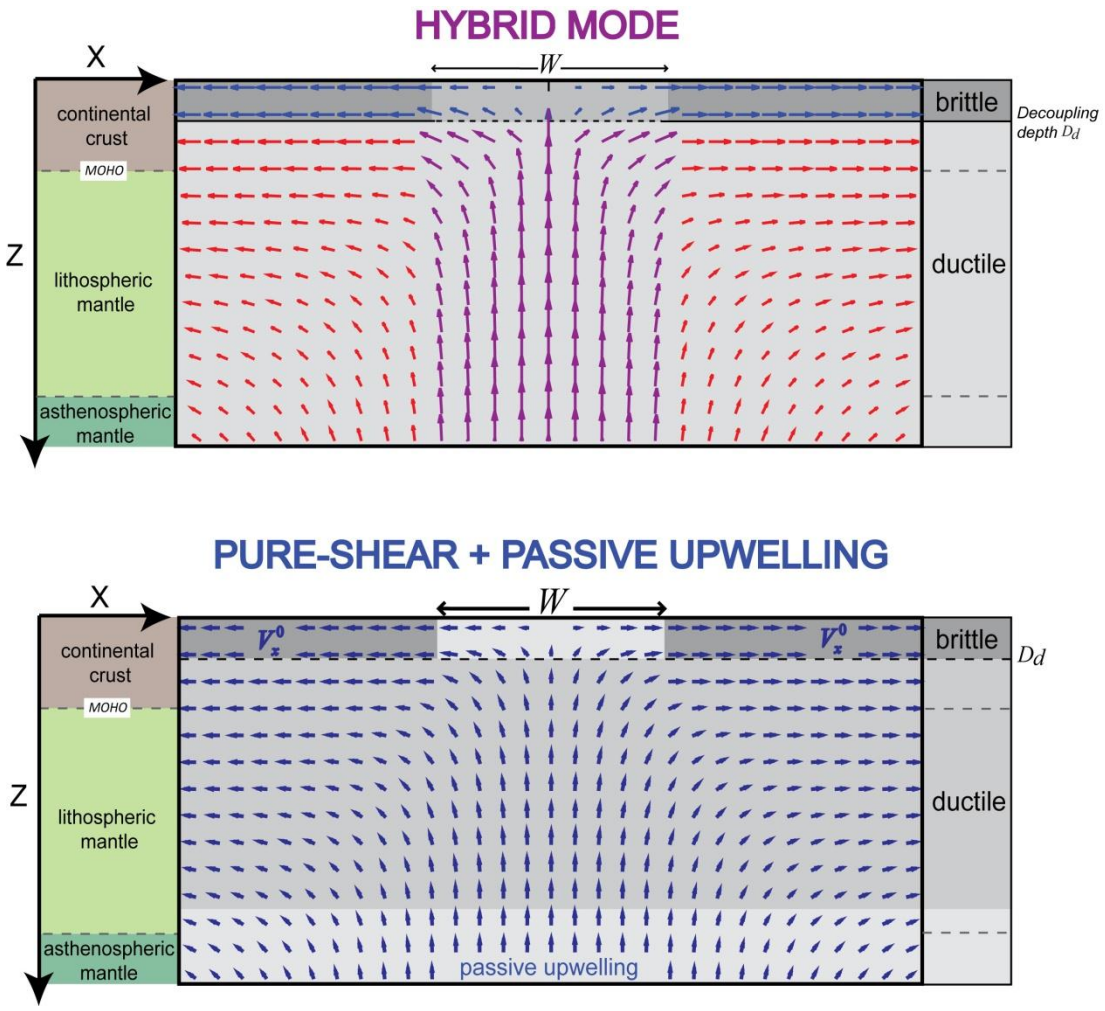

Appendix A: Comparison between the hybrid deformation mode, consisting of pure-shear above upwelling-divergent flow end-members deformation modes, and the pure-shear and passive upwelling mode calculated with the finite-element viscous flow model.

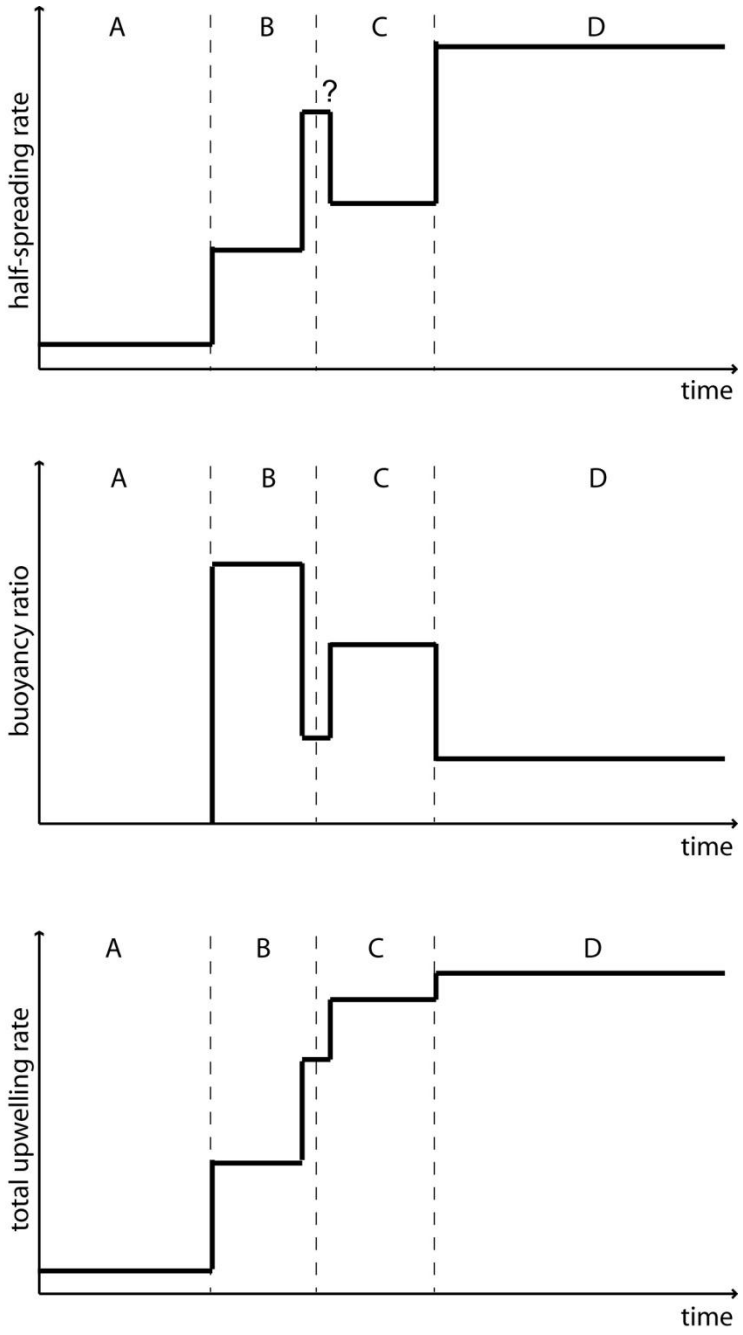

Appendix B: Schematic evolution of the extension rate, buoyancy upwelling ratio and the total upwelling rate based on the modelled predictions for the formation of magma-poor rifted margins